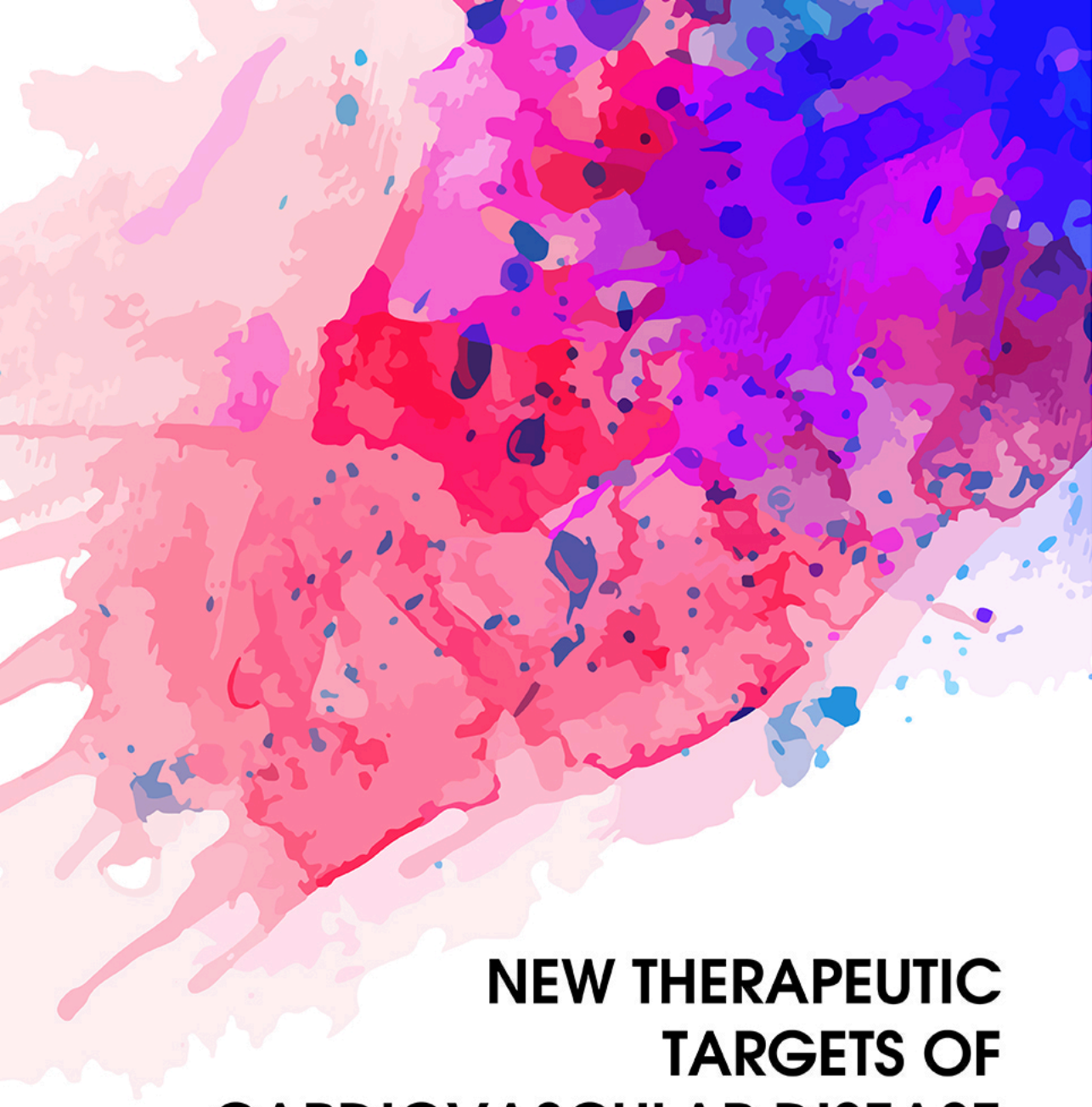

NEW THERAPEUTIC TARGETS OF CARDIOVASCULAR DISEASE

focus on the renin-angiotensin system and lipid metabolism

Yuan Sun

Invitation

To attend the public defense
of the PhD thesis

NEW THERAPEUTIC TARGETS OF CARDIOVASCULAR DISEASE

focus on the renin-angiotensin system and lipid metabolism

by Yuan Sun

y.sun.1@erasmusmc.nl

9:30 am, October 27th, 2020

Prof. Andries Queridozaal
Erasmus MC Onderwijscentrum

Zoom Live stream link will be informed later

Paranymphs

Michelle Broekhuizen
m.broekhuizen@erasmusmc.nl

Lunbo Tan
l.tan@erasmusmc.nl

Reception will be held after the defense

Stellingen

behorende bij het proefschrift

"NEW THERAPEUTIC TARGETS IN CARDIOVASCULAR DISEASE-
focus on the renin-angiotensin system and lipid metabolism"

1. The hepatic (pro)renin receptor is a regulator of lipid metabolism (this thesis).

2. Megalin is a novel endocytic receptor for prorenin and renin (this thesis).

3. Megalin-mediated internalization of (pro)renin requires the (pro)renin receptor (this thesis).

4. Placental angiotensinogen is derived from maternal blood (this thesis).

5. Hepatic angiotensinogen inhibition alone or in combination with an angiotensin receptor blocker is an effective mean to control blood pressure. (this thesis)

6. Megalin is a bridge connecting kidney, the renin-angiotensin system and atherosclerosis. (Ye *et al., ATVB* 2019; Koizumi *et al., Hypertension* 2019)

7. The (pro)renin receptor is required for normal vacuolar H^+-ATPase function but not for renin-angiotensin system activity. (Trepiccione *et al., JASN* 2016)

8. Proton pump inhibitors lower the risk of early-onset preeclampsia. (Hastie *et al., Hypertension* 2019)

9. Gut microbiota is a new path to treat obesity and hypertension. (Tang *et al., Circ. Res.* 2017)

10. Renin-angiotensin system blockers neither have advantages nor disadvantages in COVID-19.

11. Time is money, efficiency is life, innovation is that you spend your money and life to learn the basic facts.

Yuan Sun
Rotterdam,27 October, 2020

NEW THERAPEUTIC TARGETS IN CARDIOVASCULAR DISEASE

focus on the renin-angiotensin system and lipid metabolism

Yuan Sun
孙源

NEW THERAPEUTIC TARGETS IN CARDIOVASCULAR DISEASE -
focus on the renin-angiotensin system and lipid metabolism

Thesis, Erasmus University, Rotterdam. With summary in Dutch and English.

ISBN: 978-94-6416-133-5

Cover design: Yuan Sun
Layout design: Yuan Sun
Printing: Ridderprint, the Netherlands

NEW THERAPEUTIC TARGETS IN CARDIOVASCULAR DISEASE

focus on the renin-angiotensin system and lipid metabolism

Nieuwe behandelopties voor cardiovasculaire aandoeningen – focus op het renine-angiotensine systeem en lipiden metabolisme

Proefschrift

ter verkrijging van de graad van doctor aan de
Erasmus Universiteit Rotterdam
op gezag van de rector magnificus

Prof. dr. R.C.M.E. Engels

en volgens besluit van het College voor Promoties.

De openbare verdediging zal plaats vinden op
dinsdag 27 oktober 2020 om 9.30 uur

door
Yuan Sun
geboren te Gansu (China)

Erasmus University Rotterdam

PROMOTIECOMMISSIE

Promotor:	Prof. dr. A.H.J. Danser
Overige leden:	Prof. dr. E.J. Hoorn
	Prof. dr. N. Zelcer
	Prof. dr. R. Masereeuw
Copromotor:	Dr. X. Lu

Financial support by the Dutch Heart Foundation for the publication of this thesis is gratefully acknowledged.

Hartstichting

Additional financial support for publication of this thesis was generously provided by 触梦社区 .
(感谢触梦社区赞助出版此论文集)

触梦社区

SYSE Bio-Tech （常州鼠一鼠二生物科技有限公司）

SYSE
鼠一鼠二生物

In me the tiger sniffs the rose.

——*Siegfried Sassoon*

Table of contents

CHAPTER 1

Introduction and Aims

(Pro)renin Receptor as a Therapeutic Target for the Treatment of Cardiovascular Diseases?

Yuan Sun, A.H. Jan Danser and Xifeng Lu

Pharmacol Res 125: 48-56, 2017

Abstract

The discovery of the (pro)renin receptor [(P)RR] 15 years ago stimulated ideas on prorenin being more than renin's inactive precursor. Indeed, binding of prorenin to the (P)RR induces a conformational change in the prorenin molecule, allowing it to display angiotensin-generating activity, and additionally results in intracellular signaling in an angiotensin-independent manner. However, the prorenin levels required to observe these angiotensin-dependent and -independent effects of the (P)RR are many orders above its in vivo concentrations, both under normal and pathological conditions. Given this requirement, the idea that the (P)RR has a function within the renin-angiotensin system (RAS) is now being abandoned. Instead, research is now focused on the (P)RR as an accessory protein of vacuolar H^+-ATPase (V-ATPase), potentially determining its integrity. Acting as an adaptor between Frizzled co-receptor LRP6 and V-ATPase, the (P)RR appears to be indispensable for Wnt/β-catenin signaling, thus explaining why (P)RR deletion (unlike renin deletion) is lethal even when restricted to specific cells, such as cardiomyocytes, podocytes and smooth muscle cells. Furthermore, recent studies suggest that the (P)RR may play important roles in lipoprotein metabolism and overall energy metabolism. In this review, we summarize the controversial RAS-related effects of the (P)RR, and critically review the novel non-RAS-related functions of the (P)RR, ending with a discussion on the potential of targeting the (P)RR to treat cardiovascular diseases.

Introduction

The renin-angiotensin system (RAS) is a key system regulating blood pressure and controlling body fluid homeostasis. Renin is formed by cleavage of the N-terminal prosegment from its non-active precursor prorenin exclusively in the juxtaglomerular cells of the kidney and secreted into the circulation in a controlled manner. Active renin catalyzes the conversion of angiotensinogen to angiotensin (Ang) I, which is then further converted by angiotensin-converting enzyme (ACE) to Ang II, the main effector molecule of the RAS. Unlike renin, prorenin is constantly secreted into the circulation by the kidney and other organs, such as the eye, reproductive organs and adrenal gland [1]. Plasma prorenin levels are in excess of plasma renin levels under physiological conditions, and can be up to 100-fold higher under pathological conditions such as diabetes mellitus [2-4]. Since proteolytic activation of prorenin has never been demonstrated outside the juxtaglomerular cells, it seemed unlikely that prorenin would somehow contribute to angiotensin generation at tissue sites. Consequently, prorenin's function remained solely as the inactive precursor of renin until the discovery the (pro)renin receptor [(P)RR] fifteen years ago. Upon binding to the (P)

RR, prorenin is activated in a non-proteolytic manner. In addition, binding of renin and prorenin triggers intracellular signaling pathways independent from the generation of Ang II. This indicates that the (pro)renin-(P)RR interaction could be a potential target for treating cardiovascular and renal complications, and it soon drew great attention. Now, more than a decade later, it is still not clear how and to what degree the (P)RR contributes to end-organ damage and whether this involves local RAS activation. Yet, novel and Ang II-independent functions of the (P)RR have been identified, as an accessory protein of vacuolar H^+-ATPase (V-ATPase), with important roles in Wnt signaling, low-density lipoprotein (LDL) clearance, and glucose metabolism. In this review, we summarize the latest findings on the novel functions of the (P)RR and discuss the pharmacological potential of targeting the (P)RR for the treatment of cardiovascular diseases.

(P)RR and the RAS

The (P)RR is a 350-amino acid protein with a single transmembrane domain, encoded by the ATP6AP2 gene located on the X chromosome, which is highly conserved in vertebrates [5]. The C-terminal fragment (CTF) of the (P)RR is identical to the 8.9 kDa accessory protein of V-ATPase [6]. Identification and characterization of a novel 9.2-kDa membrane sector-associated protein of vacuolar proton-ATPase from chromaffin granules, and the N-terminal domain (NTD) of the (P)RR can bind both renin and prorenin [7], denoted together as (pro)renin. The (P)RR induces a conformational change in prorenin upon binding, resulting in full exposure of the catalytic cleft with the prosegment still being present [7-10]. In addition, the (P)RR also directly stimulates intracellular signaling networks, including extracellular signal-regulated kinases 1/2 (Erk1/2) activation in vascular smooth muscle cells, meningeal cells, monocytes, collecting duct cells, endothelial cells and adipocytes, and phosphatidylinositol 3-kinase/Akt (PI3K/Akt) activation in HEK293T cells [11-19] **(Figure 1)**. Activation of these signaling pathways can subsequently result in upregulation of profibrotic genes including transforming growth factor-1, plasminogen-activator inhibitor 1 (PAI-1), fibronectin and collagen-1 [12, 20, 21]. As a consequence, the (P)RR might directly (i.e., independent from Ang II formation) promote tissue damage. If true, it would be a novel target to prevent cardiovascular and renal complications. In agreement with this concept, aging transgenic rats overexpressing the human (P)RR develop proteinuria and glomerulosclerosis [22] in the absence of hypertension, and ACE inhibition, although capable of lowering Ang II, did not prevent this renal damage.

A peptidic antagonist (handle region peptide, HRP) has been designed based on the concept that the prosegment of prorenin contains a “handle region” that binds to the (P)RR [23]. HRP

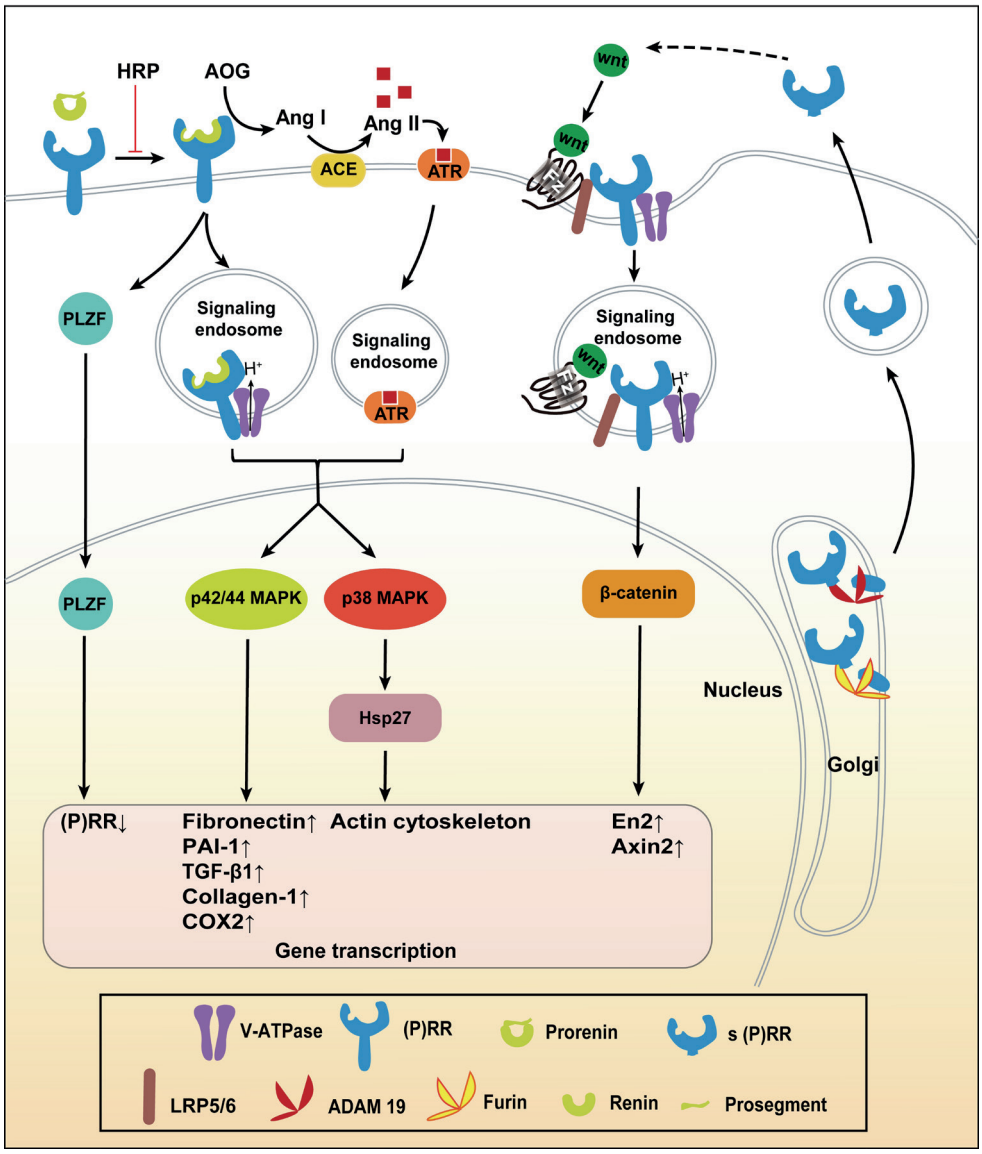

Figure 1. Potential functions of the (P)RR. Upon binding (pro)renin, the (P)RR can activate intracellular signaling pathways, via both angiotensin-dependent and -independent ways, resulting in upregulation of profibrotic genes. In addition, the (P)RR is required for Wnt/β-catenin signaling. Besides, s(P)RR can be generated from full length (P)RR by furin and ADAM19, and potentiate Wnt/β-catenin signaling. HRP, handle region peptide; ACE, angiotensin-converting enzyme; AOG, angiotensinogen; ATR, angiotensin II receptor; MAPK, mitogen-activated protein kinase; PLZF, promyelocytic leukemia zinc finger; s(P)RR, soluble (P)RR; TGF-β1, transforming growth factor-β1; PAI-1, plasminogen-activator inhibitor 1; COX2, cyclo-oxygenase 2; En2, homeobox protein engrailed-2, an important controller of development; Axin2, axin-like protein (Axil) or axis inhibition protein 2, a regulator of β-catenin stability.

should thus theoretically occupy the binding pocket of the (P)RR, preventing prorenin binding and activation. Initially, studies reported that HRP indeed prevented nephropathy and retinopathy in streptozotocin-induced diabetic human (P)RR transgenic rats [24-26] and reduced ocular inflammation, cardiac hypertrophy and cardiac fibrosis in other pathological animal models [27-30], as reviewed elsewhere [31]. However, later studies demonstrated no or even detrimental effects of HRP in hypertensive and diabetic models [30, 32-36]. In addition, *in vitro* studies showed that HRP does not prevent (pro)renin-induced signaling, not even when applied at micromolar concentrations, and that HRP might actually behave as a partial agonist of (P)RR [14, 30, 37, 38]. Even more confusing, new transgenic mice models with enhanced (P)RR expression show no alterations in blood pressure, and no damage in the heart or kidney [39, 40].

Contrasting data on the (P)RR-prorenin interaction in the brain have also been reported. Given the low, if not absent, renin levels in the brain, prorenin should be the exclusive agonist of the (P)RR. Indeed, the brain (P)RR has been suggested to play an important role in prorenin-stimulated signaling pathways associated with the pathogenesis of neurogenic hypertension [41]. Inhibiting (P)RR expression in the brain using shRNA decreased blood pressure and vasomotor sympathetic tone, possibly through a reduction in Ang II type 1 receptor expression [42]. Moreover, neuron-specific (P)RR KO mice, showing a normal cardiovascular phenotype, were resistant to salt-dependent hypertension [43]. Conceptually in line with these studies, intracerebroventricular infusion of the newly developed HRP-like (P)RR peptidic inhibitor PRO20 attenuated DOCA-salt induced hypertension [44]. Interestingly, Ang II upregulates the expression of brain (P)RR by increasing cAMP response element-binding protein binding to the promoter of the (P)RR [45]. The (P)RR is expressed in hypothalamic magnocellular neurosecretory cells and in the parasympathetic paraventricular nucleus, and prorenin stimulates the neuronal activities in these areas via both Ang II-dependent and -independent effects [46]. Nevertheless, recently, we were unable to detect prorenin in the brain, nor did brain (pro)renin levels increase following the induction of neurogenic hypertension with DOCA-salt [47]. Taken together these studies suggest that the (P)RR-prorenin interaction in the brain is highly unlikely, and that the central effects of putative (P)RR antagonists like HRP and PRO20 occur independently of the RAS [44]. Importantly, this does not exclude the possibility that the brain (P)RR plays a role in blood pressure regulation via a non RAS-mediated pathway. In fact, given the above findings, it is highly likely that there is a link between the (P)RR and neurogenic hypertension. To solve these discrepancies, a detailed pharmacological characterization of PRO20 is still anxiously awaited.

Cleavage of the NTD of the (P)RR by proteases such as furin and ADAM (a disintegrin and metalloproteinase 19) is followed by its secretion into the circulation [48, 49]. The secreted

form of the (P)RR is denoted as s(P)RR [soluble (P)RR]. Initially, s(P)RR was thought to be able to bind and activate prorenin in the circulation, resulting in chronic RAS overactivation. However, this hypothesis was incorrect [50]. In fact, to what degree the (pro)renin-(P)RR interaction truly occurs in vivo remains questionable until today. As reviewed elsewhere, to observe angiotensin-dependent and -independent effects in *in vitro* experiments, the required prorenin levels are 1000-fold and 10,000-fold, respectively, above its normal physiological (i.e., picomolar) concentrations [31]. Such elevations are unlikely to ever occur in vivo, even under pathophysiological conditions, and have also never been achieved in transgenic animal models. Although the collecting duct is believed to be a prorenin-synthesizing site which abundantly expresses the (P)RR, also in collecting duct cells 10 nmol/L prorenin was required to activate Erk1/2 [51]. This implies that even at sites where prorenin-(P)RR interaction is theoretically feasible, it may not happen easily in vivo. In agreement with this concept, a recent study using kidney-specific (P)RR knockout mice observed that renal Ang II production, sodium handling and angiotensin-dependent blood pressure regulation were not affected by (P)RR abolishment [52]. Finally, unlike other RAS components, deletion of (P)RR in mice is lethal, even when (P)RR deletion is restricted to cardiomyocytes [53], podocytes [54, 55] or nephron progenitor cells [56]. Taken together, the (pro)renin-(P)RR interaction is unlikely to occur in normal physiology, and the (P)RR is more likely to play an important role beyond the RAS.

Novel functions of the (P)RR

Table 1 summarizes the findings from recent (P)RR transgenic, knock-out (KO) and knocking-down (KD) animal models. As discussed, the CTF of the (P)RR is identical to ATPA6P2, i.e., accessory protein 2 of V-ATPase. This implies that the function of the (P)RR may be linked to V-ATPase. V-ATPase is a multisubunit proton pump that consists of a Vo domain which translocates protons and a V1 domain which hydrolyzes ATP [57]. The Vo domain contains 6 different subunits of which the a and d subunits have tissue-specific isoforms in mammalians. The V1 domain contains 8 different subunits of which the B, C, E and G subunits have tissue-specific isoforms. In addition to these complex-forming subunits, V-ATPase also has two accessory proteins which are not always co-purified with V-ATPase: ATP6AP1 (also known as Ac45) and ATP6AP2. V-ATPases are expressed in virtually all cell types on the membrane of intracellular compartments, playing an important role in vesicle trafficking, protein degradation and intracellular signaling [58]. V-ATPases are also abundantly expressed in the plasma membrane of certain cells, such as osteoclasts, intercalated cells, macrophages and tumor cells, thus contributing to bone resorption, systemic acid-base regulation and tumor metastasis [57, 59-64]. The contribution of the (P)RR to

V-ATPase function remains largely unknown. One possibility is that the (P)RR may help to maintain V-ATPase integrity [65].

Cardiomyocyte-specific (P)RR deletion in mice resulted in severe heart failure and the mice died within 3 weeks after birth [53]. Similarly, podocyte-specific ablation of the (P)RR in mice caused severe glomerulosclerosis and consequently fetal renal failure within 2-4 weeks [54, 55]. Both (P)RR-deleted cardiomyocytes and podocytes showed accumulation of multivesicle vacuoles in the perinuclear regions, indicating impaired autophagic degradation, which was attributed to deacidification of intracellular vesicles as a consequence of selective down-regulation of subunits of the Vo domain by (P)RR deletion. Complete loss of functional lysosomes was also observed in smooth muscle cell-specific (P)RR knockout animals [66]. These data suggest that the (P)RR is indeed essential for V-ATPase integrity and stability. Moreover, specific (P)RR knockout in photoreceptor cells and the ureteric bud also resulted in phenotypes related to V-ATPase defects [67, 68]. However, it is worth to note that in these in vivo studies, mRNA levels of Vo subunits were not assessed. In addition, the protein levels of the Vo subunits were marginally reduced, if at all, at an early stage of (P)RR deletion (4 days of transfection/cre expression), and became evident only at a later stage, although (P)RR deletion was apparent immediately [53-55]. This suggests that the downregulation of Vo subunits is a secondary effect of (P)RR deletion rather than a direct consequence of impaired V-ATPase assembly or integrity. Indeed, silencing the (P)RR in collecting duct cells did not affect plasma membrane V-ATPase activity and only altered the protein abundance of certain Vo subunit isoforms [38]. Moreover, lysosome-dependent protein degradation remained intact upon (P)RR silencing, suggesting that at least lysosomal V-ATPase activities were not impaired [69].

The (P)RR has been identified as a crucial player in the Wnt/-catenin signaling pathway [69]. The canonical -catenin signaling pathway contributes to embryonic development, stem cell biology, cell polarity, cell proliferation and neuron patterning, and is crucial for a normal development of the cardiovascular and renal systems [70, 71]. Mechanistic studies suggest that the (P)RR acts as an adaptor between Frizzled (Fz) co-receptor low-density lipoprotein receptor-related protein 6 (LRP6) and V-ATPase, since V-ATPase activity was required for LRP6 activation and its downstream signaling events [69]. Further studies in Drosophila revealed that (P)RR deletion disturbed Fz localization, suggesting that the (P)RR is important for Fz trafficking [72, 73]. Increased Wnt/β-catenin signaling is observed in kidneys of diabetic patients and rodents [74-76], and this may underlie, at least in part, the phenotype of (P)RR-overexpressing rats. However, *in vitro* experiments showed that overexpressing the full-length (P)RR did not activate Wnt/β-catenin signaling, while overexpressing a truncated (P)RR (its

Table 1. Summary of (pro)renin receptor [(P)RR] transgenic and knock out (KO) animal models.

Model	Species	Cardiovascular phenotype	Other phenotypes	Methods & affected tissues	Reference
cKO	Mouse	SBP ↑	Resistance to obesity Adipose tissue mass ↓ Hepatic fat deposition ↑	Adiponectin-cre; Adipocytes	Wu et al. [85]
cKO	Mouse	Unknown	Total fat mass ↑ Total lean mass ↑ Locomotor activity ↑ Basal metabolic rate ↑ Insulin sensitivity ↑ Circulating adiponectin levels ↑ Adipocyte size ↓	AP-cre; Adipocytes	Shamansurova et al. [87]
cKO	Mouse	Prevention of DOCA-induced hypertension	Unknown	Neuron-cre; Neurons	Li et al. [43]
cKO	Mouse	Unknown	Thymus atrophy Peripheral native T cells ↓	Lck-cre; T cells	Geisberger et al. [78]
cKO	Mouse	Unknown	Urine concentration defect Water intake ↑	Pax8-cre ; Nephrons	Ramkumar et al. [103]
cKO	Mouse	Unknown	Impaired nephrogenesis Proteinuria Small cystic kidney Neonatal death	Six2-EGFP/Cre; Nephron progenitors	Song et al. [56]
cKO	Mouse	Lethal heart failure	High mortality	α-MHC-Cre; cardiomyocytes	Kinouchi et al. [53]
cKO	Mouse	Sclerosis in abdominal aorta	None	Myh11-Cre; Smooth muscle cells	Kurauchi-Mito et al. [66]
cKO	Mouse	Unknown	High mortality Nephrotic syndrome Proteinuria	Podocin-Cre; Podocytes	Riediger et al. [54]
cKO	Mouse	Unknown	High mortality Renal failure Proteinuria	Podocin-Cre; Podocytes	Oshima et al. [55]
cKO	Mouse	Unknown	Impaired retinal lamination Impaired retinal function	Crx-Cre; Photoreceptor cells	Kanda et al.[67]
cKO	Mouse	None	Kidney hypoplasia Small cysts in medullary collecting ducts	Hoxb7-Cre; Ureteric bud	Song et al. [68]
Genetic mutation	Zebrafish	Unknown	Defective biliary development	Genetic mutation; Global	Eauclaire et al.[104]
KD	Drosophila	None	Impaired wing development	RNAi; Global	Buechling et al. [73]
KD	Drosophila	None	Impaired planar cell polarity	RNAi Global	Hermle et al. [72]
Constitutive h(P)RR o/e	Mouse	None	None	Knock-in at hprt locus driven by CAG promoter; Global	Rosendahl et al. [39]
Constitutive h(P)RR o/e	Mouse	None	None	Tg driven by α-MHC promoter; Cardiomyocyte	Mahmud et al. [40]
Constitutive h(P)RR o/e	Rat	SBP ↑ HR ↑	Hyperaldosteronism	Tg driven by SMMHC promoter; Smooth muscle cells	Burcklé et al.[105]
Constitutive h(P)RR o/e	Rat	None	Renal COX-2 ↑ Urinary PGE2↑ Proteinuria Glomerulosclerosis	Tg driven by CAG promoter; Global	Kaneshiro et al. [22]

Adipocyte P2 (AP2); CMV early enhancer/chicken β-actin (CAG); cone-rod homeobox (Crx); cyclo-oxygenase (COX); deoxycorticosterone acetate (DOCA); homeeobox protein Hox-b7 (Hoxb7); heart rate (HR); myosin heavy chain (MHC); myosin heavy chain 11 (Myh11); nubbin (Nub); prostaglandin E2 (PGE2); systolic blood pressure (SBP).

CTF) enhanced Wnt signaling [69]. In line with these findings, a recent study reported (P)RR upregulation in kidney biopsy samples from patients with chronic kidney disease (CKD), as well as in the renal tubular epithelium of mice with CKD induced by either ischemia-reperfusion injury (IRI), adriamycin or Ang II [76]. According to this same study, overexpressing the (P)RR in renal cells potentiated Wnt/β-catenin signaling in a V-ATPase-dependent (and renin-independent) manner, resulting in augmented expression of, among others, PAI-1 and fibronectin, i.e., exactly the profibrotic proteins that have been linked to renin-induced (P)RR stimulation. Conversely, knocking down the (P)RR ameliorated kidney injury and fibrosis in the IRI model. Based on these data, a unifying concept might be that the previously observed upregulation of profibrotic pathways by (pro)renin simply is the consequence of artificially stimulating the (P)RR- Wnt/β-catenin-V-ATPase pathway when applying (pro)renin at pharmacological concentrations. Moreover, the close interaction between the (P)RR and Wnt/β-catenin signaling provides an explanation why (P)RR deletion is lethal, even when restricted to specific cell types. Interestingly, s(P)RR lacks the CTF enhanced urine-concentrating capability by activating Wnt/β-catenin signaling [77]. However, the underlying molecular mechanisms of this phenomenon are far from clear. Finally, targeted deletion of the (P)RR in lymphocytes resulted in thymus atrophy and a profound reduction of peripheral native T cells, suggesting impaired thymus development [78]. However, T-cell-specific deletion of β-catenin resulted in a similar, but less profound phenotype [79]. This implies that the (P)RR has functions beyond regulating the Wnt/β-catenin signaling pathway.

We recently used an unbiased proteomics approach to identify the (P)RR-interactome in human embryonic kidney cells, and found sortilin-1 as a novel (P)RR-interacting protein [80]. Sortilin-1, encoded by the SORT1 gene, plays an important role in neuron survival and intracellular protein sorting, and has been identified as a determinant of LDL metabolism [81-84]. Silencing the (P)RR reduced SORT1 and low-density lipoprotein receptor (LDLR) protein levels, albeit without affecting their transcription, and consequently also diminished cellular LDL uptake in hepatocytes. (P)RR silencing-induced LDLR degradation could be reversed by lysosomal inhibitors, such as bafilomycin A1. These findings suggest that the (P)RR has a role in lipid metabolism and atherosclerosis **(Figure 2)**. Wu et al. recently also concluded that the (P)RR contributes to energy metabolism and adipogenesis [85]. Specifically knocking out the (P)RR in adipocytes almost completely abolished white adipose tissue, increased systolic blood pressure, and caused severe lipid accumulation in the liver. Moreover, adipocyte-specific (P)RR knockout mice were resistant to diet-induced obesity and displayed better glycemic control than control mice. Mechanistic studies revealed that (P)RR silencing markedly reduced the adipocyte transcript levels of peroxisome proliferator-activated receptor gamma (PPARγ), a nuclear receptor playing important roles in adipose tissues by

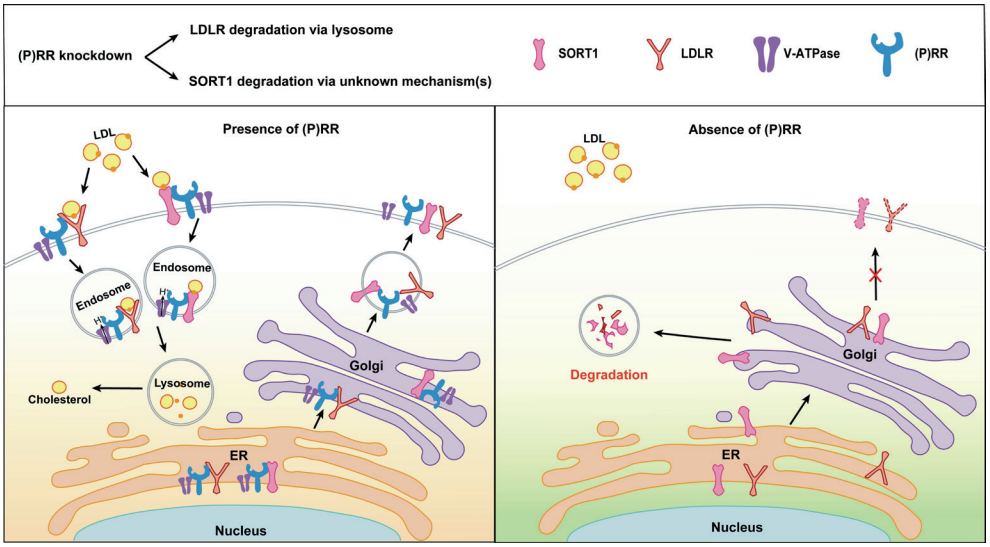

Figure 2. Novel functions of the (P)RR as a regulator of LDL metabolism. Knocking down the (P)RR reduces LDL receptor (LDLR) and SORT1 protein levels, but does not affect their transcript levels, while lysosomotropic agents like bafilomycin A1 prevents this. This suggests that the (P)RR is required for LDLR and SORT1 transportation from the Golgi apparatus to the plasma membrane, while in the absence of the (P)RR, the LDLR is transported to lysosomes for degradation, and SORT1 is degraded via unknown mechanism(s). Inhibiting (P)RR should reduce cellular LDL uptake due to the disappearance of LDLR and SORT1 on the cell surface.

regulating fat storage, lipid metabolism and glucose metabolism [86]. How this reduction in PPARγ mRNA levels occurred is still unknown. Upregulation of PPARγ is important for differentiation of pre-adipocytes to adipocytes, also known as adipogenesis. Shamansurova et al. reported similar results using adipose tissue-specific (P)RR knockout mice generated using AP2-cre rather than the adiponectin-cre applied in the previous report [87]. These knockout mice were also leaner than control mice, and had less total fat mass. Male adipose (P)RR knockout mice displayed increased O_2 consumption and CO_2 production, suggesting an increase in basal metabolic rate. Intriguingly, a high-fat/high-carbohydrate diet upregulated (P)RR expression 2-fold in adipose tissue in mice, likely caused by reduced expression of promyelocytic leukemia zinc finger protein, a transcription factor which suppresses (P)RR transcription [88]. Moreover, in insulin-resistant obese women, adipose (P)RR expression was found to be increased by 33% as compared to insulin-sensitive obese women [88].

Finally, the (P)RR has been observed to interact with the pyruvate dehydrogenase E1 subunit (PDHB) [89]. Indeed, knocking down the (P)RR reduced PDHB protein levels and therefore enzymatic activity of the PDH complex. The PDH complex is an enzyme complex converting pyruvate to acetyl-CoA, a crucial step in glucose catabolism. Consequently, reducing the PDH complex will affect the tricarboxylic acid cycle, resulting in insufficient en-

ergy supply. As a result, energy utilization from other acetyl-CoA sources, like fatty acids, is required to supplement the insufficient acetyl-CoA supply from pyruvate. This could potentially lead to increased fatty acid catabolism and reduced fat deposition. In this regard it is of interest to note that the (P)RR has recently been identified as an interacting protein of the glucagon-like peptide 1 (GLP1) receptor, so that silencing the (P)RR in pancreatic beta cells resulted in reduced GLP1-stimulated insulin secretion [90]. Since this involved impaired Ca^{2+} influx, it appears that the (P)RR is indispensable for GLP1 receptor signaling. Given the GLP1 receptor-dependent regulation of insulin secretion and blood glucose levels, and its potential contribution to blood pressure regulation [91-93], it is highly likely that the (P)RR not only plays a crucial role in lipid homeostasis, but also in energy metabolism.

(P)RR as a pharmacological target for treating cardiovascular diseases

Genome-wide association studies have revealed that single nucleotide polymorphisms in the (P)RR gene are associated with increased cardiovascular risk. The 5+169C>T polymorphism is associated with blood pressure in Japanese [94] and Caucasian men [95]. In Japanese women, the +1513A>G polymorphism is associated with the risk of lacunar infarction and left ventricular hypertrophy [96]. Two additional polymorphisms, one in the promoter region and the other in an intron region of the (P)RR, is associated with hypertension in two cardiovascular diseases cohorts, EUROPA and PROGRESS [97]. However, it is worthy to note that none of the above-mentioned polymorphisms have been validated to affect the expression or function of the (P)RR. The most interesting clinical indication was provided by a unique exonic splice enhance mutation (c.321C>T) which causes deletion of exon 4 of the (P)RR, and a profound reduction (~50%) in full length functional (P)RR protein levels [98]. Carriers of this mutation have X-linked mental retardation and epilepsy, without cardiovascular or renal abnormalities. This mutation was also found in patients with X-linked Parkinsonism with spasticity [99], and again no cardiovascular or renal phenotype was observed in these patients. Taken together, the role of the (P)RR in hypertensive disease is still ambiguous, and more studies to clarify the molecular functions of the (P)RR are urgently needed.

As reviewed above, the (P)RR seems to have a role in regulating lipid metabolism, glucose metabolism and overall energy metabolism. Since hypercholesterolemia, diabetes and obesity are well-known risk factors for cardiovascular disease, targeting these parameters via the (P)RR might indirectly affect cardiovascular disease progression. Indeed, deleting the adipose (P)RR prevented diet-induced obesity and improved glycemic control in mice [85, 87], although it simultaneously caused severe lipid deposition in the liver due to impaired adipogenesis by reduced adipocyte PPARγ levels [85]. Interestingly, a high-fat diet upregulated he-

patic PPARγ and resulted in de novo lipogenesis, also leading to liver steatosis and dyslipidemia [100-102]. Therefore, inhibiting the (P)RR in the liver may reduce high-fat diet induced lipogenesis and dyslipidemia by reducing PPARγ-mediated upregulation of lipogenic genes. However, the precise interaction between the (P)RR and PPARγ needs to be unraveled, to further understand their respective roles in the regulation of lipid metabolism. An important question that remains is whether the impaired adipogenesis caused by (P)RR deletion is not simply due to developmental issues, as observed in many previous conditional knockout models, or to suppressed adipocyte proliferation. To address this question, in the absence of specific (P)RR antagonists, inducible deletion of the (P)RR in adult animals is recommended, or antisense oligonucleotides targeting the (P)RR.

Finally, a major concern when considering the (P)RR as a therapeutic target for the treatment of cardiovascular diseases is the lethality of the (P)RR knockout. Will inhibiting the (P)RR cause (lethal) renal and cardiovascular damage as seen in the cell-specific KO models? The important role of the (P)RR during development has made investigating its molecular functions, involving the (pro)renin-binding NTD and/or the V-ATPase associated CTF, a major challenge. It is for instance possible that the CTF is indispensable for development, while the NTD is not. To address this question, it is recommended to generate transgenic mice with conditional knock-in of the CTF, expressed only after Cre-mediated recombination and deletion of the wild type (P)RR allele.

Conclusions

Fifteen years of research on the (P)RR have shown that its functions are largely, if not completely, unrelated to the RAS, implying that its name is inappropriate. The (pro)renin levels required to stimulate the (P)RR are many orders of magnitude above any (pro)renin level ever measured *in vivo*, even in transgenic animals, and the confusing data obtained with non-specified (P)RR antagonists do not support the occurrence of (pro)renin-(P)RR interaction, not even in (pro)renin synthesizing, (P)RR-expressing tissues. Therefore, the concept of inhibiting (P)RR-mediated RAS activation is currently being abandoned. Instead, (P)RR-oriented research is now focusing on its relationship with V-ATPase. Indeed, the (P)RR appears to act as an adaptor between V-ATPase and multiple receptors/proteins, such as Fz, thereby regulating signaling events, receptor trafficking, and protein degradation by V-ATPase-dependent acidification. This results, among others, in enhanced Wnt/β-catenin signaling and the upregulation of profibrotic genes. It may also contribute to neurogenic hypertension. Thus, inhibiting the (P)RR may potentially exert beneficial cardiovascular effects, e.g., with regard to blood pressure and fibrosis. However, considering the broad

presence of the Wnt/β-catenin signaling pathway, targeting the (P)RR with pharmacological tools (e.g., receptor antagonists) is likely to exert affects on vital processes in multiple, if not all, cells of the body. This will undoubtedly limit the therapeutic application of such a drug in cardiovascular diseases. This leaves the possibility of targeting the (P)RR in specific cells, e.g., with antisense oligonucleotides. Whether such an approach holds promise, e.g. to treat obesity or CKD, needs to be answered in the coming years.

Acknowledgement

This work is supported by National Natural Science Foundation of China (grant no. 81500667), Medical Scientific Research Foundation of Guangdong Province (grant no. A2015051), Shenzhen Municipal Science and Technology Innovation Council (grant no. JCYJ20160307160819191), and Shenzhen University (grant no. 068). We thank dr. Katrina Mirabito for critically reading the manuscript, and making appropriate changes where necessary.

Disclosures/Declaration of Interest

None.

References

1. Krop M, Danser AHJ. Circulating versus tissue renin-angiotensin system: On the origin of (pro)renin. *Curr. Hypertens. Rep.* 2008;10:112-118
2. Danser AHJ, Derkx FH, Schalekamp MA, Hense HW, Riegger GA, Schunkert H. Determinants of interindividual variation of renin and prorenin concentrations: Evidence for a sexual dimorphism of (pro) renin levels in humans. *J. Hypertens.* 1998;16:853-862
3. Luetscher JA, Kraemer FB, Wilson DM, Schwartz HC, Bryer-Ash M. Increased plasma inactive renin in diabetes mellitus. A marker of microvascular complications. *N. Engl. J. Med.* 1985;312:1412-1417
4. Franken AA, Derkx FH, Man in't Veld AJ, Hop WC, van Rens GH, Peperkamp E, de Jong PT, Schalekamp MA. High plasma prorenin in diabetes mellitus and its correlation with some complications. *J. Clin. Endocrinol. Metab.* 1990;71:1008-1015
5. Bader M. The second life of the (pro)renin receptor. *J. Renin Angiotensin Aldosterone Syst.* 2007;8:205-208
6. Ludwig J, Kerscher S, Brandt U, Pfeiffer K, Getlawi F, Apps DK, Schagger H. Identification and characterization of a novel 9.2-kda membrane sector-associated protein of vacuolar proton-atpase from chromaffin granules. *J. Biol. Chem.* 1998;273:10939-10947
7. Nguyen G, Delarue F, Burckle C, Bouzhir L, Giller T, Sraer JD. Pivotal role of the renin/prorenin receptor in angiotensin ii production and cellular responses to renin. *J. Clin. Invest.* 2002;109:1417-1427
8. Batenburg WW, Krop M, Garrelds IM, de Vries R, de Bruin RJ, Burckle CA, Muller DN, Bader M, Nguyen G, Danser AHJ. Prorenin is the endogenous agonist of the (pro)renin receptor. Binding kinetics of renin and prorenin in rat vascular smooth muscle cells overexpressing the human (pro)renin receptor. *J. Hypertens.* 2007;25:2441-2453
9. Batenburg WW, de Bruin RJ, van Gool JM, Muller DN, Bader M, Nguyen G, Danser AHJ. Ali-

skiren-binding increases the half life of renin and prorenin in rat aortic vascular smooth muscle cells. *Arterioscler. Thromb. Vasc. Biol.* 2008;28:1151-1157

10. Nabi AH, Kageshima A, Uddin MN, Nakagawa T, Park EY, Suzuki F. Binding properties of rat prorenin and renin to the recombinant rat renin/prorenin receptor prepared by a baculovirus expression system. *Int. J. Mol. Med.* 2006;18:483-488
11. Sakoda M, Ichihara A, Kaneshiro Y, Takemitsu T, Nakazato Y, Nabi AH, Nakagawa T, Suzuki F, Inagami T, Itoh H. (pro)renin receptor-mediated activation of mitogen-activated protein kinases in human vascular smooth muscle cells. *Hypertens. Res.* 2007;30:1139-1146
12. Huang Y, Noble NA, Zhang J, Xu C, Border WA. Renin-stimulated tgf-beta1 expression is regulated by a mitogen-activated protein kinase in mesangial cells. *Kidney Int.* 2007;72:45-52
13. Feldt S, Maschke U, Dechend R, Luft FC, Muller DN. The putative (pro)renin receptor blocker hrp fails to prevent (pro)renin signaling. *J. Am. Soc. Nephrol.* 2008;19:743-748
14. Feldt S, Batenburg WW, Mazak I, Maschke U, Wellner M, Kvakan H, Dechend R, Fiebeler A, Burckle C, Contrepas A, Danser AHJ, Bader M, Nguyen G, Luft FC, Muller DN. Prorenin and renin-induced extracellular signal-regulated kinase 1/2 activation in monocytes is not blocked by aliskiren or the handle-region peptide. *Hypertension*. 2008;51:682-688
15. Advani A, Kelly DJ, Cox AJ, White KE, Advani SL, Thai K, Connelly KA, Yuen D, Trogadis J, Herzenberg AM, Kuliszewski MA, Leong-Poi H, Gilbert RE. The (pro)renin receptor: Site-specific and functional linkage to the vacuolar h+-atpase in the kidney. *Hypertension*. 2009;54:261-269
16. Contrepas A, Walker J, Koulakoff A, Franek KJ, Qadri F, Giaume C, Corvol P, Schwartz CE, Nguyen G. A role of the (pro)renin receptor in neuronal cell differentiation. *Am. J. Physiol. Regul. Integr. Comp. Physiol.* 2009;297:R250-257
17. Shan Z, Shi P, Cuadra AE, Dong Y, Lamont GJ, Li Q, Seth DM, Navar LG, Katovich MJ, Sumners C, Raizada MK. Involvement of the brain (pro)renin receptor in cardiovascular homeostasis. *Circ. Res.* 2010;107:934-938
18. Uraoka M, Ikeda K, Nakagawa Y, Koide M, Akakabe Y, Nakano-Kurimoto R, Takahashi T, Matoba S, Yamada H, Okigaki M, Matsubara H. Prorenin induces erk activation in endothelial cells to enhance neovascularization independently of the renin-angiotensin system. *Biochem. Biophys. Res. Commun.* 2009;390:1202-1207
19. Achard V, Boullu-Ciocca S, Desbriere R, Nguyen G, Grino M. Renin receptor expression in human adipose tissue. *Am. J. Physiol. Regul. Integr. Comp. Physiol.* 2007;292:R274-282
20. Huang Y, Wongamorntham S, Kasting J, McQuillan D, Owens RT, Yu L, Noble NA, Border W. Renin increases mesangial cell transforming growth factor-beta1 and matrix proteins through receptor-mediated, angiotensin ii-independent mechanisms. *Kidney Int.* 2006;69:105-113
21. Zhang J, Noble NA, Border WA, Owens RT, Huang Y. Receptor-dependent prorenin activation and induction of pai-1 expression in vascular smooth muscle cells. *Am. J. Physiol. Endocrinol. Metab.* 2008;295:E810-819
22. Kaneshiro Y, Ichihara A, Sakoda M, Takemitsu T, Nabi AH, Uddin MN, Nakagawa T, Nishiyama A, Suzuki F, Inagami T, Itoh H. Slowly progressive, angiotensin ii-independent glomerulosclerosis in human (pro)renin receptor-transgenic rats. *J. Am. Soc. Nephrol.* 2007;18:1789-1795
23. Suzuki F, Hayakawa M, Nakagawa T, Nasir UM, Ebihara A, Iwasawa A, Ishida Y, Nakamura Y, Murakami K. Human prorenin has “gate and handle” regions for its non-proteolytic activation. *J. Biol. Chem.* 2003;278:22217-22222
24. Ichihara A, Hayashi M, Kaneshiro Y, Suzuki F, Nakagawa T, Tada Y, Koura Y, Nishiyama A, Okada H, Uddin MN, Nabi AH, Ishida Y, Inagami T, Saruta T. Inhibition of diabetic nephropathy by a decoy peptide corresponding to the “handle” region for nonproteolytic activation of prorenin. *J. Clin. Invest.* 2004;114:1128-1135
25. Ichihara A, Suzuki F, Nakagawa T, Kaneshiro Y, Takemitsu T, Sakoda M, Nabi AH, Nishiyama A, Sugaya T, Hayashi M, Inagami T. Prorenin receptor blockade inhibits development of glomerulosclerosis in diabetic angiotensin ii type 1a receptor-deficient mice. *J. Am. Soc. Nephrol.* 2006;17:1950-1961
26. Ichihara A, Sakoda M, Kurauchi-Mito A, Nishiyama A, Itoh H. Involvement of receptor-bound prorenin in development of nephropathy in diabetic db/db mice. *J. Am. Soc. Hypertens.* 2008;2:332-340
27. Satofuka S, Ichihara A, Nagai N, Yamashiro K, Koto T, Shinoda H, Noda K, Ozawa Y, Inoue M, Tsubota K, Suzuki F, Oike Y, Ishida S. Suppression of ocular inflammation in endotoxin-induced uveitis by inhibiting nonproteolytic activation of prorenin. *Invest. Ophthalmol. Vis. Sci.* 2006;47:2686-2692

28. Satofuka S, Ichihara A, Nagai N, Koto T, Shinoda H, Noda K, Ozawa Y, Inoue M, Tsubota K, Itoh H, Oike Y, Ishida S. Role of nonproteolytically activated prorenin in pathologic, but not physiologic, retinal neovascularization. *Invest. Ophthalmol. Vis. Sci.* 2007;48:422-429
29. Satofuka S, Ichihara A, Nagai N, Noda K, Ozawa Y, Fukamizu A, Tsubota K, Itoh H, Oike Y, Ishida S. (pro)renin receptor-mediated signal transduction and tissue renin-angiotensin system contribute to diabetes-induced retinal inflammation. *Diabetes*. 2009;58:1625-1633
30. Wilkinson-Berka JL, Heine R, Tan G, Cooper ME, Hatzopoulos KM, Fletcher EL, Binger KJ, Campbell DJ, Miller AG. Rillkkmpsv influences the vasculature, neurons and glia, and (pro)renin receptor expression in the retina. *Hypertension*. 2010;55:1454-1460
31. Batenburg WW, Danser AHJ. (pro)renin and its receptors: Pathophysiological implications. *Clin. Sci.* 2012;123:121-133
32. Batenburg WW, van den Heuvel M, van Esch JH, van Veghel R, Garrelds IM, Leijten F, Danser AHJ. The (pro)renin receptor blocker handle region peptide upregulates endothelium-derived contractile factors in aliskiren-treated diabetic transgenic (mren2)27 rats. *J. Hypertens.* 2013;31:292-302
33. te Riet L, van den Heuvel M, Peutz-Kootstra CJ, van Esch JH, van Veghel R, Garrelds IM, Musterd-Bhaggoe U, Bouhuizen AM, Leijten FP, Danser AHJ, Batenburg WW. Deterioration of kidney function by the (pro)renin receptor blocker handle region peptide in aliskiren-treated diabetic transgenic (mren2)27 rats. *Am. J. Physiol. Renal Physiol.* 2014;306:F1179-1189
34. van Esch JH, van Veghel R, Garrelds IM, Leijten F, Bouhuizen AM, Danser AHJ. Handle region peptide counteracts the beneficial effects of the renin inhibitor aliskiren in spontaneously hypertensive rats. *Hypertension*. 2011;57:852-858
35. Muller DN, Klanke B, Feldt S, Cordasic N, Hartner A, Schmieder RE, Luft FC, Hilgers KF. (pro)renin receptor peptide inhibitor "handle-region" peptide does not affect hypertensive nephrosclerosis in goldblatt rats. *Hypertension*. 2008;51:676-681
36. Krebs C, Weber M, Steinmetz O, Meyer-Schwesinger C, Stahl R, Danser AHJ, Garrelds I, van Goor H, Nguyen G, Muller D, Wenzel U. Effect of (pro)renin receptor inhibition by a decoy peptide on renal damage in the clipped kidney of goldblatt rats. *Kidney Int.* 2008;74:823-824
37. Batenburg WW, Lu X, Leijten F, Maschke U, Muller DN, Danser AHJ. Renin- and prorenin-induced effects in rat vascular smooth muscle cells overexpressing the human (pro)renin receptor: Does (pro)renin-(pro)renin receptor interaction actually occur? *Hypertension*. 2011;58:1111-1119
38. Lu X, Garrelds IM, Wagner CA, Danser AHJ, Meima ME. (pro)renin receptor is required for prorenin-dependent and -independent regulation of vacuolar h(+)-atpase activity in mdck.C11 collecting duct cells. *Am. J. Physiol. Renal Physiol.* 2013;305:F417-425
39. Rosendahl A, Niemann G, Lange S, Ahadzadeh E, Krebs C, Contrepas A, van Goor H, Wiech T, Bader M, Schwake M, Peters J, Stahl R, Nguyen G, Wenzel UO. Increased expression of (pro)renin receptor does not cause hypertension or cardiac and renal fibrosis in mice. *Lab. Invest.* 2014;94:863-872
40. Mahmud H, Candido WM, van Genne L, Vreeswijk-Baudoin I, Yu H, van de Sluis B, van Deursen J, van Gilst WH, Sillje HH, de Boer RA. Cardiac function and architecture are maintained in a model of cardiorestricted overexpression of the prorenin-renin receptor. *PLoS One*. 2014;9:e89929
41. Xu Q, Jensen DD, Peng H, Feng Y. The critical role of the central nervous system (pro)renin receptor in regulating systemic blood pressure. *Pharmacol. Ther.* 2016;164:126-134
42. Li W, Peng H, Cao T, Sato R, McDaniels SJ, Kobori H, Navar LG, Feng Y. Brain-targeted (pro)renin receptor knockdown attenuates angiotensin ii-dependent hypertension. *Hypertension*. 2012;59:1188-1194
43. Li W, Peng H, Mehaffey EP, Kimball CD, Grobe JL, van Gool JM, Sullivan MN, Earley S, Danser AHJ, Ichihara A, Feng Y. Neuron-specific (pro)renin receptor knockout prevents the development of salt-sensitive hypertension. *Hypertension*. 2014;63:316-323
44. Li W, Sullivan MN, Zhang S, Worker CJ, Xiong Z, Speth RC, Feng Y. Intracerebroventricular infusion of the (pro)renin receptor antagonist pro20 attenuates deoxycorticosterone acetate-salt-induced hypertension. *Hypertension*. 2015;65:352-361
45. Li W, Liu J, Hammond SL, Tjalkens RB, Saifudeen Z, Feng Y. Angiotensin ii regulates brain (pro)renin receptor expression through activation of camp response element-binding protein. *American Journal of Physiology - Regulatory, Integrative and Comparative Physiology*. 2015;309:R138-R147
46. Pitra S, Feng Y, Stern JE. Mechanisms underlying prorenin actions on hypothalamic neurons implicated in cardiometabolic control. *Mol Metab*. 2016;5:858-868

47. van Thiel BS, Goes Martini A, Te Riet L, Severs D, Uijl E, Garrelds IM, Leijten FP, van der Pluijm I, Essers J, Qadri F, Alenina N, Bader M, Paulis L, Rajkovicova R, Domenig O, Poglitsch M, Danser AHJ. Brain renin-angiotensin system: Does it exist? *Hypertension*. 2017
48. Cousin C, Bracquart D, Contrepas A, Corvol P, Muller L, Nguyen G. Soluble form of the (pro)renin receptor generated by intracellular cleavage by furin is secreted in plasma. *Hypertension*. 2009;53:1077-1082
49. Yoshikawa A, Aizaki Y, Kusano K, Kishi F, Susumu T, Iida S, Ishiura S, Nishimura S, Shichiri M, Senbonmatsu T. The (pro)renin receptor is cleaved by adam19 in the golgi leading to its secretion into extracellular space. *Hypertens. Res.* 2011;34:599-605
50. Danser AHJ. The role of the (pro)renin receptor in hypertensive disease. *Am. J. Hypertens.* 2015;28:1187-1196
51. Daryadel A, Bourgeois S, Figueiredo MF, Gomes Moreira A, Kampik NB, Oberli L, Mohebbi N, Lu X, Meima ME, Danser AHJ, Wagner CA. Colocalization of the (pro)renin receptor/atp6ap2 with h+-atpases in mouse kidney but prorenin does not acutely regulate intercalated cell h+-atpase activity. *PLoS One*. 2016;11:e0147831
52. Trepiccione F, Gerber SD, Grahammer F, Lopez-Cayuqueo KI, Baudrie V, Paunescu TG, Capen DE, Picard N, Alexander RT, Huber TB, Chambrey R, Brown D, Houillier P, Eladari D, Simons M. Renal atp6ap2/(pro)renin receptor is required for normal vacuolar h+-atpase function but not for the renin-angiotensin system. *J. Am. Soc. Nephrol.* 2016;27:3320-3330
53. Kinouchi K, Ichihara A, Sano M, Sun-Wada GH, Wada Y, Kurauchi-Mito A, Bokuda K, Narita T, Oshima Y, Sakoda M, Tamai Y, Sato H, Fukuda K, Itoh H. The (pro)renin receptor/atp6ap2 is essential for vacuolar h+-atpase assembly in murine cardiomyocytes. *Circ. Res.* 2010;107:30-34
54. Riediger F, Quack I, Qadri F, Hartleben B, Park JK, Potthoff SA, Sohn D, Sihn G, Rousselle A, Fokuhl V, Maschke U, Purfurst B, Schneider W, Rump LC, Luft FC, Dechend R, Bader M, Huber TB, Nguyen G, Muller DN. Prorenin receptor is essential for podocyte autophagy and survival. *J. Am. Soc. Nephrol.* 2011;22:2193-2202
55. Oshima Y, Kinouchi K, Ichihara A, Sakoda M, Kurauchi-Mito A, Bokuda K, Narita T, Kurosawa H, Sun-Wada GH, Wada Y, Yamada T, Takemoto M, Saleem MA, Quaggin SE, Itoh H. Prorenin receptor is essential for normal podocyte structure and function. *J. Am. Soc. Nephrol.* 2011;22:2203-2212
56. Song R, Preston G, Kidd L, Bushnell D, Sims-Lucas S, Bates CM, Yosypiv IV. Prorenin receptor is critical for nephron progenitors. *Dev. Biol.* 2016;409:382-391
57. Wagner CA, Finberg KE, Breton S, Marshansky V, Brown D, Geibel JP. Renal vacuolar h+-atpase. *Physiol. Rev.* 2004;84:1263-1314
58. Nishi T, Forgac M. The vacuolar (h+)-atpases--nature's most versatile proton pumps. *Nat. Rev. Mol. Cell Biol.* 2002;3:94-103
59. Li YP, Chen W, Liang Y, Li E, Stashenko P. Atp6i-deficient mice exhibit severe osteopetrosis due to loss of osteoclast-mediated extracellular acidification. *Nat. Genet.* 1999;23:447-451
60. Rojas JD, Sennoune SR, Martinez GM, Bakunts K, Meininger CJ, Wu G, Wesson DE, Seftor EA, Hendrix MJ, Martinez-Zaguilan R. Plasmalemmal vacuolar h+-atpase is decreased in microvascular endothelial cells from a diabetic model. *J. Cell. Physiol.* 2004;201:190-200
61. Frattini A, Orchard PJ, Sobacchi C, Giliani S, Abinun M, Mattsson JP, Keeling DJ, Andersson AK, Wallbrandt P, Zecca L, Notarangelo LD, Vezzoni P, Villa A. Defects in tcirg1 subunit of the vacuolar proton pump are responsible for a subset of human autosomal recessive osteopetrosis. *Nat. Genet.* 2000;25:343-346
62. Inoue H, Noumi T, Nagata M, Murakami H, Kanazawa H. Targeted disruption of the gene encoding the proteolipid subunit of mouse vacuolar h(+)-atpase leads to early embryonic lethality. *Biochim. Biophys. Acta*. 1999;1413:130-138
63. Karet FE, Finberg KE, Nelson RD, Nayir A, Mocan H, Sanjad SA, Rodriguez-Soriano J, Santos F, Cremers CW, Di Pietro A, Hoffbrand BI, Winiarski J, Bakkaloglu A, Ozen S, Dusunsel R, Goodyer P, Hulton SA, Wu DK, Skvorak AB, Morton CC, Cunningham MJ, Jha V, Lifton RP. Mutations in the gene encoding b1 subunit of h+-atpase cause renal tubular acidosis with sensorineural deafness. *Nat. Genet.* 1999;21:84-90
64. Cotter K, Capecci J, Sennoune S, Huss M, Maier M, Martinez-Zaguilan R, Forgac M. Activity of plasma membrane v-atpases is critical for the invasion of mda-mb231 breast cancer cells. *J. Biol. Chem.* 2015;290:3680-3692

65. Sihn G, Rousselle A, Vilianovitch L, Burckle C, Bader M. Physiology of the (pro)renin receptor: Wnt of change? *Kidney Int.* 2010;78:246-256
66. Kurauchi-Mito A, Ichihara A, Bokuda K, Sakoda M, Kinouchi K, Yaguchi T, Yamada T, Sun-Wada GH, Wada Y, Itoh H. Significant roles of the (pro)renin receptor in integrity of vascular smooth muscle cells. *Hypertens. Res.* 2014;37:830-835
67. Kanda A, Noda K, Yuki K, Ozawa Y, Furukawa T, Ichihara A, Ishida S. Atp6ap2/(pro)renin receptor interacts with par3 as a cell polarity determinant required for laminar formation during retinal development in mice. *J. Neurosci.* 2013;33:19341-19351
68. Song R, Preston G, Ichihara A, Yosypiv IV. Deletion of the prorenin receptor from the ureteric bud causes renal hypodysplasia. *PLoS One*. 2013;8:e63835
69. Cruciat CM, Ohkawara B, Acebron SP, Karaulanov E, Reinhard C, Ingelfinger D, Boutros M, Niehrs C. Requirement of prorenin receptor and vacuolar h+-atpase-mediated acidification for wnt signaling. *Science*. 2010;327:459-463
70. MacDonald BT, Tamai K, He X. Wnt/beta-catenin signaling: Components, mechanisms, and diseases. *Dev. Cell*. 2009;17:9-26
71. Arnold AC, Robertson D. Defective wnt signaling: A potential contributor to cardiometabolic disease? *Diabetes*. 2015;64:3342-3344
72. Hermle T, Saltukoglu D, Grunewald J, Walz G, Simons M. Regulation of frizzled-dependent planar polarity signaling by a v-atpase subunit. *Curr. Biol.* 2010;20:1269-1276
73. Buechling T, Bartscherer K, Ohkawara B, Chaudhary V, Spirohn K, Niehrs C, Boutros M. Wnt/frizzled signaling requires dprr, the drosophila homolog of the prorenin receptor. *Curr. Biol.* 2010;20:1263-1268
74. Pulkkinen K, Murugan S, Vainio S. Wnt signaling in kidney development and disease. *Organogenesis*. 2008;4:55-59
75. Zhou D, Tan RJ, Fu H, Liu Y. Wnt/beta-catenin signaling in kidney injury and repair: A double-edged sword. *Lab. Invest.* 2016;96:156-167
76. Li Z, Zhou L, Wang Y, Miao J, Hong X, Hou FF, Liu Y. (pro)renin receptor is an amplifier of wnt/beta-catenin signaling in kidney injury and fibrosis. *J. Am. Soc. Nephrol.* 2017
77. Lu X, Wang F, Xu C, Soodvilai S, Peng K, Su J, Zhao L, Yang KT, Feng Y, Zhou SF, Gustafsson JA, Yang T. Soluble (pro)renin receptor via beta-catenin enhances urine concentration capability as a target of liver x receptor. *Proc. Natl. Acad. Sci. U. S. A.* 2016;113:E1898-1906
78. Geisberger S, Maschke U, Gebhardt M, Kleinewietfeld M, Manzel A, Linker RA, Chidgey A, Dechend R, Nguyen G, Daumke O, Muller DN, Wright MD, Binger KJ. New role for the (pro)renin receptor in t-cell development. *Blood*. 2015;126:504-507
79. Xu Y, Banerjee D, Huelsken J, Birchmeier W, Sen JM. Deletion of beta-catenin impairs t cell development. *Nat. Immunol.* 2003;4:1177-1182
80. Lu X, Meima ME, Nelson JK, Sorrentino V, Loregger A, Scheij S, Dekkers DH, Mulder MT, Demmers JA, G MD-T, Zelcer N, Danser AHJ. Identification of the (pro)renin receptor as a novel regulator of low-density lipoprotein metabolism. *Circ. Res.* 2016;118:222-229
81. Musunuru K, Strong A, Frank-Kamenetsky M, Lee NE, Ahfeldt T, Sachs KV, Li X, Li H, Kuperwasser N, Ruda VM, Pirruccello JP, Muchmore B, Prokunina-Olsson L, Hall JL, Schadt EE, Morales CR, Lund-Katz S, Phillips MC, Wong J, Cantley W, Racie T, Ejebe KG, Orho-Melander M, Melander O, Kotelianskiy V, Fitzgerald K, Krauss RM, Cowan CA, Kathiresan S, Rader DJ. From noncoding variant to phenotype via sort1 at the 1p13 cholesterol locus. *Nature*. 2010;466:714-719
82. Kjolby M, Andersen OM, Breiderhoff T, Fjorback AW, Pedersen KM, Madsen P, Jansen P, Heeren J, Willnow TE, Nykjaer A. Sort1, encoded by the cardiovascular risk locus 1p13.3, is a regulator of hepatic lipoprotein export. *Cell Metab.* 2010;12:213-223
83. Strong A, Ding Q, Edmondson AC, Millar JS, Sachs KV, Li X, Kumaravel A, Wang MY, Ai D, Guo L, Alexander ET, Nguyen D, Lund-Katz S, Phillips MC, Morales CR, Tall AR, Kathiresan S, Fisher EA, Musunuru K, Rader DJ. Hepatic sortilin regulates both apolipoprotein b secretion and ldl catabolism. *J. Clin. Invest.* 2012;122:2807-2816
84. Linsel-Nitschke P, Heeren J, Aherrahrou Z, Bruse P, Gieger C, Illig T, Prokisch H, Heim K, Doering A, Peters A, Meitinger T, Wichmann HE, Hinney A, Reinehr T, Roth C, Ortlepp JR, Soufi M, Sattler AM, Schaefer J, Stark K, Hengstenberg C, Schaefer A, Schreiber S, Kronenberg F, Samani NJ, Schunkert H, Erdmann J. Genetic variation at chromosome 1p13.3 affects sortilin mrna expression, cellular ldl-uptake and serum ldl levels which translates to the risk of coronary artery disease. *Atherosclerosis*.

2010;208:183-189
85. Wu CH, Mohammadmoradi S, Thompson J, Su W, Gong M, Nguyen G, Yiannikouris F. Adipocyte (pro) renin-receptor deficiency induces lipodystrophy, liver steatosis and increases blood pressure in male mice. *Hypertension*. 2016;68:213-219
86. Ahmadian M, Suh JM, Hah N, Liddle C, Atkins AR, Downes M, Evans RM. Ppargamma signaling and metabolism: The good, the bad and the future. *Nat. Med.* 2013;19:557-566
87. Shamansurova Z, Tan P, Ahmed B, Pepin E, Seda O, Lavoie JL. Adipose tissue (p)rr regulates insulin sensitivity, fat mass and body weight. *Mol Metab*. 2016;5:959-969
88. Tan P, Shamansurova Z, Bisotto S, Michel C, Gauthier MS, Rabasa-Lhoret R, Nguyen TM, Schiller PW, Gutkowska J, Lavoie JL. Impact of the prorenin/renin receptor on the development of obesity and associated cardiometabolic risk factors. *Obesity (Silver Spring, Md.)*. 2014;22:2201-2209
89. Kanda A, Noda K, Ishida S. Atp6ap2/(pro)renin receptor contributes to glucose metabolism via stabilizing the pyruvate dehydrogenase e1 beta subunit. *J. Biol. Chem.* 2015;290:9690-9700
90. Dai FF, Bhattacharjee A, Liu Y, Batchuluun B, Zhang M, Wang XS, Huang X, Luu L, Zhu D, Gaisano H, Wheeler MB. A novel glp1 receptor interacting protein atp6ap2 regulates insulin secretion in pancreatic beta cells. *J. Biol. Chem.* 2015;290:25045-25061
91. Yu M, Moreno C, Hoagland KM, Dahly A, Ditter K, Mistry M, Roman RJ. Antihypertensive effect of glucagon-like peptide 1 in dahl salt-sensitive rats. *J. Hypertens.* 2003;21:1125-1135
92. von Scholten BJ, Lajer M, Goetze JP, Persson F, Rossing P. Time course and mechanisms of the anti-hypertensive and renal effects of liraglutide treatment. *Diabet. Med.* 2015;32:343-352
93. Hirata K, Kume S, Araki S, Sakaguchi M, Chin-Kanasaki M, Isshiki K, Sugimoto T, Nishiyama A, Koya D, Haneda M, Kashiwagi A, Uzu T. Exendin-4 has an anti-hypertensive effect in salt-sensitive mice model. *Biochem. Biophys. Res. Commun.* 2009;380:44-49
94. Hirose T, Hashimoto M, Totsune K, Metoki H, Asayama K, Kikuya M, Sugimoto K, Katsuya T, Ohkubo T, Hashimoto J, Rakugi H, Takahashi K, Imai Y. Association of (pro)renin receptor gene polymorphism with blood pressure in japanese men: The ohasama study. *Am. J. Hypertens.* 2009;22:294-299
95. Ott C, Schneider MP, Delles C, Schlaich MP, Hilgers KF, Schmieder RE. Association of (pro)renin receptor gene polymorphism with blood pressure in caucasian men. *Pharmacogenet. Genomics*. 2011;21:347-349
96. Hirose T, Hashimoto M, Totsune K, Metoki H, Hara A, Satoh M, Kikuya M, Ohkubo T, Asayama K, Kondo T, Kamide K, Katsuya T, Ogihara T, Izumi S, Rakugi H, Takahashi K, Imai Y. Association of (pro) renin receptor gene polymorphisms with lacunar infarction and left ventricular hypertrophy in japanese women: The ohasama study. *Hypertens. Res.* 2011;34:530-535
97. Brugts JJ, Isaacs A, de Maat MP, Boersma E, van Duijn CM, Akkerhuis KM, Uitterlinden AG, Witteman JC, Cambien F, Ceconi C, Remme W, Bertrand M, Ninomiya T, Harrap S, Chalmers J, Macmahon S, Fox K, Ferrari R, Simoons ML, Danser AHJ. A pharmacogenetic analysis of determinants of hypertension and blood pressure response to angiotensin-converting enzyme inhibitor therapy in patients with vascular disease and healthy individuals. *J. Hypertens.* 2011;29:509-519
98. Ramser J, Abidi FE, Burckle CA, Lenski C, Toriello H, Wen G, Lubs HA, Engert S, Stevenson RE, Meindl A, Schwartz CE, Nguyen G. A unique exonic splice enhancer mutation in a family with x-linked mental retardation and epilepsy points to a novel role of the renin receptor. *Hum. Mol. Genet.* 2005;14:1019-1027
99. Korvatska O, Strand NS, Berndt JD, Strovas T, Chen DH, Leverenz JB, Kiianitsa K, Mata IF, Karakoc E, Greenup JL, Bonkowski E, Chuang J, Moon RT, Eichler EE, Nickerson DA, Zabetian CP, Kraemer BC, Bird TD, Raskind WH. Altered splicing of atp6ap2 causes x-linked parkinsonism with spasticity (xpds). *Hum. Mol. Genet.* 2013;22:3259-3268
100. Inoue M, Ohtake T, Motomura W, Takahashi N, Hosoki Y, Miyoshi S, Suzuki Y, Saito H, Kohgo Y, Okumura T. Increased expression of ppargamma in high fat diet-induced liver steatosis in mice. *Biochem. Biophys. Res. Commun.* 2005;336:215-222
101. Gavrilova O, Haluzik M, Matsusue K, Cutson JJ, Johnson L, Dietz KR, Nicol CJ, Vinson C, Gonzalez FJ, Reitman ML. Liver peroxisome proliferator-activated receptor gamma contributes to hepatic steatosis, triglyceride clearance, and regulation of body fat mass. *J. Biol. Chem.* 2003;278:34268-34276
102. Zhang YL, Hernandez-Ono A, Siri P, Weisberg S, Conlon D, Graham MJ, Crooke RM, Huang LS, Ginsberg HN. Aberrant hepatic expression of ppargamma2 stimulates hepatic lipogenesis in a mouse model of obesity, insulin resistance, dyslipidemia, and hepatic steatosis. *J. Biol. Chem.* 2006;281:37603-37615

Aim of the thesis

Cardiovascular disease (CVD) is the leading cause of death world-wide. Increased blood pressure (BP), or hypertension, is a major risk factor for CVD. Hypertension, if not well treated, will cause heart and kidney damage in the longer term. Controlling BP is therefore a major goal in patients with CVD. The renin-angiotensin system (RAS) is one of the most important systems regulating blood pressure. Renin, secreted by juxtaglomerular cells in the kidney, cleaves angiotensinogen (AGT) to generate angiotensin I, which is further cleaved by angiotensin-converting enzyme (ACE) to form angiotensin II (Ang II), the effector peptide of the RAS. Prorenin, the inactive precursor of renin, can be activated both proteolytically (via prosegment cleavage) and non-proteolytically (by allowing the prosegment to move out of the enzymatic cleft, e.g. in an acid environment). About two decades ago, a receptor that binds prorenin (and to a lesser degree renin) was identified. It has been named (pro)renin receptor [(P)RR]. Binding of renin and prorenin to the (P)RR induces the activation of intracellular signaling cascades, resulting in extracellular signal-regulated kinase1/2 (Erk1/2) and p38 mitogen-activated protein kinase (MAPK) upregulation. Prorenin binding to the (P)RR has also been suggested to result in its non-proteolytic activation. Yet, apart from its role in the RAS, the (P)RR has also been identified as an accessory protein of the vacuolar H^+-ATPase (V-ATPase). V-ATPase is a multiple subunit complex, expressed in virtually all cell types, which plays an important role in the acidification of intracellular compartments, such as lysosomes, and signaling endosomes. A recent study surprisingly found that silencing the (P)RR reduces low-density-lipoprotein receptor (LDLR) protein levels via a lysosome-dependent pathway, suggesting a role of the (P)RR in lipoprotein metabolism. In **Chapter 2**, we investigated the role of (P)RR in lipid metabolism *in vivo*. We found that inhibiting the hepatic (P)RR prevents high-fat diet-induced obesity and non-alcoholic fatty liver disease and lowers plasma cholesterol and triglyceride in $LDLR^{-/-}$ mice. Mechanistically, we found that inhibition of (P)RR resulted in reduced lipid synthesis and increased fatty acid oxidation by reducing acetyl-CoA carboxylase and pyruvate dehydrogenase abundance.

RAS inhibitors, such as direct renin inhibitors (DRI), ACE inhibitors and angiotensin receptor blockers (ARBs), are the most commonly used medicines in the clinic for controlling BP. However, RAS inhibition results in a significant rise in renin due to a negative feedback loop, thus compromising the management of BP. Hence, there is a compelling need for novel therapies that circumvent this problem to better control BP. In **Chapter 3**, we tested the effect of inhibiting hepatic AGT, the initiator of RAS, on BP and hypertension-induced heart - and kidney injury in spontaneously hypertensive rats. The AGT-targeting siRNA is

stable *in vivo* and potently suppresses AGT expression in the liver over a long period. We found that abolishing AGT expression effectively lowered BP. Furthermore, we found that applying this siRNA in combination with the ARB valsartan resulted in a far greater reduction in BP and prevention of cardiac hypertrophy.

Human plasma prorenin levels are usually 10-fold higher than renin levels. Plasma prorenin and renin are filtered through the glomerulus and either reabsorbed in the proximal tubule or excreted in urine. Urinary renin levels normally amount to 6-7% of plasma renin levels, while prorenin is undetectable in urine. Moreover, in Cyp1a1-Ren2 rats whose plasma prorenin levels are increased 200-fold as compared with non-transgenic rats, urinary prorenin is still undetectable. Considering that prorenin and renin have similar molecular weights, the average glomerular sieving coefficients for filtering prorenin and renin through the glomerulus are also similar, excluding the possibility that different filtration rates account for the discrepancies in their urinary levels. This suggests that an as yet unidentified recycling receptor for prorenin may exist in the proximal tubule. Interestingly, urinary (pro)renin levels are drastically elevated in patients with Lowe syndrome and Dent's disease. Importantly, these patients carry mutations in the genes encoding for OCRL1 and CLC-5, which are known to impair megalin function. Megalin is a multi-ligand receptor that can bind and internalize nutrients or hormones in the proximal tubule. In **Chapter 4** and **5**, we summarize the current knowledge about megalin and hypothesize that megalin could be the missing receptor that explains the discrepancies in urinary prorenin and renin levels. In **Chapter 6**, we subsequently studied whether megalin binds and internalizes (pro)renin, making use of Brown Norway Rat yolk sac epithelial cells (BN16 cells) which highly express megalin. We found that BN16 cells show higher binding and internalization for prorenin than for renin, while uptake disappeared after silencing megalin. Moreover, we found that silencing the (P)RR reduced prorenin/renin internalization but not binding. Our work therefore identified megalin as a novel receptor for prorenin and renin, and shows that megalin-mediated internalization of (pro)renin requires the (P)RR.

Preeclampsia is a disease that involves the development of hypertension and proteinuria after 20 weeks of gestation in previously normotensive women. It is one of the leading causes of maternal mortality during pregnancy. The placenta is believed to play a key role in the development of preeclampsia, as preeclampsia may even occur in the absence of fetal tissue, in the form of gestational trophoblastic disease (hydatidiform mole). Many studies have suggested that a local placental RAS exists, in addition to the circulating RAS, based on the demonstration of RAS component gene expression in the placenta. Interestingly, circulating renin and AGT are suppressed in preeclampsia, while data of (pro)renin levels in the pre-

eclamptic uteroplacental unit are conflicting, with evidence for decreases, increases and no alteration. To better understand the role, if any, of the local placental RAS in preeclampsia, we compared the gene expression and protein levels of RAS components in healthy pregnant subjects and preeclamptic patients **(Chapter 7)**. We found that (pro)renin levels are comparable in preeclamptic and healthy placentas, with no alterations in their mRNA expression. (P)RR expression was increased, and the same tended to be true for megalin. AGT protein could be easily detected in healthy placentas, despite its barely detectable mRNA levels. Placental AGT levels were reduced in preeclamptic placental tissue. To further understand the origin of placental (pro)renin and AGT, we also explored the release of AGT and (pro)renin from perfused placentas. AGT release gradually declined during perfusion time, while (pro)renin release remained stable. These findings suggest that placental AGT originates from maternal blood, while (pro)renin is locally synthesized. Interestingly, the proton pump inhibitor esomeprazole blocked megalin/(pro)renin receptor-mediated renin uptake. To what degree this implies that such drugs may interfere with placental RAS activity remains to be demonstrated.

Chapter 8 puts all data into perspective and provides directions for further research.

CHAPTER 2

(Pro)renin Receptor Inhibition Reprograms Hepatic Lipid Metabolism and Protects Mice from Diet-Induced Obesity and Hepatosteatosis

Liwei Ren[#], Yuan Sun[#], Hong Lu, Dien Ye, Lijuan Han, Na Wang, Alan Daugherty, Furong Li, Miaomiao Wang, Fengting Su, Wenjun Tao, Jie Sun, Noam Zelcer, Adam E. Mullick, A.H. Jan Danser, Yizhou Jiang, Yongcheng He, Xiongzhong Ruan*, Xifeng Lu*

Circ Res 122: 730-741, 2018

[#]= equal contribution [*]= corresponding author

Abstract

Rationale: An elevated level of plasma low-density lipoprotein (LDL) is an established risk factor for cardiovascular disease. Recently, we reported that the (pro)renin receptor ([P]RR) regulates LDL metabolism *in vitro* via the LDL receptor (LDLR) and SORT1, independently of the renin-angiotensin system.

Objectives: To investigate the physiological role of (P)RR in lipid metabolism *in vivo*.

Methods and Results: We used N-Acetylgalactosamine (GalNAc) modified antisense oligonucleotides (ASO) to specifically inhibit hepatic (P)RR expression in C57BL/6J mice, and studied the consequences this has on lipid metabolism. In line with our earlier report, hepatic (P)RR silencing increased plasma LDL cholesterol. Unexpectedly, this also resulted in markedly reduced plasma triglycerides in a SORT1-independent manner in C57BL/6J mice fed a normal or high fat diet. In LDLR-deficient mice, hepatic (P)RR inhibition reduced both plasma cholesterol and triglycerides, in a diet-independent manner. Mechanistically, we found that (P)RR inhibition decreased protein abundance of acetyl-CoA carboxylase (ACC) and pyruvate dehydrogenase (PDH). This alteration reprograms hepatic metabolism, leading to reduced lipid synthesis and increased fatty acid oxidation. As a result, hepatic (P)RR inhibition attenuated diet-induced obesity and hepatosteatosis.

Conclusions: Collectively, our study suggests that (P)RR plays a key role in energy homeostasis and regulation of plasma lipids by integrating hepatic glucose and lipid metabolism.

Key Words

(P)RR/ATP6AP2, SORT1, V-ATPase, dyslipidemia, fatty liver disease

Abbreviations

ACC	acetyl-CoA carboxylase
ApoB	apolipoprotein B
ASO	antisense oligonucleotides
LDL	low-density lipoprotein
LDLR	low-density lipoprotein receptor
LPL	lipoprotein lipase
mTOR	mechanistic target of rapamycin

PCSK9	proprotein convertase subtilisin/kexin type 9
PDH	pyruvate dehydrogenase
(P)RR	(pro)renin receptor
RAS	renin-angiotensin system
SORT1	sortilin 1
V-ATPase	vacuolar H^+-ATPase
VLDL	very low-density lipoprotein

Introduction

Elevated plasma low-density lipoprotein (LDL) levels are a major risk factor for developing atherosclerosis and ensuing ischemic cardiovascular disease (CVD), a leading cause of world-wide death. LDL, which is derived by peripheral lipolysis of very low-density lipoprotein (VLDL), is primarily cleared from the circulation in the liver via the LDL receptor (LDLR) pathway.[1, 2] Hence, plasma LDL levels are determined by the dynamic balance between hepatic VLDL secretion and LDL clearance.

VLDL particles are formed by lipidation of ApoB100, the core protein of VLDL, in the ER and Golgi apparatus.[3] The assembly of VLDL particles depends on ApoB100 production and cellular availability of triglycerides. Accordingly, genetic mutations in ApoB100 are associated with altered VLDL secretion and plasma LDL levels.[4-6] Overexpression of ApoB100 results in increased VLDL secretion and plasma LDL levels in rabbits.[7] Similarly, the activity of enzymes involved in de novo lipid biosynthesis also affect VLDL assembly and secretion.[8, 9] For example, impaired loading of triglycerides into nascent VLDL particles, caused by mutations in the microsomal triglyceride carrier protein (MTP), result in defective VLDL secretion.[10]

Disturbed LDL clearance can increase plasma LDL levels and risk for cardiovascular diseases. In line with this, loss-of-function LDLR mutations are associated with elevated plasma LDL levels and cardiovascular risk.[11-13] Recently, GWAS studies have identified single-nucleotide polymorphisms (SNPs) mapping to 1p13.3 that strongly associated with plasma LDL levels and coronary heart disease.[14-19] Subsequent mechanistic studies revealed that sortilin-1 (SORT1), located within the 1p13.3 region, is a novel regulator of LDL metabolism.[20-22] Overexpression of SORT1 increases LDL clearance and decreases plasma LDL levels,[16, 21, 22] while SORT1 deficiency reduces cellular LDL uptake *in vitro* and LDL clearance *in vivo*.[22, 23] Additionally, SORT1 also plays a role in VLDL secretion. Overexpressing SORT1 promotes ApoB degradation via an endolysosome-dependent route, and

hence reduces VLDL secretion and plasma triglyceride levels.[22] Controversially, mice deficient for SORT1 also display reduced VLDL secretion and triglyceride levels.[20, 22] These opposing results highlight the complex, and not yet fully elucidated, role of SORT1 in lipoprotein metabolism.

The (pro)renin receptor ([P]RR) interacts with renin/prorenin (denoted as [pro]renin) at supra-physiological concentrations that are even several orders of magnitude higher than (patho)physiological concentrations, questioning the physiological relevance of the (P)RR-(pro)renin interaction.[24, 25] Recently, the (P)RR was reported to play a role in Wnt/β-catenin signaling pathway, vacuolar H^+-ATPase (V-ATPase) integrity and T-cell development, independently of (pro)renin.[26-30] Moreover, we have recently identified the (P)RR as a SORT1-interacting protein,[31] and demonstrated that silencing *(P)RR* expression in hepatocytes *in vitro* reduces protein abundance of SORT1 and LDLR post-transcriptionally, and consequently cellular LDL uptake. To understand the role of the (P)RR in lipoprotein metabolism *in vivo*, we studied here the consequence of hepatic (P)RR silencing on lipoprotein metabolism. We report that hepatic loss of (P)RR in mice results in a SORT1-dependent increase in plasma LDL levels, but unexpectedly also in a reduction in plasma triglycerides that was SORT1-independent that resulted from altered metabolic reprogramming of hepatocytes. Our study thus highlights hepatic (P)RR as a crucial regulator of energy and lipid metabolism.

Methods:

A detailed description of methods used in this study is available in the Online Supplemental Materials.

Results

Inhibiting hepatic (P)RR reduced both hepatic LDL clearance and VLDL secretion

We have previously reported that (P)RR inhibition attenuates cellular LDL uptake by reducing LDLR and SORT1 protein abundance in hepatocytes.[31] To understand the role of hepatic (P)RR in lipoprotein metabolism *in vivo*, we used N-Acetylgalactosamine (GalNAc) modified antisense oligos (ASOs) to inhibit hepatic *(P)RR* expression. At a dose of 3.0 mg/kg/week, GalNAc (P)RR ASO [G-(P)RR] potently reduced *(P)RR* expression in liver, but had no effects on its expression in other major organs, including heart, kidney, intestine, spleen, and different adipose tissues (***Online Figure I A , C-F***). In line with our previous report, inhibiting the (P)RR specifically reduced hepatic LDLR and SORT1 protein levels without af-

fecting their transcript levels (***Online Figure I B***). As a result of reduced hepatic LDLR and SORT1 protein abundance, (P)RR inhibition elevated plasma cholesterol levels in normal diet (ND) fed mice, primarily by increasing cholesterol content in IDL/LDL fractions (***Figure 1 A&B***). Since plasma LDL-c concentrations reflect the balance between hepatic LDL clearance and VLDL secretion, we then investigated the effects of (P)RR inhibition on LDL clearance and hepatic VLDL output. In line with decreased LDLR and SORT1, inhibiting hepatic (P)RR led to attenuated clearance of injected Dil-labeled human LDL (***Figure 1C***). Unexpectedly, (P)RR inhibition also significantly decreased plasma triglyceride concentrations (***Figure 1D***), a finding could be attributed to reduced hepatic VLDL secretion (***Figure 1E***).

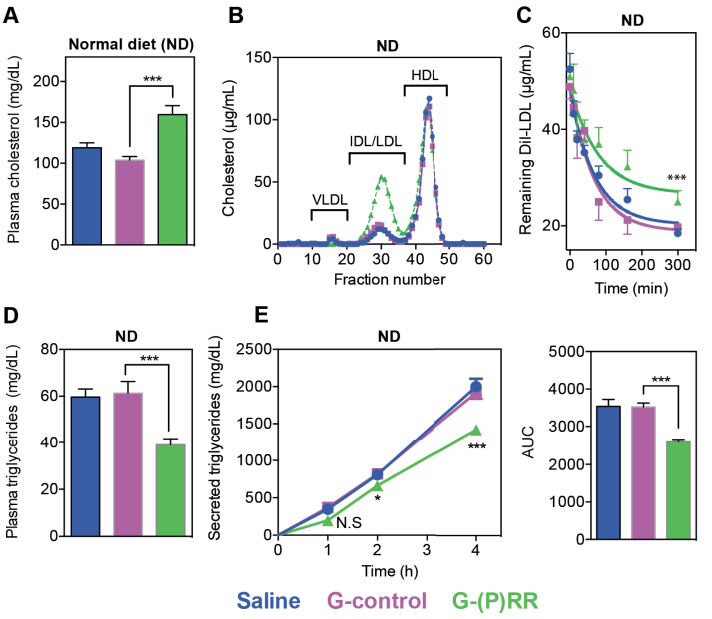

Figure 1. Inhibiting hepatic (P)RR induces hypercholesterolemia by reducing hepatic LDL clearance in normal diet (ND)-fed C57BL/6J mice. Eight-weeks-old male C57BL/6J mice were inject with either saline (blue), G-control (magenta) or G-(P)RR (green) intraperitoneally. Mice were sacrificed after 7 days and blood samples were collected for (A) determining circulating levels of cholesterol (N=12-18 per group). Each bar and error represent the mean ± SEM; ***: p<0.001, or (B) pooled plasma samples were loaded on FPLC for lipoprotein fractionation analysis, and cholesterol content in each fraction was determined. (C) 7 days after injection, mice (n=6 per group) were injected with 50 µg Dil-labeled human LDL. Blood samples were drawn retro-orbitally at the indicated time points and the Dil-LDL was determined. Each point represents the mean ± SEM and the area-under curve (AUC) was constructed for each group and used to compare the difference in LDL clearance. ***: p<0.001. (D) Blood was collected as in (A) and used to determine plasma triglyceride levels. (N=12-18 per group); Each bar and error represent the mean ± SEM ***: p<0.001. (E) 7 days after injection, mice (n=6 per group) were fasted for 6 hours, and injected with Pluronic F127 to inhibit lipoprotein lipase. Blood samples were drawn retro-orbitally at the indicated time points and the concentration of triglycerides was determined. The mean VLDL secretion for saline-, G-control-, or G-(P)RR-injected mice is 474 ± 16 mg/dL*h, 460 ± 14 mg/dL*h, and 342 ± 10 mg/dL*h, respectively. The AUC was calculated for individual mice and used to compare the differences in the rate of VLDL secretion. ***: p<0.001; G-control vs. G-(P)RR.

We then asked if silencing *(P)RR* in hepatocytes could aggravate hypercholesterolemia in C57BL/6J mice fed a high-fat diet (HFD). Like in ND-fed mice, 1 week after (P)RR inhibition, plasma cholesterol levels were 3~4 fold higher than those measured in GalNAc control ASO (G-control) injected mice (***Figure 2A***). This elevation was primarily attributed to a marked increase in cholesterol content in the IDL/LDL fraction (***Figure 2B***). Notably, (P)RR inhibition also increased cholesterol contents in the VLDL fraction and reduced cholesterol contents in the HDL fraction. Unexpectedly, within two weeks, plasma cholesterol levels of G-(P)RR injected mice normalized and were similar to those in the saline or G-control injected mice (***Figure 2 A&C, Online Figure I G***). This contrasts with the sustained increase in plasma cholesterol levels in C57BL/6J mice fed with ND (***Online Figure I H***). Nevertheless, (P)RR inhibition in HFD-fed mice reduced hepatic LDL clearance and VLDL secretion (***Figure 2 D&E***). Plasma triglycerides and VLDL triglycerides were both lower in G-(P)RR injected mice as compared to saline or G-control injected mice (***Figure 2 F&G***), thus mimicking the pattern seen under ND feeding. Importantly, plasma lipoprotein lipase (LPL) activity was not affected by hepatic (P)RR inhibition (***Figure 2H***). This excludes the possibility that increased triglyceride hydrolysis underpins reduced levels of plasma triglycerides in (P)RR-silenced mice.

Since SORT1 deficiency *in vivo* reduces VLDL secretions and plasma triglycerides and (P)RR-silencing decreases SORT1,[20, 22, 31] we wondered if the effect of (P)RR inhibition on hepatic lipid output is SORT1-dependent. To address this possibility, we studied plasma lipid levels in (P)RR-silenced mice in which we overexpressed human SORT1 (hSORT1). Exogenous hSORT1 protein was detected in liver, and hSORT1 partially rescued the (P)RR-inhibition-induced LDLR protein reduction (***Online Figure II***). Given that SORT1 itself is a clearance receptor for LDL,[20-22] it is not surprising that hSORT1 overexpression reversed the (P)RR-inhibition-induced increase in plasma cholesterol levels, primarily by decreasing the cholesterol content in the VLDL and IDL/LDL fractions (***Figure 3 A&B***). However, hSORT1 overexpression did not prevent the reduction in plasma triglycerides caused by (P)RR inhibition (***Figure 3C***), implying that (P)RR inhibition reduced plasma triglycerides in a SORT1-independent manner.

Hepatic (P)RR inhibition reduced plasma cholesterol levels in LDLR deficient mice

As (P)RR affects both hepatic LDL clearance and VLDL secretion, it is possible that (P)RR has a differential role in governing plasma cholesterol levels under distinct diet conditions. Under ND, LDL clearance may govern plasma cholesterol levels, while under HFD VLDL secretion may become more prominent in determining plasma cholesterol levels. To address this issue, we tested the effects of hepatic (P)RR inhibition on plasma cholesterol levels in

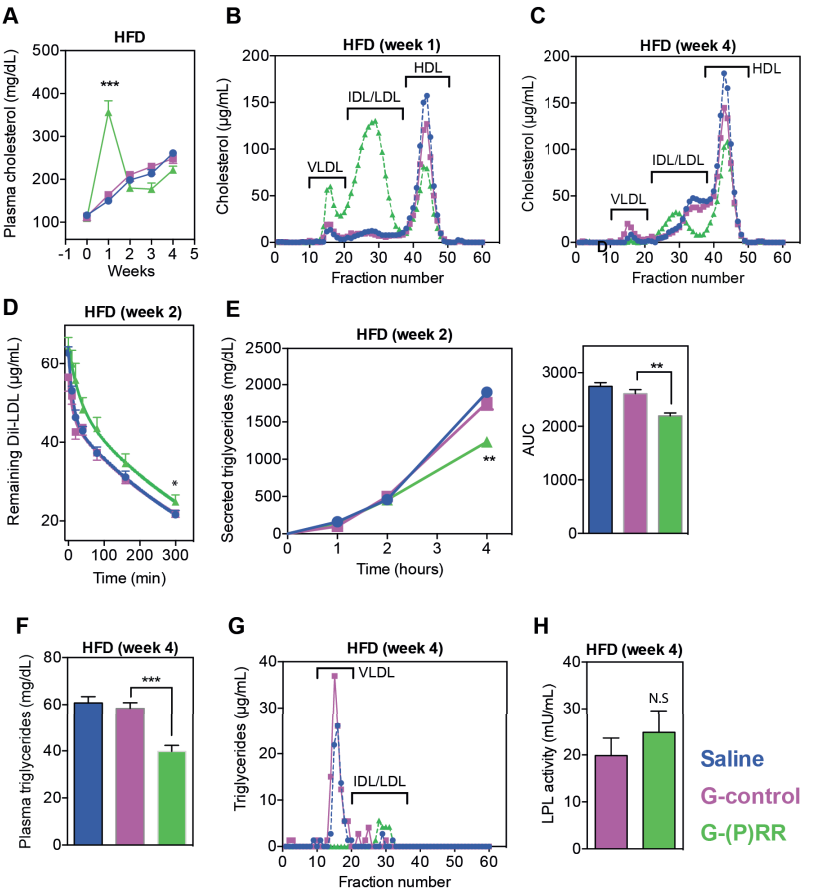

Figure 2. Inhibiting hepatic (P)RR does not result in hypercholesterolemia in HFD-fed C57BL/6J mice. Eight-weeks-old male C57BL/6J mice were injected with either saline (blue), G-control (magenta) or G-(P)RR (green), and fed a HFD for 4 weeks. **(A)** Plasma cholesterol concentrations were determined weekly and each point represents the mean ± SEM. N=10 per group; ***: p<0.001; G-control vs. G-(P)RR. (B,C) Pooled plasma samples were collected after the **(B)** 1st week of diet, or **(C)** following 4 weeks of diet and the lipoprotein distribution was determined. The cholesterol content in each fraction was determined and is plotted. **(D)** Two weeks after start of HFD diet, mice (n=6 per group) were injected with 50 µg DiI-labeled human LDL, and LDL clearance was assessed. Each point represent the mean ± SEM and the AUC was constructed for each treatment and used to compare the differences in LDL clearance. *: p<0.05. **(E)** Two weeks after (P)RR inhibition, mice were fasted for 6 hours and VLDL secretion was assessed (n=6 per group) by injecting mice with Pluronic F127 to inhibit lipoprotein lipase. Blood samples were drawn retro-orbitally at the indicated time points and the concentration of triglycerides was determined and the AUC was calculated and used to compare the differences in the rate of VLDL secretion. **: p<0.01; G-control vs. G-(P)RR. **(F,G)** Plasma triglyceride levels were analyzed in samples collected following 4 weeks of HFD. Each bar represents the mean ± SEM, N=10 per group. ***: p<0.001, or **(G)** pooled plasma samples were analyzed by FPLC. (H) Plasma lipoprotein lipase (LPL) activity was determined for mice were injected with G-control or G-(P)RR and fed HFD for 4 weeks. N=9/ group.

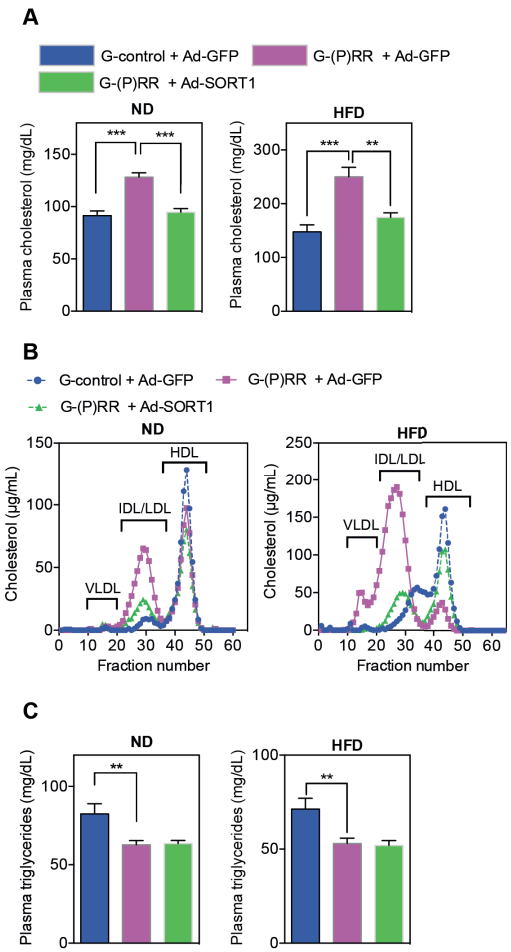

Figure 3. SORT1 overexpression prevents PRR-dependent hypercholesterolemia, but does not affect reduction in plasma triglycerides. Eight-week-old male C57BL/6J mice were injected with G-control or G-(P)RR intraperitoneally, and subsequently injected with either adenovirus carrying GFP (Ad-GFP) or adenovirus carrying human SORT1 (Ad-SORT1) via the tail-vein. Mice were fed with ND or HFD for 1 week and **(A)** plasma cholesterol levels were determined. Each bar represents the mean ± SEM (N=6 per group). **: p<0.01; ***: p<0.001. Alternatively, **(B)** Lipoprotein composition in pooled plasma samples was analyzed by fractionation. **(C)** Plasma was collected as in **(A)** and analyzed for triglyceride content. Each bar and error represent the mean ± SEM (N=6 per group). **: p<0.01.

mice with impaired LDL clearance by injecting adeno-associated virus (AAVs) expressing the gain-of-function PCSK9 D377Y mutant [32, 33] and in LDLR$^{-/-}$ mice. As expected, injecting C57BL/6J mice with the PCSK9 D377Y-encoding AAVs led to a marked increase in the circulating levels of LDL cholesterol (from 77 ± 2 mg/dL to 167 ± 2 mg/dL, n=39). We subsequently injected these mice with either saline, G-control, or G-(P)RR for 4 weeks, and fed either ND or HFD. We found that after this treatment period, (P)RR inhibition reduced

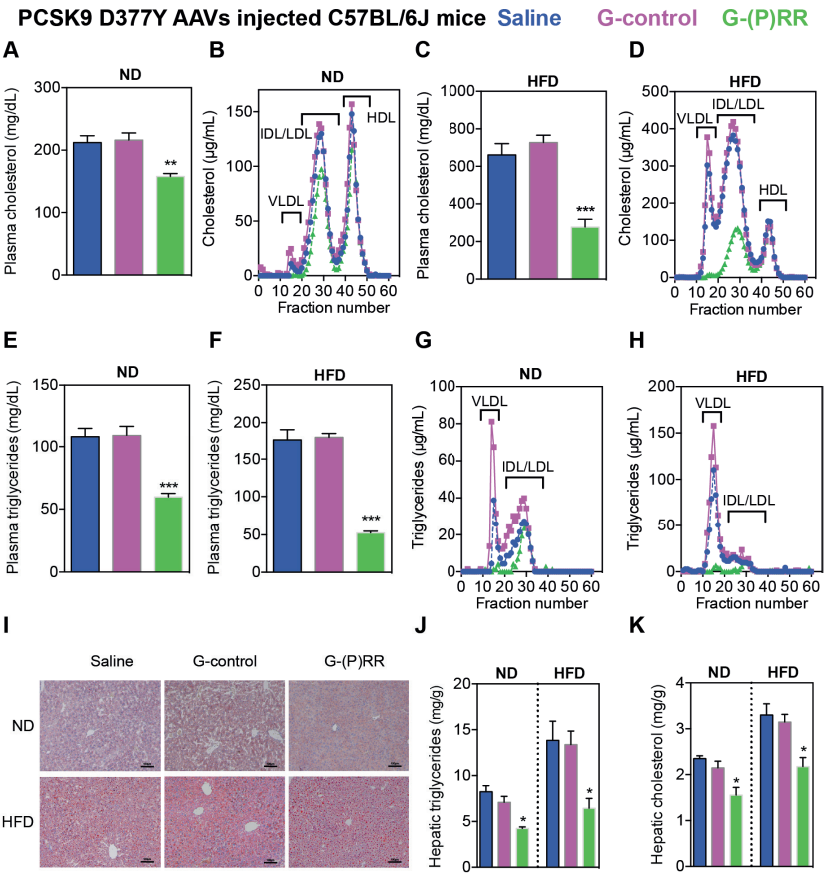

Figure 4. Hepatic (P)RR inhibition in the absence of LDLR reduces plasma lipid levels and hepatic lipid deposition. Eight-week-old male C57BL/6J mice were injected intraperitoneally with 10×10^{10} genomic copies of mouse PCSK9D377Y AAV, and fed with ND for 4 weeks. Subsequently, mice were injected with either saline (blue), G-control (magenta) or G-(P)RR (green) and fed with ND or HFD for an additional 4 weeks. **(A-D)** Plasma cholesterol levels and lipoprotein profiles at the end of study were determined for ND fed **(A,B)** and HFD fed **(C,D)** mice. **(E-H)** Plasma triglycerides and lipoprotein distribution were determined for ND fed **(E,G)** and HFD fed **(F,H)** mice. (N=6 per group). **: p<0.01; ***: p<0.001; G-control vs. G-(P)RR. **(I)** Representative images of Oil Red O stained liver samples from above-indicated mice fed with ND or HFD for 4 weeks. scale bar = 100 μm. **(J,K)** Lipids were extracted from liver samples and analyzed for triglycerides and cholesterol levels. *: p<0.05; G-control v.s G-(P)RR.

plasma cholesterol levels in both ND and HFD fed mice, despite the lack of functional LDLR-mediated clearance (***Figure 4 A-D***). Similarly, inhibiting hepatic (P)RR in $LDLR^{-/-}$ mice induced a sustained decrease in plasma cholesterol levels independent of diet (***Online Figure III A&B***). These results confirm that LDL clearance is more dominant than VLDL secretion in determining circulating LDL levels in mice fed ND. Similar to the observation in wildtype C57BL/6J mice, plasma triglycerides and VLDL-associated triglycerides were

reduced by (P)RR inhibition under ND or HFD feeding (***Figure 4 E-H***), in PCSK9-induced LDLR deficient mice. Moreover, in $LDLR^{-/-}$ mice, hypertriglyceridemia was prevented by hepatic (P)RR inhibition (***Online Figure III C&D***). We reasoned that if (P)RR inhibition primarily affects lipid export pathways, we should observe lipid accumulation in liver, especially under HFD feeding. However, we found that hepatic lipid levels were also reduced by (P)RR inhibition (***Figure 4 I-K, Online Figure IV)***, implying that the reduced plasma lipid levels are not the result of impaired lipid secretion.

Hepatic (P)RR inhibition attenuated diet-induced obesity and improved metabolic disorders

(P)RR inhibition resulted in decreased hepatic VLDL secretion without concomitant hepatic lipid accumulation. This could point towards (P)RR regulating hepatic lipid biosynthesis, an important facet of fatty liver disease and obesity.[34] We therefore questioned whether hepatic (P)RR inhibition can ameliorate diet-induced fatty liver disease and obesity. To address this, we inhibited hepatic *(P)RR* expression in C57BL/6J mice fed a HFD for 14 weeks. In line with our hypothesis, loss of hepatic (P)RR attenuated diet-induced obesity in C57BL/6J mice (***Figure 5A***). Body composition analyses using EchoMRI revealed that inhibiting hepatic (P)RR lowered fat weight of the mice, but did not affect the weight of lean mass (***Figure 5B, Online Figure V A***). Furthermore, the size of the livers and white adipose tissues (WATs) of G-(P)RR injected mice were smaller than control mice (***Figure 5 C&D***). Under HFD, lipid accumulates in liver and increases liver weight. Mean liver weight of saline or G-control injected mice was ~2 gram, which was nearly twice the mean liver weight (1.07 ± 0.02 gram, $n=12$, $p<0.001$) of ND fed C57BL/6J mice at same age (22 weeks old). Hepatic (P)RR inhibition attenuated HFD-induced liver weight gain and prevented abnormal lipid deposition in the liver (***Figure 5 E&F***). Liver/body weight ratios of G-(P)RR injected mice were also significantly lower than that of G-control injected mice, and resembled the ratio of ND fed C57BL/6J mice at the same age (***Online Figure V B***). Moreover, mice in which hepatic (P)RR was inhibited had smaller adipocytes in inguinal WATs (***Online Figure V C***), but normal brown adipose tissues weight (***Figure 5D***). In agreement with reduced adipose tissues, plasma leptin concentrations were also reduced by hepatic (P)RR inhibition (***Online Figure V D***). However, plasma adiponectin concentrations were unaltered by (P)RR inhibition despite the marked reduction in adipose tissue weight (***Online Figure V E***), likely due to increased expression of adiponectin in white adipose tissues (***Online Figure I C&E***). This suggests that hepatic (P)RR inhibition can indirectly affect adipokines secretion by adipose tissues, thereby contributing to improved metabolic control.

Accompanied by less body weight gain, fasting blood glucose concentrations were reduced

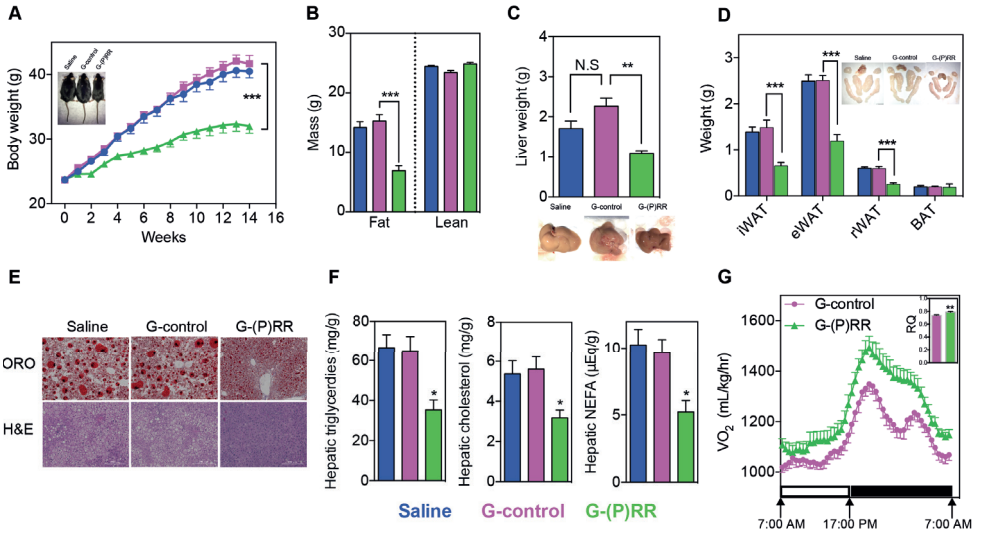

Figure 5. Hepatic (P)RR inhibition attenuates diet-induced obesity and metabolic deregulation. Eight-week-old mice were injected with saline (blue), G-control (magenta) or G-(P)RR (green) and fed a HFD for 14 weeks. (N=10 per group). (A) Body weight was monitored during the study period and each point and error represent the mean ± SEM. ***: p<0.001. Representative picture showing that G-(P)RR injected mice are leaner than control mice. **(B)** Fat and lean mass were measured by EchoMRI. Each bar and error represent the mean ± SEM. ***: p<0.001. **(C)** Liver weight, and representative pictures showing G-(P)RR treated mice have less fatty liver. **: p<0.01. **(D)** Weight and representative picture of different adipose tissue depots. Brown fat tissue of saline and G-control injected mice were surrounded with white fat which was removed to give a correct estimation of the weight of the brown fat. ***: p<0.001. **(E)** Representative images of Oil Red O and H&E staining of the livers (scale bar = 200 μm). **(F)** Hepatic lipids were extracted and measured. *: p<0.05; G-control vs. G-(P)RR. **(G)** Oxygen consumption and 24h average respiratory quotient (RQ) of G-control injected and G-(P)RR injected mice was monitored with a metabolic monitoring system 4 days prior to sacrifice. N=8 per group.

by (P)RR inhibition (***Online Figure V F***), which also improved glucose tolerance and lowered plasma insulin levels (***Online Figure V G&H***). Plasma AST, ALT and AST/ALT ratio indicates (P)RR inhibition did not cause liver damage (***Online Figure V I***). In addition, H&E staining also revealed improved liver morphology by (P)RR inhibition (***Figure 5E***). Cumulative food intake of the mice during the 14 weeks experimental period was also recorded. G-(P)RR injected mice consumed slightly less food than saline or G-control injected mice, but when corrected for their body weight, their food consumption was actually higher (***Online Figure V J***), suggesting that the reduced body weight gain is not due to reduced food intake. In addition, we did not observe any difference in blood pressure or heart rate between saline, G-control or G-(P)RR injected mice (***Online Figure V K&L***), suggesting that the activity of the autonomic nervous system was not affected. We then monitored oxygen consumption and physical activity of the mice using metabolic cages. Inhibiting hepatic (P)RR increased oxygen consumption and 24h respiratory quotient (RQ) of the mice, implying increased catabolism of energy sources (***Figure 5G***). Yet, physical activities of the

mice were not different (***Online Figure V M***). Collectively, these results support the beneficial metabolic effects of (P)RR inhibition.

Inhibiting the (P)RR up-regulated genes involved in fatty acid oxidation

Currently recognized functions of the (P)RR are not linked with lipid biosynthesis and energy homeostasis. To understand how (P)RR may regulate these processes, we transcriptionally profiled mice following (P)RR inhibition. Male mice (8-weeks old) were injected either with saline or G-(P)RR for 5 days, and liver samples were collected and extracted for total RNA and RNAseq analysis. We identified that (P)RR inhibition led to up- and down-regulation of 199 genes and 202 genes, respectively (***Online Table III***). GO enrichment analysis revealed that metabolic pathways, including fatty acid (FA) degradation and elongation, were strongly affected by (P)RR inhibition (***Online Figure VI A&B***). Among the affected genes, several genes involved in FA β-oxidation, such as *Hadha*, *Acaa2*, *Acadvl*, and *Acadl*, were up-regulated by (P)RR inhibition, as confirmed by qPCR (***Online Figure VII***). As such, increased FA β-oxidation may contribute to increased oxygen consumption and reduced hepatic lipid content.

Inhibiting (P)RR reduced protein abundance of ACC and PDH

To complement the RNAseq analysis and to better understand the function(s) of the (P)RR, we next performed comparative quantitative proteomics to identify hepatic proteins which are affected by (P)RR inhibition. Through this unbiased approach, we identified 191 and 116 proteins that were down- and up-regulated, respectively, following (P)RR inhibition during feeding of either ND and HFD (***Online Table IV***). As reported previously, LDLR protein abundance was decreased by (P)RR inhibition (***Online Table IV***), validating the effectiveness of this approach to identify proteins with altered abundance. GO enrichment analyses revealed that proteins involved in lipid biosynthesis, lipid metabolism, and cholesterol metabolism were markedly affected by (P)RR inhibition (***Online Figure VI C&D).*** Among the identified proteins, pyruvate dehydrogenase (PDH), acetyl-CoA carboxylase α (ACCα), and acetyl-CoA carboxylase β (ACCβ) were markedly decreased. PDH is the enzyme responsible for converting pyruvate to acetyl-CoA, and is a central metabolic node.[35] ACC catalyzes the formation of malonyl-CoA, an essential substrate for FA synthesis and a potent inhibitor of FA oxidation.[36] ACC is crucial in determining lipid storage and overall energy metabolism.[37] Thus, reduced PDH and ACC may contribute to increased FA oxidation and decreased lipid synthesis. To confirm this, we examined ACCα/β and PDH protein abundance in the liver of saline, G-control or G-(P)RR injected C57BL/6J mice fed with HFD for 14 weeks. Corroborating the proteomic-based approach, hepatic ACCα/β, PDHA, and PDHB were reduced by ~40-60% after hepatic (P)RR inhibition (***Figure 6A***), whereas

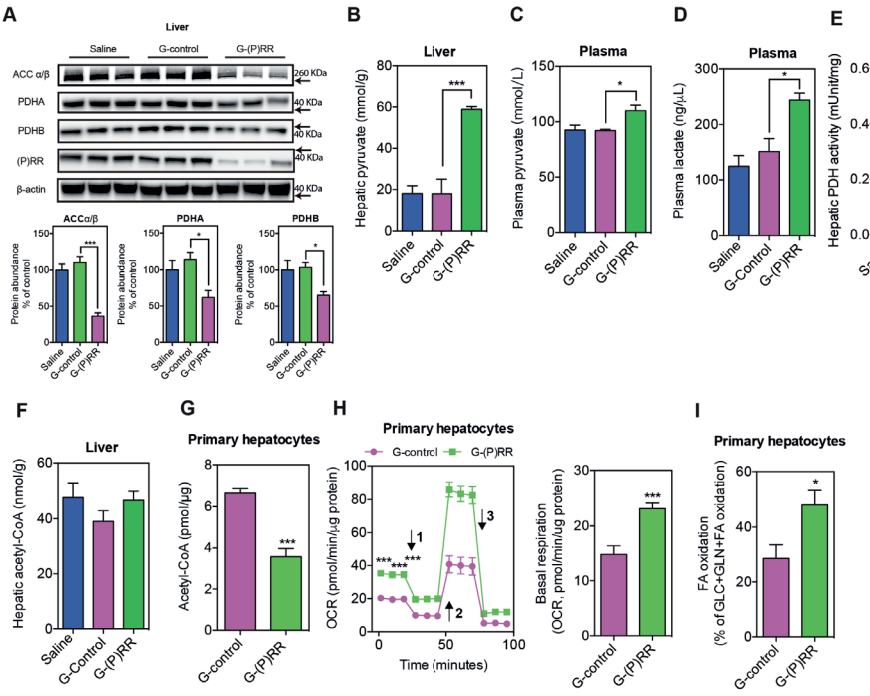

Figure 6. Inhibiting the (P)RR reduces PDH and ACC protein abundance and activity. (A) Representative blot of liver samples from mice injected with saline, G-control, or G-(P)RR, and fed a HFD for 14 weeks. The protein abundance of PDHA, PDHB, and ACCα/β was quantified and normalized to the level of β-actin in the same lysate. (N=6 per group); *: p<0.05; ***: p<0.001. **(B)** C57BL/6J mice were treated with ASOs and fed with HFD for 14 weeks. Hepatic pyruvate concentrations (B), plasma pyruvate concentrations **(C)**, plasma lactate concentrations **(D)**, hepatic PDH activity **(E)**, and acetyl-CoA concentrations **(F)** were determined. **(G)** Mouse primary hepatocytes were treated with G-control or G-(P)RR for 36 hours, and cellular Acetyl-CoA concentrations were determined. Three independent experiments in triplicates were performed. ***: p<0.001. Oxygen consumption rate (OCR) **(H)** and fuel dependency **(I)** were measured in mouse primary hepatocytes treated with G-control or G-(P)RR for 36 hours. Arrow 1-3 indicates addition of oligomycin, FCCP and the mixture of rotenone and antimycin, respectively. N=6 per group. *: p<0.05; ***: p<0.001.

the transcript abundance of *ACCα/β*, *PDHA*, and *PDHB* remained unaltered (***Online Figure VII***). Inhibiting the (P)RR in human hepatoma HepG2 cells with siRNAs also reduced protein abundances of ACCα/β, PDHA, and PDHB (***Online Figure VIII A***), suggesting that this outcome is conserved in both mouse and humans. The (P)RR knockdown induced reduction in ACCα/β protein abundance was partially reversed by the lysosome inhibitor bafilomycin A1 (BafA1), but was not affected by the autophagy inhibitor 3-methyladenine (3-MA) or the proteasome inhibitor MG-132 (***Online Figure VIII B***), suggesting accelerated lysosome-dependent degradation of ACCα/β by (P)RR inhibition. In contrast, BafA1, 3-MA and MG-132 were unable to rescue (P)RR knockdown induced reduction in PDHA and PDHB, implying that a different mechanism underlies the control of these proteins by (P)RR.

(P)RR inhibition reduced cellular acetyl-CoA abundance and FA synthesis in hepatocytes
Collectively, our results suggest that by reducing protein abundance of PDH, (P)RR inhibition reduces pyruvate to acetyl-CoA conversion, and therefore reduces cellular acetyl-CoA production from glucose. Lower cellular acetyl-CoA levels will limit cellular FA and cholesterol synthesis. This biosynthetic block will be compounded by reduced ACC abundance, which will further limit FA synthesis and reduce plasma triglyceride levels. To test this hypothesis, we first measured relevant hepatic metabolites in mice injected with saline, G-control, or G-(P)RR and fed with HFD for 14 weeks. As expected, G-(P)RR injected mice displayed hepatic pyruvate accumulation (***Figure 6B***), increased plasma pyruvate and lactate concentrations (***Figure 6 C&D***), and decreased hepatic PDH activity (***Figure 6E***). Nevertheless, despite these changes, hepatic acetyl-CoA concentrations were unaltered by (P)RR inhibition (***Figure 6F***). Yet importantly, cellular acetyl-CoA levels in isolated mouse primary hepatocytes in which (P)RR was inhibited using G-(P)RR ASO, were reduced (***Figure 6G***). Similarly, acetyl-CoA levels were decreased by (P)RR inhibition in HepG2 cells, combined with a decrease in cellular PDH activity, increased cellular pyruvate concentrations and medium lactate concentrations, and reduced cellular lipid levels (***Online Figure VIII C-G***). These data support our hypothesis, and simultaneously suggest that *in vivo*, alternative sources, especially fatty acids supply, are available to overcome reduced pyruvate to acetyl-CoA conversion. This may also explain why acetyl-CoA levels were not reduced in the liver, as they were in HepG2 cells and primary hepatocytes. It is plausible that increased FA oxidation provides additional acetyl-CoA to compensate the increased energetic demand, which could also explain the increased oxygen consumption observed in G-(P)RR injected mice. Therefore, we examined if (P)RR inhibition affects the oxygen consumption rate (OCR) in mouse primary hepatocytes and HepG2 cells. As expected, inhibiting the (P)RR significantly increased basal OCR by ~50% in mouse primary hepatocytes (***Figure 6H***) and ~30% in HepG2 cells (***Online Figure VIII H***) and, implying increased energy expenditure and utilization of high-oxygen-consuming fuels such as FA. To fully understand the mechanism, we further examined cellular fuel dependency on long chain FA (LCFA) in mouse primary hepatocytes and HepG2 cells. In the presence of 50 μmmol/L oleic acid, LCFA accounted for ~20-30% oxidized fuels (glucose, glutamine and LCFA together) in control cells, while it accounted for more than 40% oxidized fuels in primary mouse hepatocytes and HepG2 cells with (P)RR inhibited (***Figure 6I, Online Figure VIII I***). These data suggest that reduced acetyl-CoA supply from pyruvate is compensated by increased FA oxidation, as a mechanism to sustain cellular energy needs.

Discussion

We recently reported that the (P)RR is a novel modulator of LDL metabolism *in vitro*.[31] In the current study, we demonstrate that also *in vivo,* inhibiting the (P)RR in hepatocytes leads to defective LDL clearance as a result of reduced SORT1 and LDLR protein abundance. SORT1 is a recently identified hepatic clearance receptor for LDL, which also regulates VLDL secretion and plasma triglycerides.[16, 20-22, 38] SORT1 deficiency reduces VLDL secretion and plasma triglycerides,[20] and in line with this, we found that (P)RR inhibition reduced VLDL secretion and plasma triglycerides, likely as a consequence of reduced SORT1. However, hepatic overexpression of hSORT1 in mice with (P)RR silencing was unable to prevent the reduction in plasma triglycerides, despite completely preventing the increase in plasma LDL-c. This implies that the (P)RR regulates plasma triglycerides via a SORT1-independent manner. Furthermore, plasma LPL activity was not affected by (P)RR inhibition, excluding the possibility that increased triglyceride hydrolysis accounts for the reduced plasma triglycerides. In fact, hepatic lipid concentrations, including triglycerides and cholesterol, were both markedly reduced by (P)RR inhibition, indicating that lipid synthesis is diminished. Indeed, we found that the protein abundance of ACC, the crucial enzyme catalyzing the first step in fatty acid synthesis, was markedly reduced by (P)RR inhibition. As a consequence, limited amounts of lipid being available for ApoB lipidation likely caused the reduction in plasma triglycerides. This may also explain why (P)RR inhibition even reduced plasma cholesterol levels in LDLR deficient mice, in whom SORT1-depedendent LDL clearance is impaired.

Our results raise the question of how the (P)RR regulates cellular lipid levels. Intriguingly, vacuolar H^+-ATPase (V-ATPase) has recently been identified as a component of the mechanistic target of rapamycin complex 1 (mTORC1) pathway.[39] Indeed, acidification of lysosomes by V-ATPase is crucial for mTOR activation and function.[40] Increased mTORC1 activity is observed in genetic, and HFD-induced obesity, and has been implicated in the regulation of lipogenesis and VLDL secretion.[41-43] Knocking down the (P)RR reduces the protein levels of several subunits of the V-ATPase complex.[28-30, 44] Consequently, (P)RR inhibition may prevent mTORC1 activation. Nevertheless, this seems unlikely as a recent report found that mTORC1 signaling was unaffected by (P)RR.[45]

An alternative explanation for the effect of (P)RR on hepatic lipid metabolism may be related to the renin-angiotensin system, which has been linked with obesity and lipid metabolism.[46] However, this too seems unlikely, as the affinity of (P)RR to (pro)renin is very low, and in fact their interaction requires supraphysiological concentrations of (pro)renin.

Rather, by using a combined unbiased transcriptome and proteomic approach, we now identified PDH and ACC as downstream effectors of (P)RR inhibition. (P)RR inhibition has previously been reported to reduce PDHB protein levels via a tyrosine-phosphorylation dependent manner in mouse retina and human retinal pigment epithelium cells.[47] We found that both PDHA and PDHB were reduced by (P)RR inhibition. PDH is a ubiquitously expressed enzyme complex that catalyzes the conversion of pyruvate to acetyl-CoA,[48, 49] acting as a central node that links lipid metabolism, glucose metabolism and the tricarboxylic acid (TCA) cycle. We thus speculated that by reducing PDH protein abundance and activity, (P)RR inhibition would reduce acetyl-CoA production from glucose, and consequently diminish FA synthesis and increase FA oxidation (***Figure 7***).[50] Indeed, this is what we observe in the livers of (P)RR-silenced mice. Additionally, (P)RR inhibition also reduced ACC protein abundance. ACC plays an essential role in regulating FA synthesis and degradation.[37] Genetic deletion, or inhibition, of ACC reduces body-weight gain and fat mass, suppresses triglycerides synthesis, and increases FA oxidation and energy expenditure,[51, 52] which resembles the phenotype of hepatic (P)RR inhibition. Moreover, *PPARγ* expression was reduced by (P)RR inhibition by ~50% (***Online Figure VII***), and this may also have contributed to the reduced hepatic lipogenesis, as hepatic PPARγ plays important roles in HFD-induced upregulation of lipogenic genes and *de novo* lipogenesis.[53-55] Recent studies have reported that genetically deleting adipose (P)RR in mice resulted in resistance to diet-induced obesity[56] and accelerated oxygen consumption,[57] yet causing severe hepatosteatosis.[56] Unaltered (P)RR expression in both white adipose tissues and brown adipose tissues excluded the possibility that adipose (P)RR deficiency also contributed to the observed phenotype in our study. However, it raises the question whether inhibiting the (P)RR in both adipose tissue and liver would provide additional beneficial effects in treating metabolic disorders.

Post-transcriptional regulation of ACC and PDH is not well understood, and thus novel studies are required to fully understand their protein degradational regulation, and the role of the (P)RR in this process. TRB3 has been reported to control ACC degradation under fasting conditions by coupling ACC to the E3 ligase COP1.[58] Interestingly, (P)RR inhibitions upregulated the expression of several E3 ligases, including HECTD1 (***Online Table III***), and both ACCα and ACCβ have been reported to interact with HECTD1.[59] It is therefore conceivable that (P)RR inhibition accelerates ACC degradation via lysosomes by upregulating HECTD1. Simultaneously, the (P)RR-inhibition-induced reduction in PDH abundance is more difficult to understand. Inhibiting either autophagy, the lysosome or the proteasome did not rescue this reduction, nor did was inhibiting mitophagy, a special form of autophagy involved in degradation of mitochondrial proteins (data not shown). This may suggest that (P)RR inhibition regulates PDH abundance via an as yet unsolved mechanism,

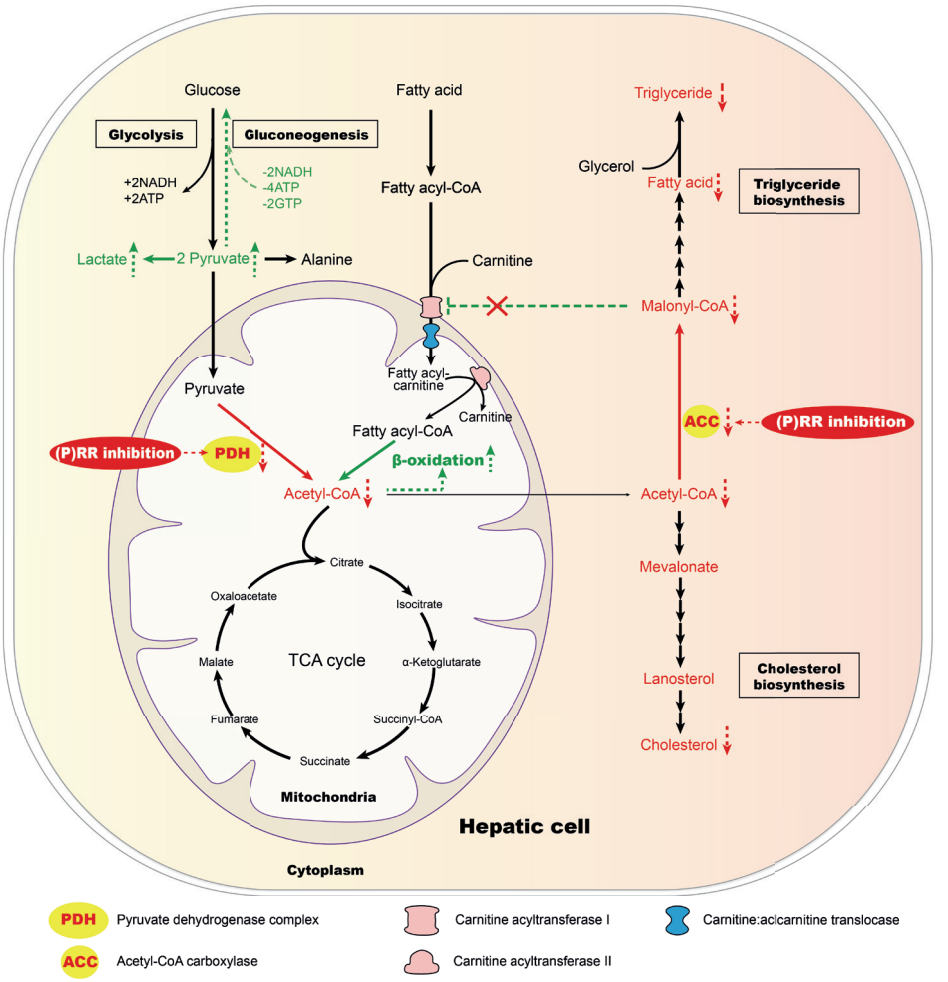

Figure 7. Model for reprogramed hepatic metabolism by (P)RR inhibition. Inhibiting hepatic (P)RR reduces PDH activity, impairing pyruvate metabolism and reducing acetyl-CoA supply from pyruvate, which limits FA biosynthesis. (P)RR inhibition further limits FA biosynthesis by reducing protein abundance of ACC, the crucial enzyme in FA biosynthesis. It further signals to increase FA oxidation via reduced malonyl-CoA, an inhibitor of FA oxidation that blocks the transportation of long-chain fatty acyl-carnitine by carnitine acyltransferase I (CAT1).

as seems to be the case with SORT1 as well.[31]

In conclusion, we report that hepatic (P)RR is a crucial regulator of lipid metabolism. Inhibiting hepatic (P)RR reduced ACC and PDH protein levels, and consequently increases FA oxidation and reduces lipid synthesis, thus attenuating diet-induced obesity and liver steatosis, as well as improving glycemic controls in C57BL/6J mice. Taken together, our study highlights the potential of inhibiting hepatic (P)RR as a therapeutic treatment for metabolic disorders such as fatty liver diseases, and familial hypercholesterolemia.

Sources of Funding

X. Lu is supported by National Natural Science Foundation of China (grant no. 81500667), Shenzhen Municipal Science and Technology Innovation Council (grant no. JCYJ20160307160819191), Shenzhen Peacock Plan (start-up fund). Y. Jiang is supported by National Natural Science Foundation of China (grant no. 81500354). X. Ruan is supported by Shenzhen Peacock Plan (grant no. KQTD20140630100746562), and Shenzhen Municipal Science and Technology Innovation Council (grant no. JCYJ20140509172719310, CXZZ20150601140615135). N. Zelcer is supported by a European Research Council Consolidator grant (617376) and is an Established Investigator of the Dutch Heart Foundation (2013T111). A.H. Jan Danser is supported by the Top Institute Pharma (T2-301).

Disclosures

Adam E. Mullick is an employee and shareholder of Ionis Pharmaceuticals.

References

1. Brown MS, Goldstein JL. A receptor-mediated pathway for cholesterol homeostasis. Science. 1986;232:34-47
2. Spady DK. Hepatic clearance of plasma low density lipoproteins. Semin Liver Dis. 1992;12:373-385
3. Olofsson SO, Stillemark-Billton P, Asp L. Intracellular assembly of vldl: Two major steps in separate cell compartments. Trends Cardiovasc Med. 2000;10:338-345
4. Hooper AJ, van Bockxmeer FM, Burnett JR. Monogenic hypocholesterolaemic lipid disorders and apolipoprotein b metabolism. Crit Rev Clin Lab Sci. 2005;42:515-545
5. Innerarity TL, Mahley RW, Weisgraber KH, Bersot TP, Krauss RM, Vega GL, Grundy SM, Friedl W, Davignon J, McCarthy BJ. Familial defective apolipoprotein b-100: A mutation of apolipoprotein b that causes hypercholesterolemia. J Lipid Res. 1990;31:1337-1349
6. Young SG, Hubl ST, Smith RS, Snyder SM, Terdiman JF. Familial hypobetalipoproteinemia caused by a mutation in the apolipoprotein b gene that results in a truncated species of apolipoprotein b (b-31). A unique mutation that helps to define the portion of the apolipoprotein b molecule required for the formation of buoyant, triglyceride-rich lipoproteins. J Clin Invest. 1990;85:933-942
7. Fan J, McCormick SP, Krauss RM, Taylor S, Quan R, Taylor JM, Young SG. Overexpression of human apolipoprotein b-100 in transgenic rabbits results in increased levels of ldl and decreased levels of hdl. Arterioscler Thromb Vasc Biol. 1995;15:1889-1899
8. Bou Khalil M, Sundaram M, Zhang HY, Links PH, Raven JF, Manmontri B, Sariahmetoglu M, Tran K, Reue K, Brindley DN, Yao Z. The level and compartmentalization of phosphatidate phosphatase-1 (lipin-1) control the assembly and secretion of hepatic vldl. J Lipid Res. 2009;50:47-58
9. Yamazaki T, Sasaki E, Kakinuma C, Yano T, Miura S, Ezaki O. Increased very low density lipoprotein secretion and gonadal fat mass in mice overexpressing liver dgat1. J Biol Chem. 2005;280:21506-21514
10. Sharp D, Blinderman L, Combs KA, Kienzle B, Ricci B, Wager-Smith K, Gil CM, Turck CW, Bouma ME, Rader DJ, et al. Cloning and gene defects in microsomal triglyceride transfer protein associated with abetalipoproteinaemia. Nature. 1993;365:65-69
11. Hobbs HH, Brown MS, Goldstein JL. Molecular genetics of the ldl receptor gene in familial hypercholesterolemia. Hum Mutat. 1992;1:445-466

12. Khachadurian AK, Uthman SM. Experiences with the homozygous cases of familial hypercholesterolemia. A report of 52 patients. Nutr Metab. 1973;15:132-140
13. Soutar AK, Naoumova RP. Mechanisms of disease: Genetic causes of familial hypercholesterolemia. Nat Clin Pract Cardiovasc Med. 2007;4:214-225
14. Kathiresan S, Willer CJ, Peloso GM, et al. Common variants at 30 loci contribute to polygenic dyslipidemia. Nat Genet. 2009;41:56-65
15. Kathiresan S, Melander O, Guiducci C, et al. Six new loci associated with blood low-density lipoprotein cholesterol, high-density lipoprotein cholesterol or triglycerides in humans. Nat Genet. 2008;40:189-197
16. Linsel-Nitschke P, Heeren J, Aherrahrou Z, et al. Genetic variation at chromosome 1p13.3 affects sortilin mrna expression, cellular ldl-uptake and serum ldl levels which translates to the risk of coronary artery disease. Atherosclerosis. 2010;208:183-189
17. Muendlein A, Geller-Rhomberg S, Saely CH, Winder T, Sonderegger G, Rein P, Beer S, Vonbank A, Drexel H. Significant impact of chromosomal locus 1p13.3 on serum ldl cholesterol and on angiographically characterized coronary atherosclerosis. Atherosclerosis. 2009;206:494-499
18. Sandhu MS, Waterworth DM, Debenham SL, et al. Ldl-cholesterol concentrations: A genome-wide association study. Lancet. 2008;371:483-491
19. Willer CJ, Sanna S, Jackson AU, et al. Newly identified loci that influence lipid concentrations and risk of coronary artery disease. Nat Genet. 2008;40:161-169
20. Kjolby M, Andersen OM, Breiderhoff T, Fjorback AW, Pedersen KM, Madsen P, Jansen P, Heeren J, Willnow TE, Nykjaer A. Sort1, encoded by the cardiovascular risk locus 1p13.3, is a regulator of hepatic lipoprotein export. Cell Metab. 2010;12:213-223
21. Musunuru K, Strong A, Frank-Kamenetsky M, et al. From noncoding variant to phenotype via sort1 at the 1p13 cholesterol locus. Nature. 2010;466:714-719
22. Strong A, Ding Q, Edmondson AC, et al. Hepatic sortilin regulates both apolipoprotein b secretion and ldl catabolism. J Clin Invest. 2012;122:2807-2816
23. Tveten K, Strom TB, Cameron J, Berge KE, Leren TP. Mutations in the sort1 gene are unlikely to cause autosomal dominant hypercholesterolemia. Atherosclerosis. 2012;225:370-375
24. Batenburg WW, Lu X, Leijten F, Maschke U, Muller DN, Danser AH. Renin- and prorenin-induced effects in rat vascular smooth muscle cells overexpressing the human (pro)renin receptor: Does (pro)renin-(pro)renin receptor interaction actually occur? Hypertension. 2011;58:1111-1119
25. Batenburg WW, Danser AH. (pro)renin and its receptors: Pathophysiological implications. Clin Sci (Lond). 2012;123:121-133
26. Cruciat CM, Ohkawara B, Acebron SP, Karaulanov E, Reinhard C, Ingelfinger D, Boutros M, Niehrs C. Requirement of prorenin receptor and vacuolar h+-atpase-mediated acidification for wnt signaling. Science. 2010;327:459-463
27. Geisberger S, Maschke U, Gebhardt M, Kleinewietfeld M, Manzel A, Linker RA, Chidgey A, Dechend R, Nguyen G, Daumke O, Muller DN, Wright MD, Binger KJ. New role for the (pro)renin receptor in t-cell development. Blood. 2015;126:504-507
28. Kinouchi K, Ichihara A, Sano M, Sun-Wada GH, Wada Y, Kurauchi-Mito A, Bokuda K, Narita T, Oshima Y, Sakoda M, Tamai Y, Sato H, Fukuda K, Itoh H. The (pro)renin receptor/atp6ap2 is essential for vacuolar h+-atpase assembly in murine cardiomyocytes. Circ Res. 2010;107:30-34
29. Oshima Y, Kinouchi K, Ichihara A, et al. Prorenin receptor is essential for normal podocyte structure and function. J Am Soc Nephrol. 2011;22:2203-2212
30. Riediger F, Quack I, Qadri F, et al. Prorenin receptor is essential for podocyte autophagy and survival. J Am Soc Nephrol. 2011;22:2193-2202
31. Lu X, Meima ME, Nelson JK, Sorrentino V, Loregger A, Scheij S, Dekkers DH, Mulder MT, Demmers JA, G MD-T, Zelcer N, Danser AH. Identification of the (pro)renin receptor as a novel regulator of low-density lipoprotein metabolism. Circ Res. 2016;118:222-229
32. Lu H, Howatt DA, Balakrishnan A, Graham MJ, Mullick AE, Daugherty A. Hypercholesterolemia induced by a pcsk9 gain-of-function mutation augments angiotensin ii-induced abdominal aortic aneurysms in c57bl/6 mice-brief report. Arterioscler Thromb Vasc Biol. 2016;36:1753-1757
33. Goettsch C, Hutcheson JD, Hagita S, Rogers MA, Creager MD, Pham T, Choi J, Mlynarchik AK, Pieper B, Kjolby M, Aikawa M, Aikawa E. A single injection of gain-of-function mutant pcsk9 adeno-associated virus vector induces cardiovascular calcification in mice with no genetic modification.

Atherosclerosis. 2016;251:109-118
34. Postic C, Girard J. Contribution of de novo fatty acid synthesis to hepatic steatosis and insulin resistance: Lessons from genetically engineered mice. J Clin Invest. 2008;118:829-838
35. Sugden MC, Holness MJ. Recent advances in mechanisms regulating glucose oxidation at the level of the pyruvate dehydrogenase complex by pdks. Am J Physiol Endocrinol Metab. 2003;284:E855-862
36. Foster DW. Malonyl-coa: The regulator of fatty acid synthesis and oxidation. J Clin Invest. 2012;122:1958-1959
37. Tong L. Acetyl-coenzyme a carboxylase: Crucial metabolic enzyme and attractive target for drug discovery. Cell Mol Life Sci. 2005;62:1784-1803
38. Teslovich TM, Musunuru K, Smith AV, et al. Biological, clinical and population relevance of 95 loci for blood lipids. Nature. 2010;466:707-713
39. Zoncu R, Bar-Peled L, Efeyan A, Wang S, Sancak Y, Sabatini DM. Mtorc1 senses lysosomal amino acids through an inside-out mechanism that requires the vacuolar h(+)-atpase. Science. 2011;334:678-683
40. Hu Y, Carraro-Lacroix LR, Wang A, Owen C, Bajenova E, Corey PN, Brumell JH, Voronov I. Lysosomal ph plays a key role in regulation of mtor activity in osteoclasts. J Cell Biochem. 2016;117:413-425
41. Li S, Brown MS, Goldstein JL. Bifurcation of insulin signaling pathway in rat liver: Mtorc1 required for stimulation of lipogenesis, but not inhibition of gluconeogenesis. Proc Natl Acad Sci U S A. 2010;107:3441-3446
42. Peterson TR, Sengupta SS, Harris TE, Carmack AE, Kang SA, Balderas E, Guertin DA, Madden KL, Carpenter AE, Finck BN, Sabatini DM. Mtor complex 1 regulates lipin 1 localization to control the srebp pathway. Cell. 2011;146:408-420
43. Ai D, Baez JM, Jiang H, et al. Activation of er stress and mtorc1 suppresses hepatic sortilin-1 levels in obese mice. J Clin Invest. 2012;122:1677-1687
44. Lu X, Garrelds IM, Wagner CA, Danser AH, Meima ME. (pro)renin receptor is required for prorenin-dependent and -independent regulation of vacuolar h(+)-atpase activity in mdck.C11 collecting duct cells. Am J Physiol Renal Physiol. 2013;305:F417-425
45. Kissing S, Rudnik S, Damme M, Lullmann-Rauch R, Ichihara A, Kornak U, Eskelinen EL, Jabs S, Heeren J, De Brabander JK, Haas A, Saftig P. Disruption of the vacuolar-type h+-atpase complex in liver causes mtorc1-independent accumulation of autophagic vacuoles and lysosomes. Autophagy. 2017;13:670-685
46. Engeli S, Negrel R, Sharma AM. Physiology and pathophysiology of the adipose tissue renin-angiotensin system. Hypertension. 2000;35:1270-1277
47. Kanda A, Noda K, Ishida S. Atp6ap2/(pro)renin receptor contributes to glucose metabolism via stabilizing the pyruvate dehydrogenase e1 beta subunit. J Biol Chem. 2015;290:9690-9700
48. Patel MS, Nemeria NS, Furey W, Jordan F. The pyruvate dehydrogenase complexes: Structure-based function and regulation. J Biol Chem. 2014;289:16615-16623
49. Harris RA, Bowker-Kinley MM, Huang B, Wu P. Regulation of the activity of the pyruvate dehydrogenase complex. Adv Enzyme Regul. 2002;42:249-259
50. Sun Y, Danser AHJ, Lu X. (pro)renin receptor as a therapeutic target for the treatment of cardiovascular diseases? Pharmacological Research. 2017;In press
51. Choi CS, Savage DB, Abu-Elheiga L, Liu ZX, Kim S, Kulkarni A, Distefano A, Hwang YJ, Reznick RM, Codella R, Zhang D, Cline GW, Wakil SJ, Shulman GI. Continuous fat oxidation in acetyl-coa carboxylase 2 knockout mice increases total energy expenditure, reduces fat mass, and improves insulin sensitivity. Proc Natl Acad Sci U S A. 2007;104:16480-16485
52. Abu-Elheiga L, Matzuk MM, Abo-Hashema KA, Wakil SJ. Continuous fatty acid oxidation and reduced fat storage in mice lacking acetyl-coa carboxylase 2. Science. 2001;291:2613-2616
53. Inoue M, Ohtake T, Motomura W, Takahashi N, Hosoki Y, Miyoshi S, Suzuki Y, Saito H, Kohgo Y, Okumura T. Increased expression of ppargamma in high fat diet-induced liver steatosis in mice. Biochem Biophys Res Commun. 2005;336:215-222
54. Gavrilova O, Haluzik M, Matsusue K, Cutson JJ, Johnson L, Dietz KR, Nicol CJ, Vinson C, Gonzalez FJ, Reitman ML. Liver peroxisome proliferator-activated receptor gamma contributes to hepatic steatosis, triglyceride clearance, and regulation of body fat mass. J Biol Chem. 2003;278:34268-34276
55. Zhang YL, Hernandez-Ono A, Siri P, Weisberg S, Conlon D, Graham MJ, Crooke RM, Huang LS,

Ginsberg HN. Aberrant hepatic expression of ppargamma2 stimulates hepatic lipogenesis in a mouse model of obesity, insulin resistance, dyslipidemia, and hepatic steatosis. J Biol Chem. 2006;281:37603-37615

56. Wu CH, Mohammadmoradi S, Thompson J, Su W, Gong M, Nguyen G, Yiannikouris F. Adipocyte (pro) renin-receptor deficiency induces lipodystrophy, liver steatosis and increases blood pressure in male mice. Hypertension. 2016;68:213-219
57. Shamansurova Z, Tan P, Ahmed B, Pepin E, Seda O, Lavoie JL. Adipose tissue (p)rr regulates insulin sensitivity, fat mass and body weight. Mol Metab. 2016;5:959-969
58. Qi L, Heredia JE, Altarejos JY, et al. Trb3 links the e3 ubiquitin ligase cop1 to lipid metabolism. Science. 2006;312:1763-1766
59. Rouillard AD, Gundersen GW, Fernandez NF, Wang Z, Monteiro CD, McDermott MG, Ma'ayan A. The harmonizome: A collection of processed datasets gathered to serve and mine knowledge about genes and proteins. Database (Oxford). 2016;2016

Supplemental Materials

Methods

Animals

C57BL/6 mice and LDLR$^{-/-}$ mice were obtained from Model Animal Research Center of Nanjing University (Nanjing, China), and were housed at a 10-hour light/14-hour dark cycle. 8-week old male C57BL6 mice were injected weekly with saline, GalNAc control ASOs (G-conrol), or GalNAc (P)RR ASOs [G-(P)RR] subcutaneously. For experiments ≤ 4 weeks, ASOs were dosed at 3 mg/kg/week. For experiments ≥ 4 weeks, ASOs were dosed at 3 mg/kg/week in the first 4 weeks, and were then reduced to 1.5 mg/kg/week until end of the experiment. Mice were either fed with ND (Harlan Teklad) or HFD (42% kcal fat, 0.2% cholesterol, Harlan Teklad). LDLR$^{-/-}$ mice were treated in the same way as C57BL/6 mice. Body weight was monitored weekly. Food consumption of each cage hosting 6 mice was recorded weekly. Blood samples were collected via submandibular bleeding after 6h fasting. Plasma lipid TC and TG levels were monitored bi-weekly, unless indicated elsewhere. Experimental procedures were approved by local animal ethnic committee (no. 2014-0140).

Antisense Oligonucleotides (ASOs)

ASOs with 5'-methyl modified cytosine and a phosphorothioate backbone containing 2-O, 4-C-[(S)-ethylidene]-D-ribose (cEt) modified sugars were synthesized as described previously.[1] Chimeric ASOs containing 16mer cEt chemistries were used with the gapmer design of 3-10-3 wherein the terminal 5' and 3' nucleotides contained the cET modified sugars that flanked 10 nucleotides with unmodified sugars. The liver targeting conjugate GalNAc was connected through a trishexylamino-(THA)-C6 linker at the 5' end of the ASO.[2] Extensive *in vitro* activity screens were performed followed by *in vivo* tolerability and activity studies to identify the lead (P)RR ASO with the following nucleotide sequence AGATATTGGTCCATTT. A control ASO that did not hybridize to any known rodent mRNA was used and had the following nucleotide sequence, GGCCAATACGCCGTCA.

Intraperitoneal glucose tolerance test (IPGTT)

IPGTT was performed as described elsewhere,[3] one week prior to the end of the study. Briefly, following 16h fasting, 2 g/kg glucose was injected intraperitoneally to mice. Blood samples were collected from tail vain at 0, 15, 30, 60 and 120 min after glucose injection, and blood glucose was measured using a glucometer (Roche). Glucose levels at each time point were compared, and overall differences in glycemic control were compared using

area under curve (AUC).

***In vivo* LDL clearance assay**

In vivo LDL clearance was measured as described before.[4] In short, mice were injected with 50 μg human Dil-labeled LDL (AngYuBio, Shanghai) via a tail-vein. Then, blood samples were collected retro-orbitally at 2, 10, 20, 40, 80, 160, and 300 min after injection. A standard curve was constructed by serial dilution of the human Dil-labeled LDL into mice plasma. Dil-LDL concentrations at 2 min after injection were the highest and were thus set as the baseline value for further analysis. Differences in VLDL secretion were compared using area under curve (AUC).

Hepatic VLDL secretion

To determine VLDL-TG secretion rate, mice were fasted for 4 hours and injected intraperitoneally with 1 mg/g Pluronic F127 (Sigma Aldrich), a detergent that inhibits lipolysis. Subsequently, blood samples were collected by retroorbital bleeding at 0, 1, 2 and 4 hours after Pluronic F127 injection. Differences in VLDL secretion were compared using area under curve (AUC).

Fast Protein Liquid Chromatography (FPLC) analysis of plasma lipoproteins

FPLC analysis of plasma lipoproteins was performed as described before.[5] In short, plasma samples were pooled, and cleared by centrifugation and filtering through a 0.22 μm filter. 200 μL cleared plasma samples were loaded for FPLC analysis using an AKTA purifier (GE) and Superose-6 Increase 10/300 GL (GE). Flow rate was set to 0.5 mL/min, and fractions between 10-16 mL were collected at intervals of 0.25 mL/fraction. Cholesterol and triglycerides content in each fraction was measured.

Oxygen consumption and physical activity measurement

Metabolic and physical activity of the mice were measured using an indirect open-circuit calorimeter (Oxylet, Panlab).[6] Mice were housed individually in metabolic chambers and oxygen consumption, CO_2 production, and physical activity were recorded at 30 min intervals for consecutive 48 hours. For accuracy, the recorded data from the first 12-14 hours after the mice have been housed in the chamber were not analyzed.

Body composition analysis

Fat and lean mass composition of the mice were evaluated by EchoMRI (Echo Medical Systems, Houston, TX, USA) before sacrifice. Weights of different fat tissues were measured using a scale balance with 0.0001-gram accuracy (Sartorius).

H&E staining and Oil Red O staining

Hematoxylin and eosin (H&E) staining was performed on 5 μm tissue sections which were Bouin's-fixed and paraffin-embedded. Oil Red O staining was used to detected hepatic neutral lipids. Fresh liver and adipose tissues embedded in OCT were cryosectioned for 7 μm. After fixation with 4% paraformaldehyde, sections were stained with 0.3% oil red o following standard procedures [7] and then counterstained with hematoxylin. Images were scanned using Cytation 5 Cell Imaging Multi-mode reader (Biotek).

Measurement of ALT and AST

Blood samples were pre-cleared by centrifugation at 3,000×g for 5 minutes. Plasma alanine aminotransferase (ALT) and aspartate aminotransferase (AST) activities were measured by commercial kits (Biosino) following the manufacture's protocol.

Adenovirus and Adeno-associated virus

Adeno-associated virus (AAV) expressing the D377Y PCSK9 mutant and their use was previously described.[8] Eight-week-old mice were intraperitoneally with AAV-PCSK9 at a concentration of 10×10^{10} genomic copies, and fed a chow-diet for 4 weeks to induce LDLR degradation. Afterwards, mice were treated with saline, G-control, or G-(P)RR for 4 weeks, and fed with chow or HFD. Human SORT1 under control of a CMV promotor was cloned and inserted in to pAd-EF1a-GFP vector (Vigenebio, China). Packaging of adenovirus was performed by linearization of the plasmid and transfection of 293A cells. Adenoviral particles were purified by ultracentrifugation, and virus titer was determined by serial dilution and plaque formation. 8-weeks old male mice were injected with 1.5×10^{9} pfu Ad-hSORT1 or Ad-GFP (purchased from Vigenebio) via tail-vein. Mice were fed with chow or HFD for 7 days, and sacrificed after 6h fasting.

Transcriptome analysis

To assess whether silencing hepatic (P)RR affects gene expression in the liver, we injected mice (3 mice/group) intraperitoneally with saline or G-(P)RR as described above. After 5 days, the mice were sacrificed after 6h fasting, and liver samples were collected immediately and stored in Trizol at -80 °C until use. Total RNA was extracted and a RNA sequencing library was constructed for each sample using the Illumina mRNA-Seq Prep Kit. Paired-End libraries were prepared following Illumina's protocols and sequenced on the Illumina HiSeq X10 platform. RNA Sequencing reads were analyzed following the reported protocol with HISAT, StringTie and Ballgown.[9] More specifically, high quality sequencing reads were firstly mapped to the mouse reference genome (version Ensembl GRCm38) using HISAT with default parameters.[10] Transcriptomic expression at gene and transcript

level, characterized by FPKM (Fragments Per Kilobase of transcript per Million mapped reads), was then quantified by StringTie.[9] The Ballgown package was used to identify differential expressed genes (DEGs) with P <0.05 between G-(P)RR and saline control.[11] Functional analysis of all DEGs was preformed using DAVID functional annotation clustering tool.[12] Gene numbers were calculated for each Gene ontology (GO) category, and a hypergeometric test was used to identify significantly enriched GO categories in DEGs.

Comparative proteomics using iTRAQ

To understand how does (P)RR inhibition affects lipid metabolism and energy metabolism, we performed comparative proteomics analysis. Mice (n=3/group) were treated with G-control or G-(P)RR for 4 weeks, and fed with chow or HFD. Mice were sacrificed after 6h fasting. Livers were collected and homogenized in lysis buffer by TissueLyzer. Proteins were precipitated by acetone and resuspended with dissolving buffer containing 6 M guanidine hydrochloride and 300 mM TEAB (triethylammonium bicarbonate). Protein concentrations were determined by BCA, and equal amounts of proteins from individual samples per group were mixed and processed for iTRAQ labeling. Labeled samples were fractionated by high pH separation using Acquity UPLC H-Class Bio system (Waters Corporation, Milford, MA) connected to a reverse phase column (XBridge C18 column, 2.1 mm×150 mm, 3.5 μm, 300 Å, Waters Corporation, Milford, MA). High pH separation was performed using a linear gradient, starting from 5% B to 35% B in 40 min (B: 5 mM ammonium formate in 90% acetonitrile, pH 10.0, adjusted with ammonium hydroxide). The column flow rate was maintained at 200 μL/min and column temperature was maintained at room temperature. Ten fractions were collected. Each fraction was dried in a vacuum concentrator for the next step. The peptide samples were resuspended with 30 μL solvent A respectively (A: water with 0.1% formic acid; B: acetonitrile with 0.1% formic acid), separated by nano-RPLC (EASY-nLC 1000, Thermo Fisher Scientific) and analyzed by on-line electrospray tandem mass spectrometry (Q Exactive mass spectrometer, Thermo Fisher Scientific). 5 μL peptide sample was loaded onto the trap column (Thermo Scientific Acclaim PepMap C18, 75 μm × 2 cm), and subsequently separated on the analytical column (Acclaim PepMap C18, 75 μm × 15 cm) with a linear gradient, from 5% B to 35% B in 70 min, at a flow rate of 300 nL/min. The electrospray voltage of 1.6 kV versus the inlet of the mass spectrometer was used. The Q Exactive mass spectrometer was operated in the data-dependent mode to switch automatically between MS and MS/MS acquisition. Survey full-scan MS spectra (m/z 300-1600) were acquired in Orbitrap with a mass resolution of 70,000 at m/z 200. The AGC target was set to 1 000 000, and the maximum injection time was 20 ms. The ten most intense peaks were isolated in the quadrupole with isolation window of 2.0 m/z units. Ions with charge states 2+, 3+, and 4+ were sequentially fragmented by higher

energy collisional dissociation (HCD) with a normalized collision energy of 27%, fixed first mass was set at 100, and further analyzed in the Orbitrap mass analyzer with 17,500 resolution. The AGC target was set to 500,000, and the maximum injection time was 200 ms. In all cases, one microscan was recorded using dynamic exclusion of 35 seconds.

The expression ratio [G-(P)RR/G-control] was calculated for each protein, under different diet conditions. Cut-off value was set to 1.2-fold [G-(P)RR/G-control >1.2 or <0.083]. Proteins with altered abundance were compared between HFD and chow, and only proteins that were regulated in the same trend by (P)RR inhibition were identified as differential expressed proteins (DEPs). Functional analysis of all DEGs was preformed using DAVID functional annotation clustering tool. Gene numbers were calculated for each Gene ontology (GO) category, and hypergeometric test was used to identify significantly enriched GO categories in DEGs.

Measurement of pyruvate, acetyl-CoA, lactate and PDH activity

Plasma pyruvate and lactate levels were detected using Pyruvate Assay kit (Sigma Aldrich) and Lactate Assay kit (Sigma Aldrich), following the manufacture's protocols. To measure hepatic pyruvate, acetyl-CoA, and PDH activity, liver samples (~25 mg) were homogenized in the assay buffers provided with the kits, and measurements were performed according to the manufacture's protocol. To measure cellular pyruvate levels, HepG2 cells were transfected with either control siRNA (siNC) or (P)RR siRNA [si(P)RR] for 48 hours. Cells were then detached using TrypLE and collected by centrifugation at 4 °C at 100×g, followed by washing with ice-cold PBS for three times. Measurement of pyruvate levels from an equal number of cells was performed according to manufacturer's protocol, and normalized to cell number. Acetyl-CoA levels were measured using the PicoProbe Activity Microplate Assay kit (Abcam) in a similar approach, except that protein concentration was used to normalize acetyl-CoA levels. To measure lactate concentration, 24h after transfection, cells were switched to conditional medium (CM) that does not contain phenol red for 24 hours. Lactate levels in CM were then measured using the Lactate Assay kit (Sigma Aldrich). PDH activity was detected by a commercial kit (Sigma Aldrich), following the manufacture's protocol.

Measurement of lipoprotein lipase (LPL) activity

Mice were treated with saline, G-control, or G-(P)RR and fed an HFD for 4 weeks. To measure LPL activity, mice were injected with 0.2 U/g heparin via tail-vein, and blood were drawn 15 min after heparin injection. Plasma LPL activity were then measured with a commercial kit from Abcam (catalog nr. ab204721).

Measurement of plasma insulin

Mice were treated with saline, G-control, or G-(P)RR and fed an HFD for 14 weeks. At 12th week, after 6-hour-fasting, plasma samples were collected and measured for insulin levels with an ultrasensitive mouse insulin ELISA kit from ALPCO (catalog nr. 80-INSMSU-E01), following the standard manufacturer's protocol.

Isolation and culture of primary hepatocytes

Primary hepatocytes were isolated from C57BL/6J mice using previously described two-step collagenase perfusion method with modifications.[13] Briefly, mice were first perfused with O2 gassed perfusion buffer (5 mmol/L HEPES, 4 mmol/L KCl, 120 mmol/L NaCl, 1 mmol/L KH_2PO_4, 2.4 mmol/L $MgSO_4$, 40 mmol/L $NaHCO_3$, 20 mmol/L glucose) supplemented with 0.1 mmol/L EDTA, for 5-7 minutes at a constant flow rate at 7 mL/min. Perfusion path was set to flow into liver via inferior vena cava and flow out through portal vein. After the first perfusion step, mice were then perfused with O_2 gassed perfusion buffer supplemented with 2.7 mmol/L $CaCl_2$ and 1.6 mg/mL Type IV collagenase (Sigma Aldrich, catalog nr. C5138), for 3-4 minutes at a constant flow rate at 6 mL/min. Primary hepatocytes were released by removing liver capsule, and filtered through 100 μm filtered. Then, primary hepatocytes were washed with ice-cold DMEM and centrifuged at 50×g for 2 min, which was repeated for three times. Primary hepatocytes were seeded at a density of 600,000 cells/well or 8,000 cells/well into collagen coated 6-well plate or Seahorse 24-well plate, respectively, and cultured with DMEM GlutaMax™ high glucose supplemented with 5% FBS. To inhibit (P)RR expression in mouse primary hepatocytes, 0.05 mg/mL G-(P)RR ASO was added to culture medium 3 hours after seeding cells.

Seahorse XFe24 analyzer

HepG2 cells were seeded to Seahorse 24-well plate, and cultured with DMEM GlutaMax™ high glucose with 10% FBS. HepG2 cells were transfected with siNC or si(P)RR for 48 hours. Mouse primary hepatocytes were isolated, seeded to Seahorse 24 well plate, and cultured with DMEM GlutaMax™ high glucose supplemented with 5% FBS. To inhibit (P)RR expression, mouse primary hepatocytes were treated with 0.05 μg/mL final concentration of G-(P)RR ASOs for 36 hours. Mitochondrial function and cellular fuel dependency were then measured using Seahorse XF Cell Mito Stress Test Kit and Seahorse XF Mito Fuel Flex Test Kit, following manufacturer's protocol, with the exception that for FA dependency assay oleic acid was added to a final concentration of 50 μmol/L to the cell culture medium 4 hours prior to the start of the assay.

Immunoblotting

For protein expression and phosphorylation studies, 50 mg mouse liver samples were homogenized in RIPA buffer (50 mM Tris-HCl, 150mM NaCl, 1% Triton X-100, 1% sodium deoxycholate, 0.1% SDS, pH 7.4) with phosphatase inhibitor cocktail (Sigma Aldrich) and protease inhibitors cocktail (Roche) using TissueLyzer (Qiagen). Homogenates were centrifuged at 10,000×g at 4 °C for 10 minutes to clear any cell debris or insoluble proteins. Protein concentrations were then determined using BCA assay (Pierce). Equal amounts of proteins (30-40 mg) were loaded and separated on 4-20% Bis-Tris gels (GenScript), and transferred to PVDF membranes using iBlot® 2 Dry Blotting System (Thermo Fisher Scientific). For high-molecular weight proteins such as acetyl-CoA carboxylase (ACC), samples were loaded and separated on 6% SDS-PAGE gels with ice-cold buffers for 3-5 hours, and transferred to PVDF membranes using traditional wet transferring system at 4 °C for 16 hours. The blots were then probed with the antibodies listed in **Online Table I** and detected by ClarityTM Western Substrate (Bio-rad). The intensities of bands were analyzed using ImageJ.

Online Table I. Antibodies used in the study.

Target	Species originated	Dilution	Source	Catalog number
(P)RR	Rabbit	1：1000	Sigma	HPA003156
SORT1	Mouse	1：1000	BD Bioscience	612100
LDLR	Rabbit	1：1000	Thermo Fisher Scientific	PA5-22976
PDHA	Rabbit	1：1000	Proteintech	18068-1-AP
PDHB	Rabbit	1：1000	Proteintech	14744-1-AP
ACCα/β	Rabbit	1：1000	Cell Signaling Technology	9957
PPARγ	Rabbit	1：1000	Cell Signaling Technology	2435
Adiponectin	Rabbit	1：1000	Cell Signaling Technology	2789
β-actin	Mouse	1：3000	Proteintech	60008-1

RNA isolation and qPCR analysis

Liver samples were homogenized with Trizol (Thermo Fisher Scientific) and total RNA was extracted using Direct-zolTM RNA MiniPrep kit (ZYMO Research). One microgram of total RNA was reverse transcribed with Prime ScriptTM RT Master Mix (TaKaRa). SYBR Green real-time quantitative PCR assays were performed on a qTOWER apparatus (Analytic Jena) using SYBR®Premix Ex TaqTM II kit (TaKaRa). Primers used in the study were listed in **Online Table II**.

Hepatic lipids extraction and measurement

To measure hepatic lipid contents, lipids in the liver were extracted using Folch's method.[14] In short, 50 mg liver samples were homogenized using Tissue lyzer (60Hz, 30s) in chloroform and methanol mixture (2:1) followed by adding methanol, chloroform and

MQ. Extracted lipids were dried with N_2 gas and dissolved with 200μL PBS containing 1% Triton X-100. Cholesterol, triglycerides and non-esterified fatty acid (NEFA) were measured using colorimetric kits (Wako).

Statistics

All values were presented as mean ± SEM. For experiments with n number ≥ 8/group, D'Agostino-Pearson omnibus test was performed to test normality. For experiments with less n number, Kolmogorov-Smirnov test was performed for normality test. After passing normality test, one-way ANOVA followed by the Bonferroni test was performed for comparison of more than two groups. And student t-test was used to compare the differences between two groups. P values of <0.05 were considered significant.

Online Table II.List of qPCR primer sequences.

Gene		Sequence
(P)RR	Forward	5'-GGGTGGATAAACTGGCACTTC-3'
	Reverse	5'-TGGAATTTGCAACGCTGTC-3'
SORT1	Forward	5'-TGAGGACATGGTCTTCATGC-3'
	Reverse	5'-GGTAAAGATGGTGCCAAACC-3'
LDLR	Forward	5'-GATGGCTATACCTACCCCTCAA-3'
	Reverse	5'-TGCTCATGCCACATCGTC-3'
PDHA	Forward	5'-GGCATCGTTGGAGCTCAG-3'
	Reverse	5'-ACAGACCTCATCTTTTCCATTGT-3'
PDHB	Forward	5'-GAGCTGAGATTTGTGCCAGA-3'
	Reverse	5'-ACATCAGCACCAGTGACACG-3'
ACCα	Forward	5'-GGCTCAAACTGCAGGTATCC-3'
	Reverse	5'-TTGCCAATCCACTCGAAGA-3'
ACCβ	Forward	5'-TGAATCTCACGCGCCTACTA-3'
	Reverse	5'-TTGTGTTCTCGGCCTCTCTT-3'
PPARγ	Forward	5'-GAAAGACAACGGACAAATCACC-3'
	Reverse	5'-GGGGGTGATATGTTTGAACTTG-3'
Adiponectin	Forward	5'-GGGGGTGATATGTTTGAACTTG-3'
	Reverse	5'-CTTTCCTGCCAGGGGTTC-3'
UCP-1	Forward	5'-GGCCTCTACGACTCAGTCCA-3'
	Reverse	5'-TAAGCCGGCTGAGATCTTGT-3'
Hadha	Forward	5'-GAAATGGATAATATCTTGGCAAATC-3'
	Reverse	5'-TGGACGTCTTCATCAGAGGAG-3'
Acaa2	Forward	5'-AAATGTGCGCTTCGGAAC-3'
	Reverse	5'-CGTTAATCCTGCCCACAAAG-3'
Acadvl	Forward	5'-GGTGGTTTGGGCCTCTCTA-3'
	Reverse	5'-TCCCAGGGTAACGCTAACAC-3'
Acadl	Forward	5'-GCTTATGAATGTGTGCAACTCC-3'
	Reverse	5'-CCGAGCATCCACGTAAGC-3'
β-actin	Forward	5'-CTAAGGCCAACCGTGAAAAG-3'
	Reverse	5'-ACCAGAGGCATACAGGGACA-3'

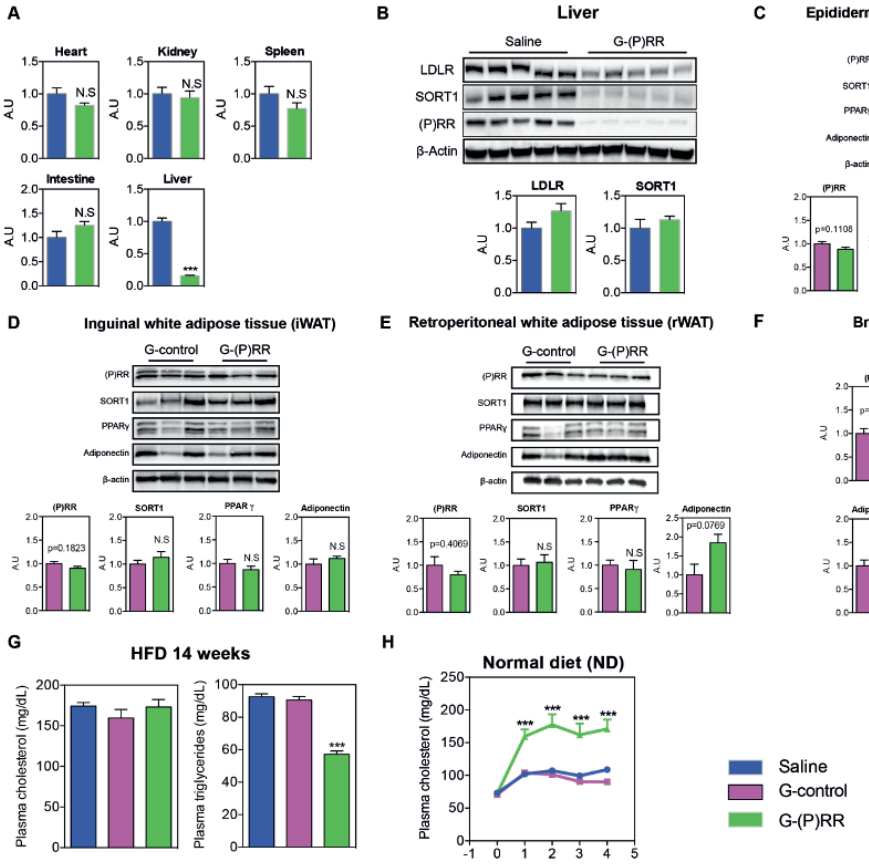

Online Figure I. GalNAc-(P)RR ASO specifically targets hepatic (P)RR and affects plasma lipid concentrations. (A) Eight-weeks-old male C57BL6 mice were injected with saline (blue) or G-(P)RR (green). After 5 days, mice were sacrificed and tissues were collected and analyzed for (P)RR expression. (P)RR expression was normalized by the geometric mean of the expression of actin, 36B4 and GAPDH. N=5/group; ***: p<0.001. **(B)** Immunoblotting of liver samples from saline or G-(P)RR treated mice. **(C-E)** (P)RR expression levels and protein abundance in epididermal white adipose tissue (eWAT), inguinal white adipose tissue (iWAT), and retroperitoneal white adipose tissue (rWAT) of mice treated with G-control or G-(P)RR for 14 weeks and fed with HFD. **(F)** (P)RR expression in brown adipose tissue (BAT) of mice treated with G-control or G-(P)RR for 14 weeks and fed with HFD. **(G)** Plasma triglycerides and cholesterol concentration of C57BL6 mice injected with saline (blue), G-control (magenta) or G-(P)RR (green), and fed HFD for 14 weeks. N=10 per group. ***: p<0.001. G-control v.s G-(P)RR. **(H)** Plasma cholesterol levels of C57BL6 mice treated as indicated, and fed ND for 4 weeks. N=12 per group. ***: p<0.001. G-control v.s G-(P)RR.

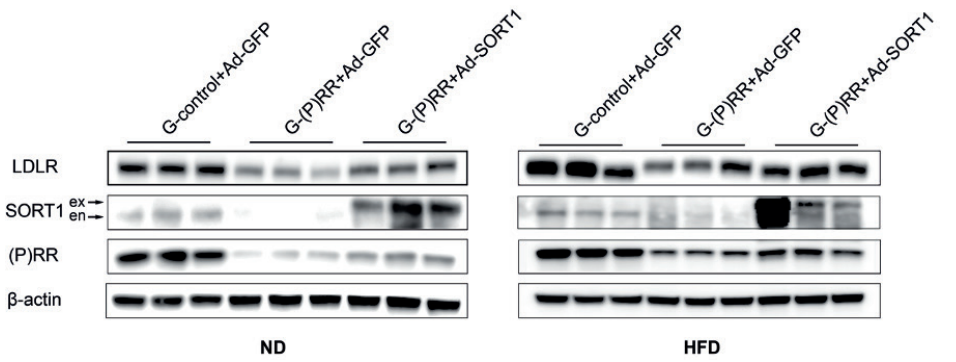

Online Figure II. SORT1 overexpression does not prevent PRR deficiency induced reduction in LDLR protein levels in the liver. Eight-week-old male mice were treated with G-control or G-(P)RR, in combination of control adenovirus (Ad-GFP) or SORT1 expressing adenovirus (Ad-SORT1). N=6 per mice. Representative blot. Ex: exogenously expressed hSORT1. En: endogenously expressed mSORT1.

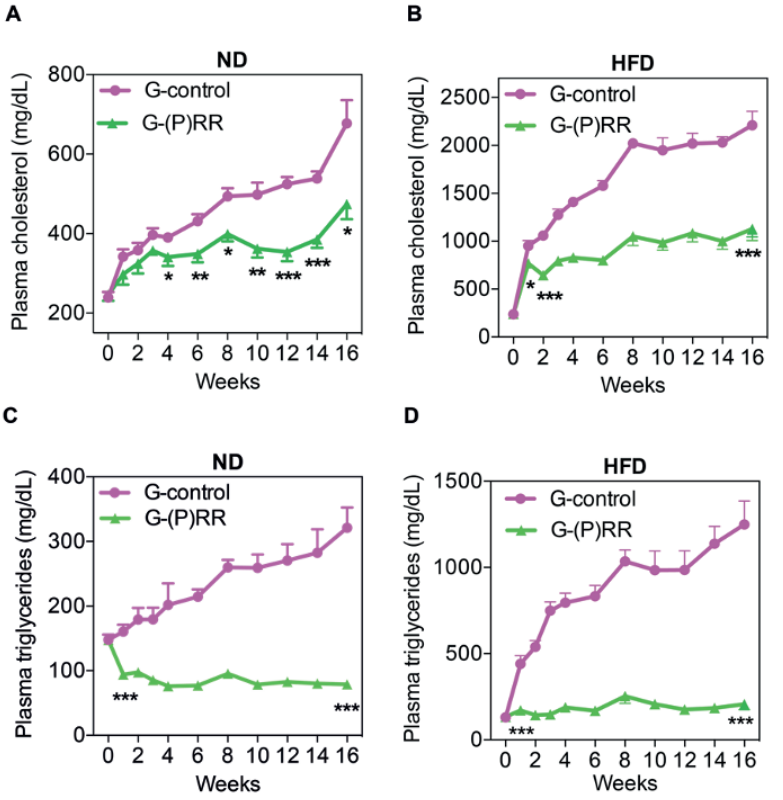

Online Figure III. Inhibiting hepatic (P)RR in LDLR$^{-/-}$ mice reduces plasma cholesterol and triglyceride levels under both chow and HFD conditions. Eight-weeks-old male mice were treated with G-control (magenta) or G-(P)RR (green), and fed with ND or HFD for 16 weeks. Plasma cholesterol levels **(A&B)** and plasma triglyceride levels **(C&D)** were monitored weekly in the first 4 weeks, and bi-weekly afterwards. N=8 per group. *: $p<0.05$; **: $p<0.01$; ***: $p<0.001$.

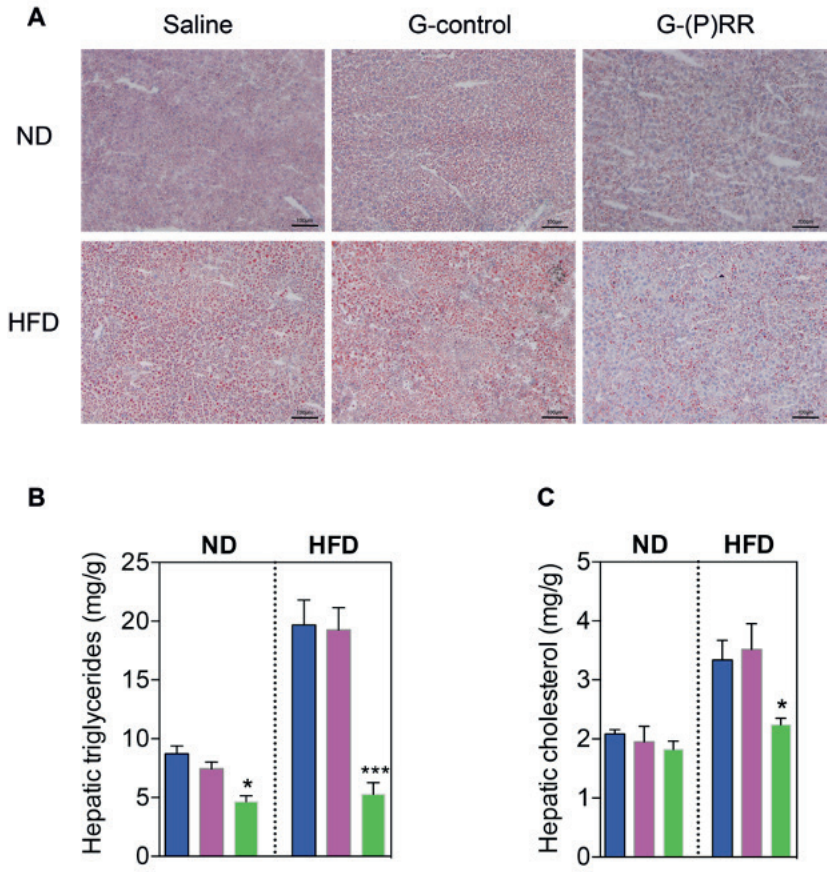

Online Figure IV. Inhibiting hepatic (P)RR in LDLR$^{-/-}$ mice reduces plasma cholesterol and triglyceride levels under both chow and HFD conditions. Eight-weeks-old male mice were treated with G-control (magenta) or G-(P)RR (green), and fed with ND or HFD for 16 weeks. Plasma cholesterol levels **(A&B)** and plasma triglyceride levels **(C&D)** were monitored weekly in the first 4 weeks, and bi-weekly afterwards. N=8 per group. *: $p<0.05$; **: $p<0.01$; ***: $p<0.001$.

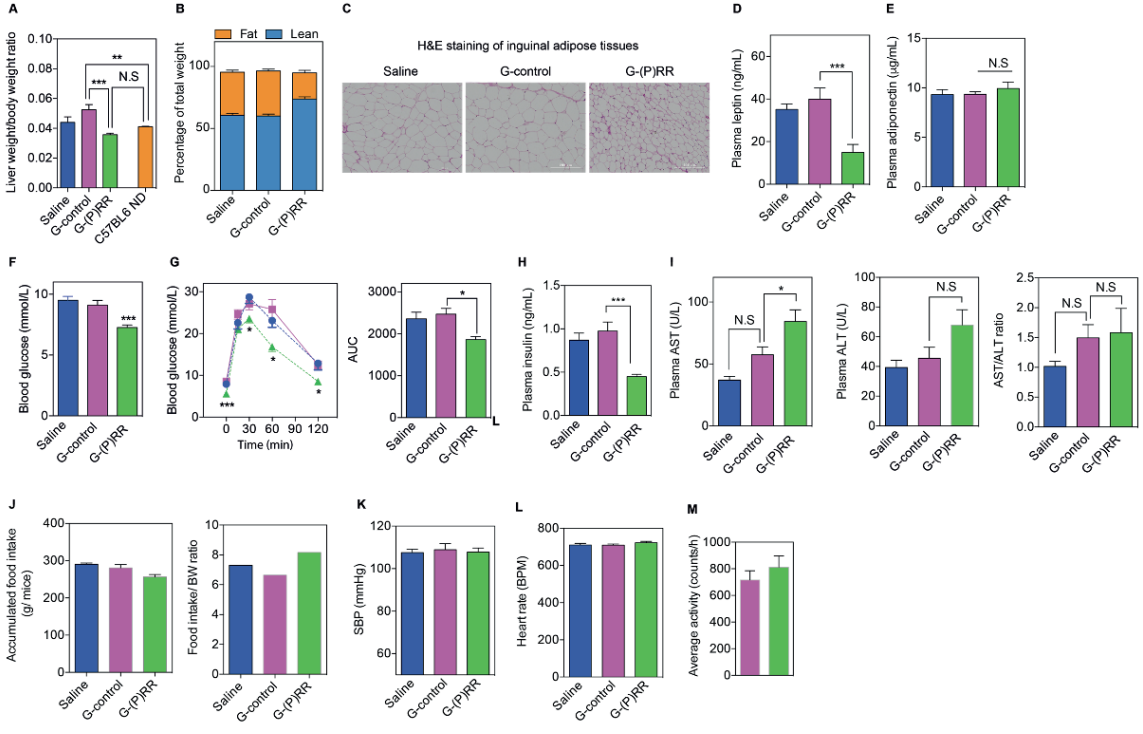

Online Figure V. Relevant information of hepatic (P)RR inhibition in C57BL6 mice fed HFD for 14 weeks. Eight-week-old male mice were treated as indicated, and fed HFD for 14 weeks. **(A)** LW/BW ratio. LW/BW of C57BL6 mice at similar age, fed ND, was used as a reference value (n=6). N=10 per group. ***: $p<0.001$. **(B)** Percentage of fat and lean mass of total weight. **(C)** Representative image of H&E staining of inguinal white adipose tissue. **(D)** Plasma leptin concentrations. **(E)** Plasma adiponectin concentrations. **(F)** Fasting glucose levels of the mice were measured on week 12 of the HFD. **(G)** Intraperitoneal glucose tolerance test (IPGTT) was performed on week 13 of the HFD. Glucose levels at each time point were compared by One-way ANOVA and * indicates significant differences between G-control and G-(P)RR injected mice. AUC was used to compare the overall differences between groups. **(H)** Fasting plasma insulin levels at 12th week. **(I)** plasma ALT and AST activity, and AST/ALT ratio. N=10 per group; *: $p<0.05$; **(J)** accumulated food intake during experimental period, and accumulated food intake adjusted by end time body weight. SBP **(K)** and heart rate **(L)** measured 7 days prior to sacrifice. N=10 per group. **(M)** 24h average physical activity of G-control injected and G-(P)RR injected mice was monitored with a metabolic monitoring system 4 days prior to sacrifice. N=8 per group.

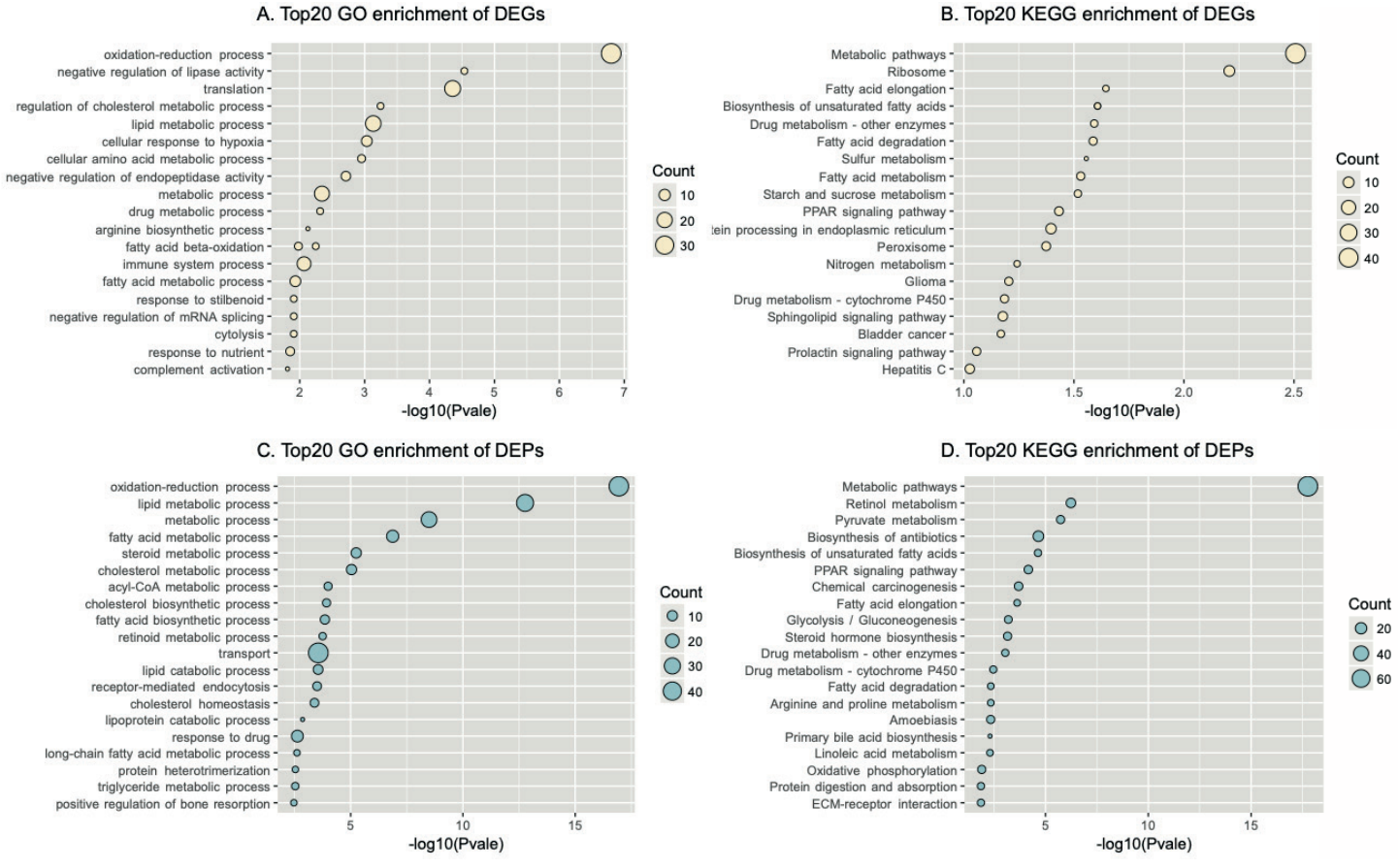

Online Figure VI. GO enrichment analysis reveals that inhibiting the (P)RR extensively affects genes involved in metabolic processes. Analysis of transcriptome (A&B), or comparative proteomics **(C&D)**. Top 20 enriched biological processes (BP) **(A&C)**. Top 20 enriched KEGG pathways **(B&D)**.

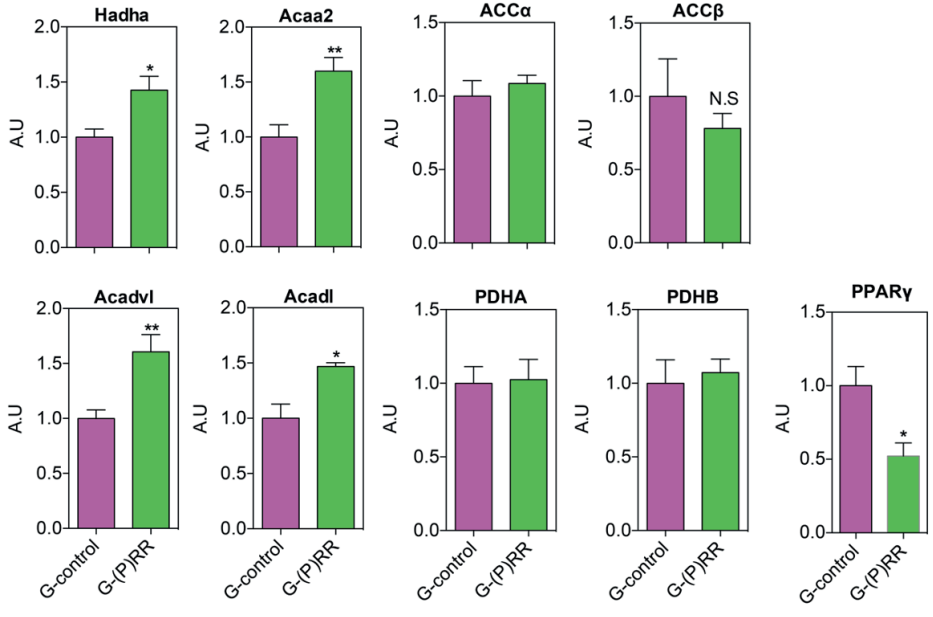

Online Figure VII. Hepatic genes expression are affected by (P)RR inhibition. Eight-week-old male C57BL6 mice were treated with G-control or G-(P)RR, fed HFD for 14 weeks. Hepatic gene expressions were analyzed, and normalized by the expression of β-actin in the same sample. N=6 per group. *: $p<0.05$; **: $p<0.01$.

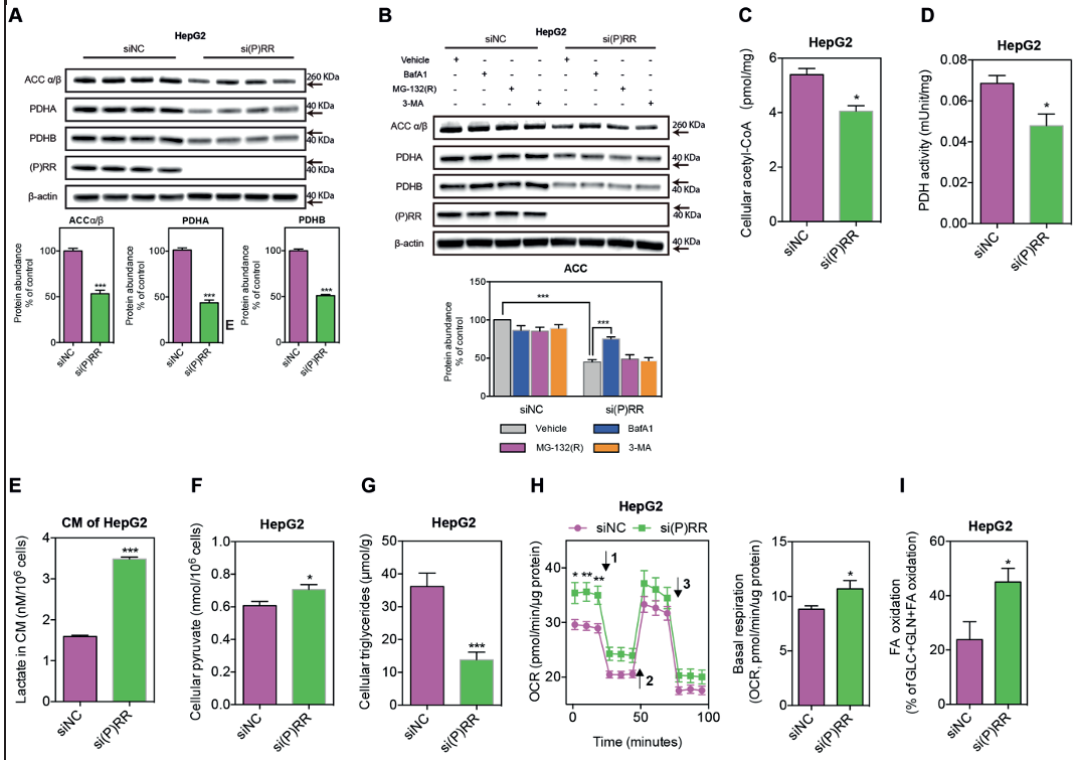

Online Figure VIII. Silencing the (P)RR in HepG2 cells reduces ACC and PDH protein abundance resulting in increased oxygen consumption and dependency on fatty acid as fuel source. (A) (P)RR expression was silenced in HepG2 cells and a representative blot of 3 independent experiments in quadruplicate is shown. Total cell lysates were immunoblotted as indicated, and the level of PDHA, PDHB, and ACCα/β protein was quantified and normalized to the level of β-actin in the same lysate. ***: p<0.001. **(B)** HepG2 cells were transfected with control or (P)RR siRNAs for 48h. Cell were incubated with vehicle control, 100 nmol/L bafilomycin A1 (BafA1), 7.5 mmol/L 3-3-Methyladenine, and 20 µmol/L MG-132(R) for 8 hours. A representative blot of 4 independent experiments and corresponding quantification is shown. **(C-G)** To measure cellular metabolites, HepG2 cells were transfected with control siRNA (siNC) or siRNA against (P)RR [si(P)RR] for 48 hours. Subsequently, cells or medium were prepared as described to measure intracellular acetyl-CoA levels **(C)**, PDH activity **(D)**, lactate levels in the conditional medium (CM) **(E)**, intracellular pyruvate levels **(F)**, and intracellular triglyceride levels **(G)**. Three independent experiments in triplicate were performed for each measurement and values were corrected with either the amount of protein or number of cells. N=9 per group; *: p<0.05; ***: p<0.001. **(H-I)** Cellular oxygen consumption rates (OCR) **(H)** and fuel dependency **(I)** were measured in HepG2 cells treated with siNC or si(P)RR for 48 hours. Arrow 1-3 indicates addition of oligomycin, FCCP and the mixture of rotenone and antimycin, respectively. N=6 per group. *: p<0.05; **: p<0.01.

References

1. Seth PP, Siwkowski A, Allerson CR, Vasquez G, Lee S, Prakash TP, Kinberger G, Migawa MT, Gaus H, Bhat B, Swayze EE. Design, synthesis and evaluation of constrained methoxyethyl (cmoe) and constrained ethyl (cet) nucleoside analogs. Nucleic Acids Symp Ser (Oxf). 2008:553-554
2. Prakash TP, Yu J, Migawa MT, et al. Comprehensive structure-activity relationship of triantennary n-acetylgalactosamine conjugated antisense oligonucleotides for targeted delivery to hepatocytes. J Med Chem. 2016;59:2718-2733
3. Bowe JE, Franklin ZJ, Hauge-Evans AC, King AJ, Persaud SJ, Jones PM. Metabolic phenotyping guidelines: Assessing glucose homeostasis in rodent models. J Endocrinol. 2014;222:G13-25
4. Wagschal A, Najafi-Shoushtari SH, Wang L, et al. Genome-wide identification of microrna regulating cholesterol and triglyceride homeostasis. Nat Med. 2015;21:1290-1297
5. Roche-Molina M, Sanz-Rosa D, Cruz FM, Garcia-Prieto J, Lopez S, Abia R, Muriana FJ, Fuster V, Ibanez B, Bernal JA. Induction of sustained hypercholesterolemia by single adeno-associated virus-mediated gene transfer of mutant hpcsk9. Arterioscler Thromb Vasc Biol. 2015;35:50-59
6. Franckhauser S, Munoz S, Elias I, Ferre T, Bosch F. Adipose overexpression of phosphoenolpyruvate carboxykinase leads to high susceptibility to diet-induced insulin resistance and obesity. Diabetes. 2006;55:273-280
7. Thatcher SE, Zhang X, Howatt DA, Lu H, Gurley SB, Daugherty A, Cassis LA. Angiotensin-converting enzyme 2 deficiency in whole body or bone marrow-derived cells increases atherosclerosis in low-density lipoprotein receptor-/- mice. Arterioscler Thromb Vasc Biol. 2011;31:758-765
8. Lu H, Howatt DA, Balakrishnan A, Graham MJ, Mullick AE, Daugherty A. Hypercholesterolemia induced by a pcsk9 gain-of-function mutation augments angiotensin ii-induced abdominal aortic aneurysms in c57bl/6 mice-brief report. Arterioscler Thromb Vasc Biol. 2016;36:1753-1757
9. Pertea M, Kim D, Pertea GM, Leek JT, Salzberg SL. Transcript-level expression analysis of rna-seq experiments with hisat, stringtie and ballgown. Nat Protoc. 2016;11:1650-1667
10. Kim D, Langmead B, Salzberg SL. Hisat: A fast spliced aligner with low memory requirements. Nat Methods. 2015;12:357-360
11. Frazee AC, Pertea G, Jaffe AE, Langmead B, Salzberg SL, Leek JT. Ballgown bridges the gap between transcriptome assembly and expression analysis. Nat Biotechnol. 2015;33:243-246
12. Huang DW, Sherman BT, Tan Q, Kir J, Liu D, Bryant D, Guo Y, Stephens R, Baseler MW, Lane HC, Lempicki RA. David bioinformatics resources: Expanded annotation database and novel algorithms to better extract biology from large gene lists. Nucleic Acids Res. 2007;35:W169-175
13. Severgnini M, Sherman J, Sehgal A, Jayaprakash NK, Aubin J, Wang G, Zhang L, Peng CG, Yucius K, Butler J, Fitzgerald K. A rapid two-step method for isolation of functional primary mouse hepatocytes: Cell characterization and asialoglycoprotein receptor based assay development. Cytotechnology. 2012;64:187-195
14. Folch J, Lees M, Sloane Stanley GH. A simple method for the isolation and purification of total lipides from animal tissues. J Biol Chem. 1957;226:497-509

Online Table III

Gene Name	Protein Accession	Description	Fold Change	pval	qval
Kyat3	NM_173763	kynurenine--oxoglutarate transaminase 3 isoform 2	0.0029	4.76E-02	8.62E-01
Vegfa	NM_001025250	vascular endothelial growth factor A isoform 1	0.0173	1.68E-03	5.12E-01
Tomm40	NM_016871	mitochondrial import receptor subunit TOM40 homolog	0.0425	1.96E-03	5.12E-01
Rai14	NM_030690	ankycorbin	0.0489	2.79E-03	5.12E-01
Keg1	NM_029550	glycine N-acyltransferase-like protein Keg1	0.0562	1.24E-03	5.12E-01
Hsf1	NM_001331154	heat shock factor protein 1 isoform alpha	0.0591	1.29E-02	7.15E-01
Fam114a2	NM_001168668	protein FAM114A2 isoform 1	0.0614	7.53E-03	6.58E-01
Vegfa	NM_009505	vascular endothelial growth factor A isoform 2	0.0643	4.03E-04	4.23E-01
Akt1	NM_001331107	RAC-alpha serine/threonine-protein kinase isoform 1	0.1002	8.24E-03	6.67E-01
Irak1	NM_001177975	interleukin-1 receptor-associated kinase 1 isoform 3	0.1096	3.64E-03	6.07E-01
H2-Q9	NM_001201460	H-2 class I histocompatibility antigen, Q9 alpha chain precursor	0.1679	4.89E-02	8.62E-01
Chn2	NM_001163640	beta-chimaerin isoform 2	0.1699	1.41E-03	5.12E-01
Zmym5	NM_144842	zinc finger MYM-type protein 5	0.1721	2.65E-02	7.81E-01
Slc39a14	NM_001135152	zinc transporter ZIP14 isoform a precursor	0.1898	1.48E-02	7.41E-01
Atp6ap2	NM_027439	renin receptor precursor	0.1979	1.38E-03	5.12E-01
Mapk8ip3	NM_001163448	C-Jun-amino-terminal kinase-interacting protein 3 isoform c	0.2059	4.25E-03	6.37E-01
Mup1	NM_001163011	major urinary protein 1 isoform a precursor	0.2155	3.81E-02	8.34E-01
Cish	NM_009895	cytokine-inducible SH2-containing protein isoform 1	0.2173	1.49E-02	7.41E-01
Zfp809	NR_028420	zinc finger protein 809	0.2179	1.04E-02	6.67E-01
Rnf152	NM_001160368	E3 ubiquitin-protein ligase RNF152	0.2184	4.57E-02	8.62E-01
Mpst	NM_001162492	3-mercaptopyruvate sulfurtransferase	0.2360	7.24E-03	6.55E-01
Sik3	NM_027498	serine/threonine-protein kinase SIK3	0.2400	8.43E-03	6.67E-01
Nr4a1	NM_010444	nuclear receptor subfamily 4 group A member 1	0.2613	3.73E-02	8.34E-01
Ethe1	NM_023154	persulfide dioxygenase ETHE1, mitochondrial precursor	0.2640	2.77E-02	7.81E-01
Gbe1	NM_028803	1,4-alpha-glucan-branching enzyme	0.2663	5.86E-03	6.55E-01
Pex16	NR_028114	peroxisomal biogenesis factor 16	0.2671	2.89E-02	7.81E-01
Larp4b	NM_001311117	la-related protein 4B isoform 2	0.2706	4.57E-02	8.62E-01
Cdk16	NM_011049	cyclin-dependent kinase 16 isoform 1	0.2959	7.47E-03	6.58E-01

Ly6e	NM_008529	lymphocyte antigen 6E precursor	0.2960	3.09E-02	7.81E-01
Scnn1a	NM_011324	amiloride-sensitive sodium channel subunit alpha	0.2967	2.95E-02	7.81E-01
Gtf2i	NM_001080746	general transcription factor II-I isoform 1	0.3069	3.65E-02	8.34E-01
Fam46a	NM_001160379	protein FAM46A isoform 2	0.3109	4.66E-02	8.62E-01
Wnk1	NM_001185021	serine/threonine-protein kinase WNK1 isoform 3	0.3123	1.64E-02	7.50E-01
Car3	NM_007606	carbonic anhydrase 3	0.3140	5.20E-03	6.55E-01
Rnf125	NM_026301	E3 ubiquitin-protein ligase RNF125	0.3224	8.70E-03	6.67E-01
Cd59a	NM_001111060	CD59A glycoprotein precursor	0.3252	3.08E-02	7.81E-01
Ddah1	NM_026993	N(G),N(G)-dimethylarginine dimethylaminohydrolase 1	0.3355	1.81E-02	7.62E-01
Atxn7l3	NM_001098836	ataxin-7-like protein 3 isoform a	0.3381	3.24E-02	8.05E-01
Mink1	NM_001045964	misshapen-like kinase 1 isoform 4	0.3502	1.45E-02	7.41E-01
Mir7085	NR_106053	microRNA 7085(Mir7085)	0.3578	3.70E-02	8.34E-01
Bud13	NM_146000	BUD13 homolog	0.3604	1.60E-02	7.50E-01
Immp2l	NM_053122	mitochondrial inner membrane protease subunit 2	0.3606	3.60E-03	6.07E-01
Lin7a	NM_001039354	protein lin-7 homolog A isoform 1	0.3667	2.20E-02	7.62E-01
Gphn	NM_145965	gephyrin isoform 1	0.3750	2.60E-03	5.12E-01
Dpyd	NM_170778	dihydropyrimidine dehydrogenase [NADP(+)]	0.3813	1.37E-02	7.34E-01
Txnl4b	NM_175646	thioredoxin-like protein 4B	0.4009	4.76E-02	8.62E-01
Tcea3	NM_011542	transcription elongation factor A protein 3	0.4076	4.19E-02	8.44E-01
Car1	NM_009799	carbonic anhydrase 1	0.4141	1.93E-02	7.62E-01
Nip7	NM_025391	60S ribosome subunit biogenesis protein NIP7 homolog isoform 1	0.4190	2.46E-02	7.81E-01
Ppp1r3g	NM_029628	protein phosphatase 1 regulatory subunit 3G	0.4208	1.75E-02	7.62E-01
Inca1	NM_001252483	protein INCA1 isoform 1	0.4261	8.66E-03	6.67E-01
Spp1	NM_009263	osteopontin isoform 4 precursor	0.4348	1.88E-03	5.12E-01
Lmf1	NM_029624	lipase maturation factor 1	0.4386	5.11E-03	6.55E-01
Def8	NM_054046	differentially expressed in FDCP 8 isoform 3	0.4428	3.85E-02	8.34E-01
Tlcd2	NM_027249	TLC domain-containing protein 2 isoform 1	0.4435	2.75E-02	7.81E-01
Hmgb3	NM_008253	high mobility group protein B3	0.4460	3.70E-02	8.34E-01
Atg9a	NM_001003917	autophagy-related protein 9A isoform a	0.4465	3.91E-02	8.34E-01
Wwox	NM_019573	WW domain-containing oxidoreductase	0.4550	1.40E-02	7.39E-01
Ppp4r1	NM_001114131	serine/threonine-protein phosphatase 4 regulatory subunit 1 isoform b	0.4599	1.92E-02	7.62E-01

Them7	NM_028747	uncharacterized protein LOC74088 isoform 1	0.4609	1.20E-02	6.82E-01
S100a11	NM_016740	protein S100-A11	0.4760	2.70E-02	7.81E-01
Mdfic	NM_175088	myoD family inhibitor domain-containing protein	0.4761	7.19E-03	6.55E-01
Tshz2	NM_080455	teashirt homolog 2	0.4845	2.18E-02	7.62E-01
Tprkb	NM_176842	EKC/KEOPS complex subunit Tprkb	0.4865	1.44E-02	7.41E-01
Atp8b1	NM_001001488	phospholipid-transporting ATPase IC	0.4879	9.05E-03	6.67E-01
Mir682	NR_030451	microRNA 682	0.4896	3.35E-02	8.10E-01
0610031O16Rik	NR_045760	RIKEN cDNA 0610031O16 gene	0.4915	2.21E-02	7.62E-01
Aspg	NM_001081169	60 kDa lysophospholipase	0.4969	2.86E-02	7.81E-01
Rogdi	NM_133185	protein rogdi homolog	0.4972	2.73E-03	5.12E-01
1500017E21Rik	NR_033510	RIKEN cDNA 1500017E21 gene	0.4997	4.72E-02	8.62E-01
D2hgdh	NM_178882	D-2-hydroxyglutarate dehydrogenase, mitochondrial isoform 2 precursor	0.4997	2.16E-02	7.62E-01
Swi5	NM_001290552	DNA repair protein SWI5 homolog isoform a	0.5024	2.45E-02	7.81E-01
Selenbp1	NM_009150	selenium-binding protein 1	0.5071	2.81E-02	7.81E-01
Cox16	NM_001309809	cytochrome c oxidase assembly protein COX16 homolog, mitochondrial isoform 3	0.5145	2.71E-02	7.81E-01
Csrp3	NM_013808	cysteine and glycine-rich protein 3	0.5152	2.03E-02	7.62E-01
Exoc4	NM_009148	exocyst complex component 4	0.5166	1.60E-02	7.50E-01
Gpr146	NM_030258	probable G-protein coupled receptor 146 isoform 1	0.5173	2.85E-02	7.81E-01
Slc6a12	NM_133661	sodium- and chloride-dependent betaine transporter	0.5316	3.78E-02	8.34E-01
Cyp2d40	NM_023623	cytochrome P450, family 2, subfamily d, polypeptide 40	0.5336	3.26E-02	8.05E-01
Pygl	NM_133198	glycogen phosphorylase, liver form	0.5356	3.95E-02	8.34E-01
Palmd	NM_023245	palmdelphin	0.5358	3.79E-02	8.34E-01
Actr10	NM_019785	actin-related protein 10	0.5363	1.04E-02	6.67E-01
Macrod1	NM_134147	O-acetyl-ADP-ribose deacetylase MACROD1	0.5406	1.70E-02	7.56E-01
Bdh2	NM_001172055	3-hydroxybutyrate dehydrogenase type 2 isoform 1	0.5458	1.64E-02	7.50E-01
Copg2	NM_017478	coatomer subunit gamma-2	0.5462	2.01E-02	7.62E-01
Ppp2r5c	NM_001081458	serine/threonine-protein phosphatase 2A 56 kDa regulatory subunit gamma isoform isoform c	0.5464	2.99E-02	7.81E-01
Ints6	NM_008715	integrator complex subunit 6	0.5494	1.09E-02	6.70E-01
Lyz2	NM_017372	lysozyme C-2 precursor	0.5520	4.46E-02	8.54E-01

Alas2	NM_009653	5-aminolevulinate synthase, erythroid-specific, mitochondrial isoform a	0.5528	9.81E-03	6.67E-01
Mlxipl	NM_021455	carbohydrate-responsive element-binding protein	0.5573	3.35E-02	8.10E-01
Reep6	NM_139292	receptor expression-enhancing protein 6 isoform 1	0.5577	4.90E-02	8.62E-01
Ccpg1os	NM_001198789	uncharacterized protein C15orf65 homolog	0.5590	6.54E-03	6.55E-01
Cyp2j6	NM_010008	cytochrome P450 2J6	0.5604	2.67E-02	7.81E-01
Slc2a9	NM_001012363	solute carrier family 2, facilitated glucose transporter member 9 isoform 2	0.5607	4.24E-02	8.45E-01
Tex2	NM_198292	testis-expressed sequence 2 protein	0.5647	5.97E-03	6.55E-01
Acmsd	NM_001033041	2-amino-3-carboxymuconate-6-semialdehyde decarboxylase	0.5657	2.96E-02	7.81E-01
Ptbp1	NM_001077363	polypyrimidine tract-binding protein 1 isoform 1	0.5679	1.47E-02	7.41E-01
Necab1	NM_178617	N-terminal EF-hand calcium-binding protein 1	0.5705	4.19E-02	8.44E-01
Ttc39c	NM_028341	tetratricopeptide repeat protein 39C	0.5730	3.11E-02	7.81E-01
Mtmr1	NM_016985	myotubularin-related protein 1 isoform A	0.5738	2.42E-02	7.81E-01
Tmem11	NM_001168507	transmembrane protein 11, mitochondrial isoform 2	0.5753	7.11E-03	6.55E-01
Decr1	NM_026172	2,4-dienoyl-CoA reductase, mitochondrial precursor	0.5768	4.94E-02	8.63E-01
Mmp19	NM_001164197	matrix metalloproteinase-19 isoform 2	0.5771	6.99E-03	6.55E-01
Cers2	NM_001320492	ceramide synthase 2	0.5773	4.34E-02	8.45E-01
Pxmp2	NM_008993	peroxisomal membrane protein 2	0.5779	4.15E-02	8.42E-01
Dcxr	NM_026428	L-xylulose reductase	0.5832	3.40E-02	8.12E-01
4930539J05Rik	NR_030689	RIKEN cDNA 4930539J05 gene	0.5862	2.49E-02	7.81E-01
Adipor2	NM_197985	adiponectin receptor protein 2	0.5897	1.87E-02	7.62E-01
Rbmxl1	NM_009033	RNA binding motif protein, X-linked-like-1	0.5900	1.67E-03	5.12E-01
Apoa2	NM_001305550	apolipoprotein A-II preproprotein	0.5959	3.83E-02	8.34E-01
Gm14403	NR_036450	predicted gene 14403	0.5976	1.81E-02	7.62E-01
BC029214	NM_153557	protein PAXX	0.6106	3.50E-02	8.21E-01
Shoc2	NM_019658	leucine-rich repeat protein SHOC-2	0.6109	3.37E-02	8.12E-01
Hspb11	NM_028394	intraflagellar transport protein 25 homolog	0.6126	2.21E-02	7.62E-01
Fdxr	NM_007997	NADPH:adrenodoxin oxidoreductase, mitochondrial precursor	0.6166	3.99E-02	8.34E-01
Ppfibp1	NM_026221	liprin-beta-1 isoform 2	0.6210	4.21E-03	6.37E-01
Etfa	NM_145615	electron transfer flavoprotein subunit alpha, mitochondrial	0.6219	1.93E-02	7.62E-01
Raf1	NM_029780	RAF proto-oncogene serine/threonine-protein kinase	0.6227	1.28E-02	7.15E-01

Rbbp6	NM_011247	E3 ubiquitin-protein ligase RBBP6 isoform 1	0.6229	1.07E-02	6.67E-01
Gsdmd	NM_026960	gasdermin-D	0.6243	4.67E-02	8.62E-01
Stra6l	NM_028788	uncharacterized protein LOC74152 isoform 1	0.6261	1.04E-02	6.67E-01
Vps13d	NM_001276465	vacuolar protein sorting-associated protein 13D isoform 2	0.6302	9.47E-03	6.67E-01
Tagln	NM_011526	transgelin	0.6310	4.90E-02	8.62E-01
Btg1	NM_007569	protein BTG1	0.6328	1.18E-02	6.82E-01
Rpl34	NM_001287581	60S ribosomal protein L34	0.6359	1.10E-02	6.70E-01
Sardh	NM_138665	sarcosine dehydrogenase, mitochondrial	0.6417	1.79E-02	7.62E-01
Usmg5	NM_023211	up-regulated during skeletal muscle growth protein 5	0.6420	6.22E-03	6.55E-01
Dnm1l	NM_001025947	dynamin-1-like protein isoform b	0.6430	4.19E-02	8.44E-01
Zfp146	NM_011980	zinc finger protein OZF	0.6468	9.55E-03	6.67E-01
Fubp1	NM_057172	far upstream element-binding protein 1	0.6477	1.57E-02	7.50E-01
Pyroxd2	NM_029011	pyridine nucleotide-disulfide oxidoreductase domain-containing protein 2	0.6566	2.67E-02	7.81E-01
Cpq	NM_176073	carboxypeptidase Q precursor	0.6582	3.31E-02	8.07E-01
Frmd8	NM_026169	FERM domain-containing protein 8	0.6583	4.83E-02	8.62E-01
Mafk	NM_010757	transcription factor MafK	0.6599	1.68E-03	5.12E-01
Ppp3ca	NM_001293622	serine/threonine-protein phosphatase 2B catalytic subunit alpha isoform isoform 2	0.6614	2.07E-02	7.62E-01
Shc1	NM_011368	SHC-transforming protein 1 isoform b	0.6643	3.91E-02	8.34E-01
Chd1	NM_007690	chromodomain-helicase-DNA-binding protein 1	0.6680	4.90E-02	8.62E-01
Pex11b	NM_011069	peroxisomal membrane protein 11B isoform 1	0.6686	3.51E-02	8.21E-01
Trp53	NM_011640	cellular tumor antigen p53 isoform a	0.6687	1.27E-02	7.13E-01
Gramd1c	NM_153528	GRAM domain-containing protein 1C	0.6692	3.02E-02	7.81E-01
Klf2	NM_008452	Krueppel-like factor 2	0.6735	9.60E-03	6.67E-01
Sparc	NM_009242	SPARC precursor	0.6904	2.01E-02	7.62E-01
Slc37a4	NM_008063	glucose-6-phosphate exchanger SLC37A4	0.6920	4.54E-02	8.62E-01
Fmc1	NM_025363	UPF0562 protein C7orf55 homolog	0.6922	2.54E-02	7.81E-01
Lyrm5	NM_133688	electron transfer flavoprotein regulatory factor 1	0.6972	3.63E-02	8.34E-01
Gm12070	NR_002890	glyceraldehyde-3-phosphate dehydrogenase pseudogene(Gm12070)	0.7003	4.01E-02	8.34E-01
Ugt1a6b	NM_201410	UDP glucuronosyltransferase 1 family, polypeptide A6B precursor	0.7027	3.40E-02	8.12E-01

Mrpl47	NM_029017	39S ribosomal protein L47, mitochondrial	0.7047	2.82E-02	7.81E-01
Cps1	NM_001080809	carbamoyl-phosphate synthase [ammonia], mitochondrial precursor	0.7064	2.17E-02	7.62E-01
Fbxl5	NM_001159963	F-box/LRR-repeat protein 5 isoform A	0.7074	4.26E-02	8.45E-01
Lgals8	NM_001199043	galectin-8 isoform 1	0.7130	1.99E-02	7.62E-01
Pigx	NM_024464	phosphatidylinositol-glycan biosynthesis class X protein isoform 1 precursor	0.7152	3.49E-02	8.21E-01
Fam32a	NM_026455	protein FAM32A	0.7162	1.47E-02	7.41E-01
Irf6	NM_016851	interferon regulatory factor 6	0.7225	1.04E-02	6.67E-01
Cox14	NM_183256	cytochrome c oxidase assembly protein COX14	0.7227	2.50E-02	7.81E-01
Map4	NM_001205330	microtubule-associated protein 4 isoform 1	0.7245	1.79E-02	7.62E-01
Oma1	NM_025909	metalloendopeptidase OMA1, mitochondrial precursor	0.7264	4.07E-02	8.35E-01
Tmem9b	NM_020050	transmembrane protein 9B precursor	0.7265	3.27E-02	8.05E-01
Tbl1x	NM_020601	F-box-like/WD repeat-containing protein TBL1X	0.7268	4.82E-02	8.62E-01
Prdx5	NM_012021	peroxiredoxin-5, mitochondrial precursor	0.7297	1.06E-02	6.67E-01
Eif3f	NM_025344	eukaryotic translation initiation factor 3 subunit F	0.7334	1.61E-02	7.50E-01
Oxld1	NM_025560	oxidoreductase-like domain-containing protein 1	0.7362	4.07E-02	8.35E-01
Commd4	NM_025417	COMM domain-containing protein 4	0.7368	2.90E-02	7.81E-01
Mrps30	NM_021556	28S ribosomal protein S30, mitochondrial	0.7415	3.04E-02	7.81E-01
Ncor1	NM_001252313	nuclear receptor corepressor 1 isoform 1	0.7494	8.52E-03	6.67E-01
Plekhj1	NM_023900	pleckstrin homology domain-containing family J member 1	0.7544	4.86E-02	8.62E-01
Baat	NM_007519	bile acid-CoA:amino acid N-acyltransferase	0.7549	2.95E-02	7.81E-01
Wipi2	NM_178398	WD repeat domain phosphoinositide-interacting protein 2	0.7608	1.80E-02	7.62E-01
Tars	NM_033074	threonine--tRNA ligase, cytoplasmic	0.7654	2.51E-02	7.81E-01
Yy1	NM_009537	transcriptional repressor protein YY1	0.7661	2.49E-02	7.81E-01
Clybl	NM_029556	citrate lyase subunit beta-like protein, mitochondrial precursor	0.7715	1.17E-02	6.82E-01
Cfhr1	NM_015780	complement factor H-related 1 precursor	0.7751	3.17E-03	5.65E-01
Dapk3	NM_001190474	death-associated protein kinase 3 isoform a	0.7778	3.43E-02	8.13E-01
C8g	NM_027062	complement component C8 gamma chain isoform 1 precursor	0.7784	2.04E-02	7.62E-01
Zc3h18	NM_001029994	zinc finger CCCH domain-containing protein 18 isoform b	0.7796	3.00E-02	7.81E-01
Usp47	NM_133758	ubiquitin carboxyl-terminal hydrolase 47 isoform 2	0.7815	3.09E-02	7.81E-01
Isca1	NM_026921	iron-sulfur cluster assembly 1 homolog, mitochondrial precursor	0.7820	5.71E-03	6.55E-01

Psmd11	NM_178616	26S proteasome non-ATPase regulatory subunit 11	0.7835	2.83E-02	7.81E-01
Zfp706	NM_026521	zinc finger protein 706	0.7863	1.18E-02	6.82E-01
Dxo	NM_001163770	decapping and exoribonuclease protein	0.7886	4.46E-02	8.54E-01
Bola1	NM_026975	bolA-like protein 1	0.7923	1.30E-03	5.12E-01
Psmg2	NM_134138	proteasome assembly chaperone 2	0.7964	2.67E-02	7.81E-01
Pigt	NM_133779	GPI transamidase component PIG-T precursor	0.7985	4.34E-02	8.45E-01
Nsfl1c	NM_001291074	NSFL1 cofactor p47 isoform b	0.8044	2.81E-02	7.81E-01
Ugt1a6a	NM_145079	UDP-glucuronosyltransferase 1-6 precursor	0.8050	3.71E-02	8.34E-01
R3hdm4	NM_177994	R3H domain-containing protein 4	0.8054	3.97E-02	8.34E-01
Rpl10a	NM_011287	60S ribosomal protein L10a	0.8108	1.19E-02	6.82E-01
Rbm17	NM_152824	splicing factor 45	0.8120	2.96E-02	7.81E-01
Ivd	NM_019826	isovaleryl-CoA dehydrogenase, mitochondrial precursor	0.8124	3.77E-02	8.34E-01
Sympk	NM_026605	symplekin	0.8126	3.67E-02	8.34E-01
Otc	NM_008769	ornithine carbamoyltransferase, mitochondrial precursor	0.8175	4.90E-02	8.62E-01
Csnk1a1	NM_146087	casein kinase I isoform alpha	0.8184	2.21E-03	5.12E-01
Idh3b	NM_130884	isocitrate dehydrogenase [NAD] subunit beta, mitochondrial	0.8223	5.35E-03	6.55E-01
Mkln1	NM_013791	muskelin	0.8228	2.47E-02	7.81E-01
Mrps2	NM_080452	28S ribosomal protein S2, mitochondrial isoform 1	0.8236	3.96E-02	8.34E-01
Hs3st3b1	NM_018805	heparan sulfate glucosamine 3-O-sulfotransferase 3B1	0.8274	3.06E-02	7.81E-01
Ndufa10	NM_024197	NADH dehydrogenase [ubiquinone] 1 alpha subcomplex subunit 10, mitochondrial precursor	0.8288	4.75E-02	8.62E-01
Ppp1cc	NM_013636	serine/threonine-protein phosphatase PP1-gamma catalytic subunit	0.8447	3.08E-02	7.81E-01
Tnpo1	NM_178716	transportin-1 isoform 1	0.8493	2.41E-02	7.81E-01
Tnks2	NM_001163635	tankyrase-2	0.8508	6.30E-03	6.55E-01
Larp1	NM_028451	la-related protein 1	0.8602	2.70E-02	7.81E-01
Eif3h	NM_080635	eukaryotic translation initiation factor 3 subunit H	0.8627	1.07E-02	6.67E-01
Arpc3	NM_019824	actin-related protein 2/3 complex subunit 3	0.8649	2.29E-02	7.73E-01
Scamp2	NM_022813	secretory carrier-associated membrane protein 2	0.8684	3.28E-02	8.05E-01
Rps7	NM_011300	40S ribosomal protein S7	0.8690	5.60E-03	6.55E-01
Abhd17c	NM_133722	protein ABHD17C	0.8731	4.82E-02	8.62E-01
Slc25a3	NM_133668	phosphate carrier protein, mitochondrial precursor	0.8771	4.04E-02	8.34E-01

Suclg1	NM_019879	succinate--CoA ligase [ADP/GDP-forming] subunit alpha, mitochondrial precursor	0.8775	1.87E-02	7.62E-01
Pds5a	NM_001081321	sister chromatid cohesion protein PDS5 homolog A	0.8776	8.80E-03	6.67E-01
Rpl17	NM_001002239	60S ribosomal protein L17	0.8850	1.64E-02	7.50E-01
Rps8	NM_009098	40S ribosomal protein S8	0.8898	1.11E-02	6.70E-01
Iscu	NM_025526	iron-sulfur cluster assembly enzyme ISCU, mitochondrial precursor	0.8906	1.05E-02	6.67E-01
Rps17	NM_009092	40S ribosomal protein S17	0.8937	3.08E-02	7.81E-01
Mrpl13	NM_026759	39S ribosomal protein L13, mitochondrial	0.8954	4.38E-02	8.45E-01
B230219D22Rik	NM_181278	UPF0461 protein C5orf24 homolog	0.8967	4.24E-02	8.45E-01
Gm15772	NR_003373	ribosomal protein L26 pseudogene	0.9102	4.54E-02	8.62E-01
Rpl18	NM_009077	60S ribosomal protein L18	0.9147	2.87E-02	7.81E-01
Fam8a1	NM_001033192	protein FAM8A1	0.9321	3.24E-02	8.05E-01
Dync1h1	NM_030238	cytoplasmic dynein 1 heavy chain 1	1.0898	8.76E-03	6.67E-01
Bcap31	NM_012060	B-cell receptor-associated protein 31	1.0923	4.20E-02	8.44E-01
Itgb1	NM_010578	integrin beta-1 precursor	1.1003	3.43E-02	8.13E-01
Slc25a5	NM_007451	ADP/ATP translocase 2	1.1009	4.35E-02	8.45E-01
Sec63	NM_153055	translocation protein SEC63 homolog	1.1243	2.59E-02	7.81E-01
Wdr26	NM_145514	WD repeat-containing protein 26	1.1248	9.06E-03	6.67E-01
Dhrs1	NM_026819	dehydrogenase/reductase SDR family member 1	1.1262	4.28E-02	8.45E-01
Cyp2e1	NM_021282	cytochrome P450 2E1	1.1325	6.55E-03	6.55E-01
Tbrg1	NM_025289	transforming growth factor beta regulator 1	1.1446	2.00E-02	7.62E-01
Prkar2a	NM_008924	cAMP-dependent protein kinase type II-alpha regulatory subunit	1.1446	2.05E-02	7.62E-01
Erp44	NM_029572	endoplasmic reticulum resident protein 44 precursor	1.1474	1.95E-02	7.62E-01
Poldip2	NM_026389	polymerase delta-interacting protein 2	1.1531	4.04E-02	8.34E-01
Arpc1a	NM_019767	actin-related protein 2/3 complex subunit 1A	1.1657	1.68E-02	7.52E-01
Nsmce4a	NM_001162855	non-structural maintenance of chromosomes element 4 homolog A	1.1717	3.83E-02	8.34E-01
Hacd2	NM_023587	very-long-chain (3R)-3-hydroxyacyl-CoA dehydratase 2	1.1748	5.44E-03	6.55E-01
Atp1a1	NM_144900	sodium/potassium-transporting ATPase subunit alpha-1 precursor	1.1784	1.96E-02	7.62E-01
Tmod3	NM_016963	tropomodulin-3	1.1837	4.03E-02	8.34E-01
Hnrnpa2b1	NR_104468	heterogeneous nuclear ribonucleoprotein A2/B1	1.1894	3.00E-02	7.81E-01

Slco1a1	NM_013797	solute carrier organic anion transporter family member 1A1	1.1908	2.24E-02	7.62E-01
Rrm1	NM_009103	ribonucleoside-diphosphate reductase large subunit	1.1979	3.26E-04	4.23E-01
Mtpn	NM_008098	myotrophin	1.1998	4.67E-02	8.62E-01
Sumf1	NM_145937	sulfatase-modifying factor 1 precursor	1.2001	2.60E-02	7.81E-01
Cfb	NM_008198	complement factor B isoform 1 precursor	1.2020	2.12E-02	7.62E-01
Setd5	NM_028385	SET domain-containing protein 5	1.2096	1.03E-02	6.67E-01
Sgpp1	NM_030750	sphingosine-1-phosphate phosphatase 1	1.2112	7.30E-03	6.55E-01
Acadvl	NM_017366	very long-chain specific acyl-CoA dehydrogenase, mitochondrial precursor	1.2159	2.62E-02	7.81E-01
Usp14	NM_021522	ubiquitin carboxyl-terminal hydrolase 14 isoform 1	1.2213	4.03E-02	8.34E-01
Tmx1	NM_028339	thioredoxin-related transmembrane protein 1 precursor	1.2313	4.67E-02	8.62E-01
Myo18a	NM_011586	unconventional myosin-XVIIIa isoform 2	1.2336	8.62E-03	6.67E-01
Glo1	NM_001113560	lactoylglutathione lyase	1.2366	4.85E-02	8.62E-01
Ifrd2	NM_025903	interferon-related developmental regulator 2	1.2370	2.13E-02	7.62E-01
Adam10	NM_007399	disintegrin and metalloproteinase domain-containing protein 10 preproprotein	1.2376	3.25E-02	8.05E-01
Rad21	NM_009009	double-strand-break repair protein rad21 homolog	1.2450	2.58E-02	7.81E-01
Tmem64	NM_181401	transmembrane protein 64	1.2528	3.76E-04	4.23E-01
Dync1li2	NM_001013380	cytoplasmic dynein 1 light intermediate chain 2	1.2536	3.04E-02	7.81E-01
Man1a2	NM_010763	mannosyl-oligosaccharide 1,2-alpha-mannosidase IB	1.2546	2.45E-02	7.81E-01
Sfr1	NM_026377	swi5-dependent recombination DNA repair protein 1 homolog	1.2578	2.31E-02	7.74E-01
Iars2	NM_198653	isoleucine--tRNA ligase, mitochondrial precursor	1.2588	4.62E-02	8.62E-01
Dnajc5	NR_073369	DnaJ heat shock protein family (Hsp40) member C5	1.2596	2.09E-02	7.62E-01
Mrps18c	NM_026826	28S ribosomal protein S18c, mitochondrial	1.2717	1.94E-02	7.62E-01
Slc35a3	NM_144902	UDP-N-acetylglucosamine transporter	1.2720	3.32E-02	8.08E-01
F5	NM_007976	coagulation factor V preproprotein	1.2752	1.64E-02	7.50E-01
Tm9sf1	NM_028780	transmembrane 9 superfamily member 1 precursor	1.2783	1.16E-03	5.12E-01
Syap1	NM_025932	synapse-associated protein 1	1.2828	9.02E-03	6.67E-01
Acaa2	NM_177470	3-ketoacyl-CoA thiolase, mitochondrial	1.2849	2.41E-03	5.12E-01
Selenop	NM_009155	selenoprotein P precursor	1.2880	4.10E-02	8.37E-01
Cyp2d26	NM_029562	cytochrome P450 2D26	1.2883	4.95E-02	8.63E-01
Ubqln4	NM_033526	ubiquilin-4	1.2921	5.54E-03	6.55E-01

Atp6v1g1	NM_024173	V-type proton ATPase subunit G 1	1.2930	3.82E-02	8.34E-01
Mpp6	NM_019939	MAGUK p55 subfamily member 6 isoform b	1.2940	2.64E-03	5.12E-01
Ier2	NM_010499	immediate early response gene 2 protein	1.2953	2.25E-02	7.63E-01
Cmas	NM_009908	N-acylneuraminate cytidylyltransferase	1.2988	2.54E-02	7.81E-01
Erp29	NM_026129	endoplasmic reticulum resident protein 29 precursor	1.3141	2.69E-02	7.81E-01
Sptlc1	NM_009269	serine palmitoyltransferase 1	1.3213	3.97E-02	8.34E-01
Hectd1	NM_144788	E3 ubiquitin-protein ligase HECTD1	1.3228	4.68E-02	8.62E-01
Apoa1	NM_009692	apolipoprotein A-I preproprotein	1.3279	4.91E-02	8.62E-01
Npr2	NM_173788	atrial natriuretic peptide receptor 2 precursor	1.3291	2.81E-02	7.81E-01
Heatr5a	NM_177171	HEAT repeat-containing protein 5A	1.3371	4.21E-02	8.44E-01
Anxa7	NM_001110794	annexin A7	1.3375	1.40E-02	7.39E-01
Chmp3	NM_025783	charged multivesicular body protein 3	1.3385	8.46E-03	6.67E-01
Hadha	NM_178878	trifunctional enzyme subunit alpha, mitochondrial precursor	1.3397	2.33E-03	5.12E-01
Ifi30	NM_023065	gamma-interferon-inducible lysosomal thiol reductase precursor	1.3451	3.74E-02	8.34E-01
Polr2a	NM_001291068	DNA-directed RNA polymerase II subunit RPB1	1.3455	1.47E-03	5.12E-01
Wwc1	NM_170779	protein KIBRA	1.3465	1.47E-02	7.41E-01
Kdm6b	NM_001017426	lysine-specific demethylase 6B	1.3544	3.58E-02	8.30E-01
Arhgap5	NM_009706	rho GTPase-activating protein 5	1.3558	3.65E-02	8.34E-01
Sra1	NM_025291	steroid receptor RNA activator 1 isoform a	1.3639	1.97E-02	7.62E-01
Dap	NM_146057	death-associated protein 1	1.3657	2.62E-02	7.81E-01
Itch	NM_008395	E3 ubiquitin-protein ligase Itchy	1.3659	2.80E-04	4.23E-01
Ncoa4	NM_001033988	nuclear receptor coactivator 4 isoform a	1.3870	3.62E-02	8.34E-01
Pacsin3	NM_028733	protein kinase C and casein kinase II substrate protein 3	1.4191	3.00E-02	7.81E-01
Fmo1	NM_010231	dimethylaniline monooxygenase [N-oxide-forming] 1 isoform 1	1.4219	3.23E-03	5.65E-01
Kctd2	NM_183285	BTB/POZ domain-containing protein KCTD2	1.4234	4.79E-02	8.62E-01
Nnt	NM_001308506	NAD(P) transhydrogenase, mitochondrial isoform 2	1.4256	1.03E-02	6.67E-01
Trappc2l	NM_021502	trafficking protein particle complex subunit 2-like protein	1.4317	2.80E-02	7.81E-01
Gpc4	NM_008150	glypican-4 precursor	1.4323	3.87E-02	8.34E-01
Cxcl12	NM_001012477	stromal cell-derived factor 1 isoform gamma precursor	1.4328	4.35E-02	8.45E-01
Mpp1	NM_008621	55 kDa erythrocyte membrane protein	1.4336	4.87E-02	8.62E-01

Ufl1	NM_026194	E3 UFM1-protein ligase 1	1.4484	2.24E-02	7.62E-01
Ap3m1	NM_018829	AP-3 complex subunit mu-1	1.4487	3.88E-02	8.34E-01
Xdh	NM_011723	xanthine dehydrogenase/oxidase	1.4517	1.05E-02	6.67E-01
Ppp2r5c	NM_001135001	serine/threonine-protein phosphatase 2A 56 kDa regulatory subunit gamma isoform isoform d	1.4586	1.21E-02	6.82E-01
Tmem131	NM_018872	transmembrane protein 131	1.4663	2.79E-03	5.12E-01
Lsm14b	NM_177727	protein LSM14 homolog B	1.4674	2.03E-02	7.62E-01
Lgals3bp	NM_011150	galectin-3-binding protein precursor	1.4702	4.37E-03	6.42E-01
Ptdss1	NM_008959	phosphatidylserine synthase 1	1.4741	1.47E-02	7.41E-01
Tmem86a	NM_026436	lysoplasmalogenase-like protein TMEM86A	1.4766	2.05E-02	7.62E-01
Slc46a3	NM_027872	solute carrier family 46 member 3 precursor	1.4778	4.90E-02	8.62E-01
Zmym5	NM_001253753	zinc finger MYM-type protein 5	1.4807	3.89E-02	8.34E-01
Psip1	NM_133948	PC4 and SFRS1-interacting protein isoform 1	1.4823	2.65E-02	7.81E-01
Tmed3	NM_025360	transmembrane emp24 domain-containing protein 3 precursor	1.4844	1.92E-02	7.62E-01
Dnajc10	NM_024181	dnaJ homolog subfamily C member 10 precursor	1.4895	1.44E-03	5.12E-01
Ipmk	NM_027184	inositol polyphosphate multikinase	1.4914	3.47E-02	8.19E-01
Zhx3	NM_177263	zinc fingers and homeoboxes protein 3	1.4961	7.24E-03	6.55E-01
Dcn	NM_007833	decorin preproprotein	1.4999	3.54E-02	8.22E-01
Rbm3	NM_001293658	RNA-binding protein 3 isoform 1	1.5020	3.52E-02	8.21E-01
Alcam	NM_009655	CD166 antigen isoform 1 precursor	1.5190	1.81E-04	4.23E-01
Gbp7	NM_001083312	guanylate binding protein 7	1.5239	2.19E-02	7.62E-01
Ctbs	NM_001293672	di-N-acetylchitobiase isoform 1 precursor	1.5243	4.64E-02	8.62E-01
Slc35g1	NM_175507	solute carrier family 35 member G1	1.5379	4.68E-02	8.62E-01
Fabp1	NM_017399	fatty acid-binding protein, liver	1.5436	1.83E-02	7.62E-01
Slk	NM_009289	STE20-like serine/threonine-protein kinase isoform 1	1.5457	1.14E-02	6.81E-01
Hipk3	NM_010434	homeodomain-interacting protein kinase 3 isoform 1	1.5477	4.31E-02	8.45E-01
Cad	NM_023525	CAD protein isoform 1	1.5559	3.79E-02	8.34E-01
Clec1b	NM_019985	C-type lectin domain family 1 member B isoform 1	1.5560	2.70E-02	7.81E-01
Spryd4	NM_025716	SPRY domain-containing protein 4	1.5584	5.47E-03	6.55E-01
Acadl	NM_007381	long-chain specific acyl-CoA dehydrogenase, mitochondrial precursor	1.5594	5.96E-03	6.55E-01
Pzp	NM_007376	pregnancy zone protein precursor	1.5598	2.84E-02	7.81E-01

Cdip1	NM_025670	cell death-inducing p53-target protein 1	1.5646	2.65E-03	5.12E-01
Lurap1l	NM_026821	leucine rich adaptor protein 1-like	1.5670	4.86E-02	8.62E-01
Hook1	NM_030014	protein Hook homolog 1	1.5716	7.03E-03	6.55E-01
Srsf4	NM_020587	serine/arginine-rich splicing factor 4	1.5828	3.15E-05	2.31E-01
Sec14l4	NM_146013	SEC14-like protein 4	1.6040	1.48E-02	7.41E-01
Spin1	NM_146043	spindlin-1 isoform 2	1.6082	4.01E-02	8.34E-01
Fcna	NM_007995	ficolin-1 precursor	1.6132	2.63E-02	7.81E-01
Pptc7	NM_177242	protein phosphatase PTC7 homolog	1.6473	6.17E-03	6.55E-01
Pde6d	NM_008801	retinal rod rhodopsin-sensitive cGMP 3',5'-cyclic phosphodiesterase subunit delta	1.6830	4.74E-02	8.62E-01
Aifm2	NM_001039194	apoptosis-inducing factor 2 isoform 2	1.6894	9.09E-04	5.12E-01
Slc25a20	NM_020520	mitochondrial carnitine/acylcarnitine carrier protein	1.6970	2.19E-02	7.62E-01
Arfgap3	NM_025445	ADP-ribosylation factor GTPase-activating protein 3	1.7002	2.76E-02	7.81E-01
Suco	NM_172645	SUN domain-containing ossification factor precursor	1.7063	4.43E-02	8.51E-01
Slc16a10	NM_001114332	monocarboxylate transporter 10 isoform 1	1.7105	1.18E-02	6.82E-01
Irf1	NM_008390	interferon regulatory factor 1 isoform a	1.7135	4.54E-02	8.62E-01
Tspyl2	NM_029836	testis-specific Y-encoded-like protein 2	1.7145	3.40E-02	8.12E-01
Slc16a12	NM_172838	monocarboxylate transporter 12	1.7274	2.23E-02	7.62E-01
Cks1b	NM_016904	cyclin-dependent kinases regulatory subunit 1	1.7580	5.07E-03	6.55E-01
Irak1	NM_008363	interleukin-1 receptor-associated kinase 1 isoform 4	1.7820	3.77E-02	8.34E-01
Slc29a1	NM_001199116	equilibrative nucleoside transporter 1 isoform 2	1.7837	1.37E-02	7.34E-01
Sirt3	NM_001177804	NAD-dependent protein deacetylase sirtuin-3 isoform 3	1.8037	1.89E-02	7.62E-01
Serinc3	NM_012032	serine incorporator 3 precursor	1.8079	4.84E-02	8.62E-01
Dhx9	NM_007842	ATP-dependent RNA helicase A	1.8281	1.01E-02	6.67E-01
Zfp703	NM_001101502	zinc finger protein 703 isoform 1	1.8608	1.54E-02	7.49E-01
Cap1	NM_007598	adenylyl cyclase-associated protein 1	1.8621	2.36E-02	7.81E-01
Slc25a13	NM_001177572	calcium-binding mitochondrial carrier protein Aralar2 isoform 2	1.8789	7.24E-03	6.55E-01
Cln6	NM_001033175	ceroid-lipofuscinosis neuronal protein 6	1.8823	3.12E-02	7.81E-01
Cmpk2	NM_020557	UMP-CMP kinase 2, mitochondrial precursor	1.9072	7.31E-03	6.55E-01
Mcm2	NM_008564	DNA replication licensing factor MCM2	1.9089	1.89E-02	7.62E-01

Sult1d1	NM_016771	sulfotransferase 1 family member D1	1.9387	6.92E-03	6.55E-01
Mir22hg	NR_030711	Mir22 host gene (non-protein coding)	1.9430	1.50E-02	7.42E-01
Gemin2	NM_025656	gem-associated protein 2	1.9651	3.90E-03	6.09E-01
Ifit3	NM_010501	interferon-induced protein with tetratricopeptide repeats 3	1.9673	7.71E-03	6.66E-01
Inhbc	NM_010565	inhibin beta C chain preproprotein	2.0562	2.94E-02	7.81E-01
Abhd6	NM_001331064	monoacylglycerol lipase ABHD6 isoform 1	2.0623	3.88E-03	6.09E-01
Stat2	NM_019963	signal transducer and activator of transcription 2	2.0800	1.67E-02	7.52E-01
Plpp5	NM_028000	phospholipid phosphatase 5 isoform 1	2.0802	2.04E-02	7.62E-01
P4ha2	NM_001136076	prolyl 4-hydroxylase subunit alpha-2 isoform 1 precursor	2.1283	2.87E-02	7.81E-01
Golga2	NM_133852	golgin subfamily A member 2 isoform a	2.1368	1.53E-02	7.49E-01
Cd163	NM_001170395	scavenger receptor cysteine-rich type 1 protein M130 isoform 1 precursor	2.1647	4.12E-02	8.37E-01
Hsdl2	NM_024255	hydroxysteroid dehydrogenase-like protein 2 isoform 1	2.1779	4.08E-02	8.35E-01
Clec2d	NM_053109	C-type lectin domain family 2 member D	2.2068	1.76E-02	7.62E-01
Atxn7l3	NM_001098837	ataxin-7-like protein 3 isoform b	2.2307	3.73E-02	8.34E-01
Igf1	NM_001111276	insulin-like growth factor I isoform 5 precursor	2.2524	3.74E-03	6.09E-01
Por	NM_008898	NADPH--cytochrome P450 reductase	2.2881	1.35E-02	7.33E-01
Gin1	NM_026250	gypsy retrotransposon integrase-like protein 1 isoform 1	2.2909	1.05E-02	6.67E-01
Cpeb2	NM_001177379	cytoplasmic polyadenylation element-binding protein 2 isoform 2	2.3236	2.70E-02	7.81E-01
Ifit3b	NM_001005858	interferon-induced protein with tetratricopeptide repeats 3-like	2.3317	2.48E-03	5.12E-01
Pcp4l1	NM_025557	Purkinje cell protein 4-like protein 1	2.3643	9.41E-04	5.12E-01
Rbm3	NM_001166410	RNA-binding protein 3 isoform 2	2.3717	1.75E-02	7.62E-01
Shc1	NM_001113331	SHC-transforming protein 1 isoform a	2.3869	1.58E-02	7.50E-01
Usp18	NM_011909	ubl carboxyl-terminal hydrolase 18	2.4061	5.88E-03	6.55E-01
C8a	NM_001290645	complement component C8 alpha chain isoform 2	2.4234	2.46E-02	7.81E-01
Cyp39a1	NM_018887	24-hydroxycholesterol 7-alpha-hydroxylase isoform 1	2.4420	2.20E-02	7.62E-01
Tsc22d3	NM_001077364	TSC22 domain family protein 3 isoform 1	2.4790	9.63E-03	6.67E-01
Ivns1abp	NM_054102	influenza virus NS1A-binding protein homolog isoform 2	2.5089	2.35E-02	7.81E-01
Tmem41a	NM_025693	transmembrane protein 41A precursor	2.5292	4.96E-02	8.63E-01
Irf7	NM_001252600	interferon regulatory factor 7 isoform 2	2.5961	4.32E-02	8.45E-01
Gimap9	NM_174960	GTPase, IMAP family member 9	2.6738	2.88E-02	7.81E-01

Pck1	NM_011044	phosphoenolpyruvate carboxykinase, cytosolic [GTP]	2.7370	2.42E-03	5.12E-01
Il15ra	NM_001271498	interleukin-15 receptor subunit alpha isoform 3	2.7375	2.55E-02	7.81E-01
Gss	NM_001291111	glutathione synthetase isoform b	2.7462	1.58E-03	5.12E-01
C8a	NM_001316667	complement component C8 alpha chain isoform 3 precursor	2.7556	1.97E-02	7.62E-01
Usp47	NM_177249	ubiquitin carboxyl-terminal hydrolase 47 isoform 1	2.8029	2.54E-02	7.81E-01
Ciart	NM_001033302	circadian-associated transcriptional repressor	2.8831	3.96E-02	8.34E-01
Shoc2	NM_001168505	leucine-rich repeat protein SHOC-2	2.9274	4.37E-02	8.45E-01
Plin5	NM_025874	perilipin-5	2.9994	5.69E-03	6.55E-01
Kyat3	NM_001293560	kynurenine--oxoglutarate transaminase 3 isoform1	3.0010	2.81E-02	7.81E-01
Hsf1	NM_008296	heat shock factor protein 1 isoform beta	3.0486	2.14E-02	7.62E-01
Ubtf	NM_001302955	nucleolar transcription factor 1 isoform 3	3.0897	2.74E-03	5.12E-01
Wdr45	NM_172372	WD repeat domain phosphoinositide-interacting protein 4 isoform a	3.0914	3.90E-02	8.34E-01
Ifit1	NM_008331	interferon-induced protein with tetratricopeptide repeats 1	3.1347	3.31E-02	8.07E-01
Mgme1	NM_001289630	mitochondrial genome maintenance exonuclease 1	3.1610	1.99E-03	5.12E-01
Vegfa	NM_001287058	vascular endothelial growth factor A isoform 9 precursor	3.1809	7.81E-03	6.67E-01
Cdk16	NM_001310456	cyclin-dependent kinase 16 isoform 2	3.5516	2.44E-03	5.12E-01
Snord2	NR_030705	small nucleolar RNA, C/D box 2	3.5642	2.87E-02	7.81E-01
Ap2a1	NM_007458	AP-2 complex subunit alpha-1 isoform a	3.8308	1.09E-02	6.70E-01
Vegfa	NM_001287056	vascular endothelial growth factor A isoform 7 precursor	3.8963	1.82E-02	7.62E-01
Slc19a2	NM_001276455	thiamine transporter 1 isoform b	3.9868	2.58E-03	5.12E-01
Zfp385b	NM_001113400	zinc finger protein 385B isoform 3	4.0568	1.34E-02	7.33E-01
Cyp4a31	NM_001252539	cytochrome P450, family 4, subfamily a, polypeptide 31 isoform 2	4.2487	9.44E-03	6.67E-01
Mfsd2a	NM_029662	sodium-dependent lysophosphatidylcholine symporter 1	4.2783	4.59E-02	8.62E-01
Fmo5	NM_010232	dimethylaniline monooxygenase [N-oxide-forming] 5	4.3163	6.73E-03	6.55E-01
Mtmr1	NM_001313703	myotubularin-related protein 1 isoform B	4.5761	1.58E-02	7.50E-01
Lgals8	NM_001291055	galectin-8 isoform 2	4.5841	5.45E-03	6.55E-01
Ss18	NM_001161369	protein SSXT isoform 2	4.6064	1.77E-03	5.12E-01
Fmo5	NM_001161763	dimethylaniline monooxygenase [N-oxide-forming] 5	4.7097	2.14E-02	7.62E-01
Enpp2	NM_001285994	ectonucleotide pyrophosphatase/phosphodiesterase family member 2 isoform 3	5.2148	4.37E-02	8.45E-01

Cyp4a31	NM_201640	cytochrome P450, family 4, subfamily a, polypeptide 31 isoform 1	5.5627	1.81E-04	4.23E-01
Zfp740	NM_001289690	zinc finger protein 740 isoform 1	6.1417	1.27E-03	5.12E-01
Rab3a	NM_009001	ras-related protein Rab-3A	7.3806	1.66E-02	7.52E-01
Rnf185	NR_110959	ring finger protein 185	10.9233	4.34E-02	8.45E-01
Dynll2	NM_001168472	dynein light chain 2, cytoplasmic	22.1209	8.06E-03	6.67E-01
Rai14	NM_001166408	ankycorbin	25.6938	1.38E-03	5.12E-01
Ly6e	NM_001164040	lymphocyte antigen 6E precursor	346.1442	6.70E-03	6.55E-01
Hbb-b1	NM_001278161	hemoglobin subunit beta-1	1295.3357	2.97E-02	7.81E-01

Online Table IV

Index	Protein Accession	Description	MW [kDa]	G-(P)RR_chow/G-control_chow	G-(P)RR_HFD/G-control_HFD	Regulation
1	O35728	Cytochrome P450 4A14 OS=Mus musculus GN=Cyp4a14 PE=1 SV=1 - [CP4AE_MOUSE]	58.7	0.400	0.205	DOWN
2	P56654	Cytochrome P450 2C37 OS=Mus musculus GN=Cyp2c37 PE=1 SV=2 - [CP237_MOUSE]	55.6	0.402	0.720	DOWN
3	P27786	Steroid 17-alpha-hydroxylase/17 20 lyase OS=Mus musculus GN=Cyp17a1 PE=1 SV=1 - [CP17A_MOUSE]	57.6	0.429	0.516	DOWN
4	O55137	Acyl-coenzyme A thioesterase 1 OS=Mus musculus GN=Acot1 PE=1 SV=1 - [ACOT1_MOUSE]	46.1	0.436	0.416	DOWN
5	Q05117	Tartrate-resistant acid phosphatase type 5 OS=Mus musculus GN=Acp5 PE=1 SV=2 - [PPA5_MOUSE]	36.8	0.458	0.679	DOWN
6	P06801	NADP-dependent malic enzyme OS=Mus musculus GN=Me1 PE=1 SV=2 - [MAOX_MOUSE]	63.9	0.467	0.448	DOWN
7	Q9Z1G4	V-type proton ATPase 116 kDa subunit a isoform 1 OS=Mus musculus GN=Atp6v0a1 PE=1 SV=3 - [VPP1_MOUSE]	96.4	0.475	0.542	DOWN
8	O88833	Cytochrome P450 4A10 OS=Mus musculus GN=Cyp4a10 PE=2 SV=2 - [CP4AA_MOUSE]	58.3	0.479	0.299	DOWN
9	Q9DCY0	Glycine N-acyltransferase-like protein Keg1 OS=Mus musculus GN=Keg1 PE=1 SV=1 - [KEG1_MOUSE]	33.7	0.482	0.640	DOWN
10	Q9CQS7	Developmental pluripotency-associated protein 5A OS=Mus musculus GN=Dppa5a PE=1 SV=2 - [DPA5A_MOUSE]	13.8	0.483	0.760	DOWN

11	Q9CQ01	Ribonuclease T2 OS=Mus musculus GN=Rnaset2 PE=1 SV=1 - [RNT2_MOUSE]	29.6	0.521	0.599	DOWN
12	Q9CQN6	Transmembrane protein 14C OS=Mus musculus GN=Tmem14c PE=1 SV=1 - [TM14C_MOUSE]	11.6	0.543	0.567	DOWN
13	P04444	Hemoglobin subunit beta-H1 OS=Mus musculus GN=Hbb-bh1 PE=2 SV=3 - [HBBZ_MOUSE]	16.5	0.551	0.742	DOWN
14	P07744	Keratin type II cytoskeletal 4 OS=Mus musculus GN=Krt4 PE=1 SV=2 - [K2C4_MOUSE]	56.2	0.551	0.775	DOWN
15	P03987	Ig gamma-3 chain C region OS=Mus musculus PE=1 SV=2 - [IGHG3_MOUSE]	43.9	0.560	0.801	DOWN
16	Q62264	Thyroid hormone-inducible hepatic protein OS=Mus musculus GN=Thrsp PE=1 SV=1 - [THRSP_MOUSE]	17.1	0.560	0.394	DOWN
17	P02088	Hemoglobin subunit beta-1 OS=Mus musculus GN=Hbb-b1 PE=1 SV=2 - [HBB1_MOUSE]	15.8	0.564	0.810	DOWN
18	Q64458	Cytochrome P450 2C29 OS=Mus musculus GN=Cyp2c29 PE=1 SV=2 - [CP2CT_MOUSE]	55.7	0.566	0.598	DOWN
19	P13516	Acyl-CoA desaturase 1 OS=Mus musculus GN=Scd1 PE=1 SV=2 - [ACOD1_MOUSE]	41	0.568	0.267	DOWN
20	P52431	DNA polymerase delta catalytic subunit OS=Mus musculus GN=Pold1 PE=1 SV=2 - [DPOD1_MOUSE]	123.7	0.568	0.651	DOWN
21	O88829	Lactosylceramide alpha-2 3-sialyltransferase OS=Mus musculus GN=St3gal5 PE=2 SV=2 - [SIAT9_MOUSE]	47.3	0.571	0.510	DOWN
22	Q9QYR7	Acyl-coenzyme A thioesterase 3 OS=Mus musculus GN=Acot3 PE=1 SV=1 - [ACOT3_MOUSE]	47.5	0.573	0.447	DOWN
23	Q14DH7	Acyl-CoA synthetase short-chain family member 3 mitochondrial OS=Mus musculus GN=Acss3 PE=1 SV=2 - [ACSS3_MOUSE]	74.5	0.579	0.356	DOWN
24	Q9WU79	Proline dehydrogenase 1 mitochondrial OS=Mus musculus GN=Prodh PE=1 SV=2 - [PROD_MOUSE]	68	0.581	0.675	DOWN
25	Q60648	Ganglioside GM2 activator OS=Mus musculus GN=Gm2a PE=1 SV=2 - [SAP3_MOUSE]	20.8	0.581	0.740	DOWN
26	Q3UHQ6	Protein dopey-2 OS=Mus musculus GN=Dopey2 PE=1 SV=3 - [DOP2_MOUSE]	257.3	0.586	0.722	DOWN
27	Q9Z2U2	Zinc finger protein 292 OS=Mus musculus GN=Zfp292 PE=1 SV=2 - [ZN292_MOUSE]	300.9	0.589	0.311	DOWN
28	P24721	Asialoglycoprotein receptor 2 OS=Mus musculus GN=Asgr2 PE=1 SV=1 - [ASGR2_MOUSE]	34.9	0.596	0.657	DOWN

11	Q9CQ01	Ribonuclease T2 OS=Mus musculus GN=Rnaset2 PE=1 SV=1 - [RNT2_MOUSE]	29.6	0.521	0.599	DOWN
12	Q9CQN6	Transmembrane protein 14C OS=Mus musculus GN=Tmem14c PE=1 SV=1 - [TM14C_MOUSE]	11.6	0.543	0.567	DOWN
13	P04444	Hemoglobin subunit beta-H1 OS=Mus musculus GN=Hbb-bh1 PE=2 SV=3 - [HBBZ_MOUSE]	16.5	0.551	0.742	DOWN
14	P07744	Keratin type II cytoskeletal 4 OS=Mus musculus GN=Krt4 PE=1 SV=2 - [K2C4_MOUSE]	56.2	0.551	0.775	DOWN
15	P03987	Ig gamma-3 chain C region OS=Mus musculus PE=1 SV=2 - [IGHG3_MOUSE]	43.9	0.560	0.801	DOWN
16	Q62264	Thyroid hormone-inducible hepatic protein OS=Mus musculus GN=Thrsp PE=1 SV=1 - [THRSP_MOUSE]	17.1	0.560	0.394	DOWN
17	P02088	Hemoglobin subunit beta-1 OS=Mus musculus GN=Hbb-b1 PE=1 SV=2 - [HBB1_MOUSE]	15.8	0.564	0.810	DOWN
18	Q64458	Cytochrome P450 2C29 OS=Mus musculus GN=Cyp2c29 PE=1 SV=2 - [CP2CT_MOUSE]	55.7	0.566	0.598	DOWN
19	P13516	Acyl-CoA desaturase 1 OS=Mus musculus GN=Scd1 PE=1 SV=2 - [ACOD1_MOUSE]	41	0.568	0.267	DOWN
20	P52431	DNA polymerase delta catalytic subunit OS=Mus musculus GN=Pold1 PE=1 SV=2 - [DPOD1_MOUSE]	123.7	0.568	0.651	DOWN
21	O88829	Lactosylceramide alpha-2 3-sialyltransferase OS=Mus musculus GN=St3gal5 PE=2 SV=2 - [SIAT9_MOUSE]	47.3	0.571	0.510	DOWN
22	Q9QYR7	Acyl-coenzyme A thioesterase 3 OS=Mus musculus GN=Acot3 PE=1 SV=1 - [ACOT3_MOUSE]	47.5	0.573	0.447	DOWN
23	Q14DH7	Acyl-CoA synthetase short-chain family member 3 mitochondrial OS=Mus musculus GN=Acss3 PE=1 SV=2 - [ACSS3_MOUSE]	74.5	0.579	0.356	DOWN
24	Q9WU79	Proline dehydrogenase 1 mitochondrial OS=Mus musculus GN=Prodh PE=1 SV=2 - [PROD_MOUSE]	68	0.581	0.675	DOWN
25	Q60648	Ganglioside GM2 activator OS=Mus musculus GN=Gm2a PE=1 SV=2 - [SAP3_MOUSE]	20.8	0.581	0.740	DOWN
26	Q3UHQ6	Protein dopey-2 OS=Mus musculus GN=Dopey2 PE=1 SV=3 - [DOP2_MOUSE]	257.3	0.586	0.722	DOWN
27	Q9Z2U2	Zinc finger protein 292 OS=Mus musculus GN=Zfp292 PE=1 SV=2 - [ZN292_MOUSE]	300.9	0.589	0.311	DOWN
28	P24721	Asialoglycoprotein receptor 2 OS=Mus musculus GN=Asgr2 PE=1 SV=1 - [ASGR2_MOUSE]	34.9	0.596	0.657	DOWN

29	Q8BWG9	Calcium release-activated calcium channel protein 1 OS=Mus musculus GN=Orai1 PE=2 SV=1 - [CRCM1_MOUSE]	33	0.597	0.756	DOWN
30	Q9D6Y9	1 4-alpha-glucan-branching enzyme OS=Mus musculus GN=Gbe1 PE=1 SV=1 - [GLGB_MOUSE]	80.3	0.599	0.511	DOWN
31	Q3V1M1	Immunoglobulin superfamily member 10 OS=Mus musculus GN=Igsf10 PE=2 SV=2 - [IGS10_MOUSE]	285.4	0.605	0.561	DOWN
32	Q920A5	Retinoid-inducible serine carboxypeptidase OS=Mus musculus GN=Scpep1 PE=1 SV=2 - [RISC_MOUSE]	50.9	0.608	0.831	DOWN
33	P20852	Cytochrome P450 2A5 OS=Mus musculus GN=Cyp2a5 PE=2 SV=1 - [CP2A5_MOUSE]	56.7	0.614	0.749	DOWN
34	P31651	Sodium- and chloride-dependent betaine transporter OS=Mus musculus GN=Slc6a12 PE=2 SV=1 - [S6A12_MOUSE]	69.6	0.618	0.716	DOWN
35	Q80XD1	Beta-chimaerin OS=Mus musculus GN=Chn2 PE=1 SV=2 - [CHIO_MOUSE]	38.2	0.622	0.471	DOWN
36	Q61205	Platelet-activating factor acetylhydrolase IB subunit gamma OS=Mus musculus GN=Pafah1b3 PE=1 SV=1 - [PA1B3_MOUSE]	25.8	0.625	0.775	DOWN
37	P55302	Alpha-2-macroglobulin receptor-associated protein OS=Mus musculus GN=Lrpap1 PE=1 SV=1 - [AMRP_MOUSE]	42.2	0.629	0.713	DOWN
38	Q6PB93	Polypeptide N-acetylgalactosaminyltransferase 2 OS=Mus musculus GN=Galnt2 PE=1 SV=1 - [GALT2_MOUSE]	64.5	0.630	0.614	DOWN
39	P34927	Asialoglycoprotein receptor 1 OS=Mus musculus GN=Asgr1 PE=1 SV=4 - [ASGR1_MOUSE]	32.6	0.636	0.632	DOWN
40	Q9Z0M5	Lysosomal acid lipase/cholesteryl ester hydrolase OS=Mus musculus GN=Lipa PE=1 SV=2 - [LICH_MOUSE]	45.3	0.636	0.628	DOWN
41	P00920	Carbonic anhydrase 2 OS=Mus musculus GN=Ca2 PE=1 SV=4 - [CAH2_MOUSE]	29	0.638	0.812	DOWN
42	P47740	Fatty aldehyde dehydrogenase OS=Mus musculus GN=Aldh3a2 PE=1 SV=2 - [AL3A2_MOUSE]	53.9	0.641	0.392	DOWN
43	A2ATU0	Probable 2-oxoglutarate dehydrogenase E1 component DHKTD1 mitochondrial OS=Mus musculus GN=Dhtkd1 PE=1 SV=1 - [DHTK1_MOUSE]	102.7	0.644	0.756	DOWN
44	Q9JIY8	Probable N-acetyltransferase CML3 OS=Mus musculus GN=Cml3 PE=1 SV=1 - [CMLO3_MOUSE]	25.9	0.645	0.538	DOWN
45	A2ARZ3	Fibrous sheath-interacting protein 2 OS=Mus musculus GN=Fsip2 PE=1 SV=3 - [FSIP2_MOUSE]	784.4	0.645	0.482	DOWN

46	E9Q4Z2	Acetyl-CoA carboxylase 2 OS=Mus musculus GN=Acacb PE=1 SV=1 - [ACACB_MOUSE]	275.6	0.646	0.618	DOWN
47	Q61543	Golgi apparatus protein 1 OS=Mus musculus GN=Glg1 PE=1 SV=1 - [GSLG1_MOUSE]	133.6	0.654	0.637	DOWN
48	P45700	Mannosyl-oligosaccharide 1 2-alpha-mannosidase IA OS=Mus musculus GN=Man1a1 PE=1 SV=1 - [MA1A1_MOUSE]	73.2	0.660	0.705	DOWN
49	Q8BYH8	Chromodomain-helicase-DNA-binding protein 9 OS=Mus musculus GN=Chd9 PE=1 SV=2 - [CHD9_MOUSE]	323.7	0.661	0.712	DOWN
50	Q9QXG4	Acetyl-coenzyme A synthetase cytoplasmic OS=Mus musculus GN=Acss2 PE=1 SV=2 - [ACSA_MOUSE]	78.8	0.663	0.753	DOWN
51	Q6XVG2	Cytochrome P450 2C54 OS=Mus musculus GN=Cyp2c54 PE=1 SV=1 - [CP254_MOUSE]	55.8	0.667	0.799	DOWN
52	Q9DBG1	Sterol 26-hydroxylase mitochondrial OS=Mus musculus GN=Cyp27a1 PE=1 SV=1 - [CP27A_MOUSE]	60.7	0.670	0.800	DOWN
53	P61939	Thyroxine-binding globulin OS=Mus musculus GN=Serpina7 PE=2 SV=1 - [THBG_MOUSE]	47	0.672	0.488	DOWN
54	O09158	Cytochrome P450 3A25 OS=Mus musculus GN=Cyp3a25 PE=1 SV=1 - [CP3AP_MOUSE]	58.1	0.674	0.745	DOWN
55	P13634	Carbonic anhydrase 1 OS=Mus musculus GN=Ca1 PE=1 SV=4 - [CAH1_MOUSE]	28.3	0.678	0.755	DOWN
56	Q9JJQ0	GPI mannosyltransferase 3 OS=Mus musculus GN=Pigb PE=2 SV=2 - [PIGB_MOUSE]	63.1	0.681	0.826	DOWN
57	A7XV04	Selection and upkeep of intraepithelial T-cells protein 7 OS=Mus musculus GN=Skint7 PE=2 SV=2 - [SKIT7_MOUSE]	45.2	0.681	0.779	DOWN
58	Q80XI6	Mitogen-activated protein kinase kinase kinase 11 OS=Mus musculus GN=Map3k11 PE=1 SV=1 - [M3K11_MOUSE]	93.2	0.687	0.722	DOWN
59	Q06770	Corticosteroid-binding globulin OS=Mus musculus GN=Serpina6 PE=1 SV=1 - [CBG_MOUSE]	44.7	0.687	0.632	DOWN
60	Q9JI02	Secretoglobin family 2B member 20 OS=Mus musculus GN=Scgb2b20 PE=2 SV=1 - [S2B20_MOUSE]	12.6	0.689	0.619	DOWN
61	Q8BWN8	Acyl-coenzyme A thioesterase 4 OS=Mus musculus GN=Acot4 PE=1 SV=1 - [ACOT4_MOUSE]	46.5	0.694	0.485	DOWN
62	Q9DB76	ER membrane protein complex subunit 9 OS=Mus musculus GN=Emc9 PE=1 SV=1 - [EMC9_MOUSE]	22.8	0.695	0.817	DOWN
63	Q3USZ8	Deleted in autism protein 1 homolog OS=Mus musculus PE=1 SV=2 - [DIA1_MOUSE]	49.4	0.695	0.808	DOWN

64	P03888	NADH-ubiquinone oxidoreductase chain 1 OS=Mus musculus GN=Mtnd1 PE=1 SV=3 - [NU1M_MOUSE]	36	0.697	0.745	DOWN
65	P70190	F-actin-capping protein subunit alpha-3 OS=Mus musculus GN=Capza3 PE=2 SV=1 - [CAZA3_MOUSE]	34.9	0.698	0.547	DOWN
66	P09813	Apolipoprotein A-II OS=Mus musculus GN=Apoa2 PE=1 SV=2 - [APOA2_MOUSE]	11.3	0.699	0.523	DOWN
67	Q8K339	DNA/RNA-binding protein KIN17 OS=Mus musculus GN=Kin PE=1 SV=1 - [KIN17_MOUSE]	44.7	0.701	0.782	DOWN
68	P70245	3-beta-hydroxysteroid-Delta(8) Delta(7)-isomerase OS=Mus musculus GN=Ebp PE=1 SV=3 - [EBP_MOUSE]	26.2	0.702	0.639	DOWN
69	P55096	ATP-binding cassette sub-family D member 3 OS=Mus musculus GN=Abcd3 PE=1 SV=2 - [ABCD3_MOUSE]	75.4	0.702	0.731	DOWN
70	Q9QYR9	Acyl-coenzyme A thioesterase 2 mitochondrial OS=Mus musculus GN=Acot2 PE=1 SV=2 - [ACOT2_MOUSE]	49.6	0.705	0.580	DOWN
71	O89106	Bis(5'-adenosyl)-triphosphatase OS=Mus musculus GN=Fhit PE=1 SV=3 - [FHIT_MOUSE]	17.2	0.708	0.739	DOWN
72	P28571	Sodium- and chloride-dependent glycine transporter 1 OS=Mus musculus GN=Slc6a9 PE=1 SV=3 - [SC6A9_MOUSE]	76.5	0.709	0.729	DOWN
73	Q7TN22	Thioredoxin domain-containing protein 16 OS=Mus musculus GN=Txndc16 PE=2 SV=1 - [TXD16_MOUSE]	92	0.712	0.758	DOWN
74	Q8BH24	Transmembrane 9 superfamily member 4 OS=Mus musculus GN=Tm9sf4 PE=1 SV=1 - [TM9S4_MOUSE]	74.6	0.713	0.688	DOWN
75	Q8BFZ2	Lipid phosphate phosphatase-related protein type 1 OS=Mus musculus GN=Lppr1 PE=1 SV=1 - [LPPR1_MOUSE]	35.9	0.714	0.687	DOWN
76	Q71KT5	Delta(14)-sterol reductase OS=Mus musculus GN=Tm7sf2 PE=1 SV=2 - [ERG24_MOUSE]	46.5	0.716	0.674	DOWN
77	Q64459	Cytochrome P450 3A11 OS=Mus musculus GN=Cyp3a11 PE=1 SV=1 - [CP3AB_MOUSE]	57.8	0.716	0.707	DOWN
78	Q9JJL3	Solute carrier organic anion transporter family member 1B2 OS=Mus musculus GN=Slco1b2 PE=1 SV=1 - [SO1B2_MOUSE]	76.7	0.720	0.814	DOWN
79	Q3V1L6	Myotubularin-related protein 11 OS=Mus musculus GN=Mtmr11 PE=2 SV=1 - [MTMRB_MOUSE]	78.3	0.721	0.668	DOWN
80	P49222	Erythrocyte membrane protein band 4.2 OS=Mus musculus GN=Epb42 PE=1 SV=3 - [EPB42_MOUSE]	76.7	0.723	0.795	DOWN

81	Q99J47	Dehydrogenase/reductase SDR family member 7B OS=Mus musculus GN=Dhrs7b PE=1 SV=1 - [DRS7B_MOUSE]	35	0.728	0.606	DOWN
82	Q91V92	ATP-citrate synthase OS=Mus musculus GN=Acly PE=1 SV=1 - [ACLY_MOUSE]	119.7	0.729	0.713	DOWN
83	Q9Z139	Inactive tyrosine-protein kinase transmembrane receptor ROR1 OS=Mus musculus GN=Ror1 PE=2 SV=2 - [ROR1_MOUSE]	104	0.730	0.806	DOWN
84	P24472	Glutathione S-transferase A4 OS=Mus musculus GN=Gsta4 PE=1 SV=3 - [GSTA4_MOUSE]	25.5	0.730	0.626	DOWN
85	O88502	High affinity cAMP-specific and IBMX-insensitive 3' 5'-cyclic phosphodiesterase 8A OS=Mus musculus GN=Pde8a PE=1 SV=1 - [PDE8A_MOUSE]	93.1	0.730	0.792	DOWN
86	Q3THK3	General transcription factor IIF subunit 1 OS=Mus musculus GN=Gtf2f1 PE=1 SV=2 - [T2FA_MOUSE]	57.2	0.734	0.817	DOWN
87	Q3UHN9	Bifunctional heparan sulfate N-deacetylase/N-sulfotransferase 1 OS=Mus musculus GN=Ndst1 PE=1 SV=2 - [NDST1_MOUSE]	100.7	0.736	0.782	DOWN
88	P52792	Glucokinase OS=Mus musculus GN=Gck PE=1 SV=1 - [HXK4_MOUSE]	52.1	0.738	0.749	DOWN
89	Q9CQ62	2 4-dienoyl-CoA reductase mitochondrial OS=Mus musculus GN=Decr1 PE=1 SV=1 - [DECR_MOUSE]	36.2	0.740	0.650	DOWN
90	Q8BZ09	Mitochondrial 2-oxodicarboxylate carrier OS=Mus musculus GN=Slc25a21 PE=1 SV=1 - [ODC_MOUSE]	33.2	0.740	0.675	DOWN
91	Q8VCT4	Carboxylesterase 1D OS=Mus musculus GN=Ces1d PE=1 SV=1 - [CES1D_MOUSE]	61.7	0.742	0.716	DOWN
92	Q64505	Cholesterol 7-alpha-monooxygenase OS=Mus musculus GN=Cyp7a1 PE=2 SV=2 - [CP7A1_MOUSE]	57.2	0.744	0.759	DOWN
93	Q8K0R6	Glycolipid transfer protein domain-containing protein 2 OS=Mus musculus GN=Gltpd2 PE=1 SV=1 - [GLTD2_MOUSE]	34.4	0.744	0.710	DOWN
94	Q9QYY9	Alcohol dehydrogenase 4 OS=Mus musculus GN=Adh4 PE=1 SV=4 - [ADH4_MOUSE]	40.2	0.745	0.764	DOWN
95	Q91WL5	Cytochrome P450 4A12A OS=Mus musculus GN=Cyp4a12a PE=1 SV=2 - [CP4CA_MOUSE]	58.3	0.746	0.790	DOWN
96	Q9CPU2	NADH dehydrogenase [ubiquinone] 1 beta subcomplex subunit 2 mitochondrial OS=Mus musculus GN=Ndufb2 PE=1 SV=1 - [NDUB2_MOUSE]	12	0.747	0.781	DOWN
97	Q9D6Y7	Mitochondrial peptide methionine sulfoxide reductase OS=Mus musculus GN=Msra PE=1 SV=1 - [MSRA_MOUSE]	26	0.748	0.594	DOWN

81	Q99J47	Dehydrogenase/reductase SDR family member 7B OS=Mus musculus GN=Dhrs7b PE=1 SV=1 - [DRS7B_MOUSE]	35	0.728	0.606	DOWN
82	Q91V92	ATP-citrate synthase OS=Mus musculus GN=Acly PE=1 SV=1 - [ACLY_MOUSE]	119.7	0.729	0.713	DOWN
83	Q9Z139	Inactive tyrosine-protein kinase transmembrane receptor ROR1 OS=Mus musculus GN=Ror1 PE=2 SV=2 - [ROR1_MOUSE]	104	0.730	0.806	DOWN
84	P24472	Glutathione S-transferase A4 OS=Mus musculus GN=Gsta4 PE=1 SV=3 - [GSTA4_MOUSE]	25.5	0.730	0.626	DOWN
85	O88502	High affinity cAMP-specific and IBMX-insensitive 3' 5'-cyclic phosphodiesterase 8A OS=Mus musculus GN=Pde8a PE=1 SV=1 - [PDE8A_MOUSE]	93.1	0.730	0.792	DOWN
86	Q3THK3	General transcription factor IIF subunit 1 OS=Mus musculus GN=Gtf2f1 PE=1 SV=2 - [T2FA_MOUSE]	57.2	0.734	0.817	DOWN
87	Q3UHN9	Bifunctional heparan sulfate N-deacetylase/N-sulfotransferase 1 OS=Mus musculus GN=Ndst1 PE=1 SV=2 - [NDST1_MOUSE]	100.7	0.736	0.782	DOWN
88	P52792	Glucokinase OS=Mus musculus GN=Gck PE=1 SV=1 - [HXK4_MOUSE]	52.1	0.738	0.749	DOWN
89	Q9CQ62	2 4-dienoyl-CoA reductase mitochondrial OS=Mus musculus GN=Decr1 PE=1 SV=1 - [DECR_MOUSE]	36.2	0.740	0.650	DOWN
90	Q8BZ09	Mitochondrial 2-oxodicarboxylate carrier OS=Mus musculus GN=Slc25a21 PE=1 SV=1 - [ODC_MOUSE]	33.2	0.740	0.675	DOWN
91	Q8VCT4	Carboxylesterase 1D OS=Mus musculus GN=Ces1d PE=1 SV=1 - [CES1D_MOUSE]	61.7	0.742	0.716	DOWN
92	Q64505	Cholesterol 7-alpha-monooxygenase OS=Mus musculus GN=Cyp7a1 PE=2 SV=2 - [CP7A1_MOUSE]	57.2	0.744	0.759	DOWN
93	Q8K0R6	Glycolipid transfer protein domain-containing protein 2 OS=Mus musculus GN=Gltpd2 PE=1 SV=1 - [GLTD2_MOUSE]	34.4	0.744	0.710	DOWN
94	Q9QYY9	Alcohol dehydrogenase 4 OS=Mus musculus GN=Adh4 PE=1 SV=4 - [ADH4_MOUSE]	40.2	0.745	0.764	DOWN
95	Q91WL5	Cytochrome P450 4A12A OS=Mus musculus GN=Cyp4a12a PE=1 SV=2 - [CP4CA_MOUSE]	58.3	0.746	0.790	DOWN
96	Q9CPU2	NADH dehydrogenase [ubiquinone] 1 beta subcomplex subunit 2 mitochondrial OS=Mus musculus GN=Ndufb2 PE=1 SV=1 - [NDUB2_MOUSE]	12	0.747	0.781	DOWN
97	Q9D6Y7	Mitochondrial peptide methionine sulfoxide reductase OS=Mus musculus GN=Msra PE=1 SV=1 - [MSRA_MOUSE]	26	0.748	0.594	DOWN

98	P00158	Cytochrome b OS=Mus musculus GN=Mt-Cyb PE=1 SV=1 - [CYB_MOUSE]	43.2	0.748	0.696	DOWN
99	Q91YD9	Neural Wiskott-Aldrich syndrome protein OS=Mus musculus GN=Wasl PE=1 SV=1 - [WASL_MOUSE]	54.2	0.749	0.825	DOWN
100	P48410	ATP-binding cassette sub-family D member 1 OS=Mus musculus GN=Abcd1 PE=1 SV=1 - [ABCD1_MOUSE]	81.8	0.754	0.667	DOWN
101	Q8VCH0	3-ketoacyl-CoA thiolase B peroxisomal OS=Mus musculus GN=Acaa1b PE=1 SV=1 - [THIKB_MOUSE]	44	0.754	0.355	DOWN
102	Q3TA59	JmjC domain-containing protein 8 OS=Mus musculus GN=Jmjd8 PE=2 SV=2 - [JMJD8_MOUSE]	35.5	0.755	0.742	DOWN
103	P23953	Carboxylesterase 1C OS=Mus musculus GN=Ces1c PE=1 SV=4 - [EST1C_MOUSE]	61	0.755	0.815	DOWN
104	Q61391	Neprilysin OS=Mus musculus GN=Mme PE=1 SV=3 - [NEP_MOUSE]	85.6	0.758	0.665	DOWN
105	P58021	Transmembrane 9 superfamily member 2 OS=Mus musculus GN=Tm9sf2 PE=1 SV=1 - [TM9S2_MOUSE]	75.3	0.758	0.822	DOWN
106	Q9R1Q9	V-type proton ATPase subunit S1 OS=Mus musculus GN=Atp6ap1 PE=1 SV=1 - [VAS1_MOUSE]	51	0.759	0.709	DOWN
107	Q9Z2Z6	Mitochondrial carnitine/acylcarnitine carrier protein OS=Mus musculus GN=Slc25a20 PE=1 SV=1 - [MCAT_MOUSE]	33	0.760	0.768	DOWN
108	O88962	7-alpha-hydroxycholest-4-en-3-one 12-alpha-hydroxylase OS=Mus musculus GN=Cyp8b1 PE=1 SV=1 - [CP8B1_MOUSE]	57.7	0.762	0.780	DOWN
109	P40936	Indolethylamine N-methyltransferase OS=Mus musculus GN=Inmt PE=1 SV=1 - [INMT_MOUSE]	29.4	0.763	0.554	DOWN
110	Q5SWU9	Acetyl-CoA carboxylase 1 OS=Mus musculus GN=Acaca PE=1 SV=1 - [ACACA_MOUSE]	265.1	0.765	0.752	DOWN
111	Q3UP75	UDP-glucuronosyltransferase 3A1 OS=Mus musculus GN=Ugt3a1 PE=1 SV=1 - [UD3A1_MOUSE]	59.7	0.766	0.611	DOWN
112	Q920L5	Elongation of very long chain fatty acids protein 6 OS=Mus musculus GN=Elovl6 PE=1 SV=1 - [ELOV6_MOUSE]	31.6	0.766	0.566	DOWN
113	P97325	CMP-N-acetylneuraminate-beta-1 4-galactoside alpha-2 3-sialyltransferase OS=Mus musculus GN=St3gal3 PE=2 SV=2 - [SIAT6_MOUSE]	42.1	0.767	0.631	DOWN
114	Q8BK48	Pyrethroid hydrolase Ces2e OS=Mus musculus GN=Ces2e PE=1 SV=1 - [EST2E_MOUSE]	62.3	0.767	0.595	DOWN

115	Q9QUH0	Glutaredoxin-1 OS=Mus musculus GN=Glrx PE=1 SV=3 - [GLRX1_MOUSE]	11.9	0.769	0.814	DOWN
116	P00405	Cytochrome c oxidase subunit 2 OS=Mus musculus GN=Mtco2 PE=1 SV=1 - [COX2_MOUSE]	26	0.769	0.826	DOWN
117	P58854	Gamma-tubulin complex component 3 OS=Mus musculus GN=Tubgcp3 PE=1 SV=2 - [GCP3_MOUSE]	103.4	0.770	0.783	DOWN
118	Q64176	Carboxylesterase 1E OS=Mus musculus GN=Ces1e PE=1 SV=1 - [EST1E_MOUSE]	61.5	0.772	0.624	DOWN
119	O54749	Cytochrome P450 2J5 OS=Mus musculus GN=Cyp2j5 PE=1 SV=1 - [CP2J5_MOUSE]	57.7	0.773	0.822	DOWN
120	Q91VS7	Microsomal glutathione S-transferase 1 OS=Mus musculus GN=Mgst1 PE=1 SV=3 - [MGST1_MOUSE]	17.5	0.773	0.659	DOWN
121	Q8QZR3	Pyrethroid hydrolase Ces2a OS=Mus musculus GN=Ces2a PE=1 SV=1 - [EST2A_MOUSE]	61.9	0.776	0.742	DOWN
122	P10648	Glutathione S-transferase A2 OS=Mus musculus GN=Gsta2 PE=1 SV=3 - [GSTA2_MOUSE]	25.5	0.776	0.485	DOWN
123	Q61586	Glycerol-3-phosphate acyltransferase 1 mitochondrial OS=Mus musculus GN=Gpam PE=1 SV=2 - [GPAT1_MOUSE]	93.6	0.778	0.787	DOWN
124	P35576	Glucose-6-phosphatase OS=Mus musculus GN=G6pc PE=1 SV=2 - [G6PC_MOUSE]	40.4	0.778	0.798	DOWN
125	Q8CHR6	Dihydropyrimidine dehydrogenase [NADP(+)] OS=Mus musculus GN=Dpyd PE=1 SV=1 - [DPYD_MOUSE]	111.2	0.778	0.657	DOWN
126	Q9CQN3	Mitochondrial import receptor subunit TOM6 homolog OS=Mus musculus GN=Tomm6 PE=3 SV=1 - [TOM6_MOUSE]	7.9	0.779	0.761	DOWN
127	Q9CXR1	Dehydrogenase/reductase SDR family member 7 OS=Mus musculus GN=Dhrs7 PE=1 SV=2 - [DHRS7_MOUSE]	38.1	0.782	0.718	DOWN
128	Q8BVW3	Tripartite motif-containing protein 14 OS=Mus musculus GN=Trim14 PE=1 SV=2 - [TRI14_MOUSE]	49.6	0.788	0.819	DOWN
129	Q8BS35	Alkylglycerol monooxygenase OS=Mus musculus GN=Agmo PE=1 SV=1 - [ALKMO_MOUSE]	51.7	0.788	0.734	DOWN
130	P24549	Retinal dehydrogenase 1 OS=Mus musculus GN=Aldh1a1 PE=1 SV=5 - [AL1A1_MOUSE]	54.4	0.789	0.539	DOWN
131	P54761	Ephrin type-B receptor 4 OS=Mus musculus GN=Ephb4 PE=1 SV=2 - [EPHB4_MOUSE]	108.8	0.789	0.831	DOWN

132	O35490	Betaine--homocysteine S-methyltransferase 1 OS=Mus musculus GN=Bhmt PE=1 SV=1 - [BHMT1_MOUSE]	45	0.789	0.549	DOWN
133	Q6PGB8	Probable global transcription activator SNF2L1 OS=Mus musculus GN=Smarca1 PE=1 SV=1 - [SMCA1_MOUSE]	121.6	0.791	0.744	DOWN
134	P03893	NADH-ubiquinone oxidoreductase chain 2 OS=Mus musculus GN=Mtnd2 PE=1 SV=2 - [NU2M_MOUSE]	38.7	0.791	0.502	DOWN
135	Q9D938	Transmembrane protein 160 OS=Mus musculus GN=Tmem160 PE=2 SV=1 - [TM160_MOUSE]	19.6	0.791	0.337	DOWN
136	P35951	Low-density lipoprotein receptor OS=Mus musculus GN=Ldlr PE=1 SV=2 - [LDLR_MOUSE]	94.9	0.791	0.564	DOWN
137	Q925N0	Sideroflexin-5 OS=Mus musculus GN=Sfxn5 PE=1 SV=2 - [SFXN5_MOUSE]	37.3	0.792	0.752	DOWN
138	Q9QZD8	Mitochondrial dicarboxylate carrier OS=Mus musculus GN=Slc25a10 PE=1 SV=2 - [DIC_MOUSE]	31.7	0.793	0.655	DOWN
139	P59266	Fat storage-inducing transmembrane protein 2 OS=Mus musculus GN=Fitm2 PE=1 SV=1 - [FITM2_MOUSE]	30	0.794	0.701	DOWN
140	Q8K3K7	1-acyl-sn-glycerol-3-phosphate acyltransferase beta OS=Mus musculus GN=Agpat2 PE=1 SV=1 - [PLCB_MOUSE]	31	0.795	0.598	DOWN
141	Q9Z2P8	Vesicle-associated membrane protein 5 OS=Mus musculus GN=Vamp5 PE=1 SV=1 - [VAMP5_MOUSE]	11.4	0.795	0.816	DOWN
142	Q60848	Lymphocyte-specific helicase OS=Mus musculus GN=Hells PE=1 SV=2 - [HELLS_MOUSE]	95.1	0.796	0.810	DOWN
143	Q8BW75	Amine oxidase [flavin-containing] B OS=Mus musculus GN=Maob PE=1 SV=4 - [AOFB_MOUSE]	58.5	0.797	0.742	DOWN
144	P00687	Alpha-amylase 1 OS=Mus musculus GN=Amy1 PE=1 SV=2 - [AMY1_MOUSE]	57.6	0.797	0.750	DOWN
145	B2RX12	Canalicular multispecific organic anion transporter 2 OS=Mus musculus GN=Abcc3 PE=1 SV=1 - [MRP3_MOUSE]	169	0.797	0.739	DOWN
146	Q3UGP9	Leucine-rich repeat-containing protein 58 OS=Mus musculus GN=Lrrc58 PE=2 SV=1 - [LRC58_MOUSE]	40.1	0.797	0.760	DOWN
147	O54824	Pro-interleukin-16 OS=Mus musculus GN=Il16 PE=1 SV=3 - [IL16_MOUSE]	141.3	0.798	0.677	DOWN
148	Q8BMF4	Dihydrolipoyllysine-residue acetyltransferase component of pyruvate dehydrogenase complex mitochondrial OS=Mus musculus GN=Dlat PE=1 SV=2 - [ODP2_MOUSE]	67.9	0.798	0.776	DOWN

149	Q791T5	Mitochondrial carrier homolog 1 OS=Mus musculus GN=Mtch1 PE=1 SV=1 - [MTCH1_MOUSE]	41.5	0.802	0.829	DOWN
150	Q3UI66	Coiled-coil domain-containing protein 34 OS=Mus musculus GN=Ccdc34 PE=2 SV=1 - [CCD34_MOUSE]	42.2	0.803	0.814	DOWN
151	Q9JIY7	N-acetyltransferase 8 OS=Mus musculus GN=Nat8 PE=1 SV=1 - [NAT8_MOUSE]	25.6	0.803	0.808	DOWN
152	Q3UBG2	PTB-containing cubilin and LRP1-interacting protein OS=Mus musculus GN=Pid1 PE=1 SV=2 - [PCLI1_MOUSE]	24.8	0.804	0.826	DOWN
153	Q3TPX4	Exocyst complex component 5 OS=Mus musculus GN=Exoc5 PE=1 SV=2 - [EXOC5_MOUSE]	81.7	0.804	0.813	DOWN
154	Q04899	Cyclin-dependent kinase 18 OS=Mus musculus GN=Cdk18 PE=1 SV=1 - [CDK18_MOUSE]	51.8	0.804	0.666	DOWN
155	O88428	Bifunctional 3'-phosphoadenosine 5'-phosphosulfate synthase 2 OS=Mus musculus GN=Papss2 PE=1 SV=2 - [PAPS2_MOUSE]	70.3	0.806	0.773	DOWN
156	P29758	Ornithine aminotransferase mitochondrial OS=Mus musculus GN=Oat PE=1 SV=1 - [OAT_MOUSE]	48.3	0.806	0.697	DOWN
157	P47934	Carnitine O-acetyltransferase OS=Mus musculus GN=Crat PE=1 SV=3 - [CACP_MOUSE]	70.8	0.807	0.524	DOWN
158	P52623	Uridine-cytidine kinase 1 OS=Mus musculus GN=Uck1 PE=1 SV=2 - [UCK1_MOUSE]	31	0.807	0.481	DOWN
159	Q64133	Amine oxidase [flavin-containing] A OS=Mus musculus GN=Maoa PE=1 SV=3 - [AOFA_MOUSE]	59.6	0.808	0.829	DOWN
160	P37040	NADPH--cytochrome P450 reductase OS=Mus musculus GN=Por PE=1 SV=2 - [NCPR_MOUSE]	77	0.809	0.793	DOWN
161	Q8BGT5	Alanine aminotransferase 2 OS=Mus musculus GN=Gpt2 PE=1 SV=1 - [ALAT2_MOUSE]	57.9	0.809	0.698	DOWN
162	Q64FW2	All-trans-retinol 13 14-reductase OS=Mus musculus GN=Retsat PE=1 SV=3 - [RETST_MOUSE]	67.3	0.810	0.782	DOWN
163	Q9CWQ0	Diphthine methyl ester synthase OS=Mus musculus GN=Dph5 PE=1 SV=2 - [DPH5_MOUSE]	31.2	0.812	0.826	DOWN
164	Q9CQJ8	NADH dehydrogenase [ubiquinone] 1 beta subcomplex subunit 9 OS=Mus musculus GN=Ndufb9 PE=1 SV=3 - [NDUB9_MOUSE]	22	0.812	0.831	DOWN
165	Q8R1V4	Transmembrane emp24 domain-containing protein 4 OS=Mus musculus GN=Tmed4 PE=1 SV=1 - [TMED4_MOUSE]	26	0.813	0.695	DOWN

166	Q8BK03	Protein FAM73B OS=Mus musculus GN=Fam73b PE=1 SV=1 - [FA73B_MOUSE]	65.5	0.814	0.738	DOWN
167	Q8VCC1	15-hydroxyprostaglandin dehydrogenase [NAD(+)] OS=Mus musculus GN=Hpgd PE=1 SV=1 - [PGDH_MOUSE]	29.2	0.816	0.616	DOWN
168	Q7TNE1	Succinate--hydroxymethylglutarate CoA-transferase OS=Mus musculus GN=Sugct PE=1 SV=2 - [SUCHY_MOUSE]	47.7	0.816	0.748	DOWN
169	Q9D154	Leukocyte elastase inhibitor A OS=Mus musculus GN=Serpinb1a PE=1 SV=1 - [ILEUA_MOUSE]	42.5	0.816	0.549	DOWN
170	Q8BXA1	Golgi integral membrane protein 4 OS=Mus musculus GN=Golim4 PE=1 SV=1 - [GOLI4_MOUSE]	76.7	0.816	0.830	DOWN
171	Q8R127	Saccharopine dehydrogenase-like oxidoreductase OS=Mus musculus GN=Sccpdh PE=1 SV=1 - [SCPDL_MOUSE]	47.1	0.817	0.726	DOWN
172	A2RSJ4	UHRF1-binding protein 1-like OS=Mus musculus GN=Uhrf1bp1l PE=1 SV=2 - [UH1BL_MOUSE]	161.8	0.819	0.772	DOWN
173	P35486	Pyruvate dehydrogenase E1 component subunit alpha somatic form mitochondrial OS=Mus musculus GN=Pdha1 PE=1 SV=1 - [ODPA_MOUSE]	43.2	0.819	0.775	DOWN
174	Q61268	Apolipoprotein C-IV OS=Mus musculus GN=Apoc4 PE=1 SV=1 - [APOC4_MOUSE]	14.3	0.819	0.744	DOWN
175	Q8BZB2	Phosphopantothenoylcysteine decarboxylase OS=Mus musculus GN=Ppcdc PE=1 SV=1 - [COAC_MOUSE]	22.3	0.820	0.586	DOWN
176	Q920E5	Farnesyl pyrophosphate synthase OS=Mus musculus GN=Fdps PE=1 SV=1 - [FPPS_MOUSE]	40.6	0.821	0.785	DOWN
177	Q9JJN5	Carboxypeptidase N catalytic chain OS=Mus musculus GN=Cpn1 PE=1 SV=1 - [CBPN_MOUSE]	51.8	0.822	0.827	DOWN
178	Q91X83	S-adenosylmethionine synthase isoform type-1 OS=Mus musculus GN=Mat1a PE=1 SV=1 - [METK1_MOUSE]	43.5	0.822	0.767	DOWN
179	Q05920	Pyruvate carboxylase mitochondrial OS=Mus musculus GN=Pc PE=1 SV=1 - [PYC_MOUSE]	129.6	0.823	0.779	DOWN
180	P53657	Pyruvate kinase PKLR OS=Mus musculus GN=Pklr PE=1 SV=1 - [KPYR_MOUSE]	62.3	0.825	0.752	DOWN
181	Q5NBX1	Protein cordon-bleu OS=Mus musculus GN=Cobl PE=1 SV=1 - [COBL_MOUSE]	143.8	0.827	0.654	DOWN

182	Q8BK30	NADH dehydrogenase [ubiquinone] flavoprotein 3 mitochondrial OS=Mus musculus GN=Ndufv3 PE=1 SV=1 - [NDUV3_MOUSE]	11.8	0.827	0.783	DOWN
183	Q8R1T4	UDP-N-acetylglucosamine transporter OS=Mus musculus GN=Slc35a3 PE=2 SV=1 - [S35A3_MOUSE]	36	0.828	0.786	DOWN
184	O89020	Afamin OS=Mus musculus GN=Afm PE=1 SV=2 - [AFAM_MOUSE]	69.3	0.829	0.810	DOWN
185	O88630	Golgi SNAP receptor complex member 1 OS=Mus musculus GN=Gosr1 PE=1 SV=2 - [GOSR1_MOUSE]	28.5	0.830	0.778	DOWN
186	Q3U3R4	Lipase maturation factor 1 OS=Mus musculus GN=Lmf1 PE=1 SV=1 - [LMF1_MOUSE]	65.8	0.830	0.750	DOWN
187	Q8C1E7	Transmembrane protein 120A OS=Mus musculus GN=Tmem120a PE=1 SV=1 - [T120A_MOUSE]	40.7	0.831	0.615	DOWN
188	P07758	Alpha-1-antitrypsin 1-1 OS=Mus musculus GN=Serpina1a PE=1 SV=4 - [A1AT1_MOUSE]	46	0.832	0.825	DOWN
189	Q8BQP8	Rab11 family-interacting protein 4 OS=Mus musculus GN=Rab11fip4 PE=1 SV=1 - [RFIP4_MOUSE]	71.9	0.833	0.548	DOWN
190	Q80Y98	Phospholipase DDHD2 OS=Mus musculus GN=Ddhd2 PE=1 SV=3 - [DDHD2_MOUSE]	79.5	0.833	0.765	DOWN
191	D3YYU8	Obscurin-like protein 1 OS=Mus musculus GN=Obsl1 PE=1 SV=1 - [OBSL1_MOUSE]	197.8	1.203	1.495	UP
192	Q8BMK4	Cytoskeleton-associated protein 4 OS=Mus musculus GN=Ckap4 PE=1 SV=2 - [CKAP4_MOUSE]	63.7	1.205	1.211	UP
193	Q7TPR4	Alpha-actinin-1 OS=Mus musculus GN=Actn1 PE=1 SV=1 - [ACTN1_MOUSE]	103	1.206	1.228	UP
194	Q8K182	Complement component C8 alpha chain OS=Mus musculus GN=C8a PE=1 SV=1 - [CO8A_MOUSE]	66	1.206	1.221	UP
195	Q9CZT8	Ras-related protein Rab-3B OS=Mus musculus GN=Rab3b PE=1 SV=1 - [RAB3B_MOUSE]	24.7	1.207	1.772	UP
196	P29391	Ferritin light chain 1 OS=Mus musculus GN=Ftl1 PE=1 SV=2 - [FRIL1_MOUSE]	20.8	1.210	1.324	UP
197	P29699	Alpha-2-HS-glycoprotein OS=Mus musculus GN=Ahsg PE=1 SV=1 - [FETUA_MOUSE]	37.3	1.210	1.268	UP
198	Q9JKR6	Hypoxia up-regulated protein 1 OS=Mus musculus GN=Hyou1 PE=1 SV=1 - [HYOU1_MOUSE]	111.1	1.211	1.225	UP

199	Q64282	Interferon-induced protein with tetratricopeptide repeats 1 OS=Mus musculus GN=Ifit1 PE=1 SV=2 - [IFIT1_MOUSE]	53.7	1.211	1.285	UP
200	P19157	Glutathione S-transferase P 1 OS=Mus musculus GN=Gstp1 PE=1 SV=2 - [GSTP1_MOUSE]	23.6	1.212	1.783	UP
201	Q64112	Interferon-induced protein with tetratricopeptide repeats 2 OS=Mus musculus GN=Ifit2 PE=1 SV=1 - [IFIT2_MOUSE]	55	1.212	1.317	UP
202	Q9CX80	Cytoglobin OS=Mus musculus GN=Cygb PE=1 SV=1 - [CYGB_MOUSE]	21.5	1.214	1.400	UP
203	Q4QQM4	Tumor protein p53-inducible protein 11 OS=Mus musculus GN=Trp53i11 PE=1 SV=1 - [P5I11_MOUSE]	20.9	1.218	1.381	UP
204	E9Q414	Apolipoprotein B-100 OS=Mus musculus GN=Apob PE=1 SV=1 - [APOB_MOUSE]	509.1	1.219	1.433	UP
205	P14211	Calreticulin OS=Mus musculus GN=Calr PE=1 SV=1 - [CALR_MOUSE]	48	1.220	1.245	UP
206	P10404	MLV-related proviral Env polyprotein OS=Mus musculus PE=1 SV=3 - [ENV1_MOUSE]	69.6	1.220	1.420	UP
207	Q99PL5	Ribosome-binding protein 1 OS=Mus musculus GN=Rrbp1 PE=1 SV=2 - [RRBP1_MOUSE]	172.8	1.221	1.203	UP
208	Q60872	Eukaryotic translation initiation factor 1A OS=Mus musculus GN=Eif1a PE=2 SV=3 - [IF1A_MOUSE]	16.5	1.224	1.313	UP
209	Q8K3J9	G-protein coupled receptor family C group 5 member C OS=Mus musculus GN=Gprc5c PE=1 SV=2 - [GPC5C_MOUSE]	48.4	1.227	1.456	UP
210	P27661	Histone H2AX OS=Mus musculus GN=H2afx PE=1 SV=2 - [H2AX_MOUSE]	15.1	1.228	1.749	UP
211	P51880	Fatty acid-binding protein brain OS=Mus musculus GN=Fabp7 PE=1 SV=2 - [FABP7_MOUSE]	14.9	1.228	1.676	UP
212	Q61043	Ninein OS=Mus musculus GN=Nin PE=1 SV=3 - [NIN_MOUSE]	234.6	1.228	1.461	UP
213	P70194	C-type lectin domain family 4 member F OS=Mus musculus GN=Clec4f PE=1 SV=1 - [CLC4F_MOUSE]	61.2	1.230	1.242	UP
214	Q8K2T1	NmrA-like family domain-containing protein 1 OS=Mus musculus GN=Nmral1 PE=1 SV=1 - [NMRL1_MOUSE]	34.4	1.232	1.319	UP
215	Q9QY73	Transmembrane protein 59 OS=Mus musculus GN=Tmem59 PE=1 SV=2 - [TMM59_MOUSE]	36.3	1.232	1.444	UP
216	P97463	Neurturin OS=Mus musculus GN=Nrtn PE=1 SV=1 - [NRTN_MOUSE]	22.2	1.234	1.328	UP

217	Q5F2E7	Nuclear fragile X mental retardation-interacting protein 2 OS=Mus musculus GN=Nufip2 PE=1 SV=1 - [NUFP2_MOUSE]	75.6	1.234	1.204	UP
218	Q62351	Transferrin receptor protein 1 OS=Mus musculus GN=Tfrc PE=1 SV=1 - [TFR1_MOUSE]	85.7	1.238	1.256	UP
219	Q62000	Mimecan OS=Mus musculus GN=Ogn PE=1 SV=1 - [MIME_MOUSE]	34	1.239	1.472	UP
220	P50543	Protein S100-A11 OS=Mus musculus GN=S100a11 PE=1 SV=1 - [S10AB_MOUSE]	11.1	1.241	1.283	UP
221	P51150	Ras-related protein Rab-7a OS=Mus musculus GN=Rab7a PE=1 SV=2 - [RAB7A_MOUSE]	23.5	1.243	1.325	UP
222	Q9JJG0	Transforming acidic coiled-coil-containing protein 2 OS=Mus musculus GN=Tacc2 PE=1 SV=2 - [TACC2_MOUSE]	124.1	1.244	1.368	UP
223	P35330	Intercellular adhesion molecule 2 OS=Mus musculus GN=Icam2 PE=1 SV=1 - [ICAM2_MOUSE]	31.4	1.248	1.214	UP
224	O08800	Serpin B8 OS=Mus musculus GN=Serpinb8 PE=1 SV=2 - [SPB8_MOUSE]	42.1	1.248	1.248	UP
225	Q6PFR5	Transformer-2 protein homolog alpha OS=Mus musculus GN=Tra2a PE=1 SV=1 - [TRA2A_MOUSE]	32.3	1.250	1.222	UP
226	Q9QUR7	Peptidyl-prolyl cis-trans isomerase NIMA-interacting 1 OS=Mus musculus GN=Pin1 PE=1 SV=1 - [PIN1_MOUSE]	18.4	1.252	1.200	UP
227	P21278	Guanine nucleotide-binding protein subunit alpha-11 OS=Mus musculus GN=Gna11 PE=1 SV=1 - [GNA11_MOUSE]	42	1.254	1.351	UP
228	P20029	78 kDa glucose-regulated protein OS=Mus musculus GN=Hspa5 PE=1 SV=3 - [GRP78_MOUSE]	72.4	1.257	1.251	UP
229	Q80SU7	Interferon-induced very large GTPase 1 OS=Mus musculus GN=Gvin1 PE=1 SV=1 - [GVIN1_MOUSE]	280.6	1.257	1.423	UP
230	P63028	Translationally-controlled tumor protein OS=Mus musculus GN=Tpt1 PE=1 SV=1 - [TCTP_MOUSE]	19.4	1.260	1.228	UP
231	O08638	Myosin-11 OS=Mus musculus GN=Myh11 PE=1 SV=1 - [MYH11_MOUSE]	226.9	1.265	1.205	UP
232	P08226	Apolipoprotein E OS=Mus musculus GN=Apoe PE=1 SV=2 - [APOE_MOUSE]	35.8	1.266	1.344	UP
233	P84075	Neuron-specific calcium-binding protein hippocalcin OS=Mus musculus GN=Hpca PE=1 SV=2 - [HPCA_MOUSE]	22.4	1.269	1.319	UP

234	P24369	Peptidyl-prolyl cis-trans isomerase B OS=Mus musculus GN=Ppib PE=1 SV=2 - [PPIB_MOUSE]	23.7	1.269	1.290	UP
235	O89001	Carboxypeptidase D OS=Mus musculus GN=Cpd PE=1 SV=2 - [CBPD_MOUSE]	152.3	1.272	1.504	UP
236	Q9D958	Signal peptidase complex subunit 1 OS=Mus musculus GN=Spcs1 PE=2 SV=3 - [SPCS1_MOUSE]	18.2	1.275	1.246	UP
237	Q9DCZ1	GMP reductase 1 OS=Mus musculus GN=Gmpr PE=1 SV=1 - [GMPR1_MOUSE]	37.5	1.276	2.170	UP
238	Q8R2Q8	Bone marrow stromal antigen 2 OS=Mus musculus GN=Bst2 PE=1 SV=1 - [BST2_MOUSE]	19.1	1.277	1.534	UP
239	Q02788	Collagen alpha-2(VI) chain OS=Mus musculus GN=Col6a2 PE=1 SV=3 - [CO6A2_MOUSE]	110.3	1.279	1.371	UP
240	Q8C0S1	DIS3-like exonuclease 1 OS=Mus musculus GN=Dis3l PE=1 SV=2 - [DI3L1_MOUSE]	120.2	1.280	1.379	UP
241	Q8BGN3	Ectonucleotide pyrophosphatase/phosphodiesterase family member 6 OS=Mus musculus GN=Enpp6 PE=1 SV=1 - [ENPP6_MOUSE]	50.6	1.281	1.535	UP
242	Q8VHF2	Cadherin-related family member 5 OS=Mus musculus GN=Cdhr5 PE=1 SV=1 - [CDHR5_MOUSE]	88.2	1.282	1.531	UP
243	Q61490	CD166 antigen OS=Mus musculus GN=Alcam PE=1 SV=3 - [CD166_MOUSE]	65.1	1.284	1.251	UP
244	Q8CIE0	Serpin A11 OS=Mus musculus GN=Serpina11 PE=2 SV=1 - [SPA11_MOUSE]	47.2	1.286	1.307	UP
245	A7XUY5	Selection and upkeep of intraepithelial T-cells protein 5 OS=Mus musculus GN=Skint5 PE=2 SV=1 - [SKIT5_MOUSE]	165.8	1.287	1.313	UP
246	Q922F4	Tubulin beta-6 chain OS=Mus musculus GN=Tubb6 PE=1 SV=1 - [TBB6_MOUSE]	50.1	1.289	1.353	UP
247	P05532	Mast/stem cell growth factor receptor Kit OS=Mus musculus GN=Kit PE=1 SV=3 - [KIT_MOUSE]	109.3	1.290	1.559	UP
248	Q61646	Haptoglobin OS=Mus musculus GN=Hp PE=1 SV=1 - [HPT_MOUSE]	38.7	1.293	1.421	UP
249	P70429	Ena/VASP-like protein OS=Mus musculus GN=Evl PE=1 SV=2 - [EVL_MOUSE]	44.3	1.297	1.235	UP
250	P16406	Glutamyl aminopeptidase OS=Mus musculus GN=Enpep PE=1 SV=1 - [AMPE_MOUSE]	107.9	1.298	1.208	UP

251	Q3UG98	N-acetyltransferase 9 OS=Mus musculus GN=Nat9 PE=1 SV=2 - [NAT9_MOUSE]	27.6	1.302	1.875	UP
252	Q9R092	17-beta-hydroxysteroid dehydrogenase type 6 OS=Mus musculus GN=Hsd17b6 PE=1 SV=1 - [H17B6_MOUSE]	36.1	1.306	1.376	UP
253	P39061	Collagen alpha-1(XVIII) chain OS=Mus musculus GN=Col18a1 PE=1 SV=4 - [COIA1_MOUSE]	182.1	1.310	1.215	UP
254	Q6WVG3	BTB/POZ domain-containing protein KCTD12 OS=Mus musculus GN=Kctd12 PE=1 SV=1 - [KCD12_MOUSE]	35.9	1.310	1.204	UP
255	Q9Z1M8	Protein Red OS=Mus musculus GN=Ik PE=1 SV=2 - [RED_MOUSE]	65.6	1.312	1.237	UP
256	Q9CXI5	Mesencephalic astrocyte-derived neurotrophic factor OS=Mus musculus GN=Manf PE=1 SV=1 - [MANF_MOUSE]	20.4	1.316	1.348	UP
257	Q91VM5	RNA binding motif protein X-linked-like-1 OS=Mus musculus GN=Rbmxl1 PE=2 SV=1 - [RMXL1_MOUSE]	42.1	1.317	1.693	UP
258	Q9D1M7	Peptidyl-prolyl cis-trans isomerase FKBP11 OS=Mus musculus GN=Fkbp11 PE=1 SV=1 - [FKB11_MOUSE]	22.1	1.319	1.712	UP
259	Q922W5	Pyrroline-5-carboxylate reductase 1 mitochondrial OS=Mus musculus GN=Pycr1 PE=1 SV=1 - [P5CR1_MOUSE]	32.4	1.319	1.564	UP
260	P81117	Nucleobindin-2 OS=Mus musculus GN=Nucb2 PE=1 SV=2 - [NUCB2_MOUSE]	50.3	1.319	1.376	UP
261	P08122	Collagen alpha-2(IV) chain OS=Mus musculus GN=Col4a2 PE=1 SV=4 - [CO4A2_MOUSE]	167.2	1.320	1.248	UP
262	A6H584	Collagen alpha-5(VI) chain OS=Mus musculus GN=Col6a5 PE=1 SV=4 - [CO6A5_MOUSE]	289.4	1.320	1.202	UP
263	Q7TQD2	Tubulin polymerization-promoting protein OS=Mus musculus GN=Tppp PE=1 SV=1 - [TPPP_MOUSE]	23.6	1.323	1.262	UP
264	Q00915	Retinol-binding protein 1 OS=Mus musculus GN=Rbp1 PE=1 SV=2 - [RET1_MOUSE]	15.8	1.325	1.350	UP
265	Q922R8	Protein disulfide-isomerase A6 OS=Mus musculus GN=Pdia6 PE=1 SV=3 - [PDIA6_MOUSE]	48.1	1.327	1.312	UP
266	Q61144	Presenilin-2 OS=Mus musculus GN=Psen2 PE=1 SV=3 - [PSN2_MOUSE]	50	1.329	1.388	UP
267	Q07797	Galectin-3-binding protein OS=Mus musculus GN=Lgals3bp PE=1 SV=1 - [LG3BP_MOUSE]	64.4	1.336	1.231	UP

CHAPTER 3

Strong and Sustained Antihypertensive Effect of Small Interfering RNA Targeting Liver Angiotensinogen

Estrellita Uijl[#], Katrina M. Mirabito Colafella[#], Yuan Sun, Liwei Ren, Richard Van Veghel, Ingrid M. Garrelds, RenÉ De Vries, Marko Poglitsch, Ivan Zlatev, Jae B. Kim, Ewout J. Hoorn, Don Foster, A.h. Jan Danser

Hypertension 73:1249-1257, 2019

[#]= equal contribution

Abstract

Small interfering ribonucleic acids (siRNA) targeting hepatic angiotensinogen (Agt) may provide long-lasting antihypertensive effects, but the optimal approach remains unclear. Here we assessed the efficacy of a novel AGT siRNA in spontaneously hypertensive rats (SHRs). SHRs were treated with vehicle, siRNA (10 mg/kg fortnightly; subcutaneous), valsartan (31 mg/kg/day; oral), captopril (100 mg/kg/day; oral), valsartan+siRNA, or captopril+valsartan for four weeks (all groups n=8). Mean arterial pressure (recorded via radiotelemetry) was lowered the most by valsartan+siRNA (-68±4 mmHg), followed by captopril+valsartan (-54±4 mmHg), captopril (-23±2 mmHg), siRNA (-14±2 mmHg) and valsartan (-10±2mmHg). siRNA and captopril monotherapies improved cardiac hypertrophy equally, but less than the dual therapies, which also lowered NT-proBNP. Glomerular filtration rate, urinary neutrophil gelatinase-associated lipocalin and albuminuria were unaffected by treatment. siRNA lowered circulating AGT by 97.9±1.0%, and by 99.8±0.1% in combination with valsartan. Although siRNA greatly reduced renal angiotensin I, only valsartan+-siRNA suppressed circulating and renal angiotensin II. This coincided with decreased renal sodium hydrogen exchanger type 3 and phosphorylated sodium chloride co-transporter abundances. Renin and plasma K^+ increased with every treatment, but especially during valsartan+siRNA; no effects on aldosterone were observed. Collectively, these data indicate that angiotensin II elimination requires >99% suppression of circulating AGT. Maximal blockade of the renin-angiotensin system (RAS), achieved by valsartan+siRNA, yielded the greatest reduction in blood pressure and cardiac hypertrophy, while AGT lowering alone was as effective as conventional RAS inhibitors. Given its stable and sustained efficacy, lasting weeks, RNA interference may offer a unique approach to improving therapy adherence and treating hypertension.

Keywords

Treatment resistant hypertension, novel therapeutics, small interfering RNA, renin-angiotensin-aldosterone system, acute kidney injury, hypertensive heart disease

Introduction

Treatment of hypertension generally requires multiple antihypertensive drugs, but is hampered by reduced adherence with every drug added to the treatment regimen.[1, 2] The management of hypertension is further complicated by the upregulation of counterbalancing mechanisms, e.g., the rise in renin during blockade of the renin-angiotensin system (RAS).

As a consequence, angiotensin (Ang) II levels are often restored to their original, pre-treatment levels during the chronic treatment phase.[3-5] All angiotensin stems from angiotensinogen (AGT), and blockade of the RAS at this level may ultimately annihilate RAS activity. Indeed, subcutaneously-delivered Agt-directed antisense oligonucleotides (ASO) and intravenous injection of lipid nanoparticles containing small interfering ribonucleic acids (siRNA) targeting Agt effectively lower blood pressure in hypertensive rats.[6, 7] Still, these approaches typically require weekly doses and may have a less-ideal safety profile.[8] Ongoing efforts to optimize siRNA designs have now yielded hepatocyte-directed, N-acetylgalactosamine (GalNAc)-conjugated molecules with long-term, single-dose efficacy. In fact, stable suppression of proprotein convertase subtilisin/kexin type 9 (PCSK9) has been achieved in a phase 2 clinical trial, employing biannual dosing of one such siRNA.[9] In the current study we set out to investigate the efficacy of a GalNAc-conjugated siRNA targeting Agt in spontaneously hypertensive rats (SHR), making a detailed comparison with the ACE inhibitor (ACEi) captopril and the angiotensin receptor blocker (ARB) valsartan, as well as with dual RAS blockade (AGT siRNA+valsartan and captopril+valsartan). We focused not only on blood pressure, but also unraveled the underlying RAS biochemistry and monitored the renal effects of these treatments, given the well-known side effects of RAS blockade, i.e., hypotension, renal dysfunction and hyperkalemia.[10] Using this approach, we demonstrate a sustained antihypertensive and cardioprotective effect of AGT siRNA.

Concise Methods

All supporting data are available within the article and its online-only Data Supplement.

Animal studies

All studies were performed under the regulation and permission of the Animal Care Committee of the Erasmus MC (protocol number 16-511-01). Male, 12-week old spontaneously hypertensive rats (SHRs), receiving a standard sodium diet, were treated for four weeks with vehicle, valsartan (31 mg/kg/day dissolved in drinking water), captopril (100 mg/kg/day dissolved in drinking water), captopril+valsartan, AGT siRNA (10 mg/kg fortnightly; subcutaneous injection; provided by Alnylam Pharmaceuticals, Cambridge MA, USA), or valsartan+siRNA (all groups n=8). Conjugation of siRNA to triantennary GalNAc ensures selective delivery to hepatocytes. Although single and biweekly dosing provided similar AGT suppression **(Supplemental Table S1)**, fortnightly dosing of 10 mg/kg AGT siRNA was selected to ensure maximal target silencing over the four-week period. For valsartan and captopril, water intake was checked every other day, and drug concentrations were adjusted to achieve the described daily doses. Blood pressure, heart rate and activity were re-

corded continuously via radiotelemetry. Oligonucleotide synthesis and complete procedures are described in the Supplemental Material.

Biochemical measurements, qPCR, siRNA quantification and Western blotting

In plasma, AGT and active plasma renin concentration (APRC) were measured by enzyme kinetic assays. In the cases that measurements were at or below the lower limit of detection (LLOD), this limit was applied to allow for statistical analysis. Urinary AGT was measured by direct AGT radioimmunoassay, and plasma aldosterone by solid-phase radioimmunoassay. Angiotensin and bradykinin (BK) metabolites in blood and renal tissue were measured by LC-MS/MS analysis as described before. Procedures and LLOD are described in the Supplemental Material.

Total RNA was isolated from selected tissues and reverse transcribed into cDNA. Gene expression was quantified using primers designed with NCBI (Primer-BLAST; **Supplemental Table S2**). A gene specific TaqMan assay was used for Agt mRNA quantification. The ΔΔCt method was used for relative quantification of mRNA expression levels.

siRNA quantification was performed as described previously. Antisense levels in siRNA standard curve dilutions, kidney and liver samples were quantified by stem loop reverse transcription followed by qPCR. Primer and probe sequences are described in the Supplemental Material. Ct values derived from samples were interpolated onto the standard curve, adjusted for sample dilution, and expressed as micrograms of antisense strand per gram of tissue.

Whole kidney protein extract was separated by electrophoresis, transferred to a membrane and incubated overnight at 4°C with primary antibodies against renal transporters described in the Supplemental Material. Signals were detected by chemiluminescence and quantified using ImageQuant. Samples (n=8 per group) were divided over two blots (n=4 per group per blot). To allow for combined statistical analysis, samples were first normalized to the loading control actin, followed by normalization to the average of the vehicle-treated rats from the respective immunoblot.

Kidney function

GFR in awake rats was measured prior to treatment (baseline), and after two and four weeks of treatment via transcutaneous measurement of fluorescein isothiocyanate (FITC)-labeled sinistrin, administered via the tail vein. A non-invasive clearance (NIC)-kidney fluorescent detection device together with partner software generates the elimination kinetics curve of

FITC-sinistrin. Excretion half-life ($t_{1/2}$) is used to derive GFR using a conversion factor and formula validated for rats:
GFR (mL/min per 100g body weight (BW)) = 31.26 (mL/100g BW) / $t_{1/2}$ FITC-sinistrin (minutes).

Histology
Cardiomyocyte size was measured after Gomori silver staining of sections (5μm) of the left ventricle of the heart. Sirius red staining was applied to visualize collagen as a measure of cardiac fibrosis.

Myograph studies
Responses of iliac arteries were measured in a Mulvany myograph as changes in isometric force. Exposure to 100 mmol/l potassium chloride determined the maximum contractile response. Concentration response curves (CRCs) were constructed to endothelin-1 (ET-1) in the absence or presence of ET_A or ET_B receptor antagonists. Iliac arteries were preconstricted with U46619 to construct CRCs to the endothelium-dependent vasodilator acetylcholine, in the absence or presence of the NO synthase inhibitor L-NAME, the small conductance Ca^{2+}-activated K^+ channel inhibitor apamin and the intermediate conductance Ca^{2+}-activated K^+ channel inhibitor TRAM34.

Statistical analysis
Data are expressed as mean values ± SEM. Data were analyzed with a one-way analysis of variance (ANOVA; for data obtained at a single point in time) or a repeated-measures ANOVA (for data obtained at multiple points in time) using Prism v7 (Graphpad Software Inc., La Jolla, USA). Post-hoc correction according to Bonferroni was performed in case of multiple comparisons. To conform to normality, non-parametric data were transformed to natural logarithms before statistical testing (AGT, renin, angiotensin metabolites, albuminuria). Univariate linear associations were assessed by calculation of Pearson's coefficient of correlation. Two-tailed P values <0.05 were considered statistically significant.

Results

AGT siRNA causes a similar antihypertensive effect as valsartan or captopril
Mean arterial pressure (MAP) at baseline was 137±2 mm Hg and progressively increased over time in vehicle-treated rats (9±1 mm Hg; $P \leq 0.001$ vs. baseline; **Figure 1A-B**). After four weeks, valsartan+siRNA lowered MAP the most (-68±4 mm Hg; $P \leq 0.05$ vs. captopril+valsartan), followed by combined treatment with captopril+valsartan (-54±4 mm Hg;

P≤0.0001 vs. captopril; **Figure 1B**). Monotherapy with either captopril, AGT siRNA or valsartan lowered MAP similarly (-23±2, -14±2, and -10±2 mmHg, respectively; P=0.12 captopril vs. siRNA, P>0.99 siRNA vs. valsartan, all P≤0.0001 vs. vehicle). None of the treatments affected heart rate **(Figure 1C)** or locomotor activity **(Figure 1D)**.

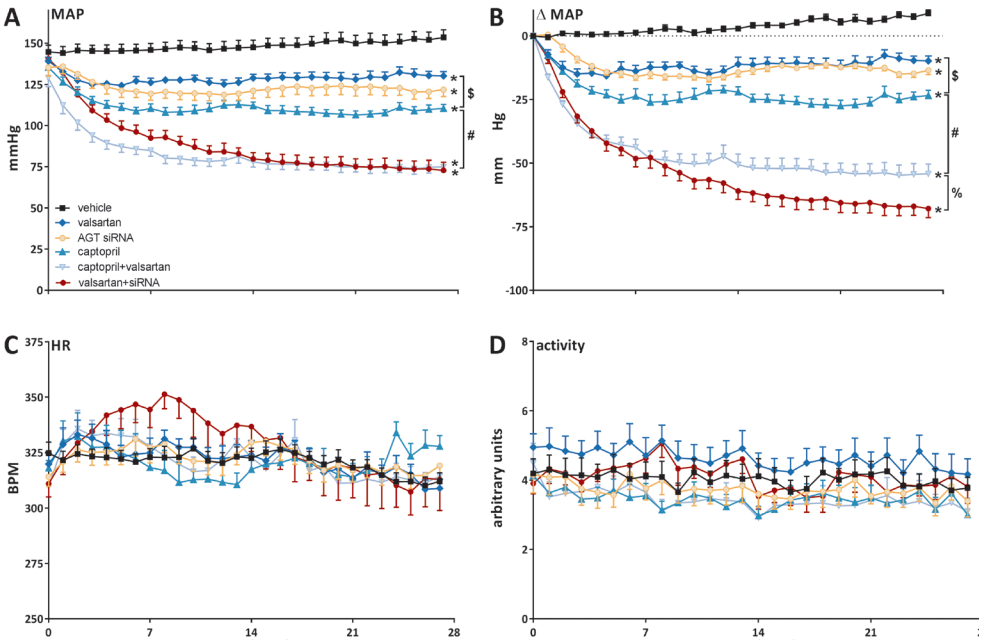

Figure 1. Mean arterial pressure, heart rate and locomotor activity. SHRs were treated for 28 days with vehicle, valsartan, AGT siRNA, captopril, valsartan+siRNA or captopril+valsartan (all groups n=8). **A)** Mean arterial pressure (MAP), **B)** change from baseline MAP (Δ MAP), **C)** heart rate (HR) and **D)** locomotor activity were recorded via radiotelemetry. Data, represented as means ± SEM, were analyzed using two-way ANOVA and post-hoc Bonferroni (* P≤0.0001 vs. vehicle; $ P≤0.01; # P≤0.0001; % P≤0.05). Abbreviations: BPM, beats per minute.

Near-complete AGT depletion is required for lowering plasma Ang II

Plasma AGT levels amounted to 651±50 pmol/mL at baseline. They were lowered by 97.9±1.0% after four weeks of treatment with AGT siRNA, and this increased to 99.8±0.1% in combination with valsartan (P≤0.0001 vs. siRNA; **Figure 2A**). Captopril with or without valsartan reduced plasma AGT levels by 86±4% and 44±13%, respectively (both P≤0.05 vs. baseline), while valsartan alone had no effect on AGT. Reductions in AGT concentrations were paralleled by increases in APRC in all treatment groups, the highest rise occurring after valsartan+siRNA **(Figure 2B)**. In agreement with previous observations,[11, 12] APRC exhibited a negative correlation with both circulating AGT and MAP (P<0.001; **Supplemental Figure S1A and S1B**). The well-known correlation between APRC and Ang I (r=0.80, P<0.0001 in non-siRNA-exposed rats, data not shown) disappeared when including

siRNA-treated rats in the analysis **(Supplemental Figure S1C)**. In fact, now AGT correlated with Ang I **(Supplemental Figure S1D)**. This was anticipated, since at very low AGT levels an increase in renin no longer results in a parallel rise Ang I. Accordingly, circulating Ang I levels were elevated after four weeks of treatment with valsartan, captopril and captopril+valsartan (all P≤0.01 vs. vehicle; **Figure 2C**). Valsartan alone also increased Ang II (P≤0.0001 vs. vehicle; **Figure 2C**). Captopril, with or without valsartan, did not lower Ang II levels, although, consistent with ACE inhibition, it did diminish the Ang II/Ang I ratio **(Figure 2C-D)**. Remarkably, only valsartan+siRNA lowered plasma Ang II (-76±5%;

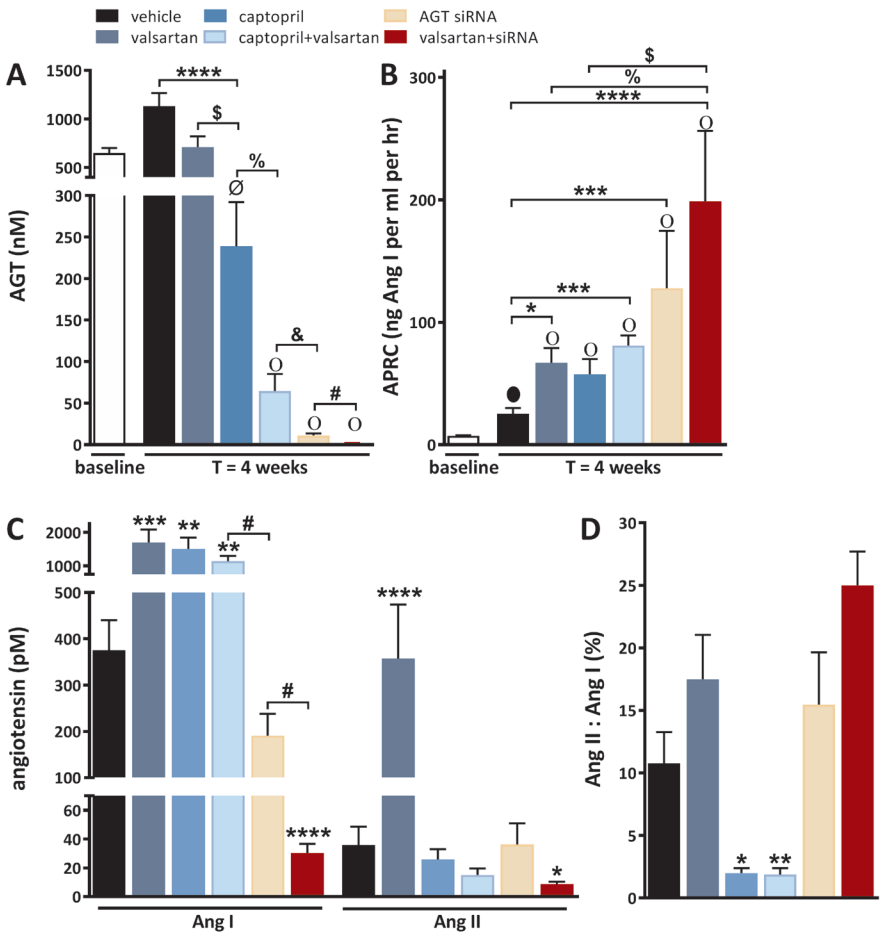

Figure 2. RAS parameters in plasma. Plasma levels of **A)** angiotensinogen (AGT) and **B)** active plasma renin concentration (APRC) of SHRs prior to treatment (baseline) and after four weeks of vehicle, valsartan, captopril, AGT siRNA, captopril+valsartan or valsartan+siRNA treatment (all groups n=8). Plasma **C)** angiotensin (Ang) levels and **D)** Ang II/Ang I ratio after four weeks of treatment. Data are represented as means ± SEM. Natural log-transformed data were analyzed using repeated measures or one-way ANOVA and post-hoc Bonferroni (ø P≤0.05, Φ P≤0.01, O P≤0.0001 vs. baseline; * P≤0.05, ** P≤0.01, *** P≤0.001, **** P≤0.0001 vs. vehicle or otherwise indicated in graph).

P≤0.05 vs. vehicle; **Figure 2C**). No treatment altered plasma aldosterone after four weeks **(Supplemental Table S3)**.

AGT siRNA reduces renal Ang I, but requires valsartan for simultaneous Ang II lowering

After four weeks, hepatic siRNA levels amounted to 36±13 μg/g tissue, versus 3.7±0.5 μg/g in the kidneys of rats treated with siRNA with or without valsartan. No siRNA could be detected in control rats. Given average liver and kidney weights of 12±1 and 2.3±0.1 g, this translates to a ≈50-fold siRNA enrichment in liver versus kidney. In agreement with this, siRNA lowered hepatic Agt mRNA levels to 0.7±0.1% of control, while renal Agt mRNA levels remained unaffected (88±8% of control; **Supplemental Figure S2A**). Of note, Agt mRNA levels in the liver of control animals were approximately 170-fold higher than in the kidneys of these animals, based on Gapdh-normalized Agt ΔCt values (kidney ΔCt 8.2 ±0.5 vs. liver ΔC_t 0.8±0.3).

Although liver-targeted Agt silencing did not affect renal Agt expression, dual blockade with valsartan+siRNA did lower urinary AGT by 89±2% **(Figure 3A)**. Valsartan and captopril increased renal Ang I (both P<0.01 vs. vehicle), while captopril+valsartan did not affect renal Ang I **(Figure 3B)**. Only siRNA with or without valsartan lowered renal Ang I by 97±1% and 86±1% respectively (both P<0.0001 vs. vehicle). Yet, valsartan did not affect renal Ang II, siRNA and captopril modestly lowered renal Ang II (P=NS for siRNA), and only dual blockade greatly reduced renal Ang II (P<0.0001; **Figure 3B**). As a consequence, the renal Ang II/Ang I ratio was increased 4-fold after siRNA (P<0.0001), reduced by >70% after valsartan, captopril and captopril+valsartan (all P<0.0001) and unaltered after siRNA+valsartan **(Figure 3C)**. Renal Ang-(1-7) was increased after valsartan and captopril, unchanged after captopril+valsartan, and reduced after siRNA with or without valsartan **(Supplemental Table S3)**. Captopril with or without valsartan impaired the renal degradation of BK-(1-9) into BK-(1-7), as reflected by reduced BK-(1-7)/BK-(1-9) ratios, without increasing BK-(1-9) levels **(Figure 3D and E)**. Systemic bradykinin levels were all below the LLOD.

Dual RAS blockade synergistically improves cardiac hypertrophy

Cardiac weight (indexed to tibia length) exhibited a strong positive correlation to MAP (r=0.84; P≤0.0001; **Figure 4A**). Proportional to the magnitude of blood pressure reductions achieved, AGT siRNA and captopril monotherapies improved the cardiac weight/tibia length ratio equally, but less than dual RAS blockade **(Figure 4B)**. Whereas valsartan+siRNA lowered this ratio the most (P≤0.01 vs. captopril+valsartan), valsartan monotherapy had no effect. Likewise, all treatments, except for valsartan, decreased cardiomyocyte sur-

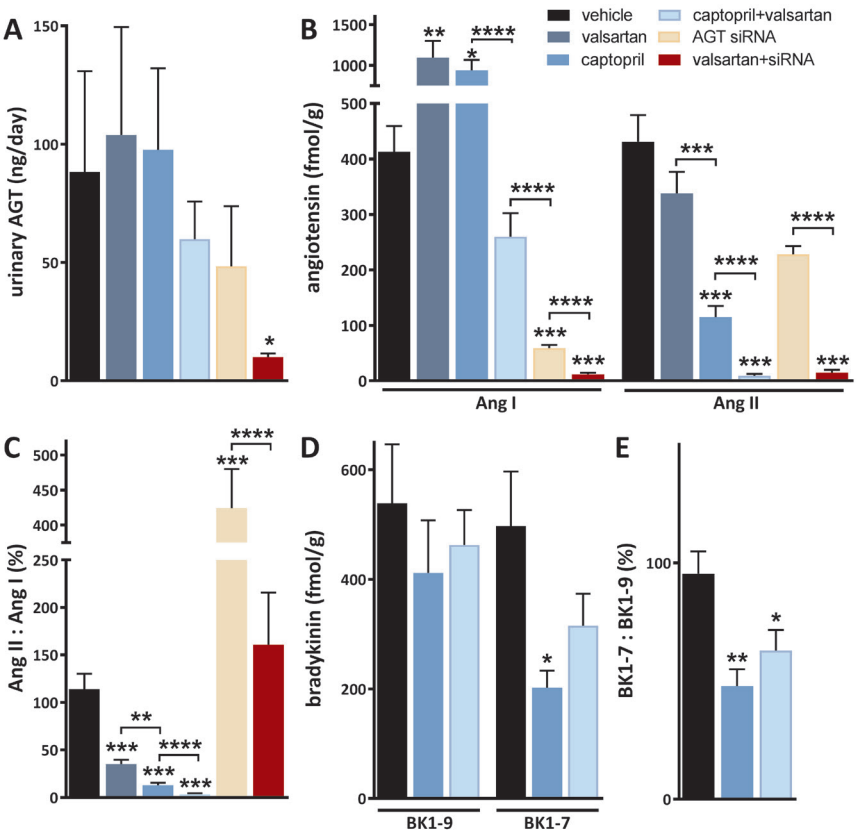

Figure 3. Renal RAS and bradykinin levels. A) Urinary angiotensinogen (AGT) and renal **B)** angiotensin (Ang) levels, **C)** Ang II/Ang I ratio, **D)** bradykinin (BK) levels and **E)** BK 1-7/1-9 ratio of SHRs after four weeks of vehicle, valsartan, captopril, AGT siRNA, captopril+valsartan or valsartan+siRNA treatment (all groups n=8). Data are represented as means ± SEM. Natural log-transformed data were analyzed using ANOVA and post-hoc Bonferroni (* P≤0.05, ** P≤0.01, *** P≤0.0001 vs. vehicle or otherwise indicated in graph).

face area **(Figure 4C)**. Between-group differences were no longer detectable. Only captopril+valsartan lowered plasma NT-proBNP levels (P≤0.05 vs. vehicle), and a similar trend was observed for valsartan+siRNA (P=0.07 vs. vehicle; **Figure 4D**). At this stage, cardiac fibrosis had yet to develop (left ventricular collagen content 0.3±0.1% in vehicle-treated rats). Hence, this could not be improved by any treatment (data not shown).

None of the treatments caused acute kidney injury

GFR at baseline was 1.3±0.1 mL/min per 100 g body weight and remained stable throughout the four-week treatment period in all groups (P≥0.65 vs. baseline; **Figure 5A**). Daily urine production was 4-fold higher after captopril and doubled after valsartan+siRNA

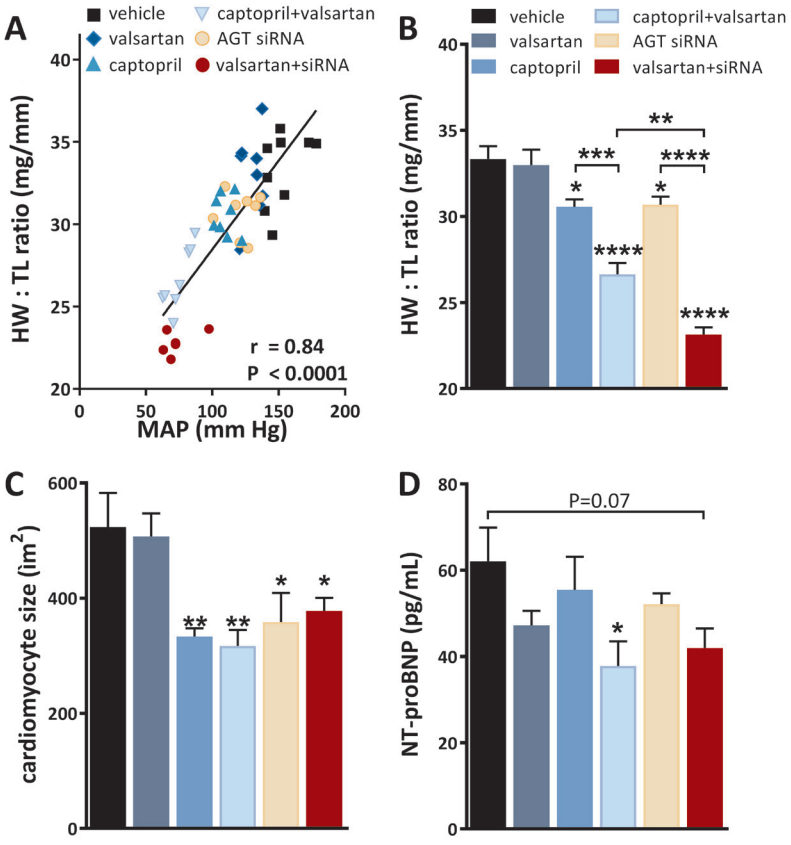

Figure 4. Indices of cardiac hypertrophy. A) Relationship between heart weight (HW) indexed for tibia length (TL) and mean arterial pressure (MAP), **B)** HW:TL ratio, **C)** cardiomyocyte surface area and **D)** plasma NT-proBNP levels in SHRs after four weeks of vehicle, valsartan, captopril, AGT siRNA, captopril+valsartan or valsartan+siRNA treatment (all groups n=8). r denotes Pearson's correlation coefficient. Data, represented as means ± SEM, were analyzed using a one-way ANOVA and post-hoc Bonferroni (* P≤0.05, ** P≤0.01, **** P≤0.0001 vs. vehicle or otherwise indicated in graph).

(P≤0.0001 vs. captopril; both P≤0.0001 vs. baseline; **Figure 5B**). This was due to equivalent increases in water intake **(Supplemental Table S4)**. None of the treatments decreased urine output or increased urinary neutrophil gelatinase-associated lipocalin (NGAL) levels, a biomarker for early manifestations of kidney damage which precede renal function decline in acute kidney injury (**Figure 5C**). Pre-existing chronic kidney disease was negated by very low levels of albuminuria at baseline (0.6±0.1 mg/day), which could not be improved further by any treatment **(Figure 5D)**. None of the treatments affected natriuresis **(Figure 5E)**. Plasma potassium levels tended to increase in all groups (P≤0.001 for linear trend), significance being reached only with valsartan+siRNA (P≤0.01 vs. vehicle; **Figure**

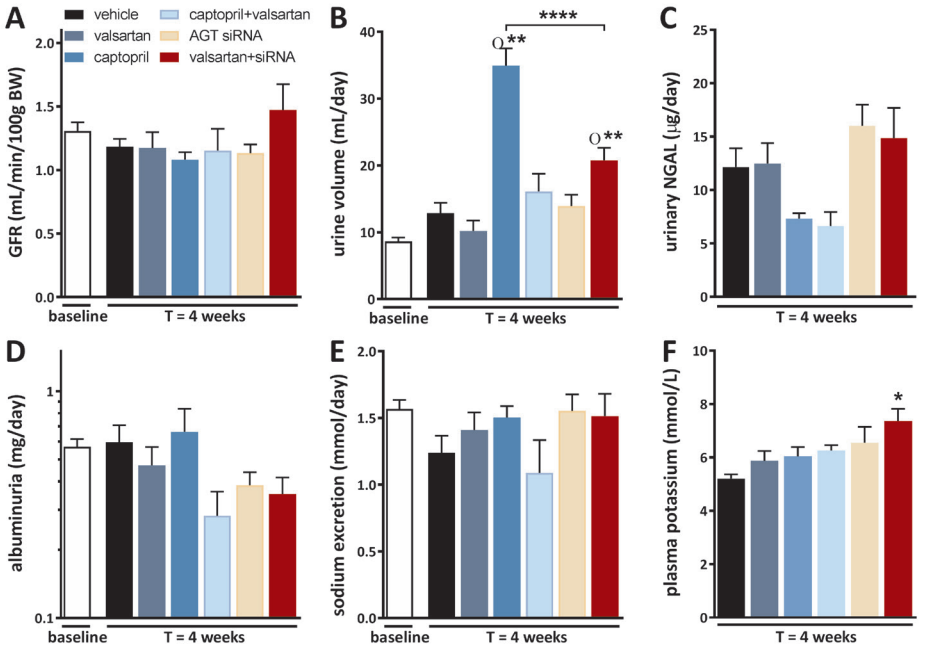

Figure 5. Indices of kidney damage. A) Glomerular filtration rate (GFR), determined by transcutaneous measurement of FITC-sinistrin clearance curves, **B)** 24-hour urine production, **C)** urinary neutrophil gelatinase-associated lipocalin (NGAL) levels, **D)** 24-hour albuminuria and E) 24-hour sodium (Na^+) excretion of SHRs prior to treatment (baseline) and after four weeks of vehicle, valsartan, captopril, AGT siRNA, captopril+valsartan or valsartan+siRNA treatment (all groups n=8). F) Plasma potassium (K^+) levels after four weeks of treatment. Data, represented as means ± SEM, were analyzed using repeated measures or one-way ANOVA and post-hoc Bonferroni (O P≤0.0001 vs. baseline; * P≤0.01, ** P≤0.0001 vs. vehicle or otherwise indicated in graph).

5F). Both types of dual blockade attenuated normal growth (as indicated by body weight) from the second week of treatment onwards, without altering food intake **(Supplemental Table S4)**.

Treatment did not alter renal AT_1 or ACE expression, but reduced NHE3, pNCC and γ-ENaC

AT_{1a} receptor expression in cortex or medulla was not affected by any treatment **(Supplemental Figure S2)**. AT_{1b} receptor expression in the cortex was reduced after valsartan+siRNA (P≤0.01 vs. control), and a similar trend was found for captopril+valsartan (P=0.07 vs. control). All treatments decreased AT_2 receptor expression in the medulla. Captopril+valsartan increased AT_2 and ACE expression in the cortex. None of the treatments affected ACE2 or (pro)renin receptor expression. As anticipated, all treatments increased renin expression in the renal cortex (paralleling the changes in plasma renin), while dual blockade additionally increased medullary renin expression.

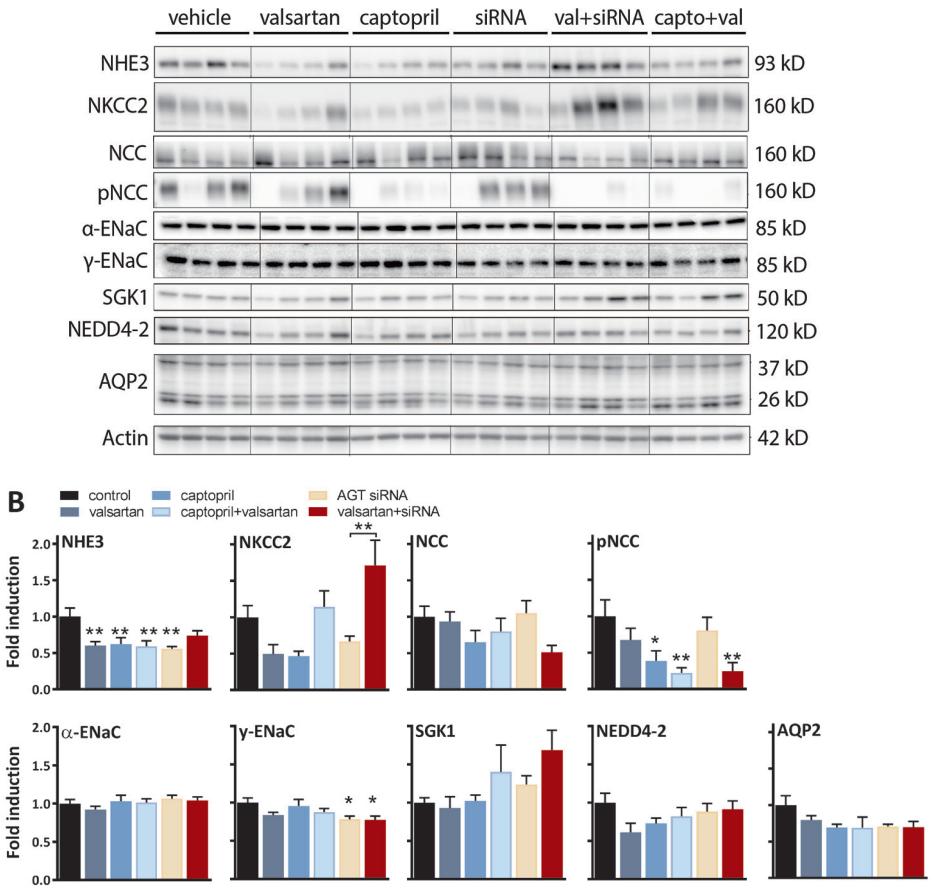

Figure 6. Renal sodium transporter protein abundance. A) Representative immunoblots showing protein abundances of renal sodium transporters: sodium-hydrogen exchanger type 3 (NHE3), Na-K-Cl co-transporter (NKCC2), Na-Cl co-transporter (NCC), NCC phosphorylated at Thr58 (pNCC), α- and γ-subunit of the epithelial sodium channel (α-ENaC; γ-ENaC), serum- and glucocorticoid-regulated kinase 1 (SGK1), neural precursor cell expressed, developmentally downregulated protein 4-2 (NEDD4-2), aquaporin-2 (AQP2) and β-actin in whole kidney homogenates after four weeks of vehicle, valsartan, captopril, AGT siRNA, captopril+valsartan or valsartan+siRNA treatment. **B)** Data, expressed as fold induction relative to vehicle-treated control (means ± SEM; all groups n=8), were analyzed using one-way ANOVA and post-hoc Bonferroni (* P≤0.05, ** P≤0.01 vs. vehicle or otherwise indicated in graph).

All treatments reduced sodium-hydrogen exchanger type 3 (NHE3) abundance (P<0.01; **Figure 6**), although the reduction was non-significant in the case of valsartan+siRNA (P=0.1). Significant reductions in the phosphorylated (at threonine-58) form of the sodium-chloride co-transporter (pNCC) were seen in the groups with the largest blood pressure decreases (captopril and the two dual-blockade groups with modest non-significant changes in the other groups). NCC abundance changes followed this pattern. Valsartan+siRNA increased the abundance of sodium-potassium-chloride co-transporter (NKCC2; P=0.07 vs. control; P<0.01 vs. AGT siRNA). Only siRNA with or without valsartan decreased the

γ-subunit of the epithelial sodium channel (γ-ENaC; P<0.05 vs. control). None of the treatments affected aquaporin-2, neural precursor cell expressed, developmentally downregulated protein 4-2, serum- and glucocorticoid-regulated kinase 1, or α-ENaC. In summary, these data confirm that blood pressure lowering during RAS blockade is accompanied by NHE3 and NCC inhibition, while the observed potassium rise may have occurred secondary to decreased ENaC activity.

Endothelial function and ET-1 responsiveness were not affected by any treatment

Acetylcholine relaxed preconstricted iliac arteries of vehicle-treated rats by 89±7% **(Supplemental Figure S3A)**. Blockade of both NO and EDHF was required to prevent this effect. None of the treatments altered this outcome. ET-1 potently constricted iliac arteries of control SHR (pEC_{50} [the negative logarithm of the half-maximal effective concentration] 8.2±0.6). ET_A receptor blockade (pEC_{50} 7.6±0.1; P≤0.5), but not ET_B receptor blockade (pEC_{50} 8.2±0.2), prevented this effect in control SHR. Single RAS blockade did not alter this outcome, while after dual RAS blockade ET_B receptor blockade resulted in a leftward shift, suggesting ET_B receptor-mediated vasodilation, with the rightward shift after ET_A receptor blockade being significant only when compared to the ET-1 curve in the presence of BQ788 **(Supplemental Figure S3B)**.

Discussion

This is the first study comparing liver-directed AGT siRNA treatment with single and dual RAS blockade in a well-established hypertension animal model, the SHR. The results show that AGT siRNA is as effective in lowering blood pressure as single RAS blockade, while impressive synergy occurs in combination with a second RAS blocker, valsartan **(Supplemental Figure S4)**. Remarkably, the data also reveal that siRNA-induced suppression of hepatic Agt mRNA, which reduced circulating AGT by almost 98%, did not significantly lower plasma or renal Ang II levels. This is reminiscent of clinical observations after chronic ACE inhibition, which also did not result in chronic Ang II suppression, despite an acute initial decrease in Ang II.[4, 13] This Ang II 'escape' can be explained by the rise in renin following treatment. Previous studies in humans, applying high renin inhibitor doses, demonstrated that the capacity of the body to upregulate renin expression is almost unlimited, with elevations of several hundred-fold possible.[11] In fact, a low AGT/high renin condition naturally occurs in mice.[14] Their AGT levels are in the same range as those in SHR after AGT siRNA, while their renin levels are 2-3 orders of magnitude above those in rats, pigs and humans.[15] Yet, mouse Ang II levels are identical to those in the latter species.[16, 17] Thus, the body has a tremendous capacity to restore Ang II levels, simply by upregulating renin.

Nevertheless, at a very high degree of RAS blockade (obtained in this study by combining AGT siRNA+valsartan), the limit of this mechanism is reached: the high renin levels then essentially deplete any remaining AGT, and thus Ang II levels fall. As a consequence, blood pressure decreased sharply, resulting in the largest reduction in cardiac hypertrophy of all treatment groups. Such strong antihypertensive effects in rodents have been described previously during dual RAS blockade, particularly under low-salt conditions, and were accompanied by a similar degree of weight loss as observed in the present study as well as renal insufficiency.[18, 19] Indeed, dual RAS blockade with conventional RAS blockers is known to result in renal dysfunction, both in animals and humans.[10] Renal dysfunction was not apparent in the present study, most likely because renal function (reflected by GFR, albuminuria and NGAL levels) was normal at the start of the study. Yet, siRNA+valsartan did raise potassium, possibly because low angiotensin II levels reduced ENaC activity. Plasma aldosterone levels were not suppressed after four weeks of treatment, suggestive for its well-known restoration in an Ang II-independent manner after prolonged RAS blockade.[13, 20]

A question raised by these data is why AGT suppression lowered blood pressure in the absence of changes in plasma Ang II. Such observations are typically attributed to alterations in tissue angiotensin levels, e.g., in the kidney. Agt mRNA is present in renal tissue, as confirmed in the present study. Yet, based on the ΔCt values, these levels are approximately 170-fold lower than the hepatic Agt mRNA levels, and were unaffected by liver-targeted AGT siRNA. Nevertheless, AGT siRNA did lower renal Ang I levels by >85% (single treatment) or >95% (combined treatment with valsartan), and under the latter conditions, urinary AGT virtually disappeared. Therefore, as has been concluded before in renal and hepatic Agt KO mice,[21, 22] renal angiotensin generation entirely depends on hepatic AGT, which suggests that renal AGT has no function, even when some of it is released into urine. Secondly, given the fact that renal Ang I levels already dropped during single AGT siRNA treatment, while circulating Ang I levels still remained intact, it appears that tissue angiotensin generation is even more sensitive to decreases in hepatic AGT synthesis. This has been observed before in cardiac tissue of heart failure patients,[23] and most likely reflects the difficulty of circulating AGT diffusing into the tissue interstitium.[24] Despite the substantial reduction in renal Ang I production, AGT siRNA alone did not significantly reduce renal Ang II levels. Here it is important to realize that tissue Ang II is bound to AT_1 receptors, i.e., it is located either on the cell surface or internalized.[16, 25, 26] An increase in AT_1 receptor density will therefore result in a rise in tissue Ang II levels.[25] Alternatively, ACE upregulation might overcome the reduction in Ang II formation.[27] Quantification of AT_{1a} receptor, AT_{1b} receptor, and ACE expression in the kidney ruled out these possibilities. Most likely therefore, factors affecting Ang II internalization (e.g., AT_1 receptor-associated protein[28]) are

responsible for maintaining near-normal renal Ang II levels, even when renal Ang I generation is diminished. Preventing internalization should then lower tissue Ang II levels. This is indeed what was observed during AT_1 receptor blockade with valsartan co-administered with AGT siRNA: renal Ang II now decreased in parallel with Ang I, and the renal Ang II/I ratio was no longer different from control.

Ang II is a well-known regulator of both NHE3[29] and NCC, thus determining sodium balance.[30, 31] In the present study, changes in pNCC fully paralleled the changes in blood pressure, i.e., the largest pNCC reductions were seen in the rats with the largest blood pressure reduction. Alterations in renal Ang II synthesis and internalization (not necessarily reflected by reduced renal Ang II levels) may underlie these pNCC reductions, which then in combination with the RAS blockade-induced suppression of NHE3, may explain, at least in part, the antihypertensive (circulating RAS-independent) effect of RAS blockade. An additional explanation is that the higher plasma potassium concentrations inhibited pNCC.[32]

We did not quantify tissue Ang II levels in the heart, vascular wall or adrenal gland, but given their dependency on hepatic AGT,[15, 33, 34] it is reasonable to assume that alterations in their Ang II content paralleled those in the kidney. Such alterations, as for example reflected by the occurrence of ET_B receptor-mediated vasodilation, may have contributed to the blood pressure-lowering effect. The virtual disappearance of Ang-(1-7) after AGT siRNA suggests that a contribution of this metabolite is unlikely. Similarly, the lack of BK-(1-9) accumulation during ACE inhibition in renal tissue argues against a major role for BK-(1-9), although the BK-(1-7)/BK-(1-9) ratio did decrease during this treatment. Together with the reduction in Ang II/Ang I ratio, this latter observation at least confirms that ACE inhibition was achieved at the tissue level.

Perspectives

In SHRs, near-elimination of hepatocyte-derived AGT with siRNA+valsartan depleted angiotensin, causing a synergistic reduction in blood pressure and cardiac hypertrophy, greater than that induced by captopril+valsartan. Yet, renal function was preserved. AGT siRNA as monotherapy provided similar antihypertensive and cardioprotective efficacy as conventional small-molecule RAS inhibitors. Unique to AGT siRNA is the long-term effectiveness of a single subcutaneous injection. Indeed, preliminary studies in cynomolgus monkeys support AGT suppression for >100 days after a single siRNA injection of 10 mg/kg (n=3; unpublished observations). As medication nonadherence is associated with greater cardiovascular risk, long-acting agents have the potential to significantly improve outcomes. Such

efforts are already underway for the management of hypercholesterolemia. Inclisiran, a GalNAc-conjugated siRNA targeting PCSK9 now in phase 3 trials, requires only biannual dosing. Future studies should better define the relationship between AGT suppression and blood pressure to establish optimal dosing, as well as safety and efficacy in the context of common comorbidities, such as heart failure and chronic kidney disease, and in combination with other RAS blockers or a low-salt diet. Such studies should also address whether the massive renin rise in the absence of AGT involves recruitment of renin secreting cells outside the juxtaglomerular apparatus and/or juxtaglomerular hypertrophy.[35]

Funding

This work was partially supported by Alnylam Pharmaceuticals.

Conflict of Interest

D.F., J.K. and I.Z. are employees of Alnylam Pharmaceuticals. A.H.J.D. received a grant from Alnylam Pharmaceuticals which has partially supported this work. M.P. is an employee of Attoquant Diagnostics. K.M.M.C. was supported by a National Health and Medical Research Council of Australia CJ Martin Fellowship #1112125.

References

1. Gupta P, Patel P, Strauch B, Lai FY, Akbarov A, Maresova V, White CMJ, Petrak O, Gulsin GS, Patel V, Rosa J, Cole R, Zelinka T, Holaj R, Kinnell A, Smith PR, Thompson JR, Squire I, Widimsky J, Jr., Samani NJ, Williams B, Tomaszewski M. Risk factors for nonadherence to antihypertensive treatment. Hypertension. 2017;69:1113-1120

2. Cushman WC, Ford CE, Cutler JA, Margolis KL, Davis BR, Grimm RH, Black HR, Hamilton BP, Holland J, Nwachuku C, Papademetriou V, Probstfield J, Wright JT, Jr., Alderman MH, Weiss RJ, Piller L, Bettencourt J, Walsh SM, Group ACR. Success and predictors of blood pressure control in diverse north american settings: The antihypertensive and lipid-lowering treatment to prevent heart attack trial (allhat). J Clin Hypertens (Greenwich). 2002;4:393-404

3. van den Meiracker AH, Admiraal PJ, Janssen JA, Kroodsma JM, de Ronde WA, Boomsma F, Sissmann J, Blankestijn PJ, Mulder PG, Man In 't Veld AJ, et al. Hemodynamic and biochemical effects of the at1 receptor antagonist irbesartan in hypertension. Hypertension. 1995;25:22-29

4. Mooser V, Nussberger J, Juillerat L, Burnier M, Waeber B, Bidiville J, Pauly N, Brunner HR. Reactive hyperreninemia is a major determinant of plasma angiotensin ii during ace inhibition. Journal of cardiovascular pharmacology. 1990;15:276-282

5. Sealey JE, Laragh JH. Aliskiren, the first renin inhibitor for treating hypertension: Reactive renin secretion may limit its effectiveness. Am J Hypertens. 2007;20:587-597

6. Mullick AE, Yeh ST, Graham MJ, Engelhardt JA, Prakash TP, Crooke RM. Blood pressure lowering and safety improvements with liver angiotensinogen inhibition in models of hypertension and kidney injury. Hypertension. 2017;70:566-576

7. Olearczyk J, Gao S, Eybye M, Yendluri S, Andrews L, Bartz S, Cully D, Tadin-Strapps M. Targeting of hepatic angiotensinogen using chemically modified sirnas results in significant and sustained blood pressure

lowering in a rat model of hypertension. Hypertension research : official journal of the Japanese Society of Hypertension. 2014;37:405-412
8. Crooke ST, Witztum JL, Bennett CF, Baker BF. Rna-targeted therapeutics. Cell metabolism. 2018;27:714-739
9. Ray KK, Landmesser U, Leiter LA, Kallend D, Dufour R, Karakas M, Hall T, Troquay RP, Turner T, Visseren FL, Wijngaard P, Wright RS, Kastelein JJ. Inclisiran in patients at high cardiovascular risk with elevated ldl cholesterol. N Engl J Med. 2017;376:1430-1440
10. Makani H, Bangalore S, Desouza KA, Shah A, Messerli FH. Efficacy and safety of dual blockade of the renin-angiotensin system: Meta-analysis of randomised trials. Bmj. 2013;346:f360
11. Balcarek J, Seva Pessoa B, Bryson C, Azizi M, Menard J, Garrelds IM, McGeehan G, Reeves RA, Griffith SG, Danser AH, Gregg R. Multiple ascending dose study with the new renin inhibitor vtp-27999: Nephrocentric consequences of too much renin inhibition. Hypertension. 2014;63:942-950
12. Danser AH, Derkx FH, Schalekamp MA, Hense HW, Riegger GA, Schunkert H. Determinants of interindividual variation of renin and prorenin concentrations: Evidence for a sexual dimorphism of (pro)renin levels in humans. J Hypertens. 1998;16:853-862
13. MacFadyen RJ, Lee AF, Morton JJ, Pringle SD, Struthers AD. How often are angiotensin ii and aldosterone concentrations raised during chronic ace inhibitor treatment in cardiac failure? Heart (British Cardiac Society). 1999;82:57-61
14. van Thiel BS, Goes Martini A, Te Riet L, Severs D, Uijl E, Garrelds IM, Leijten FPJ, van der Pluijm I, Essers J, Qadri F, Alenina N, Bader M, Paulis L, Rajkovicova R, Domenig O, Poglitsch M, Danser AHJ. Brain renin-angiotensin system: Does it exist? Hypertension. 2017;69:1136-1144
15. de Lannoy LM, Danser AH, van Kats JP, Schoemaker RG, Saxena PR, Schalekamp MA. Renin-angiotensin system components in the interstitial fluid of the isolated perfused rat heart. Local production of angiotensin i. Hypertension. 1997;29:1240-1251
16. van Esch JH, Gembardt F, Sterner-Kock A, Heringer-Walther S, Le TH, Lassner D, Stijnen T, Coffman TM, Schultheiss HP, Danser AH, Walther T. Cardiac phenotype and angiotensin ii levels in at1a, at1b, and at2 receptor single, double, and triple knockouts. Cardiovascular research. 2010;86:401-409
17. Alexiou T, Boon WM, Denton DA, Nicolantonio RD, Walker LL, McKinley MJ, Campbell DJ. Angiotensinogen and angiotensin-converting enzyme gene copy number and angiotensin and bradykinin peptide levels in mice. J Hypertens. 2005;23:945-954
18. Griffiths CD, Morgan TO, Delbridge LM. Effects of combined administration of ace inhibitor and angiotensin ii receptor antagonist are prevented by a high nacl intake. J Hypertens. 2001;19:2087-2095
19. Richer-Giudicelli C, Domergue V, Gonzalez MF, Messadi E, Azizi M, Giudicelli JF, Ménard J. Haemodynamic effects of dual blockade of the renin-angiotensin system in spontaneously hypertensive rats: Influence of salt. J Hypertens. 2004;22:619-627
20. Sato A, Saruta T. Aldosterone breakthrough during angiotensin-converting enzyme inhibitor therapy. American journal of hypertension. 2003;16:781-788
21. Matsusaka T, Niimura F, Shimizu A, Pastan I, Saito A, Kobori H, Nishiyama A, Ichikawa I. Liver angiotensinogen is the primary source of renal angiotensin ii. J Am Soc Nephrol. 2012;23:1181-1189
22. Ye F, Wang Y, Wu C, Howatt DA, Wu CH, Balakrishnan A, Mullick AE, Graham MJ, Danser AHJ, Wang J, Daugherty A, Lu HS. Angiotensinogen and megalin interactions contribute to atherosclerosis-brief report. Arteriosclerosis, thrombosis, and vascular biology. 2019;39:150-155
23. Klotz S, Burkhoff D, Garrelds IM, Boomsma F, Danser AHJ. The impact of left ventricular assist device-induced left ventricular unloading on the myocardial renin-angiotensin-aldosterone system: Therapeutic consequences? Eur Heart J. 2009;30:805-812
24. de Lannoy LM, Danser AH, Bouhuizen AM, Saxena PR, Schalekamp MA. Localization and production of angiotensin ii in the isolated perfused rat heart. Hypertension. 1998;31:1111-1117
25. van Kats JP, van Meegen JR, Verdouw PD, Duncker DJ, Schalekamp MA, Danser AH. Subcellular localization of angiotensin ii in kidney and adrenal. J Hypertens. 2001;19:583-589
26. van Kats JP, de Lannoy LM, Jan Danser AH, van Meegen JR, Verdouw PD, Schalekamp MA. Angiotensin ii type 1 (at1) receptor-mediated accumulation of angiotensin ii in tissues and its intracellular half-life in vivo. Hypertension. 1997;30:42-49
27. Danser AH, Batenburg WW, van den Meiracker AH, Danilov SM. Ace phenotyping as a first step toward personalized medicine for ace inhibitors. Why does ace genotyping not predict the therapeutic efficacy of ace inhibition? Pharmacology & therapeutics. 2007;113:607-618

28. Lopez-Ilasaca M, Liu X, Tamura K, Dzau VJ. The angiotensin ii type i receptor-associated protein, atrap, is a transmembrane protein and a modulator of angiotensin ii signaling. Molecular biology of the cell. 2003;14:5038-5050
29. Dixit MP, Xu L, Xu H, Bai L, Collins JF, Ghishan FK. Effect of angiotensin-ii on renal na+/h+ exchanger-nhe3 and nhe2. Biochimica et biophysica acta. 2004;1664:38-44
30. Sandberg MB, Riquier AD, Pihakaski-Maunsbach K, McDonough AA, Maunsbach AB. Ang ii provokes acute trafficking of distal tubule na+-cl(-) cotransporter to apical membrane. Am J Physiol Renal Physiol. 2007;293:F662-669
31. Talati G, Ohta A, Rai T, Sohara E, Naito S, Vandewalle A, Sasaki S, Uchida S. Effect of angiotensin ii on the wnk-osr1/spak-ncc phosphorylation cascade in cultured mpkdct cells and in vivo mouse kidney. Biochemical and biophysical research communications. 2010;393:844-848
32. Sorensen MV, Grossmann S, Roesinger M, Gresko N, Todkar AP, Barmettler G, Ziegler U, Odermatt A, Loffing-Cueni D, Loffing J. Rapid dephosphorylation of the renal sodium chloride cotransporter in response to oral potassium intake in mice. Kidney Int. 2013;83:811-824
33. van Kats JP, Chai W, Duncker DJ, Schalekamp MA, Danser AH. Adrenal angiotensin: Origin and site of generation. American journal of hypertension. 2005;18:1104-1110
34. Hilgers KF, Veelken R, Müller DN, Kohler H, Hartner A, Botkin SR, Stumpf C, Schmieder RE, Gomez RA. Renin uptake by the endothelium mediates vascular angiotensin formation. Hypertension. 2001;38:243-248
35. Oka M, Medrano S, Sequeira-Lomicronpez MLS, Gomez RA. Chronic stimulation of renin cells leads to vascular pathology. Hypertension. 2017;70:119-128

Novelty and significance

What is new?

Small interfering RNA targeting liver angiotensinogen (AGT) provides antihypertensive and cardioprotective efficacy comparable to that of single RAS blockade.

Angiotensin II elimination requires >99% suppression of circulating AGT, and under such circumstances blood pressure decreases substantially.

What is relevant?

Given its stable and sustained efficacy, lasting weeks, RNA interference may offer a unique approach to improving therapy adherence and treating hypertension.

Summary

Maximal blockade of the renin-angiotensin system (RAS), achieved by valsartan+siRNA, yielded the greatest reduction in blood pressure and cardiac hypertrophy, while AGT lowering alone was as effective as conventional RAS inhibitors. In clinical practice, RNA interference at the AGT level may not only prevent RAS reactivation, but also improve cardiovascular outcome and medication adherence, due to its long-lasting and stable efficacy after a single subcutaneous injection.

Supplemental Material

Methods

Animal studies

All studies were performed under the regulation and permission of the Animal Care Committee of the Erasmus MC (protocol number 16-511-01). Male, 12-week old spontaneously hypertensive rats (SHRs) were obtained from Charles River, Germany (n=20), and, due to temporary unavailability of the SHR strain at Charles River, additionally from Janvier Labs, France (n=28). Rats were housed in individual cages and maintained on a 12-h light-dark cycle with access to standard rat chow and water ad libitum. Radiotelemetry transmitters (HD-S10, Data Sciences International, St. Paul, USA) were implanted for continuous measurement of blood pressure, heart rate and activity.[1] After a one-week recovery period, SHRs were treated for four weeks with vehicle, valsartan (31 mg/kg/day dissolved in drinking water; Santa Cruz Biotechnology, Heidelberg, Germany),[2, 3] captopril (100 mg/kg/day dissolved in drinking water; Sigma Aldrich, Zwijndrecht, The Netherlands),[4] captopril+valsartan, AGT siRNA (10 mg/kg; subcutaneous fortnightly injection; provided by Alnylam Pharmaceuticals, Cambridge, MA, USA), or valsartan+siRNA (all groups n=8). The siRNA consisted of a chemically modified antisense strand with sequence UUGAUUUUUGCCCAGGAUAGCUC, hybridized with a chemically modified sense strand of sequence GCUAUCCUGGGCAAAAAUCAA, with a triantennary GalNAc (a high-affinity ligand for the hepatocyte-specific asialoglycoprotein receptor, resulting in selective and efficient delivery to hepatocytes) attached to the 3' end of the sense strand.5 To identify a dosing regimen for AGT siRNA, suppression of circulating AGT by AGT siRNA was evaluated in male, 16-week old SHRs (Charles River), treated with a single dose of phosphate buffered saline (PBS), 3 mg/kg, or 10 mg/kg siRNA on Day 0; 3 mg/kg or 10 mg/kg on Day 0 and 14; or 10 mg/kg on Day 0, 7, 14, and 21. Circulating AGT levels were determined by enzyme kinetic assay as described below in serum collected at baseline (defined as Day 0), at two, and at four weeks post study start. While the various dosing regimens performed similarly (**Supplemental Table S1**), fortnightly dosing of 10 mg/kg was selected to ensure maximal target silencing over the four-week period for assessment of efficacy. For valsartan and captopril, water intake was checked every other day, and drug concentrations were adjusted to achieve the described daily doses. During the study, blood plasma was collected from the lateral tail vein by venipuncture and 24-h urine was collected in metabolic cages prior to treatment (baseline), and after two and four weeks of treatment for biochemical measurements. At the end of antihypertensive treatment, rats were anaesthetized by inhalation of isoflurane and sacrificed by exsanguination: 1

mL blood was collected in 4 mol/L guanine thiocyanate (Sigma Aldrich), and remaining blood was supplemented with EDTA and centrifuged at 13000 rpm to obtain plasma. Kidneys and heart were excised, weighed, divided into transverse segments and fixated in 4% paraformaldehyde for histological analysis, or snap frozen in liquid nitrogen for gene expression and protein analysis.

Oligonucleotide synthesis

Oligonucleotides were synthesized on a MerMade-12 DNA/RNA synthesizer. Sterling solvents/reagents from Glen Research, 500-Å CPG solid-supports from Prime Synthesis, custom 2′-trivalent GalNAc 500-Å CPG solid-support, and 2′-O-methyl (2′-OMe), 2′-deoxy-2′-fluoro (2′-F) ribonucleoside-phosphoramidites from Hongene were all used as received.[5] Low-water content acetonitrile was purchased from EMD Chemicals. Oligonucleotides were synthesized using modified synthesis cycles, based on those provided with the instrument. A solution of 0.6 M 5-(S-ethylthio)-1H-tetrazole in acetonitrile was used as the activator. The phosphoramidite solutions were 0.15 M in anhydrous acetonitrile with 15% dimethylformamide as a co-solvent for 2′-OMe uridine and cytidine. The oxidizing reagent was 0.02 M I2 in THF/pyridine/H_2O. N,N-Dimethyl-N′-(3-thioxo-3H-1,2,4-dithiazol-5-yl)methanimidamide (DDTT), 0.09 M in pyridine, was used as the sulfurizing reagent. The detritylation reagent was 3% dichloroacetic acid (DCA) in dichloromethane (DCM). After completion of the solid-phase synthesis, the CPG solid support was washed with 5% (v/v) piperidine in anhydrous acetonitrile three times with 5-minute holds after each flow. The support was then washed with anhydrous acetonitrile and dried with argon. The oligonucleotide was then incubated with 28-30% (w/v) NH_4OH, 35°C, 20 h.[6] The solvent was collected by filtration and the support was rinsed with water prior to analysis. Oligonucleotide solutions of ~ 1 OD_{260} Units/mL were used for analysis of the crude material, where 30 – 50 µL of solution were injected. LC/ESI-MS was performed on an Agilent 6130 single quadrupole LC/MS system using an XBridge C8 column (2.1 × 50 mm, 2.5 µm) at 60°C. Buffer A consisted of 200 mM 1,1,1,3,3,3-hexafluoro-2-propanol (HFIP) and 16.3 mM triethylamine (TEA) in H_2O, and buffer B was 100% methanol. A gradient from 0% to 40% of buffer B over 10 min followed by washing and recalibration at a flow rate of 0.70 mL/min. The column temperature was 75°C. Crude oligonucleotides were purified by anion-exchange HPLC using a linear gradient of 0.17 M to 0.45 M NaBr buffer of pH 8.5/10% (v) acetonitrile in 120-150 min at room temperature. All single strands were purified to >85% HPLC (260 nm) purity and then desalted by size exclusion chromatography using an AP-2 glass column (20 × 300 mm, Waters) custom-packed with Sephadex G25 (GE Healthcare), eluted with sterile nuclease-free water. Hybridization to generate siRNA duplexes was performed by mixing equimolar amounts of

complementary strands to a final siRNA concentration of 10 mg/mL in 1×PBS buffer, pH 7.4, and by heating in a water bath at 95°C for 5 minutes followed by slow cooling to room temperature.

Biochemical measurements, RT-PCR, siRNA quantification and Western blotting

In plasma, AGT was measured by enzyme kinetic assay as the maximum quantity of angiotensin (Ang) I generated during incubation, at pH 7.4 and 37°C, with rat kidney renin in the presence of a mixture of ACE, angiotensinase, and serine protease inhibitors.[7, 8] The lower limit of detection (LLOD) of this assay was 0.2 pmol/mL. In the cases that measurements were at or below the LLOD, this limit was applied to allow statistical analysis. For comparison, in a selected set of samples, plasma AGT was also measured by direct AGT radioimmunoassay (Immuno-Biological Laboratories Co. Ltd., Japan), and AGT in urine was measured exclusively with this kit (LLOD 0.32 ng/mL or 0.006 pmol/mL). Measurements by direct AGT radioimmunoassay fully confirmed the measurements by enzyme kinetic assay (n=36, data not shown), although levels in absolute terms were 5-10 times lower with the direct assay as compared to those measured with the enzyme-kinetic assay. This is most likely due to the fact that the standard of the direct AGT assay, when determined by enzyme-kinetic assay (applying Ang I as standard), yielded 5-10-fold higher levels than predicted. Similar observations have been made with a human direct AGT assay.[9]

Active plasma renin concentration (APRC) was measured by enzyme kinetic assay, by quantifying Ang I generation in the presence of excess porcine angiotensinogen (LLOD 10 fmol/ml.hr).[7] Plasma aldosterone was measured by solid-phase radioimmunoassay (LLOD 14.8 pg/mL; Diagnostic Products Corporation; Siemens Medical Solutions Diagnostics, Los Angeles, USA). NT-proBNP was measured with a rat ELISA NT-proBNP kit (LLOD 15.6 pg/mL; Aviva Systems Biology, San Diego, USA). Angiotensin and bradykinin (BK) metabolites in plasma and renal tissue were measured by LC-MS/MS analysis as described before.[10, 11] Briefly, tissue samples were homogenized under liquid N2 and extracted with a guanidinium based extraction buffer. Stabilized whole blood and tissue extracts were spiked with stable isotope labelled internal standards for each individual target analyte (Sigma Aldrich) before being subjected to C18 based solid phase extraction and subsequent LC-MS/MS analysis. The lower limit of quantification (LLOQ) in blood/tissue were 4/8 (Ang I), 1/3 (Ang II), 7/17 (Ang-(1–7)), 1/9 (Ang-(1–5)), 3/6 (Ang-(2–8)), 1/8 (Ang-(3–8)), 11/11 (BK-(1-9)) and 2/6 (BK-(1-7)) pg per mL or g tissue, respectively. In 24-h urine, albumin was measured with a rat albumin ELISA kit (LLOD 7 µg/mL; Abcam, Cambridge, UK) and NGAL with a rat NGAL ELISA kit (LLOD 0.1 pg/mL; Abcam, Cambridge, UK). Plasma

potassium and urinary sodium and total protein (both 24-hour urine) were measured at the clinical chemistry laboratory of the Erasmus MC.

Total RNA was isolated from snap-frozen kidney cortex and medulla using TRI Reagent (Sigma Aldrich, Zwijndrecht, The Netherlands) and reverse transcribed into cDNA using the QuantiTect Reverse Transcription Kit (Qiagen, Venlo, The Netherlands). cDNA was amplified in 40 cycles in triplicate (denaturation at 95°C for 3 min; thermal cycling at 95°C for 3 sec, annealing/extension at 60°C for 20 sec) followed by a melt curve with a CFX384 (Bio-rad) using Kapa SYBR® Fast (Kapa Biosystems). The intron-spanning oligonucleotide primers were designed with NCBI (Primer-BLAST; **Supplemental Table S2**). The ΔΔCt method was used for relative quantification of mRNA expression levels, using the geometric mean of housekeeping genes β_2-microglobulin (B2M) and β-actin (Actb) for normalization.

For quantification of Agt mRNA, snap-frozen liver and kidney samples of a subset of rats (vehicle-, AGT siRNA- and valsartan+siRNA-treated; n=3/group) were homogenized in a SPEX GenoGrinder (250 strokes per second, 1x speed, 120 seconds). Total RNA was isolated with a RNAqueous 96 Total RNA Isolation kit (ThermoFisher) and reverse transcribed into cDNA according to manufacturer protocol (Applied Biosystems). Multiplex qPCR reactions were performed in duplicate using a gene specific TaqMan assay for Agt (ThermoFisher Scientific #Rn00593114_m1) and rat Gapdh (#4352338E) as an endogenous control. Real-Time PCR was performed on a Roche LightCycler 480 using LightCycler 480 Probes Master Mix (Roche). Data were analyzed using the ΔΔCt method, normalizing AGT expression to Gapdh, followed by normalization to the average of the control-treated animals. Data were expressed as percent of control.

siRNA quantification was performed as previously described.[12] Briefly, tissue powder from homogenized livers and kidneys (vehicle-, AGT siRNA- and valsartan+siRNA-treated; n=3/group) was reconstituted in PBS containing 0.25% Triton-X 100 at a concentration of 10 mg/mL. A standard curve of siRNA comprised of ten four-fold serial dilutions from 8 ng/μL duplex (3.7 ng/μL antisense strand) was implemented for quantification of antisense strand. Samples and standard curve dilutions were then heated at 95°C for 10 minutes, followed by incubation on ice for 10 minutes and centrifugation at 15,000 × g for 10 minutes at 4°C. The supernatants were then transferred to new tubes. Kidney samples were diluted 1:1 in PBS with 0.25% Triton-X 100 prior to RT, while liver samples were diluted 1:500. Antisense levels were quantified by stem loop reverse transcription followed by qPCR based on previously-described methods.[13, 14] The primer and probe sequences were GTCGTATCC AGTGCAGGGTCCGAGGTATTCGCACTGGATACGACGAGCTATCCT (RT primer),

GCCGCGCTTGATTTTTGCCC (Forward qPCR primer), CTGGATACGACGAGCTATCC (Taqman probe), GTGCAGGGTCCGAGGT (Reverse qPCR primer), using 5' FAM and 3' MGBNFQ for the probe. Ct values derived from samples were interpolated onto the standard curve for the antisense strand, adjusted for sample dilution, and expressed as micrograms of antisense strand per gram of tissue.

To perform immunoblotting, kidneys were cut into 4 equal pieces, and one piece was homogenized on ice in a buffer containing 0.3 M sucrose, 50mM Tris-HCl pH 7.5, 1mM EDTA, 1mM EGTA, 1mM DTT supplemented with protease inhibitors. Protein (40-60 ug; DC™ protein assay kit, Bio-Rad) were separated by electrophoresis on a Criterion TGX precast protein gel (Bio-Rad) and transferred to a membrane using the Trans-Blot Turbo Transfer System (Bio-Rad). Membranes were incubated with 5% bovine serum albumin (BSA) or 5% milk powder in Tris-buffered saline containing 0.1% Tween-20. Next, blots were incubated overnight at 4°C with primary antibodies against the following proteins: sodium-hydrogen exchanger type 3 (NHE3; StressMarq; 1:1000), sodium-potassium-chloride co-transporter (NKCC2; StressMarq; 1:1000); sodium-chloride co-transporter (NCC; StressMarq; 1:500) and its phosphorylated form at threonine-58 (pNCC; a kind gift by Dr. R.A. Fenton[15]; 1:500), the α- and β-subunits of the epithelial sodium channel (ENaC; both StressMarq; 1:1000), serum- and glucocorticoid-regulated kinase 1 (SGK1; Millipore; 1:1000), neural precursor cell expressed, developmentally downregulated protein 4-2 (NEDD4-2, 1:1000, Abcam, Cambridge, UK), aquaporin-2 (AQP2; StressMarq; 1:1000). β-actin (Millipore; 1:50,000) was used for normalization of protein levels. After washing, blots were incubated with horseradish peroxidase-conjugated secondary antibodies (1:3000; Bio-Rad, Veenendaal, The Netherlands). Signals were detected by chemiluminescence (Clarity Western ECL substrate; Bio-Rad) and quantified using ImageQuant LAS 4000 (GE Healthcare, Diegem, Belgium). Samples (n=8 per group) were divided over two maxi-blots (n=4 per group per blot). To allow for combined statistical analysis, samples were first normalized to the loading control actin, followed by normalization to the average of the vehicle-treated rats from the respective immunoblot.

Kidney function

GFR was determined prior to treatment (baseline), and at two and four weeks of treatment via transcutaneous measurement of fluorescein isothiocyanate (FITC)-labeled sinistrin clearance curves using a miniaturized non-invasive clearance (NIC)-kidney fluorescent detection device (Mannheim Pharma & Diagnostics GmbH, Mannheim, Germany).[16] Briefly, rats were lightly anesthetized (2–2.5% v/v isoflurane). The NIC-Kidney device was attached to a depilated region on the back of the rat using a double-sided adhesive patch

and adhesive tape. Following a 3 to 5-minute baseline period, a bolus of FITC-sinistrin (3 mg/100 g made up in 0.9% sodium chloride solution) was administered via the tail vein. The rat was then returned to its cage for 2 hours. At the end of the 2-hour recording period, rats were lightly anesthetized and the NIC-kidney device was removed. The collected data were subsequently analyzed using NIC-kidney device partner software. The software generates the elimination kinetics curve of FITC-sinistrin from which excretion half-life (t1/2) was determined using a one-compartment model. The derived $t_{1/2}$ was converted into GFR using a validated conversion factor and formula for rats previously described[17, 18]:
GFR (mL/min per 100g body weight (BW)) = 31.26 (mL/100g BW) / $t_{1/2}$ FITC-sinistrin (minutes).

Histology

Fixated heart sections were dehydrated and paraffin-embedded. Gomori silver staining was applied to deparaffinized sections (5μm) of the left ventricle of the heart to visualize individual cardiomyocytes. Sirius red staining was applied to visualize collagen as a measure of cardiac fibrosis. Cardiomyocyte size and the amount of collagen was measured using Qwin (Leica, Cambridge, UK). Only transversally cut cells showing a nucleus were used to determine the cardiomyocyte area.

Myograph studies

Following isolation, iliac arteries were cut into segments of ≈2 mm length and mounted in a Mulvany myograph (Danish Myo Technology, Aarhus, Denmark) with separated 6-mL organ baths containing Krebs bicarbonate solution, aerated with 95% O_2 and 5% CO_2, and maintained at 37°C.[19] Tissue responses were measured as changes in isometric force, using Powerlab with Labchart software (AD Instruments, Oxford, UK). Following a 30-min stabilization period, the optimal internal diameter was set to a tension equivalent of 0.9 times the estimated diameter at 100 mm Hg effective transmural pressure, as described by Mulvany and Halpern.[20] Subsequently, to determine the maximum contractile response, the tissue was exposed to 100 mmol/L KCl. The segments were then allowed to equilibrate in fresh organ bath fluid for 30 min. Next, segments were preincubated for 30 min with the NO synthase inhibitor L-NAME (N^{ω}-nitro-L-arginine methyl ester hydrochloride; 100 μmol/L), the small conductance Ca^{2+}-activated K^+ channel inhibitor apamin (100 μmol/L), the intermediate conductance Ca^{2+}-activated K^+ channel inhibitor TRAM34 (10 μmol/L), the ETA receptor antagonist BQ123 (1μmol/L), and the ETB receptor antagonist BQ788 (1μmol/L). Thereafter, CRCs were constructed to ET-1. To construct CRCs to the endothelium-dependent vasodilator acetylcholine (ACh), iliac arteries were preconstricted with U46619 (0.1–0.3 μmol/L). All drugs were from Sigma-Aldrich.

Statistical analysis

Statistical tests were performed using Graphpad Prism version 7.0 for Windows (Graphpad Software Inc., La Jolla, USA). Data are expressed as mean values ± standard deviation (± SEM in figures). For comparisons between multiple groups, a one-way analysis of variance (ANOVA) was used to analyse data obtained at a single point in time, a repeated-measures ANOVA was used to analyse data obtained at multiple points in time. Post-hoc correction according to Bonferroni was performed in case of multiple comparisons. To conform to normality, non-parametric data were transformed to natural logarithms before statistical testing (AGT, renin, angiotensin metabolites, albuminuria). Univariate linear associations were assessed by calculation of Pearson's coefficient of correlation. Two-tailed P values <0.05 were considered statistically significant.

References

1. van Esch JHM, Moltzer E, van Veghel R, Garrelds IM, Leijten F, Bouhuizen AM, Danser AHJ. Beneficial cardiac effects of the renin inhibitor aliskiren in spontaneously hypertensive rats. J Hypertens. 2010;28:2145-2155.
2. Tominaga N, Robert A, Izuhara Y, Ohtomo S, Dan T, Chihara K, Kurokawa K, Van Ypersele de Strihou C, Miyata T. Very high doses of valsartan provide renoprotection independently of blood pressure in a type 2 diabetic nephropathy rat model. Nephrology. 2009;14:581-587.
3. Kusaka H, Sueta D, Koibuchi N, Hasegawa Y, Nakagawa T, Lin B, Ogawa H, Kim-Mitsuyama S. Lcz696, angiotensin ii receptor-neprilysin inhibitor, ameliorates high-salt-induced hypertension and cardiovascular injury more than valsartan alone. Am J Hypertension. 2015;28:1409-1417.
4. Antonaccio MJ, Rubin B, Horovitz ZP, Laffan RJ, Goldberg ME, High JP, Harris DN, Zaidi I. Effects of chronic treatment with captopril (sq 14,225), an orally active inhibitor of angiotensin i-converting enzyme, in spontaneously hypertensive rats. Jpn J Pharmacol. 1979;29:285-294.
5. Nair JK, Willoughby JL, Chan A, Charisse K, Alam MR, Wang Q, Hoekstra M, Kandasamy P, Kel'in AV, Milstein S, Taneja N, O'Shea J, Shaikh S, Zhang L, van der Sluis RJ, Jung ME, Akinc A, Hutabarat R, Kuchimanchi S, Fitzgerald K, Zimmermann T, van Berkel TJ, Maier MA, Rajeev KG, Manoharan M. Multivalent n-acetylgalactosamine-conjugated sirna localizes in hepatocytes and elicits robust rnai-mediated gene silencing. J Am Chem Soc. 2014;136:16958-16961.
6. O'Shea J, Theile CS, Das R, Babu IR, Charisse K, Manoharan M, Maier MA, Zlatev I. An efficient deprotection method for 5′-[o,o-bis(pivaloyloxymethyl)]-(e)-vinylphosphonate containing oligonucleotides. Tetrahedron. 2018;74:6182-6186.
7. de Lannoy LM, Danser AHJ, van Kats JP, Schoemaker RG, Saxena PR, Schalekamp MADH. Renin-angiotensin system components in the interstitial fluid of the isolated perfused rat heart. Local production of angiotensin i. Hypertension. 1997;29:1240-1251.
8. van den Heuvel M, Batenburg WW, Jainandunsing S, Garrelds IM, van Gool JM, Feelders RA, van den Meiracker AH, Danser AHJ. Urinary renin, but not angiotensinogen or aldosterone, reflects the renal renin-angiotensin-aldosterone system activity and the efficacy of renin-angiotensin-aldosterone system blockade in the kidney. J Hypertens. 2011;29:2147-2155.
9. Verdonk K, Saleh L, Lankhorst S, Smilde JE, van Ingen MM, Garrelds IM, Friesema EC, Russcher H, van den Meiracker AH, Visser W, Danser AHJ. Association studies suggest a key role for endothelin-1 in the pathogenesis of preeclampsia and the accompanying renin-angiotensin-aldosterone system suppression. Hypertension. 2015;65:1316-1323.
10. Domenig O, Manzel A, Grobe N, Konigshausen E, Kaltenecker CC, Kovarik JJ, Stegbauer J, Gurley

SB, van Oyen D, Antlanger M, Bader M, Motta-Santos D, Santos RA, Elased KM, Saemann MD, Linker RA, Poglitsch M. Neprilysin is a mediator of alternative renin-angiotensin-system activation in the murine and human kidney. Sci Rep. 2016;6:33678.
11. Basu R, Poglitsch M, Yogasundaram H, Thomas J, Rowe BH, Oudit GY. Roles of angiotensin peptides and recombinant human ace2 in heart failure. J Am Coll Cardiol. 2017;69:805-819.
12. Parmar RG, Brown CR, Matsuda S, Willoughby JLS, Theile CS, Charisse K, Foster DJ, Zlatev I, Jadhav V, Maier MA, Egli M, Manoharan M, Rajeev KG. Facile synthesis, geometry, and 2'-substituent-dependent in vivo activity of 5'-(e)- and 5'-(z)-vinylphosphonate-modified sirna conjugates. J Med Chem. 2018;61:734-744.
13. Chen C, Ridzon DA, Broomer AJ, Zhou Z, Lee DH, Nguyen JT, Barbisin M, Xu NL, Mahuvakar VR, Andersen MR, Lao KQ, Livak KJ, Guegler KJ. Real-time quantification of microrna by stem-loop rt-pcr. Nucleic Acids Res. 2005;33:e179.
14. Cheng A, Li M, Liang Y, Wang Y, Wong L, Chen C, Vlassov AV, Magdaleno S. Stem-loop rt-PCR quantification of siRNAs in vitro and in vivo. Oligonucleotides. 2009;19:203-208.
15. Pedersen NB, Hofmeister MV, Rosenbaek LL, Nielsen J, Fenton RA. Vasopressin induces phosphorylation of the thiazide-sensitive sodium chloride cotransporter in the distal convoluted tubule. Kidney Int. 2010;78:160-169.
16. Schock-Kusch D, Xie Q, Shulhevich Y, Hesser J, Stsepankou D, Sadick M, Koenig S, Hoecklin F, Pill J, Gretz N. Transcutaneous assessment of renal function in conscious rats with a device for measuring fitc-sinistrin disappearance curves. Kidney Int. 2011;79:1254-1258.
17. Schock-Kusch D, Sadick M, Henninger N, Kraenzlin B, Claus G, Kloetzer HM, Weiss C, Pill J, Gretz N. Transcutaneous measurement of glomerular filtration rate using fitc-sinistrin in rats. Nephrol Dial Transplant. 2009;24:2997-3001.
18. Yu W, Sandoval RM, Molitoris BA. Rapid determination of renal filtration function using an optical ratiometric imaging approach. Am J Physiol Renal Physiol. 2007;292:F1873-1880
19. Lu X, Krop M, Batenburg WW, Musterd-Bhaggoe UM, Garrelds IM, Danser AHJ. Renin inhibitor VTP-27999 differs from aliskiren: Focus on their intracellular accumulation and the (pro)renin receptor. J Hypertens. 2014;32:1255-1263.
20. Mulvany MJ, Halpern W. Contractile properties of small arterial resistance vessels in spontaneously hypertensive and normotensive rats. Circ Res. 1977;41:19-26.

Supplemental Table S1. Identification of a dosing regimen in SHRs treated with a single dose of PBS, 3 mg/kg, or 10 mg/kg siRNA on Day 0; 3 mg/kg or 10 mg/kg on Day 0 and 14; or 10 mg/kg on Day 0, 7, 14, and 21. Circulating AGT levels were determined in serum collected at baseline (defined as Day 0), at two, and at four weeks post study start. Data are expressed as percentage of predose levels and presented as mean ± SD. Abbreviations: q2w, once every 2 weeks; qw, once per week.

Circulating AGT (% Predose)			Day 14		Day 28	
Group	Dose	Frequency	Mean	SD	Mean	SD
1	PBS		100.6	35.2	80.1	19.5
2	3	Single	4.0	1.5	9.3	1.6
3	3	q2w	5.5	1.5	4.2	1.9
4	10	Single	2.3	0.6	4.4	2.5
5	10	q2w	3.6	1.0	2.6	1.3
6	10	qw	3.3	0.7	4.3	2.2

Supplemental Table S2. Sequences of primers for RT-PCR. Abbreviations: AT_{1a}, angiotensin II type 1a receptor; AT_{1b}, angiotensin II type 1b receptor; AT_2, angiotensin II type 2 receptor; ACE, angiotensin converting enzyme; Ren, renin; (P)RR, (pro)renin receptor; ACTB, β-actin; B2M, β_2-microglobulin.

Gene		Sequences (5' to 3')
AT_{1a}	Forward primer	ATCACCAGGTCAAGTGGATTTCG
	Reverse primer	TTCCCACCACAAAGATGATGC
AT_{1b}	Forward primer	CTGAATCTTGCCCTGGCTGA
	Reverse primer	ACATAGGTGGTTGCCGAAGG
AT_2	Forward primer	AAGGAATCCCTGGCAAGCATC
	Reverse primer	TGGCAATGAGGACAGACAAGC
ACE	Forward primer	CTTCCCCAACAAGACTGCCA
	Reverse primer	GTTTCGTGAGGAAGCCAGGA
ACE2	Forward primer	AGATGAAGCGGGAGATCGTTG
	Reverse primer	CATGGAACAGAGATGCAGGGT
Ren	Forward primer	TGTGGTAACTGTGGGTGGAAT
	Reverse primer	GCATGAAGGGTATCAGGGGC
(P)RR	Forward primer	TCTTCTCTGGTGTCGAGTGC
	Reverse primer	CTTCCTTCACAGAGAAGCCC
Actb	Forward primer	GGGAAATCGTGCGTGACATT
	Reverse primer	GCGGCAGTGGCCATCTC
B2M	Forward primer	ATGGCTCGCTCGGTGACCG
	Reverse primer	TGGGGAGTTTTCTGAATGGCAAGCA

Supplemental Table S3. Renin-angiotensin-aldosterone system (RAAS) parameters in blood and kidney after four weeks of vehicle, valsartan, captopril, AGT siRNA, captopril+valsartan or valsartan+siRNA treatment (all groups n=8). Data, represented as means ± SD, were analysed using ANOVA and post-hoc Bonferroni (*P≤0.05, †P≤0.01, ‡P≤0.001, §P≤0.0001 vs. vehicle).

parameter	vehicle	valsartan	captopril	captopril+ valsartan	AGT siRNA	valsartan+ siRNA
Blood						
Aldosterone (pg/mL)	22 ± 6	27 ± 13	24 ± 8	31 ± 10	31 ± 23	23 ± 10
RAS metabolite (fmol/mL)						
Ang(1-10) = Ang I	375 ± 196	1697 ± 1080‡	1503 ± 896†	1144 ± 427†	191 ± 134	30 ± 18§
Ang(1-8) = Ang II	36 ± 36	357 ± 331§	26 ± 19	24 ± 28	36 ± 42	9 ± 5*
Ang(1-7)	<7	<7	<7	<7	<7	<7
Ang(1-5)	2 ± 0.5	14 ± 15†	<1	<1	<1	<1
Ang(2-8)	<3	18 ± 17†	<3	<3	<3	<3
Ang(3-8)	4 ± 6	25 ± 20§	3 ± 3	2 ± 3	3 ± 5	<1
Ang II/Ang I (x100)	11 ± 7	17 ± 10	2 ± 1†	2 ± 1‡	15 ± 12	25 ± 7
Kidney						
RAS metabolite (fmol/g)						
Ang(1-10) = Ang I	413 ± 139	1096 ± 580†	939 ± 339*	260 ± 120	59 ± 17§	12 ± 8§
Ang(1-8) = Ang II	431 ± 144	338 ± 110	115 ± 54§	9 ± 9§	228 ± 42	15 ± 15§
Ang(1-7)	66 ± 45	156 ± 70‡	137 ± 76*	40 ± 28	22 ± 7†	<17‡
Ang(1-5)	16 ± 6	22 ± 11	<9	<9	<9	<9
Ang(2-8)	59 ± 42	37 ± 22	<6§	<6§	20 ± 12‡	<6§
Ang(3-8)	<8	13 ± 4	<8	<8	12 ± 3	<8
Ang II/Ang I (x100)	114 ± 48	35 ± 13§	13 ± 7§	3 ± 3§	424 ± 158§	161 ± 155

Supplemental Table S4. Growth, food and water intake after four weeks of vehicle, valsartan, captopril, AGT siRNA, captopril+valsartan or valsartan+siRNA treatment (all groups n=8). Data, represented as means ± SD, were analysed using repeated measures or one-way ANOVA and post-hoc Bonferroni (*P≤0.05, †P≤0.01, ‡P≤0.001, §P≤0.0001 vs. vehicle).

	vehicle	valsartan	captopril	captopril+ valsartan	AGT siRNA	valsartan+ siRNA
Body weight (g)	361 ± 32	366 ± 32	412 ± 27*	408 ± 25*	351 ± 38	315 ± 38*
Δ treatment	54 ± 12	63 ± 16	40 ± 13	24 ± 25†	51 ± 14	20 ± 21‡
Food intake (mg/day)	17 ± 4	18 ± 4	18 ± 2	14 ± 5	21 ± 2	19 ± 4
Water intake (mL/day)	26 ± 5	24 ± 3	48 ± 10‡	29 ± 11	27 ± 6	36 ± 7*

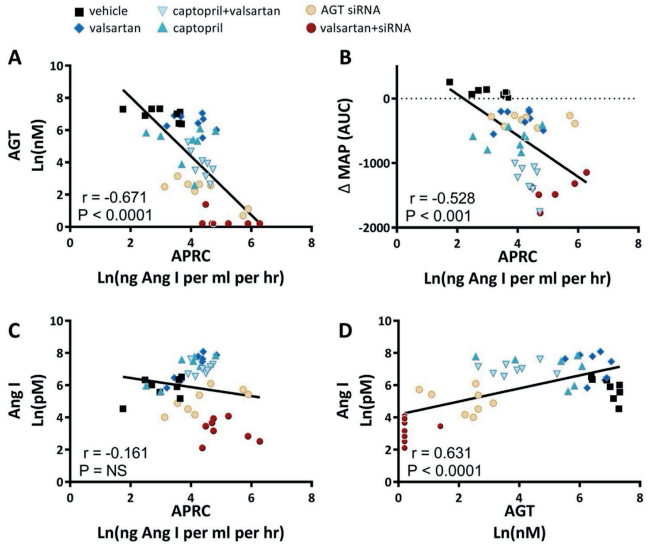

Supplemental Figure S1. Relationship between RAS parameters and antihypertensive effect. Correlation between **A)** angiotensinogen (AGT) and active plasma renin concentration (APRC), **B)** APRC and change in mean arterial pressure (ΔMAP; expressed as area under the curve), **C)** APRC and angiotensin (Ang) I, **D)** AGT and Ang I after four weeks of treatment with vehicle, valsartan, captopril, AGT siRNA, captopril+valsartan or valsartan+siRNA (all groups n=8). r denotes Pearson's correlation coefficient.

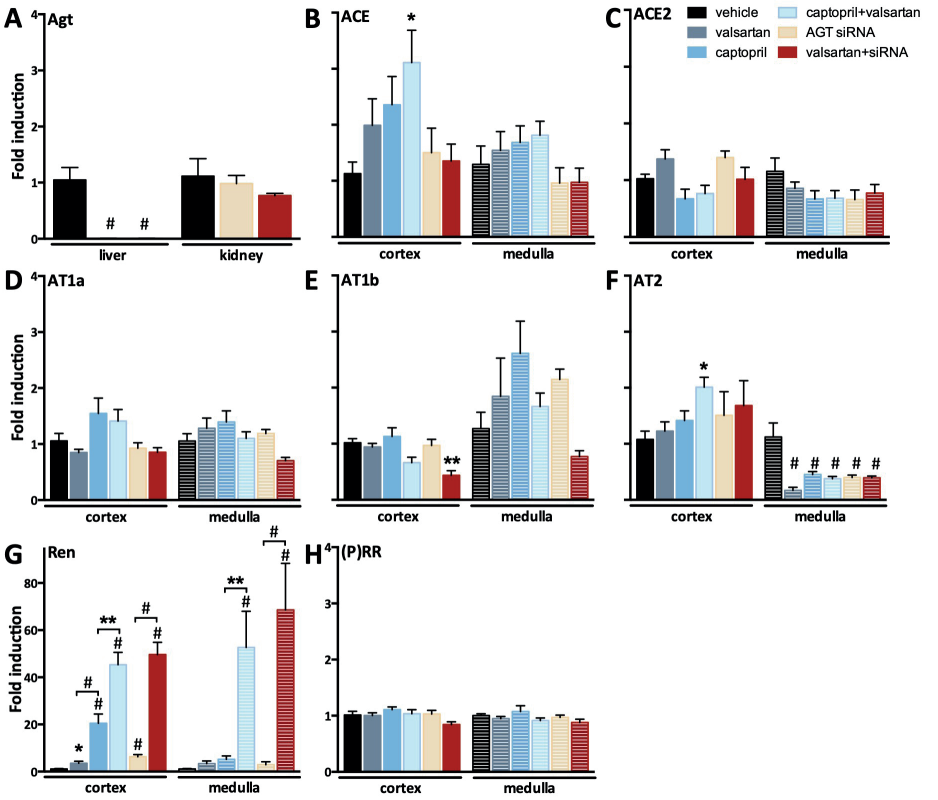

Supplemental Figure S2. Angiotensinogen, ACE, angiotensin receptor, renin and (pro)renin receptor expression. Gene expression of **A)** angiotensinogen (Agt) in liver and kidney (n=3 each for control, AGT siRNA, and valsartan+siRNA groups), **B)** angiotensin converting enzyme (ACE), **C)** ACE2, **D)** angiotensin II type Ia (*AT1a*), **E)** angiotensin II type Ib (*AT1b*), **F)** angiotensin II type 2 (*AT2*) receptors, **G)** renin and **H)** (pro)renin receptor ((P)RR) in renal cortex (closed bars) and medulla (striped bars) after four weeks of vehicle, valsartan, captopril, AGT siRNA, captopril+valsartan or valsartan+siRNA treatment (all groups n=8, except where noted). Data, expressed as fold induction relative to vehicle-treated control (means ± SEM), were analysed using one-way ANOVA and post-hoc Bonferroni (after logarithmic transformation for renin; * P≤0.05, ** P≤0.01, # P≤0.0001 vs. vehicle unless indicated otherwise in graph).

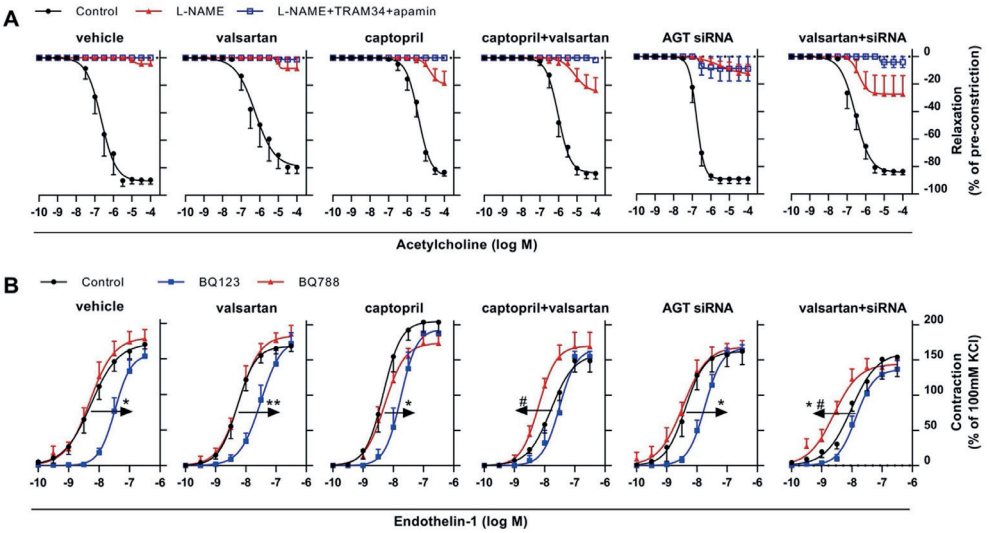

Supplemental Figure S3. Vascular responses to acetylcholine and endothelin-1. A) Relaxations to acetylcholine (% reduction of preconstriction with U46619) in the absence (control; black circles) or presence of N^{ω}-nitro-L-arginine methyl ester hydrochloride (L-NAME; red triangles) or L-NAME+TRAM34+apamin (blue squares) and **B)** contractions to endothelin-1 (% of the response to 100 mM KCl) in the absence (control; black circles) or presence of BQ123 (blue squares) or BQ788 (red triangles) in iliac arteries obtained after after four weeks of vehicle, valsartan, captopril, AGT siRNA, captopril+valsartan or valsartan+siRNA treatment (all groups n=8). Emax (maximal effect) and pEC_{50} (the negative logarithm of the half-maximal effective concentration) were analysed using one-way ANOVA and post-hoc Bonferroni (* P≤0.05, ** P≤0.01 vs. control pEC_{50}; # P≤0.01 vs. BQ123).

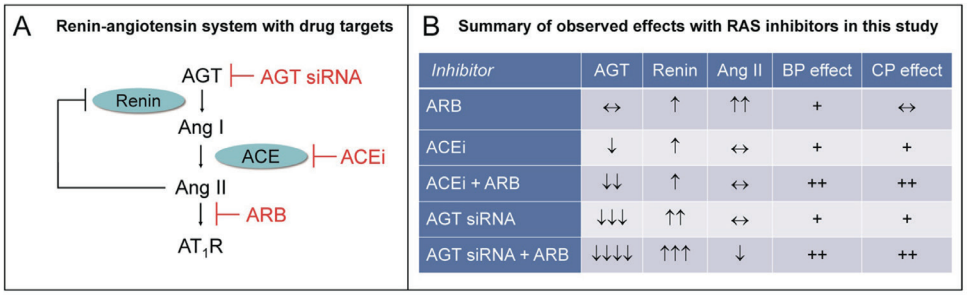

Inhibitor	AGT	Renin	Ang II	BP effect	CP effect
ARB	↔	↑	↑↑	+	↔
ACEi	↓	↑	↔	+	+
ACEi + ARB	↓↓	↑	↔	++	++
AGT siRNA	↓↓↓	↑↑	↔	+	+
AGT siRNA + ARB	↓↓↓↓	↑↑↑	↓	++	++

Supplemental Figure S4. Schematic summary of renin-angiotensin system (RAS) inhibitor drug targets and effects. Abbreviations: AGT, angiotensinogen; Ang, angiotensin; AT_1R, angiotensin II type 1 receptor; ACE(i), Angiotensin Converting Enzyme (inhibitor); ARB, angiotensin receptor blocker; BP, blood pressure; CP, cardioprotective effect.

CHAPTER 4

Tubular (Pro)renin Release: the Curtain Falls

Yuan Sun, Dominique M. Bovée and A.H. Jan Danser

Hypertension 74: 26-28, 2019

Renin was first described in urine >50 years ago.[1] Given the fact that its urinary levels usually do not correlate with plasma renin levels, a reasonable concept is that renin is released from renal tissue sites into urine under conditions where the renal renin-angiotensin system (RAS) is activated. In other words: urinary renin reflects renal RAS activity. One such condition is diabetes, which is characterized by low circulating renin levels, and a paradoxical enhanced renal response to RAS blockers, suggestive for renal RAS upregulation. Indeed, urinary renin levels are elevated in diabetic patients.[2] In this issue of *Hypertension*, Tang et al.[3] shed new light on this important issue, making use of an extensive set of experiments in humans and mice.

Of course, a logical first question is why renin release into the circulation is diminished in diabetes, while simultaneously RAS activity in the kidney is enhanced. Here the intriguing in-vitro observation that the principal cells of the collecting duct synthesize renin may come to help.[4] Remarkably, this synthesis, in contrast with renin synthesis in the juxtaglomerular apparatus, is stimulated by angiotensin II. Furthermore, these cells release prorenin rather than renin. It has even been suggested that the collecting duct is the source of the elevated circulating prorenin levels in diabetes.[4] The latter has been known for decades, but remained a mystery due to the fact that prorenin is the inactive precursor of renin. Hence, its elevation would have no functional consequences. The final piece of the puzzle appeared to be the discovery of the (pro)renin receptor, which is also present in the collecting duct, and possibly even released into urine in a soluble form.[5] Prorenin binding to this receptor allows prorenin to display activity, due to a conformational change in the prorenin molecule, not requiring actual prosegment cleavage. Subsequently, multiple effects of the prorenin-(pro) renin receptor axis in the kidney have been postulated, ranging from local angiotensin production to direct prorenin-induced effects, e.g. on water reabsorption, epithelial Na^+ channel expression, and fibrosis.[6]

However, these studies ignored the low (nanomolar) affinity of the (pro)renin receptor for prorenin, which implies that prorenin-(pro)renin receptor interaction *in vivo*, even in the kidney (with prorenin levels that might be somewhat higher than its picomolar levels in blood), would be negligible. Moreover, prorenin is normally barely detectable in urine, while urinary renin levels correspond with ≈5% of plasma renin levels.[2] Importantly, early studies had revealed that urinary renin levels rise considerably when blocking proximal tubular reabsorption with lysine.[7] Similarly, up to 40-fold higher renin levels were observed in patients with Dent's disease and Lowe syndrome in whom megalin expression and tracking is impaired, thereby resulting in tubular dysfunction.[8] In such patients prorenin also became detectable in urine, and urinary albumin levels rose in parallel with urinary renin.

These data imply that normally, there is extensive reabsorption of renin (on average 95%), and suggest that such reabsorption might even be close to 100% in the case of prorenin (hence the inability to detect prorenin in urine under normal circumstances). Studies in rodents fully confirmed megalin-dependent reabsorption of renin,[9] and accordingly massive rises in urinary renin occurred after megalin knockout, without affecting plasma renin levels.[10]

Here it is important to note that renin and prorenin, like albumin, can be filtered through the glomerulus. In fact, since both renin and prorenin are smaller than albumin, relatively larger amounts of renin and prorenin will pass the glomerulus in comparison with albumin. Not surprisingly, the glomerular sieving coefficients for renin and prorenin increase after damaging the glomerular filtration barrier.[8] The disparity between plasma and urinary renin levels might then relate to 3 factors: variation at the level of the filtration barrier (dependent on the degree of glomerular damage), variation in reabsorption (dependent on the degree of megalin expression), and release of renin (or soluble (pro)renin receptor-bound prorenin?) from tubular sites into urine. Tang et al. are the first to address these factors in the diabetic setting.

They show that urinary renin levels are higher in diabetic patients with kidney disease (albumin/creatinine ratio >300 mg/g or estimated glomerular filtration rate (eGFR) <60 mL/min per 1.73 m^2 plus albumin/creatinine ratio >30 mg/g) than in those without kidney disease, and in mice made diabetic with streptozotocin versus healthy control mice. They next confirm that lysine increases urinary renin levels, not only in normal mice, but also in diabetic mice. Since the lysine-induced urinary renin rise in diabetic mice (≈10-fold) was smaller than in normal mice (>100-fold), they speculate that reabsorption is disturbed in diabetic mice. To investigate this further, they injected recombinant human renin (single i.v. injection of 0.5 µg/g, or in a mouse of 25 gram 12.5 µg renin), which if present in urine cannot have been released from renal tissue sites. Human renin was found to be ≈25 times higher in urine of diabetic mice vs. normal mice. Unfortunately the authors did not measure human renin in plasma after injection, but 12.5 µg renin, if confined to the blood compartment, would translate to a >1000-fold higher plasma renin level than in humans. The urinary human renin levels increased after lysine in both normal (≈60-fold) and diabetic mice (≈3-fold), although the rise in diabetic mice was not significant. These data unequivocally illustrate that tubular reabsorption is disturbed in diabetes. The authors were able to confirm that this was paralleled by lower megalin expression in diabetic kidneys. Like Kang et al.,[4] they also observed diminished renin immunostaining in the juxtaglomerular apparatus and increased staining in the collecting tubules in diabetic

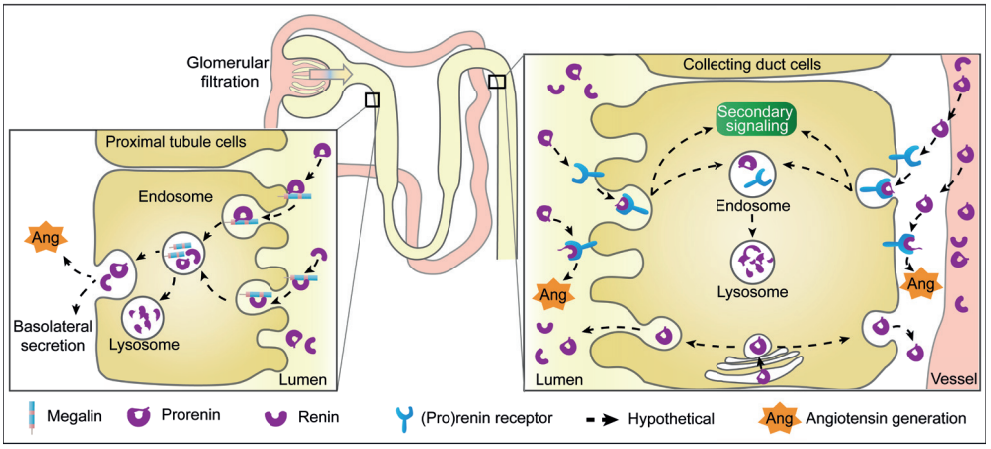

Figure. Determinants of urinary (pro)renin levels. After filtration of renin and prorenin from blood, megalin in proximal tubule cells sequesters both. This may either result in lysosomal destruction or basolateral release, thus potentially facilitating renal angiotensin generation. Megalin-mediated sequestration normally is near-complete, particularly in the case of prorenin, and thus prorenin is not detectable in urine, while urinary renin levels are ≈5% of plasma renin levels. Yet, in diabetes, megalin expression is reduced. Combined with glomerular damage (allowing more filtration) this will result in much higher urinary renin levels, even when plasma renin levels in blood in diabetics are lower. Finally, (pro)renin levels have been reported to be elevated in the collecting duct of diabetics. Initially, this was attributed to diabetes-induced prorenin production in principal cells, which through binding to the (pro)renin receptor would result in secondary signaling and local angiotensin generation. Collecting duct-derived prorenin was even suggested to be the cause of the elevated prorenin levels in diabetics.[4] The study by Tang et al.[3] now reveals that there is no such (pro)renin production in diabetes, and that the higher levels are entirely due to uptake. This is unlikely to involve the (pro)renin receptor, given its very low affinity for (pro)renin, and thus alternative possibilities need to be considered. One is that the collecting duct sequesters prorenin from peritubular capillaries.

mice. Moreover, proximal tubules renin staining was diminished in diabetic mice, in agreement with the reduced megalin expression. Yet, renin mRNA levels were unaltered in microdissected cortical collecting ducts. This argues against increased renin synthesis at this site as an explanation of the increased staining, and rather favors renin uptake. Indeed, using a renin reporter mice model (Ren1d-Cre; mT/mG), allowing tracking of the migration of kidney renin lineage cells, no evidence was found for the migration of these cells to the collecting duct. Importantly, the authors also found very few tubular epithelial structures with a co-localization of renin and renin lineage cells. Taken together, these data confirm previous results showing increased (pro)renin levels in the collecting duct of diabetic animals,[4] but now reveal that this is a matter of uptake rather than local synthesis. Thus the collecting duct can no longer be considered a source of urinary (pro)renin, not even in diabetes.

After this elegant clarification, several questions remain. What determines megalin expression/activity? One candidate is angiotensin II. Changes in urinary pH may also

play a role. Indeed, increased urinary acidification in response to acid-retention in patients with chronic kidney disease - either due to diabetes or other etiologies - is likely to inhibit megalin-(pro)renin interaction. Second, why does megalin distinguish between renin and prorenin? Is there a role for the prosegment, and might the (pro)renin receptor be involved in the endocytosis process? Third: what happens after megalin-mediated internalization? Does this result in intracellular degradation, or the release of renin/prorenin into renal interstitium or even the renal vein? Might this imply that megalin somehow determines renal RAS activity? If so, high urinary renin levels (due to low megalin levels) would be indicative for a reduction in renal RAS activity! Fourth: what determines the uptake of renin/prorenin by the collecting duct in diabetes? On the one hand, in this condition (characterized by reduced tubular reabsorption), the collecting duct is exposed to higher urinary renin/prorenin levels, allowing more binding. Yet, these urinary levels are still considerably lower than in blood, making a role for the (pro)renin receptor in the uptake very unlikely. Megalin is probably lacking at this location. A further possibility is sequestration of (pro)renin from peritubular capillaries. Since blood contains relatively high prorenin levels in diabetics, this would at least explain the predominance of prorenin in the collecting duct.

Finally, as the authors acknowledge, one has to be very careful when applying different renin and prorenin assays. Assays that rely on the recognition of renin's active site should detect renin only, while assays recognizing a common epitope on renin and prorenin will recognize both. However, a major hurdle is the fact that different assays apply different standards, and thus absolute numbers between various assays cannot be directly compared. Also, detecting prorenin release from cultured collecting duct cells does not automatically imply that these cells release prorenin in vivo, since the phenotype of renin-releasing cells may easily change in vitro.[11]

In conclusion, based on the study by Tang et al. it appears that urinary renin is strictly blood-derived and does not represent release from tubular sites. Its determinants are glomerular filtration and megalin-mediated reabsorption. Since the latter normally is in the order of 95%, a reduction to 90% or 85% would already double or triple urinary renin levels. Hence, even small variations in megalin may cause great variation in urinary renin levels for a given plasma renin level, thus explaining why plasma and urinary renin are often unrelated. Increased (pro)renin uptake and not local synthesis underlies the elevated collecting duct (pro)renin levels in the diabetic kidney. How this occurs, and what its functional consequences are, is still unknown.

Disclosures

None.

Sources of funding

None.

References

1. Brown JJ, Davies DL, Lever AF, Lloyd AM, Robertson JI, Tree M. A renin-like enzyme in normal human urine. Lancet. 1964;2:709-711
2. van den Heuvel M, Batenburg WW, Jainandunsing S, Garrelds IM, van Gool JM, Feelders RA, van den Meiracker AH, Danser AHJ. Urinary renin, but not angiotensinogen or aldosterone, reflects the renal renin-angiotensin-aldosterone system activity and the efficacy of renin-angiotensin-aldosterone system blockade in the kidney. J Hypertens. 2011;29:2147-2155
3. Tang J, Wysocki J, Ye M, Vallés PG, Rein J, Shirazi M, Bader M, Gomez RA, Sequeira-Lopez M-LS, Afkarian M, Batlle D. Urinary renin in patients with diabetic kidney disease. Hypertension. 2019;in press
4. Kang JJ, Toma I, Sipos A, Meer EJ, Vargas SL, Peti-Peterdi J. The collecting duct is the major source of prorenin in diabetes. Hypertension. 2008;51:1597-1604
5. Gonzalez AA, Lara LS, Luffman C, Seth DM, Prieto MC. Soluble form of the (pro)renin receptor is augmented in the collecting duct and urine of chronic angiotensin ii-dependent hypertensive rats. Hypertension. 2011;57:859-864
6. Ramkumar N, Kohan DE. The (pro)renin receptor: An emerging player in hypertension and metabolic syndrome. Kidney Int. 2019
7. Mazanti I, Hermann KL, Nielsen AH, Poulsen K. Ultrafiltration of renin in the mouse kidney studied by inhibition of tubular protein reabsorption with lysine. Clin Sci (Lond). 1988;75:331-336
8. Roksnoer LCW, Heijnen BF, Nakano D, Peti-Peterdi J, Walsh SB, Garrelds IM, van Gool JMG, Zietse R, Struijker-Boudier HAJ, Hoorn EJ, Danser AHJ. On the origin of urinary renin: A translational approach. Hypertension. 2016;67:927-933
9. Pohl M, Kaminski H, Castrop H, Bader M, Himmerkus N, Bleich M, Bachmann S, Theilig F. Intrarenal renin angiotensin system revisited: Role of megalin-dependent endocytosis along the proximal nephron. J Biol Chem. 2010;285:41935-41946
10. Ye F, Wang Y, Wu C, Howatt DA, Wu CH, Balakrishnan A, Mullick AE, Graham MJ, Danser AHJ, Wang J, Daugherty A, Lu HS. Angiotensinogen and megalin interactions contribute to atherosclerosis. Arterioscler Thromb Vasc Biol. 2018:150-155
11. Martini AG, Xa LK, Lacombe MJ, Blanchet-Cohen A, Mercure C, Haibe-Kains B, Friesema ECH, van den Meiracker AH, Gross KW, Azizi M, Corvol P, Nguyen G, Reudelhuber TL, Danser AHJ. Transcriptome analysis of human reninomas as an approach to understanding juxtaglomerular cell biology. Hypertension. 2017;69:1145-1155

CHAPTER 5

Megalin: a Novel Determinant of Renin-angiotensin System Activity in the Kidney?

Yuan Sun, Xifeng Lu and A.H. Jan Danser

Curr Hyp Rep 22: 30, 2020

Abstract

Megalin is well-known for its role in the reabsorption of proteins from the ultrafiltrate. Recent studies suggest that megalin also reaborbs renin and angiotensinogen. Indeed, without megalin urinary renin and angiotensinogen levels massively increase, and even prorenin becomes detectable in urine. Intriguingly, megalin might also contribute to renal angiotensin production, as evidenced from studies in megalin knockout mice. This review discusses these topics critically, concluding that urinary renin-angiotensin system components reflect diminished reabsorption rather than release from renal tissue sites, and that alterations in renal renin levels or megalin-dependent signaling need to be ruled out before concluding that angiotensin production at renal tissue sites is truly megalin-dependent. Future studies should evaluate megalin-mediated renin/angiotensinogen transcytosis (allowing interstitial angiotensin generation), and determine whether megalin prefers prorenin over renin, thus explaining why urine normally contains no prorenin.

Keywords

megalin, V-ATPase, chloride channel, renin, prorenin, angiotensinogen, proteinuria

Introduction

It is generally believed that renin-angiotensin system (RAS) activity in the kidney is independent of RAS activity in the circulation. Indeed, angiotensin (Ang) II levels in the kidney are several orders of magnitude higher than the levels of Ang II in blood, and cannot be explained by uptake from the circulation [1, 2]. Virtually all renal Ang II is cell-associated, either bound to Ang II type 1 (AT_1) receptors on the cell surface, or present intracellularly [3]. Studies in AT receptor knockout animals revealed that the intracellular presence of Ang II is dependent on AT_1 receptor-mediated internalization, i.e., there is no evidence for intracellular Ang II generation [4]. Renal angiotensin generation therefore most likely occurs in the interstitial space. Remarkably, despite evidence for local angiotensinogen synthesis in the kidney, such generation, like circulating angiotensin generation, depends on liver-derived angiotensinogen [5,6,7• ,8]. With an identical substrate source, opposing changes in RAS activity in blood and kidney must be due to other RAS-regulatory mechanisms, like the (local) release of renin and its precursor prorenin, the uptake of angiotensinogen from blood (possibly involving more than simple diffusion), and/or local alterations in ACE activity. For instance, in diabetes, the circulating RAS is suppressed, while renal RAS activity is increased [9]. This has been attributed to prorenin synthesis by the principal cells of the

collecting duct, evidenced by increased renin activity in the collecting duct and elevated urinary renin levels in this condition [10-12]. However, a recent study in diabetic mice challenged this view, and concluded that the increase in collecting duct renin under diabetic conditions reflects renin binding and not local synthesis [13••]. Moreover, the elevated urinary renin levels were due to enhanced glomerular filtration of plasma renin in combination with incomplete reabsorption by megalin, i.e, they did not reflect renin release from renal tissue sites (like the collecting duct). Surprisingly, megalin knockout even affected renal angiotensin generation [14••, 15•]. This review describes the role of megalin as a novel determinant of renal and urinary RAS activity.

What is megalin?

Megalin is a single transmembrane protein consisting of 4655 amino acids with a molecular weight of 600 kDa. It has a large extracellular domain, a transmembrane region, and a small intracellular tail of 209 amino acids. It was originally known as glycoprotein 330 [16]. Megalin belongs to the low-density lipoprotein receptor (LDLR) superfamily [17], and contains four regions that consist of cysteine-rich complement-type repeats, four regions that consist of growth factor repeats spaced by eight YWTD repeats, and a single epidermal growth factor (EGF)-like repeat in its extracellular juxtamembrane region. The regions containing complement-type repeats are believed to be important for ligand binding, while the regions containing growth factor repeats are likely required for pH-dependent ligand dissociation in the endosomal compartment [18, 19]. The overall structure of megalin resembles LDLR-related protein 1 (LRP1), and therefore megalin is also known as LRP2 [17]. The very large extracellular domain allows megalin to bind multiple ligands [20], and until now, >50 ligands for megalin have been described, including albumin, insulin, insulin-like growth factor, lipoproteins, and drugs like aprotinin and polymyxin B [18, 21, 22].

Although megalin was initially identified as an antigen in glomerular podocytes, the expression of megalin in the glomerulus is negligible versus that in the proximal tubule [23, 24, 18, 25, 16, 26]. Outside the kidney, megalin is also observed in absorptive epithelia in the lung, eye, gall bladder, placenta, and the (para)thyroid gland [18].

Megalin forms a 1:1 complex with the extracellular protein cubilin on the apical plasma membrane of proximal tubule cells, and together they mediate the endocytosis of ultrafiltrate proteins for subsequent lysosomal degradation and retrieval of their ligands and constituent amino acids into the blood. This prevents massive protein loss via urine. Megalin is a fast-recycling receptor with a long half-life, thereby making it ideal for reabsorption.

Its endocytosis depends on the enzymatic activity of an inositol 5-phosphatase encoded by the gene oculocerebrorenal syndrome protein 1 (OCRL1) [27] **(Figure 1)**. The cytosolic tail of megalin is important for recycling and degradation [28]. Among others, it binds the small GTPase Rab11, and dominant negative mutations in Rab11 result in diminished apical delivery of megalin due to disturbed recycling [29]. Autosomal recessive hypercholesterolemia (ARH), an adaptor protein that binds megalin in a similar manner as the LDLR and clathrin, retains megalin in the recycling endosomes, so that it cannot reappear on the cell surface [30]. Furthermore, phosphorylation of the cytosolic tail by glycogen synthase kinase 3β also inhibits its recycling from endosomes back to the plasma membrane [31]. Fast recycling requires rapid disruption of the megalin-ligand complex through acidification in endosomes, a process depending on voltage-gated chloride channel 5 (ClC-5) and vacuolar H^+-ATPase. Their colocalization is believed to allow ClC-5 to move out chloride as a counter-ion to the proton that is pumped by the vacuolar H^+-ATPase [32, 33], thus ensuring optimal acidification.

Genetic mutations affecting megalin

LRP2 mutations, as occurring in the Donnai-Barrow/Facio-Oculo-Acoustico-Renal syndrome, result in impaired megalin function. Patients display proteinuria [34], hypercalciuria, nephrocalcinosis, nephrolithiasis, and focal segmental glomerulosclerosis [35]. Genome-wide association studies confirmed the link between LRP2 and proteinuria [36]. Interestingly, patients with mutations in the genes encoding for OCRL1 (Lowe syndrome) and ClC-5 (Dent's disease) also display megalin dysfunction and proteinuria [37-39]. This can be explained based on the importance of OCRL1 and ClC-5 for megalin endocytosis and endosomal acidification, respectively **(Figure 1)**.

Megalin and kidney disease

Megalin knockout mice display increased albumin excretion [40], and are protected against kidney damage resulting from a high-fat diet [24]. Similar protective effects are derived from megalin inhibition (e.g., with cilastatin) in relationship to acute kidney injury due to the uptake of nephrotoxic drugs like vancomycin and cisplatin [41]. Anti-brush border antibody disease or anti-LRP2 nephropathy involves the deposit of large amounts of circulating IgG through megalin in the renal tubule. This might explain why autoantibodies induce acute kidney injury [42]. Excess albumin, as occurring in patients with chronic kidney disease (CKD), directly contributes to the development and progression of CKD by inducing tubulointerstitial inflammation and fibrosis in a megalin-dependent manner [43]. Urinary

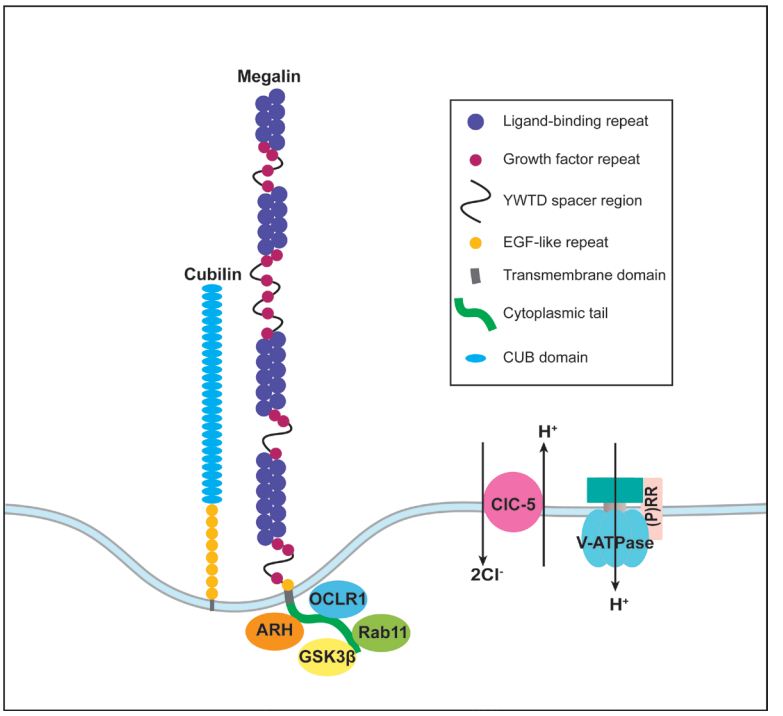

Figure 1. Megalin and its associated molecules in the proximal tubule. EGF, epidermal growth factor; OCRL1, oculocerebrorenal syndrome protein 1; ClC-5, voltage-gated chloride channel 5; ARH, autosomal recessive hypercholesterolemia; (P)RR, (pro)renin receptor; V-ATPase, vacuolar H^+-ATPase. CUB, complement subcomponents C1r and C1s,fibropellin and bone morphogenetic protein 1.

excretion of megalin associates with renal oxidative stress in CKD [44, 45], while megalin excretion in both urine and urinary extracellular vesicles correlates with the progression of albuminuria in type 2 diabetes mellitus [46, 47]. The latter implies that urinary megalin could be a biomarker for diabetic nephropathy. Yet, renal megalin expression is decreased in diabetes [13••], although increases have been observed in the early stage of type 2 diabetes [48, 49]. Among the factors that lower megalin, is Ang II [50].

Megalin and urinary RAS components

Both renin and angiotensinogen can be detected in urine, albeit at very low levels (a few percent or less) when expressed as a percentage of their concomitant plasma concentrations [12, 51]. Prorenin is undetectable in urine [12]. The latter is not due to prorenin-renin conversion in urine [12]. Remarkably, renin and angiotensinogen massively rise (up to 40-fold) in urine of patients with Dent's disease or Lowe syndrome [52], and the same occurs in urine of megalin knockdown mice [15•], or after megalin inhibition with lysine [53].

In fact, prorenin can also be detected in the urine of patients with Dent's disease or Lowe syndrome. From these data it can be concluded that RAS components are present in the ultrafiltrate, but normally are largely (>95%) reabsorbed in a megalin-dependent manner [53, 52, 54, 15•], and possibly near-completely in the case of prorenin. Indeed, all 3 RAS components are filtered through the glomerulus, and co-localize with megalin in the kidney [49, 54]. In fact, since both renin and prorenin are smaller than albumin, relatively larger amounts of renin and prorenin will pass the glomerulus in comparison with albumin. Not surprisingly, the glomerular sieving coefficients of renin, prorenin and angiotensinogen increase after damaging the glomerular filtration barrier [52], e.g., in diabetes. Moreover, in mice, the rise in urinary renin after lysine was smaller under diabetic conditions than under normal conditions (≈10-fold vs. ≈100-fold) [13••]. This is suggestive for disturbed tubular reabsorption. Therefore, the elevated urinary RAS component levels in diabetes do not reflect release from renal (tubular) tissue sites, but are the consequence of enhanced filtration from blood plasma in combination with reduced reabsorption [13••]. One more condition where urinary renin, prorenin and angiotensinogen levels are unexpectedly high, is preeclampsia [55]. Like in diabetes, this may reflect enhanced filtration; to what degree megalin is downregulated in this condition is still unknown. It is also unknown whether megalin-dependent reabsorption is different for renin and prorenin.

Megalin and renal angiotensin production

After establishing that renal angiotensin generation depends on liver-derived angiotensinogen, while renal angiotensinogen staining was limited to proximal tubule cells expressing megalin, Matsusaka and colleagues studied whether megalin is a determinant of angiotensin production at renal tissue sites [14••]. It was observed that proximal tubule-specific knockout of megalin in mice did not affect renal Ang II levels, although such knockout did massively increase urinary angiotensinogen levels. Yet, when inducing podocyte injury with the immunotoxin LMB2, the well-known rise in renal angiotensinogen and Ang II levels no longer occurred without tubular megalin. As a consequence, the Ang II-mediated Na^+ reabsorption via sodium-hydrogen exchanger 3 and the epithelial sodium channel were diminished, and thus the megalin knockout mice excreted 5 times more sodium after podocyte injury. In contrast with these findings, Ye et al. observed a profound (>70%) drop in renal Ang II levels in wildtype mice after megalin suppression based on the application of megalin antisense oligonucleotides (ASO) [15•]. The ASO approach did not affect circulating Ang II and resulted in the expected huge increase in urinary renin and angiotensinogen. Yet, even more surprising, megalin ASO reduced the atherosclerotic lesions in LDLR KO mice fed a high-fat diet. This suggests that renal Ang II, generated in a megalin-dependent

manner, contributes to atherosclerosis. However, an alternative explanation might be that the ASO approach additionally interfered with megalin at extrarenal sites (as opposed to the proximal tubule-specific knockout applied by Matsusaka et al. [14••]), and that this underlies the beneficial effect on atherosclerosis. Indeed, megalin has been reported to contribute to Ang II internalization and signaling [56, 50] and binds lipoproteins. Ideally therefore, these data are confirmed in the proximal tubule-specific knockout model. With regard to renal angiotensin generation, both studies imply that this is reduced without megalin, either selectively under pathological conditions (following podocyte injury), or possibly already under healthy conditions. Here it is important to note that we do not know the renal renin levels in these studies, and thus a final possibility is that megalin knockout has altered these levels (although it did not affect renin gene expression). In fact, under most circumstances, it is variation in renin, and not variation in angiotensinogen, which underlies variations in renal angiotensin generation, and even an angiotensinogen suppression of >95% can be matched by a rise in renin [7•]. Indeed, renin rises of >100-fold are easily achievable [57], and renal Ang II levels are unaltered when angiotensinogen is suppressed by 98% [7•].

When proposing a role for megalin in renal angiotensin generation, the question is how exactly this might occur. Obviously, endocytosis should then not result in angiotensinogen destruction. Wilson et al. [58] have reported that internalized angiotensinogen traffics intact to the mitochondria in isolated proximal tubules. However, given the absence of intracellular angiotensin generation [4], the implications of this finding are unclear. An attractive hypothesis would be that angiotensinogen is transcytosed to the basolateral membrane and released into the renal interstitium **(Figure 2)**. Such megalin-dependent transcytosis has been observed for albumin in rats [59, 60] and even for angiotensinogen in opossum kidney cells [54]. Diffusion of hepatic angiotensinogen from the circulation into the interstitial space has been reported decades ago as the most important, if not only, source of tissue angiotensin production [61]. It seems unlikely that the minute amounts of angiotensinogen in the ultrafiltrate under healthy conditions would contribute significantly to the renal interstitial angiotensinogen levels. However, under conditions of excessive protein/angiotensinogen leakage, assuming that megalin-mediated transcytosis takes place, it may indeed increase interstitial angiotensinogen and contribute to renal angiotensin production. In the case of prorenin, the acidic pH in the endosomes might even lead to prorenin activation, since a low pH results in non-proteolytic removal of the prosegment from the enzymatic cleft [62]. Yet, in previous studies we were unable to show release of activated prorenin from prorenin-synthesizing cells, possibly because activated prorenin rapidly returns to the non-activated state in a neutral pH environment [63].

Megalin and the (pro)renin receptor

Numerous studies have investigated the so-called (pro)renin receptor as a novel component of the RAS over the last 2 decades. Although this receptor was initially reported to bind and activate prorenin [64], later studies revealed that the prorenin levels required to allow such interaction are many orders above its in-vivo levels, even under pathological conditions [65, 66]. Hence, this concept is now being abandoned, also because it has become clear that the (pro)renin receptor is an accessory protein of vacuolar H^+-ATPase (also known as ATP6AP2), and thus has important functions beyond the RAS, like facilitating vesicle trafficking, intracellular signaling and lipid metabolism [67-70]. As such it may also contribute to megalin sorting and recycling, since it determines endosomal acidification in concert with ClC-5 (Figure 1). In agreement with this concept, ATP6AP2 inhibition impaired megalin protein regulation in Drosophila epithelial cells [71]. Thus, via megalin, the (pro)renin receptor may display a relationship with renin and prorenin.

Conclusions and remaining questions

Megalin is a multi-ligand receptor mainly (but not exclusively!) expressed in the kidney, determining protein reabsorption in the proximal tubule. Both genetic mutations and kidney disease (e.g., diabetes, preeclampsia) affect its function and expression, thus contributing to kidney pathology. Since megalin also binds RAS components, an intriguing new concept is that it might even play a role in angiotensin generation at renal tissue sites. If so, its internalization should not result in destruction, but, for instance via transcytosis, result in angiotensinogen release into the renal interstitial space. Such release would obviously depend on the level of angiotensinogen in the ultrafiltrate (reflecting podocyte injury), and tubular megalin expression, thus explaining why renal angiotensin generation may not always occur in concert with angiotensin generation in the circulation. Furthermore, megalin determines the level of RAS components in urine, and in the absence of megalin (like in Dent's disease or Lowe syndrome) urinary renin and angiotensinogen levels can easily rise by 2 orders of magnitude [52]. As such, urinary renin and angiotensinogen components do not reflect release from renal tissue sites (like the collecting duct) but rather diminished uptake of filtered RAS components. Given the virtual absence of prorenin (despite its filtration) in urine, except under conditions where megalin function is disturbed, it seems that megalin prefers prorenin over renin. Future studies should now address this concept, e.g., making use of megalin-expressing cells like proximal tubule epithelial cells and Brown Norway Rat yolk sac epithelial cells. Such studies might also shed light on RAS component transcytosis. Additionally, in vivo renal angiotensin generation should be verified in the presence or

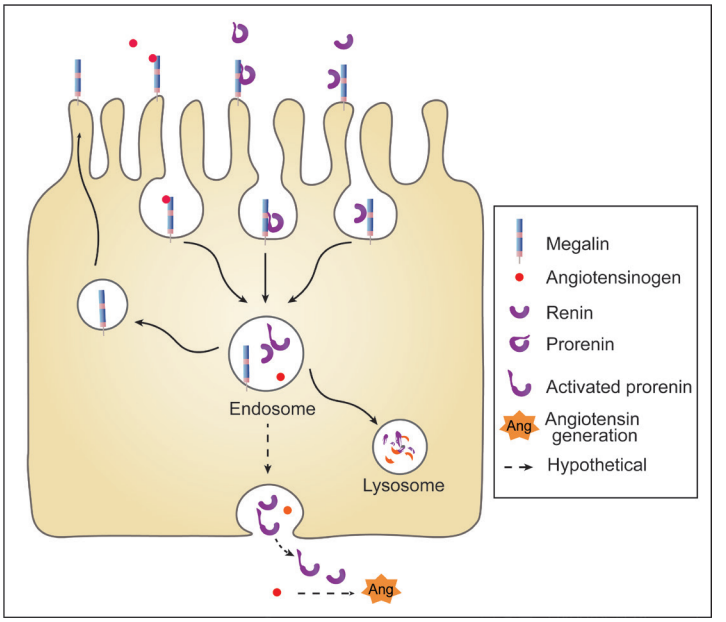

Figure 2. Megalin-mediated endocytosis of prorenin, renin and angiotensinogen, resulting in lysosomal degradation and/or transcytosis and subsequent release into the renal interstitium, allowing angiotensin generation. The low pH in endosomes may result in non-proteolytic prorenin activation (i.e., removal of the prosegment from the enzymatic cleft, resulting in 'open', active prorenin).

absence of megalin, and during inhibition of hepatic angiotensinogen synthesis, ruling out that alterations in renal renin levels and/or megalin-dependent signaling underlie the observed changes in kidney Ang II levels after megalin knockout [14••, 15••]. Knowledge on megalin expression in preeclampsia might shed light on the occurrence of prorenin in urine of women with preeclampsia [55]. Finally, we need to know what determines renin uptake in the collecting duct, reported recently by Tang et al. [13••], given that megalin is unlikely to occur in significant amounts at this location. Here the link between megalin and the (pro) renin receptor may be of particular interest.

Acknowledgement

This work was supported by National Natural Science Foundation of China (grant No. 81800383 and 81870605), Shenzhen Key Laboratory of Metabolism and Cardiovascular Homeostasis, and Shenzhen Municipal Science and Technology Innovation Council (grant no. JCYJ20160307160819191).

References

1. van Kats JP, Schalekamp MADH, Verdouw PD, Duncker DJ, Danser AHJ. Intrarenal angiotensin II: interstitial and cellular levels and site of production. Kidney Int. 2001;60:2311-7.
2. Campbell DJ, Duncan AM, Kladis A. Angiotensin-converting enzyme inhibition modifies angiotensin but not kinin peptide levels in human atrial tissue. Hypertension. 1999;34:171-5.
3. van Kats JP, van Meegen JR, Verdouw PD, Duncker DJ, Schalekamp MADH, Danser AHJ. Subcellular localization of angiotensin II in kidney and adrenal. J Hypertens. 2001;19:583-9.
4. van Esch JHM, Gembardt F, Sterner-Kock A, Heringer-Walther S, Le T, Lassner D et al. Cardiac phenotype and angiotensin II levels in AT1a, AT1b and AT2 receptor single, double and triple knockouts Cardiovasc Res. 2010;86:401-9.
5. Matsusaka T, Niimura F, Pastan I, Shintani A, Nishiyama A, Ichikawa I. Podocyte injury enhances filtration of liver-derived angiotensinogen and renal angiotensin II generation. Kidney Int. 2014;85:1068-77.
6. Matsusaka T, Niimura F, Shimizu A, Pastan I, Saito A, Kobori H et al. Liver angiotensinogen is the primary source of renal angiotensin II. J Am Soc Nephrol. 2012;23:1181-9.
• 7. Uijl E, Mirabito Colafella KM, Sun Y, Ren L, van Veghel R, Garrelds IM et al. Strong and sustained antihypertensive effect of small interfering RNA targeting liver angiotensinogen. Hypertension. 2019:1249-57. **This study reports on the consequences of hepatic angiotensinogen deletion on renal angiotensin II levels.**
8. Arendse LB, Danser AHJ, Poglitsch M, Touyz RM, Burnett JC, Jr., Llorens-Cortes C et al. Novel Therapeutic Approaches Targeting the Renin-Angiotensin System and Associated Peptides in Hypertension and Heart Failure. Pharmacol Rev. 2019;71:539-70.
9. Hollenberg NK, Fisher ND, Nussberger J, Moukarbel GV, Barkoudah E, Danser AHJ. Renal responses to three types of renin-angiotensin system blockers in patients with diabetes mellitus on a high-salt diet: a need for higher doses in diabetic patients? J Hypertens. 2011;29:2454-61.
10. Kang JJ, Toma I, Sipos A, Meer EJ, Vargas SL, Peti-Peterdi J. The collecting duct is the major source of prorenin in diabetes. Hypertension. 2008;51:1597-604.
11. Persson F, Lu X, Rossing P, Garrelds IM, Danser AHJ, Parving HH. Urinary renin and angiotensinogen in type 2 diabetes: added value beyond urinary albumin? J Hypertens. 2013;31:1646-52.
12. van den Heuvel M, Batenburg WW, Jainandunsing S, Garrelds IM, van Gool JM, Feelders RA et al. Urinary renin, but not angiotensinogen or aldosterone, reflects the renal renin-angiotensin-aldosterone system activity and the efficacy of renin-angiotensin-aldosterone system blockade in the kidney. J Hypertens. 2011;29:2147-55.
• • 13. Tang J, Wysocki J, Ye M, Vallés PG, Rein J, Shirazi M et al. Urinary renin in patients with diabetic kidney disease. Hypertension. 2019;in press:83-94. **This study shows that urinary renin in diabetes is filtered from plasma, and that there is no release of renin from the collecting duct.**
• • 14. Koizumi M, Ueda K, Niimura F, Nishiyama A, Yanagita M, Saito A et al. Podocyte Injury Augments Intrarenal Angiotensin II Generation and Sodium Retention in a Megalin-Dependent Manner. Hypertension. 2019;74:509-17. **This study elegantly unravels the role of megalin for renal angiotensin generation under normal and pathological conditions**.
• 15. Ye F, Wang Y, Wu C, Howatt DA, Wu CH, Balakrishnan A et al. Angiotensinogen and megalin interactions contribute to atherosclerosis. Arterioscler Thromb Vasc Biol. 2018:150-5. **This study reports the unexpected view that atherosclerosis depends on renal angiotensin generated in a megalin-dependent manner.**
16. Kerjaschki D, Farquhar MG. The pathogenic antigen of Heymann nephritis is a membrane glycoprotein of the renal proximal tubule brush border. Proc Natl Acad Sci U S A. 1982;79:5557-61.
17. Saito A, Pietromonaco S, Loo AK, Farquhar MG. Complete cloning and sequencing of rat gp330/"megalin," a distinctive member of the low density lipoprotein receptor gene family. Proc Natl Acad Sci U S A. 1994;91:9725-9.
18. Nielsen R, Christensen EI, Birn H. Megalin and cubilin in proximal tubule protein reabsorption: from experimental models to human disease. Kidney Int. 2016;89:58-67.
19. De S, Kuwahara S, Saito A. The endocytic receptor megalin and its associated proteins in proximal tubule epithelial cells. Membranes (Basel). 2014;4:333-55.
20. Cui S, Verroust PJ, Moestrup SK, Christensen EI. Megalin/gp330 mediates uptake of albumin in renal proximal tubule. Am J Physiol. 1996;271:F900-7.
21. Willnow TE, Christ A. Endocytic receptor LRP2/megalin-of holoprosencephaly and renal Fanconi syndrome. Pflugers Arch. 2017;469:907-16.

22. Christensen EI, Birn H. Megalin and cubilin: multifunctional endocytic receptors. Nat Rev Mol Cell Biol. 2002;3:256-66.
23. Christensen EI, Nielsen S, Moestrup SK, Borre C, Maunsbach AB, de Heer E et al. Segmental distribution of the endocytosis receptor gp330 in renal proximal tubules. Eur J Cell Biol. 1995;66:349-64.
24. Kukida M, Sawada H, Daugherty A, Lu HS. Megalin: A bridge connecting kidney, the renin-angiotensin system, and atherosclerosis. Pharmacol Res. 2019;151:104537.
25. Le Panse S, Ayani E, Nielsen S, Ronco P, Verroust P, Christensen EI. Internalization and recycling of glycoprotein 280 in epithelial cells of yolk sac. Eur J Cell Biol. 1997;72:257-67.
26. Chatelet F, Brianti E, Ronco P, Roland J, Verroust P. Ultrastructural localization by monoclonal antibodies of brush border antigens expressed by glomeruli. I. Renal distribution. Am J Pathol. 1986;122:500-11.
27. Oltrabella F, Pietka G, Ramirez IB, Mironov A, Starborg T, Drummond IA et al. The Lowe syndrome protein OCRL1 is required for endocytosis in the zebrafish pronephric tubule. PLoS Genet. 2015;11:e1005058.
28. Marzolo MP, Farfan P. New insights into the roles of megalin/LRP2 and the regulation of its functional expression. Biol Res. 2011;44:89-105.
29. Perez Bay AE, Schreiner R, Benedicto I, Paz Marzolo M, Banfelder J, Weinstein AM et al. The fast-recycling receptor Megalin defines the apical recycling pathway of epithelial cells. Nat Commun. 2016;7:11550.
30. Shah M, Baterina OY, Jr., Taupin V, Farquhar MG. ARH directs megalin to the endocytic recycling compartment to regulate its proteolysis and gene expression. J Cell Biol. 2013;202:113-27.
31. Yuseff MI, Farfan P, Bu G, Marzolo MP. A cytoplasmic PPPSP motif determines megalin's phosphorylation and regulates receptor's recycling and surface expression. Traffic. 2007;8:1215-30.
32. Lin Z, Jin S, Duan X, Wang T, Martini S, Hulamm P et al. Chloride channel (Clc)-5 is necessary for exocytic trafficking of Na+/H+ exchanger 3 (NHE3). J Biol Chem. 2011;286:22833-45.
33. Hryciw DH, Jenkin KA, Simcocks AC, Grinfeld E, McAinch AJ, Poronnik P. The interaction between megalin and ClC-5 is scaffolded by the Na(+)-H(+) exchanger regulatory factor 2 (NHERF2) in proximal tubule cells. Int J Biochem Cell Biol. 2012;44:815-23.
34. Ozdemir H, Plamondon J, Gaskin P, Asoglu MR, Turan S. A prenatally diagnosed case of Donnai-Barrow syndrome: Highlighting the importance of whole exome sequencing in cases of consanguinity. Am J Med Genet A. 2019.
35. Longoni M, Kantarci S, Donnai D, Pober BR. Donnai-Barrow Syndrome. In: Adam MP, Ardinger HH, Pagon RA, Wallace SE, Bean LJH, Stephens K et al., editors. GeneReviews((R)). Seattle (WA)1993.
36. Benonisdottir S, Kristjansson RP, Oddsson A, Steinthorsdottir V, Mikaelsdottir E, Kehr B et al. Sequence variants associating with urinary biomarkers. Hum Mol Genet. 2019;28:1199-211.
37. Eshbach ML, Weisz OA. Receptor-Mediated Endocytosis in the Proximal Tubule. Annu Rev Physiol. 2017;79:425-48.
38. De Matteis MA, Staiano L, Emma F, Devuyst O. The 5-phosphatase OCRL in Lowe syndrome and Dent disease 2. Nat Rev Nephrol. 2017;13:455-70.
39. Christensen EI, Devuyst O, Dom G, Nielsen R, Van der Smissen P, Verroust P et al. Loss of chloride channel ClC-5 impairs endocytosis by defective trafficking of megalin and cubilin in kidney proximal tubules. Proc Natl Acad Sci U S A. 2003;100:8472-7.
40. Weyer K, Storm T, Shan J, Vainio S, Kozyraki R, Verroust PJ et al. Mouse model of proximal tubule endocytic dysfunction. Nephrol Dial Transplant. 2011;26:3446-51.
41. Hori Y, Aoki N, Kuwahara S, Hosojima M, Kaseda R, Goto S et al. Megalin Blockade with Cilastatin Suppresses Drug-Induced Nephrotoxicity. J Am Soc Nephrol. 2017;28:1783-91.
42. Larsen CP, Trivin-Avillach C, Coles P, Collins AB, Merchant M, Ma H et al. LDL Receptor-Related Protein 2 (Megalin) as a Target Antigen in Human Kidney Anti-Brush Border Antibody Disease. J Am Soc Nephrol. 2018;29:644-53.
43. Liu D, Wen Y, Tang TT, Lv LL, Tang RN, Liu H et al. Megalin/Cubulin-Lysosome-mediated Albumin Reabsorption Is Involved in the Tubular Cell Activation of NLRP3 Inflammasome and Tubulointerstitial Inflammation. J Biol Chem. 2015;290:18018-28.
44. Nakatani S, Nakatani A, Ishimura E, Toi N, Tsuda A, Mori K et al. Urinary Iron Excretion is Associated with Urinary Full-Length Megalin and Renal Oxidative Stress in Chronic Kidney Disease. Kidney Blood Press Res. 2018;43:458-70.
45. Toi N, Inaba M, Ishimura E, Tsugawa N, Imanishi Y, Emoto M et al. Significance of urinary C-megalin excretion in vitamin D metabolism in pre-dialysis CKD patients. Sci Rep. 2019;9:2207.
46. De S, Kuwahara S, Hosojima M, Ishikawa T, Kaseda R, Sarkar P et al. Exocytosis-Mediated Urinary Full-

Length Megalin Excretion Is Linked With the Pathogenesis of Diabetic Nephropathy. Diabetes. 2017;66:1391-404.
47. Akour A, Kasabri V, Bulatova N, Al-Motassem Y, Fahmawi H, Momani M et al. Urinary megalin in association with progression factors of diabetic nephropathy. Bratisl Lek Listy. 2019;120:532-5.
48. Bryniarski MA, Yee BM, Jaffri I, Chaves LD, Yu JA, Guan X et al. Increased megalin expression in early type 2 diabetes: role of insulin-signaling pathways. Am J Physiol Renal Physiol. 2018;315:F1191-F207.
49. Tojo A, Kinugasa S, Fujita T, Wilcox CS. A local renal renin-angiotensin system activation via renal uptake of prorenin and angiotensinogen in diabetic rats. Diabetes Metab Syndr Obes. 2016;9:1-10.
50. Li XC, Zhuo JL. Mechanisms of AT1a receptor-mediated uptake of angiotensin II by proximal tubule cells: a novel role of the multiligand endocytic receptor megalin. Am J Physiol Renal Physiol. 2014;307:F222-33.
51. Lumbers ER, Skinner SL. Observations on the origin of renin in human urine. Circ Res. 1969;24:689-97.
52. Roksnoer LCW, Heijnen BF, Nakano D, Peti-Peterdi J, Walsh SB, Garrelds IM et al. On the origin of urinary renin: a translational approach. Hypertension. 2016;67:927-33.
53. Mazanti I, Hermann KL, Nielsen AH, Poulsen K. Ultrafiltration of renin in the mouse kidney studied by inhibition of tubular protein reabsorption with lysine. Clin Sci (Lond). 1988;75:331-6.
54. Pohl M, Kaminski H, Castrop H, Bader M, Himmerkus N, Bleich M et al. Intrarenal renin angiotensin system revisited: role of megalin-dependent endocytosis along the proximal nephron. J Biol Chem. 2010;285:41935-46.
55. Verdonk K, Saleh L, Lankhorst S, Smilde JEI, van Ingen MM, Garrelds IM et al. Association studies suggest a key role for endothelin-1 in the pathogenesis of preeclampsia and the accompanying renin-angiotensin-aldosterone system suppression. Hypertension. 2015;65:1316-23.
56. Gonzalez-Villalobos R, Klassen RB, Allen PL, Navar LG, Hammond TG. Megalin binds and internalizes angiotensin II. Am J Physiol Renal Physiol. 2005;288:F420-7.
57. Balcarek J, Sevá Pessôa B, Bryson C, Azizi M, Ménard J, Garrelds IM et al. Multiple ascending dose study with the new renin inhibitor VTP-27999: nephrocentric consequences of too much renin inhibition. Hypertension. 2014;63:942-50.
58. Wilson BA, Cruz-Diaz N, Su Y, Rose JC, Gwathmey TM, Chappell MC. Angiotensinogen import in isolated proximal tubules: evidence for mitochondrial trafficking and uptake. Am J Physiol Renal Physiol. 2017;312:F879-F86.
59. Sandoval RM, Wagner MC, Patel M, Campos-Bilderback SB, Rhodes GJ, Wang E et al. Multiple factors influence glomerular albumin permeability in rats. J Am Soc Nephrol. 2012;23:447-57.
60. Russo LM, Sandoval RM, McKee M, Osicka TM, Collins AB, Brown D et al. The normal kidney filters nephrotic levels of albumin retrieved by proximal tubule cells: retrieval is disrupted in nephrotic states. Kidney Int. 2007;71:504-13.
61. de Lannoy LM, Danser AHJ, van Kats JP, Schoemaker RG, Saxena PR, Schalekamp MADH. Renin-angiotensin system components in the interstitial fluid of the isolated perfused rat heart. Local production of angiotensin I. Hypertension. 1997;29:1240-51.
62. Schalekamp MADH, Derkx FHM, Deinum J, Danser AHJ. Newly developed renin and prorenin assays and the clinical evaluation of renin inhibitors. J Hypertens. 2008;26:928-37.
63. Martini AG, Krop M, Saleh L, Garrelds IM, Danser AH. Do prorenin-synthesizing cells release active, 'open' prorenin? J Hypertens. 2017;35:330-7.
64. Nguyen G, Delarue F, Burcklé C, Bouzhir L, Giller T, Sraer J-D. Pivotal role of the renin/prorenin receptor in angiotensin II production and cellular responses to renin. J Clin Invest. 2002;109:1417-27.
65. Batenburg WW, Danser AHJ. (Pro)renin and its receptors: pathophysiological implications. Clin Sci (Lond). 2012;123:121-33.
66. Batenburg WW, Lu X, Leijten F, Maschke U, Müller DN, Danser AHJ. Renin- and prorenin-induced effects in rat vascular smooth muscle cells overexpressing the human (pro)renin receptor: does (pro)renin-(pro)renin receptor interaction actually occur? Hypertension. 2011;58:1111-9.
67. Sun Y, Danser AHJ, Lu X. (Pro)renin receptor as a therapeutic target for the treatment of cardiovascular diseases? Pharmacol Res. 2017;125:48-56.
68. Ramkumar N, Kohan DE. The (pro)renin receptor: an emerging player in hypertension and metabolic syndrome. Kidney Int. 2019;95:1041-52.
69. Ren L, Sun Y, Lu H, Ye D, Han L, Wang N et al. (Pro)renin receptor inhibition reprograms hepatic lipid metabolism and protects mice from diet-induced obesity and hepatosteatosis. Circ Res. 2018;122:730-41.
70. Lu X, Meima ME, Nelson JK, Sorrentino V, Loregger A, Scheij S et al. Identification of the (pro)renin receptor as a novel regulator of low-density lipoprotein metabolism. Circ Res. 2016;118:222-9.
71. Gleixner EM, Canaud G, Hermle T, Guida MC, Kretz O, Helmstadter M et al. V-ATPase/mTOR signaling regulates megalin-mediated apical endocytosis. Cell Rep. 2014;8:10-9.

CHAPTER 6

Megalin: a Novel Endocytic Receptor for Prorenin and Renin?

Yuan Sun, Alexandre Goes Martini, Manoe J. Janssen, Ingrid M. Garrelds, Rosalinde Masereeuw, Xifeng Lu, A.H. Jan Danser

Hypertension 75: 1242-1250, 2020

Abstract

Megalin is an endocytic receptor contributing to protein reabsorption. Impaired expression or trafficking of megalin increases urinary renin, and allowed the detection of prorenin, which normally is absent in urine. Here, we investigated (pro)renin uptake by megalin, using both conditionally immortalized proximal tubule epithelial cells (ciPTEC) and Brown Norway Rat yolk sac cells (BN16). To distinguish binding and internalization, cells were incubated with recombinant human (pro)renin at 4°C and 37°C, respectively. (Pro)renin levels were assessed by immunoradiometric assay. At 4°C, BN16 cells bound 3 times more prorenin than renin, suggestive for a higher affinity of prorenin. Similarly, at 37°C, prorenin accumulated at 3-4-fold higher levels than renin in BN16 cells. Consequently, depletion of medium prorenin (but not renin) content occurred after 24 hours. No such differences were observed in ciPTEC, and mannose-6-phosphate (M6P) greatly reduced ciPTEC (pro) renin uptake, suggesting that these cells accumulate (pro)renin largely via M6P receptors. M6P did not affect (pro)renin uptake in BN16 cells. Yet, inhibiting megalin expression with siRNA greatly reduced (pro)renin binding and internalization by BN16 cells. Furthermore, treating BN16 cells with albumin, an endogenous ligand of megalin, also decreased binding and internalization of (pro)renin, while deleting the (pro)renin receptor affected the latter only. Exposing prorenin's prosegment with the renin inhibitor aliskiren dramatically increased prorenin binding, while after prosegment cleavage with trypsin prorenin binding was identical to that of renin. In conclusion, megalin might function as an endocytic receptor for (pro)renin, and displays a preference for prorenin. Megalin-mediated endocytosis requires the (pro)renin receptor.

Keywords

megalin – renin – prorenin - (pro)renin receptor - tubular reabsorption

Introduction

Components of the renin-angiotensin system (RAS) in urine have been suggested to reflect renal RAS activity, i.e., to be released from renal tissue sites.[1, 2] However, recent studies challenge this view and instead support the concept that urinary renin, prorenin and angiotensinogen are blood-derived (i.e., filtered through the glomerulus), and are reabsorbed in the proximal tubule.[3-5] Hence, elevated urinary RAS component levels rather reflect the net result of enhanced filtration (due to an injured glomerular barrier) and/or diminished reabsorption (due to tubular dysfunction). Remarkably, prorenin reabsorption is close to 100%,

and thus under physiological circumstances, prorenin cannot be detected in urine.[6] Since the reabsorption is megalin-dependent, prorenin can be detected in urine of patients with Dent's disease or Lowe syndrome, in whom tubular reabsorption is disturbed due to impaired renal expression and trafficking of megalin.[7] It can also be detected in urine of women with pre-eclampsia.[8]

Megalin is a 600 kDa single transmembrane protein with a small intracellular tail and a large extracellular domain containing four ligand-binding regions, allowing it to bind >40 different ligands, including albumin.[9, 10] Megalin forms a 1:1 complex with the extracellular protein cubilin. The ligand binding regions and the gross structural composition of extracellular motifs of megalin are identical in humans and rats.[11] Megalin is the major endocytic receptor in proximal tubule cells.[10] It co-localizes with renin in the proximal convoluted tubule,[12] and disruption of megalin expression in rodents resulted in a significant rise in urinary renin levels.[4] Megalin-mediated renin reabsorption amounts to ≈95%,[5, 6] and thus a reduction to 90% or 85% would already double or triple urinary renin levels. Consequently, even small variations in megalin may cause great variation in urinary renin levels for a given plasma renin level, thus explaining why plasma and urinary renin are often unrelated. Angiotensin II negatively regulates megalin expression at both the mRNA and protein levels through its type 1 receptor.[13, 14]

In the present study, we set out to compare megalin-mediated renin and prorenin uptake, making use of both human conditionally immortalized proximal tubule epithelial cells line (ciPTEC), which endogenously express multiple influx and efflux transporters, in addition to the entire endocytosis machinery,[15-17] and Brown Norway rat yolk sac epithelial cells (BN16), which are known to highly express megalin.[9] We hypothesized that megalin prefers prorenin over renin, thus explaining why urine normally contains renin only. A comparison was made versus other receptors capable of binding and/or internalizing renin and prorenin, i.e., the (pro)renin receptor [(P)RR] and the mannose-6-phosphate (M6P) receptor. We distinguished binding and internalization by performing studies at 4°C and 37°C, respectively, and made use of either receptor antagonists or siRNA to determine the contribution of each receptor separately.

Methods

Human and rat renal cortex

Rest material of one healthy human kidney cortex was supplied by the Department of Pathology. This occurred anonymously, in agreement with the Dutch regulations on medical

research. Similarly, the kidney cortex of one healthy, 12-week old Sprague Dawley rat was obtained. Both cortical tissue pieces were frozen immediately in liquid nitrogen and stored at -70°C.

Cell Culture

ciPTEC cells were derived from a healthy donor and immortalized as described.[15] Cells were cultured in phenol red-free DMEM/F12 (Invitrogen, Breda, The Netherlands) supplemented with 10% (v/v) FCS (MP Biomedicals, Uden, The Netherlands), containing insulin (5 μg/mL), transferrin (5 μg/mL), selenium (5 ng/mL), hydrocortisone (36 ng/mL), epithelial growth factor (10 ng/mL), and tri-iodothyronine (40 pg/mL). P22-24 passages of ciPTEC were used. The cells were seeded at a density of 55.000 cells per cm^2 in 96- or 24-well plates (Costar, Corning, New York, USA), cultured for 24 hours at 33°C, and matured for 7 days at 37°C, in 5% CO_2. BN16 cells[18] were cultured to confluence in a humidified incubator in 75 cm^2 flasks with Minimum Essential Media (MEM) (Gibco, Thermo Fisher Scientific, Paisley, UK) supplemented with 1×GlutaMAX (Gibco) and 10% FCS (GE Healthcare, Eindhoven, The Netherlands) at 37°C with 5% CO_2 in air. Thereafter, cells were seeded into 24-well plates and cultured for 48 hours to yield 2×10^5 cells per well (1.75 cm^2). Passages 10-14 of BN16 cells were used.

Prorenin and Renin Binding and Uptake

To study prorenin and renin binding and internalization, cells were incubated at 4°C or 37°C with 300 mL of 1000 U/L (≈2×10^6 pg/L) recombinant human prorenin or renin (a gift from Actelion Pharmaceuticals, Allschwil, Switzerland), aliskiren-pretreated recombinant human prorenin (10 mmol/L at 4°C for 48 hours) or trypsin-activated[19] recombinant human prorenin in serum-free medium. Incubations lasted up to 24 hours and were performed in the absence or presence of 10 mmol/L M6P (Sigma, St. Louis, USA), 10 mmol/L of aliskiren (a gift of Novartis, Basel, Switzerland), and/or recombinant 100 μg/L of receptor-associated protein fused to glutathione-S-transferase (RAP-GST,plasmid kindly provided by dr. de Matteis, TIGEM, Naples, Italy, recombinant protein produced as described previously[20]). To further evaluate the role of megalin and the (P)RR, identical experiments were performed after transfection of BN16 cells with negative control siRNA (siNC), LRP2 siRNA (siLRP2) or (P)RR siRNA [si(P)RR] (Invitrogen, Paisley, UK) by using RNAi max transfection reagent (Invitrogen), for 48 hours. After incubation, the medium was removed, and the cells were washed twice with ice-cold 0.5% BSA in phosphate buffered saline (PBS) and twice with ice-cold PBS. Then, the cells were lysed with ice-cold 0.2% triton X-100 (SEEVA, Heidelberg, Germany) in PBS with protease inhibitor (Roche, Mannheim, Germany), and centrifuged for 10 minutes at 4°C at 14.000×g. Supernatants were collected and stored at

-80°C. Renin in the supernatants was measured with the Renin III (Cisbio, Gif-sur-Yvette, France) immunoradiometric assay. Prorenin was also measured with this assay, after its conversion to the renin conformation (allowing its detection in the assay) by incubating it with 10 mmol/L aliskiren at 4°C.[21, 22] Prorenin measurements were performed both before and after aliskiren incubation, with levels being detected before aliskiren exposure representing prorenin that had been activated by the cells, and levels after aliskiren exposure representing the total amount of prorenin.

Albumin Uptake

To study whether M6P interferes with megalin-mediated uptake, cells were incubated in a 96-well plate setup at 37°C with 10 μg/mL fluorescently labelled BSA (BSA Alexa Fluor™ conjugate, Invitrogen, Carlsbad, USA), in the absence or presence of M6P (1 mmol-10 mmol/L) or RAP-GST (1.5-200 μg/mL) for 4 hours.[15] During the last 10 minutes, the Hoechst33342 stain (Life Technologies, Carlsbad, USA) was added to dye the nucleus. Then, the medium was removed, and the wells were washed with HBSS at room temperature. Florescence readings were performed using a CV7000S high-content imager (Yokogawa, Tokyo, Japan).

RNA isolation and qPCR analysis

Total RNA was extracted using the Direct-zol RNA kit (Zymo Research, Irvine, USA). One microgram total RNA was reverse transcribed by QuantiTect® Reverse Transcription Kit (Qiagen, Hilden, Germany). SYBR Green real-time quantitative PCR assays were performed on a One-step Plus (Thermo Fisher, Waltham, USA) using SYBR®Premix Ex TaqTM II kit (Qiagen, Venlo, The Netherlands). Primers are specified in **Table S1**.

Immunoblotting

For protein expression studies, cells were homogenized in lysis buffer (50 mmol/L Tris-HCl, 150 mmol/L NaCl, 3 mmol/L KCl, 1 mmol/L EDTA, 1% Triton X-100, complete protease inhibitor cocktail (Roche), pH 7.4). Lysates were centrifuged at 14000×g at 4°C for 10 minutes. Supernatants were collected and total protein concentrations were determined by BCA assay (Pierce, Waltham, USA). Twenty mg of total protein was loaded and separated on 6% Tris-glycine gels and transferred to PVDF membranes using Trans-Blot® Turbo™ Transfer System (Bio-Rad, Hercules, USA). The blots were probed with megalin (Santa Cruz, Dallas, USA, 1:200) and β-Actin (Merck Millipore, Darmstadt, Germany, 1:50.000) detected by Clarity Western ECL Substrate (Bio-Rad, Hercules, USA). The intensities of bands were analyzed using ImageJ software.

Data Analysis

Results are shown as mean±SEM, unless n<3. For experiments with n>3, normal distribution was verified by Kolmogorov-Smirnov test, while for experiments with n=3, the Shapiro-Wilk test was used to evaluate distribution. Once normal distribution was confirmed, differences were either tested by one-way ANOVA, followed by Bonferroni multiple comparison test, or by Student's t-test. P<0.05 were considered significant. Data below detection limit were assumed to equal the detection limit.

Results

Proximal tubule epithelial cells

Prorenin and renin binding and internalization largely depend on M6P receptors

Incubating ciPTEC with either prorenin or renin at 37°C resulted in a time-dependent increase in their cellular levels, a plateau being reached after 4-6 hours **(Figures 1A and 1C)**. The majority of cellular prorenin (up to 90%) was recognized as renin, suggestive for prorenin activation upon binding and/or internalization. In contrast, following incubation at 4°C, the majority of prorenin was in its inactive form, and the steady-state levels of both prorenin and renin were »5-10-fold lower than those at 37°C **(Figures 1B and 1D)**. At 37°C, M6P reduced the cellular accumulation of prorenin (P<0.05) and renin (P<0.01) by >80%, without altering the degree of prorenin activation. At 4°C, the blocking effect of M6P was much more modest, significance being reached only in the case of renin (P<0.05). In summary, these data demonstrate that ciPTEC bind and accumulate renin and prorenin largely via M6P receptors, and internalization is accompanied by prorenin activation. In agreement with this conclusion, M6P receptors were readily expressed in ciPTEC, while megalin was below detection limit **(Figure S1)**. Human cortical tissue did express megalin and M6P receptors, while cubilin and the (P)RR were found in both cortical tissue and ciPTEC.

RAP-GST blocks both (pro)renin and albumin internalization

At 37°C, the megalin ligand RAP-GST reduced cellular prorenin and renin accumulation after 8 hours by >80%, both in the absence and presence of M6P **(Figure 2)**. At 4°C, its blocking effects were more modest, particularly in the presence of M6P. The combined effects of RAP-GST and M6P were not significantly different from those of each blocker alone. RAP-GST blocked the uptake of labeled BSA at 37°C (IC_{50}=140 μg/mL, corresponding with 21 mmol/L; **Figure S2**). Unexpectedly, M6P blocked the uptake of labeled BSA to the same degree as RAP-GST (IC_{50}=10 mmol/L). These data suggest that either M6P is able

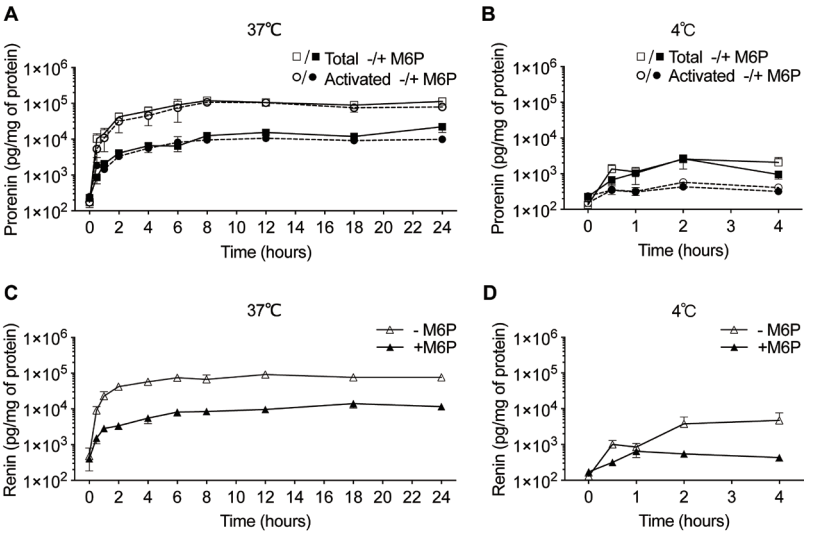

Figure 1. Cell-associated prorenin (**A&B**, distinguishing activated and total prorenin; n=5 and 4) and renin (**C&D**; n=5 and 3) levels in ciPTEC following their incubation at 37°C or 4°C with 2×10^6 pg/L prorenin or renin in the presence or absence of 10 mmol/L M6P for maximally 24 hours. Data are mean±SEM.

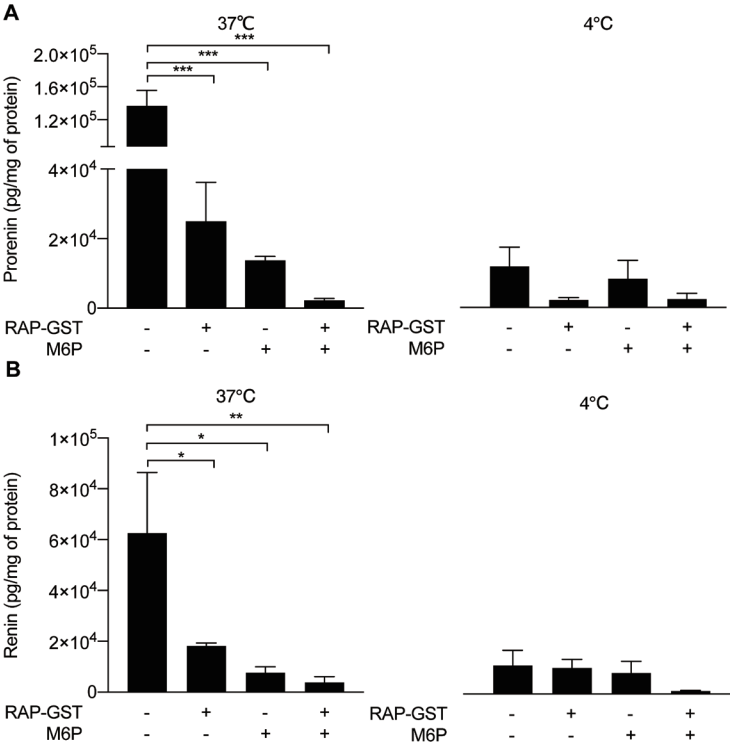

Figure 2. Cell-associated prorenin **(A)** and renin **(B)** levels in ciPTEC following their incubation at 37°C or 4°C with 2×10^6 pg/L prorenin or renin in the presence or absence of 10 mmol/L M6P and/or 100 µg/mL of RAP-GST for 4 hours. Data are mean±SEM of n=4. *P<0.05, **P<0.005, ***P<0.0005.

to interfere with the megalin/cubilin-mediated uptake of BSA, or that RAP-GST, like M6P, prevents M6P receptor-mediated uptake of BSA.

Brown Norway rat yolk sac epithelial cells

Prorenin and renin binding and internalization: no role for M6P receptors

BN16 cells accumulated prorenin and renin in a concentration-dependent manner when incubated with increasing levels at 37°C, and all cellular prorenin was found to be in the activated form **(Figure 3A)**. Importantly, for a given (pro)renin level in the incubation medium, cellular prorenin levels were 3-4-fold higher than those of renin ($P<0.05$), suggesting that prorenin uptake occurred more efficiently. A similar pattern was observed at 4°C, although now prorenin remained in the inactive form, and the cellular levels of both renin and prorenin were 3-10-fold lower than those at 37°C **(Figure 3B)**. When incubating BN16 cells with 1000 U/L prorenin or renin at 37 or 4°C, peak levels were reached after 2-4 hours under all conditions **(Figures 3C-F)**. At 37°C, in the case of renin, peak levels remained constant up to 24 hours, while in the case of prorenin the levels started to fall after 6 hours. This illustrates that after 6 hours the prorenin levels in the incubation medium had become too low to allow an equilibrium between internalization and degradation. Indeed, when measuring prorenin in the incubation medium after 24 hours, its levels had dropped to 30±8% of the levels measured at 4 hours, while in the case of renin the levels at 24 hours were still identical (86±4%) to those measured at 4°C **(Figures 3C&E)**. M6P did not affect renin and prorenin accumulation at 37°C, nor renin binding at 4°C **(Figure 3D)**. M6P did reduce prorenin binding at 4°C ($P<0.005$; **Figure 3F**). Taken together, these data indicate that BN16 cells bind and accumulate renin and prorenin largely via a non-M6P receptor-mediated mechanism (most likely megalin), and that this uptake mechanism prefers prorenin over renin. In agreement with this conclusion, BN16 cells readily expressed megalin, while M6P receptor expression was low **(Figure S1)**. Rat cortical tissue did express megalin and M6P receptors, while cubilin and the (P)RR were found in both cortical tissue and BN16 cells.

Megalin determines (pro)renin binding and internalization

To clarify whether megalin truly is the main receptor mediating (pro)renin binding and internalization in BN16 cells, we transfected BN16 cells with siRNA against megalin. This approach reduced megalin mRNA and protein by >50% and >80%, respectively **(Figures 4A&B)**. Parallel reductions were observed in the cellular renin and prorenin binding and internalization **(Figures 4C&D)**. Obviously, given the fact that megalin was not fully suppressed, this approach also did not fully suppress (pro)renin binding and internalization.

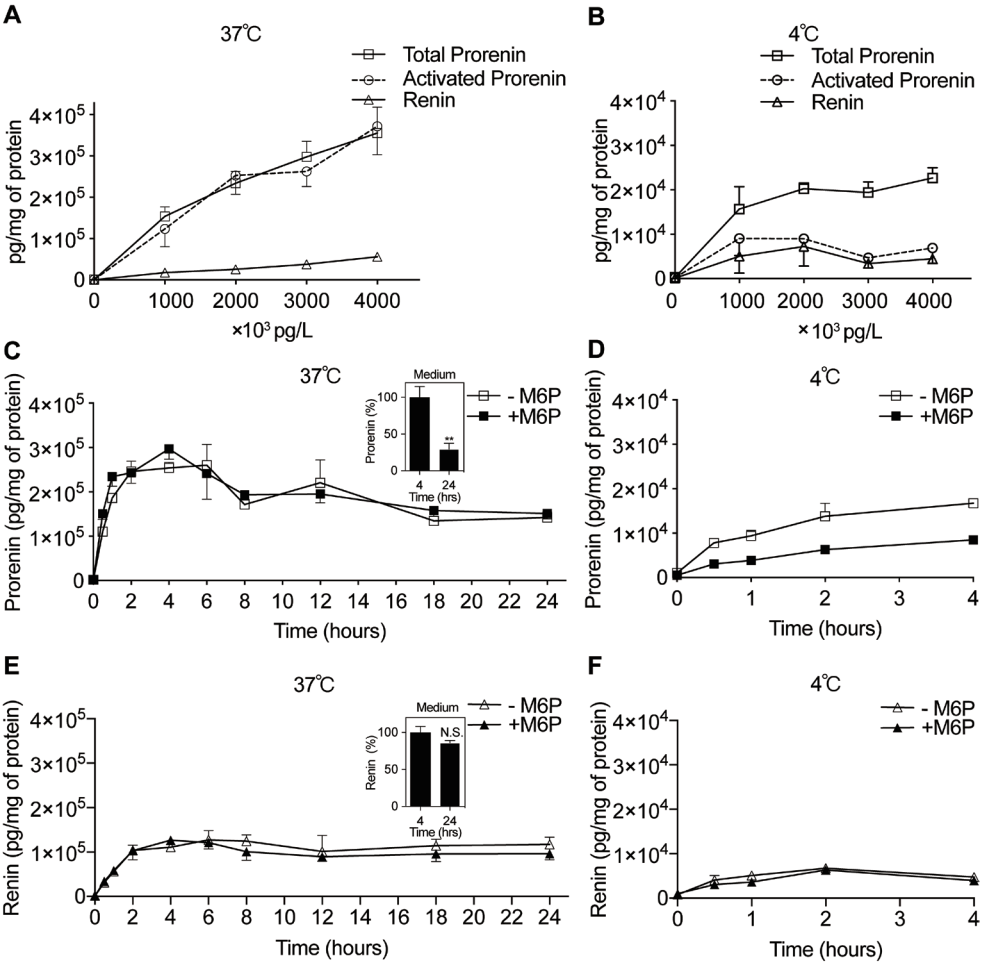

Figure 3. Cell-associated prorenin **(A-D)** and renin **(A&B, E&F)** levels in BN16 cells following their incubation at 37°C or 4°C with 2×10^6 pg/L prorenin or renin in the presence or absence of 10 mmol/L M6P for maximally 24 hours. Inserts display medium (pro)renin levels at 4 and 24 hours, expressed as a percentage of the levels at 4 hours. Data are mean±SEM of n=5.

Importantly, adding 50 µg/mL of BSA (a well-known megalin ligand) similarly reduced (pro)renin binding and internalization **(Figure S3)**. Although megalin reduction largely prevented prorenin uptake at 37°C, it did not affect prorenin activation or its intracellular degradation half-life **(Figures 4E&F)**. Taken together, these data confirm that megalin is the predominant receptor for (pro)renin binding and internalization in BN16 cells. Yet, megalin does not affect intracellular prorenin activation and degradation.

Prorenin prosegment facilitates binding to megalin, while aliskiren stabilizes renin and prorenin

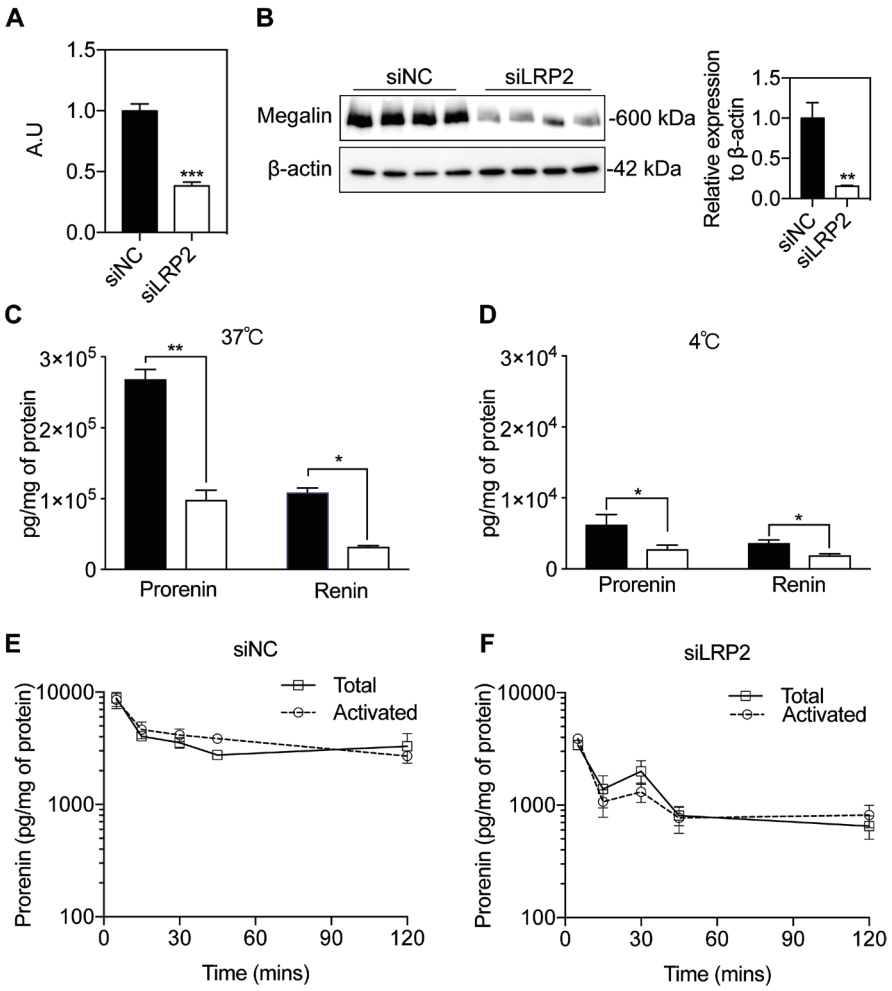

Figure 4. Megalin gene (**A**, n=5) and protein (**B**, n=5) expression levels in BN16 cells after transfection with control siRNA (siNC) or siRNA against megalin (siLRP2) for 48 hours; cell-associated prorenin (**C**, n=5) and renin (**D**, n=5) levels in BN16 cells following their incubation at 37°C or 4°C with 2×10^6 pg/L prorenin or renin for 4 hours after siNC (black bars) or siLRP2 (open bars) pretreatment; decrease in cell-associated prorenin levels after loading BN16 cells with prorenin (2×10^6 pg/L, 2 hours 37°C) following siNC (**E**, n=3) or siLRP2 (**F**, n=3) pretreatment. Data are mean±SEM, *P<0.05, **P<0.005, ***P<0.0005.

The much greater uptake of prorenin versus renin suggests a role for the prosegment. Since aliskiren is capable of removing the prosegment from the enzymatic cleft (while not cleaving it), we studied whether co-incubating the cells with aliskiren-pretreated prorenin alters prorenin binding and internalization. For comparison, renin binding and internalization were also studied in the presence of aliskiren. As shown in **Figures 5A and B**, aliskiren facilitated renin and prorenin internalization at 37°C, but its effect on prorenin was much larg-

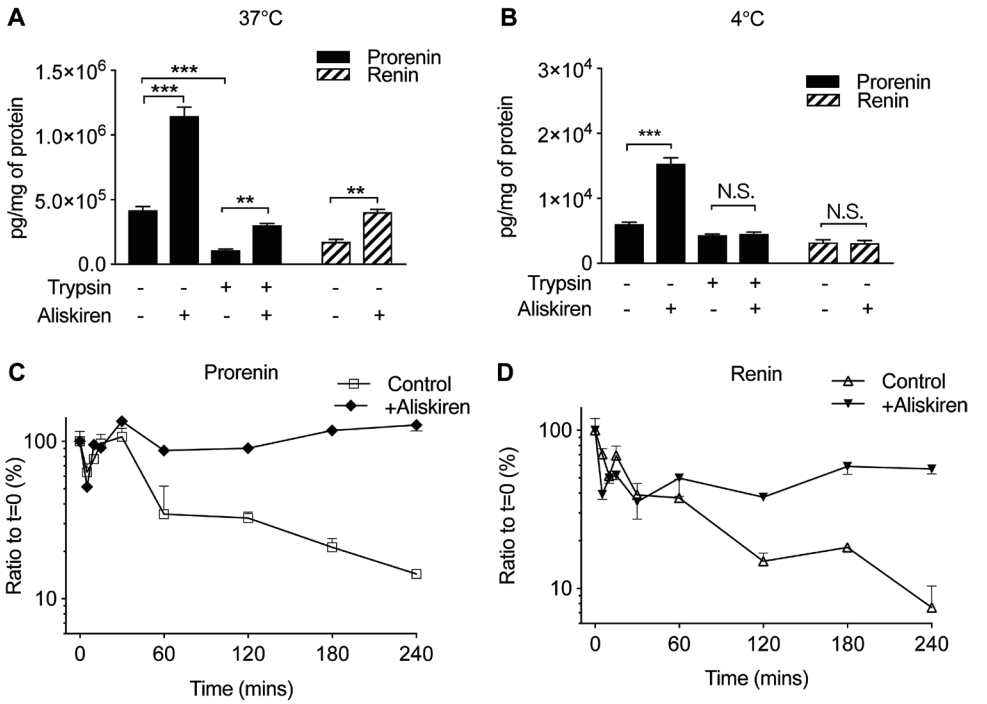

Figure 5. Cell-associated prorenin and renin levels after incubating BN16 cells with 2×10^6 pg/L prorenin or renin at 37°C (**A**, n=6) or 4°C (**B**, n=6) for 4 hours with or without prior (pro)renin exposure to trypsin or 10 µmol/L aliskiren for 48 hours; decrease in cell-associated prorenin (**C**, n=3) and renin (**D**, n=3) levels after loading BN16 cells with prorenin or renin (2×10^6 pg/L, 4 hours 37°C) with or without prior (pro)renin exposure to 10 µmol/L aliskiren for 48 hours. Data are mean±SEM, **P<0.005, ***P<0.0005.

er. At 4°C, aliskiren only facilitated prorenin binding. Incubation of prorenin with trypsin (cleaving off the prosegment) **(Figures 5A&B)** and megalin knockdown **(Figure S4)** annihilated the difference between prorenin and renin. Importantly, as has been shown before,[22] aliskiren greatly increased the intracellular half-life of both renin and prorenin (from 35 and 30 minutes, respectively, to >24 hours; **Figures 5C&D**), i.e., virtually preventing their degradation. In summary, these data show that the prosegment facilitates binding to megalin, while aliskiren binding stabilizes both renin and prorenin, thus reducing their intracellular degradation.

(P)RR contributes to prorenin internalization but does not affect prorenin binding in BN16 cells

The (P)RR binds renin and prorenin with low affinity.[23] To study (P)RR-megalin interaction, megalin and/or (P)RR expression in BN16 cells were inhibited by transfecting with their respective siRNA for 48 hours **(Figure 6A)**. Megalin knockdown again reduced prorenin

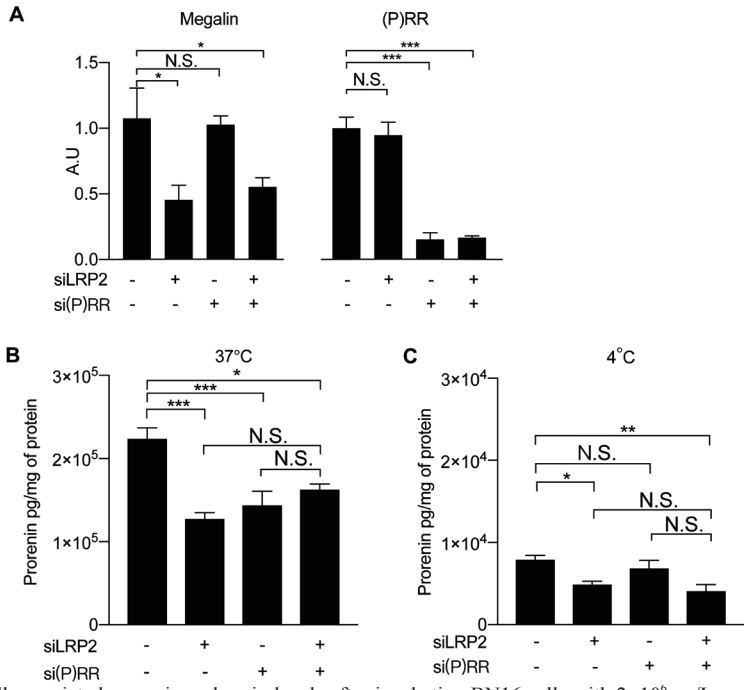

Figure 5. Cell-associated prorenin and renin levels after incubating BN16 cells with 2×10^6 pg/L prorenin or renin at 37°C (**A**, n=6) or 4°C (**B**, n=6) for 4 hours with or without prior (pro)renin exposure to trypsin or 10 µmol/L aliskiren for 48 hours; decrease in cell-associated prorenin (**C**, n=3) and renin (**D**, n=3) levels after loading BN16 cells with prorenin or renin (2×10^6 pg/L, 4 hours 37°C) with or without prior (pro)renin exposure to 10 µmol/L aliskiren for 48 hours. Data are mean±SEM, **P<0.005, ***P<0.0005.

binding and internalization by about 50% **(Figure 6B&C)**, while (P)RR inhibition reduced internalization only. Dual (P)RR/megalin inhibition induced the same effect of megalin inhibition alone. These data suggest that the (P)RR contributes to prorenin endocytosis, but not binding, and that endocytosis involves megalin and the (P)RR simultaneously.

Discussion

This study shows that megalin is an endocytic receptor binding both renin and prorenin, displaying a preference for the latter. This preference involves the prosegment, and moving out the prosegment from the enzymatic cleft further enhanced binding. Endocytosis, occurring at 37°C, depended on the (P)RR and was followed by intracellular degradation of both renin and prorenin. Aliskiren reduced degradation, most likely because renin inhibitor-binding stabilizes renin and prorenin.[22, 24]

Megalin-dependent renin binding has been demonstrated before,[12] and recent studies have shown that this process rather than tubular (pro)renin release determines urinary renin

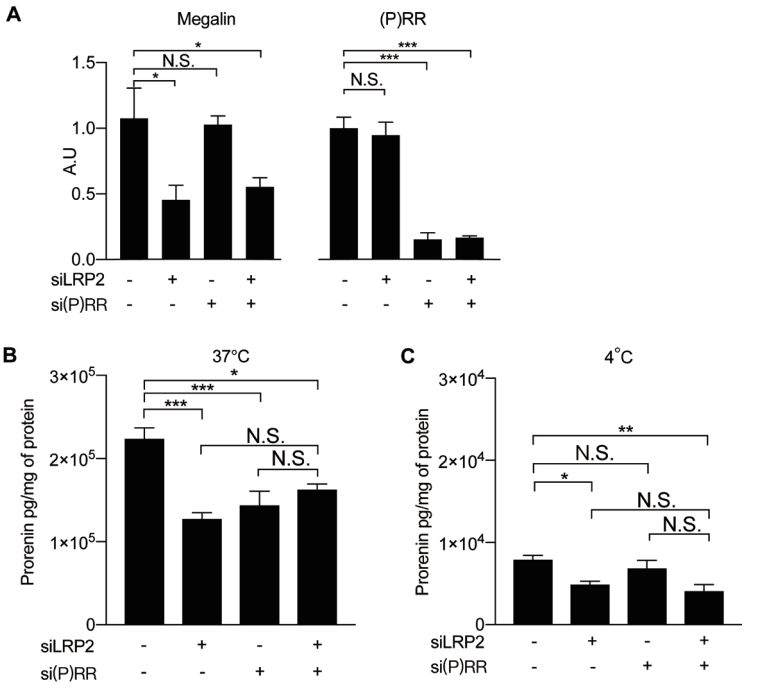

Figure 6. **A**, siRNA-induced reduction of megalin and (P)RR expression levels in BN16 cells. **B and C**, cell-associated prorenin levels after incubating BN16 cells with 2×10^6 pg/L prorenin at 37°C **(B)** or 4°C **(C)** for 4 hours in the presence or absence of megalin (LRP2) and/or the (pro)renin receptor ((P)RR). Data are mean±SEMs of n=5. *P<0.05, **P<0.005, ***P<0.0005.

levels. Indeed, blocking megalin with lysine,[25] impaired megalin trafficking[3] and megalin deletion[4] all greatly increased urinary renin levels, implying that normally >95% of filtered renin is reabsorbed in a megalin-dependent manner. Human urine did not contain detectable levels of prorenin, except in patients with Dent's disease and Lowe syndrome in whom megalin expression and trafficking is impaired, and in women with preeclampsia.[8] The current data now explain the absence of prorenin under normal conditions: its reabsorption is 4-5 times more efficient than that of renin, and thus might be closer to 100%. Tang et al. have claimed suppressed megalin expression in experimental diabetes, which, particularly in combination with the increased glomerular protein filtration in this condition, results in elevated urinary renin levels, despite the well-known circulating RAS downregulation in diabetes.[25, 26] Future studies should now evaluate whether the same is true in preeclampsia, a condition characterized by hypertension, proteinuria and RAS downregulation.[27]

Tojo et al., after infusing human prorenin in diabetic rats, reported increased renal prorenin accumulation versus non-diabetic rats, which they attributed to (P)RR and/or megalin binding.[28] Similar observations were made for human angiotensinogen, and no comparison was

made versus human renin. Given the reduced expression of megalin under diabetic conditions observed by Tang et al., these data are most likely explained on the basis of enhanced glomerular filtration of prorenin and angiotensinogen. Combined with our current findings, they suggest that the earlier reported upregulation of prorenin immunoreactivity in the collecting duct of diabetic rodents[29] is the consequence of enhanced filtration and subsequent tubular reuptake. Furthermore, we now reveal that the (P)RR contributes to the internalization of megalin-bound prorenin. Given the fact that the (P)RR is identical to ATPA6P2, i.e., accessory protein 2 of vacuolar ATPase (V-ATPase), this may not be too surprising, since V-ATPases are expressed on the membrane of intracellular compartments in virtually every cell type, and play important roles in vesicle trafficking, protein degradation and intracellular signaling.[30] Indeed, also in the case of megalin, V-ATPase ensures optimal endosomal acidification, resulting in rapid dissociation of the megalin-ligand complex and fast recycling of megalin to the cell membrane. Hence, inhibiting ATP6AP2 impairs megalin regulation.[31]

Our data subsequently illustrate that, at least under the applied cell culture conditions, megalin/(P)RR-mediated (pro)renin uptake results in intracellular degradation of both renin and prorenin, with a half-life of »30 minutes. In the case of prorenin, this metabolic process involves prosegment removal, i.e., prorenin-renin conversion.[32] As has been shown before,[22, 24] aliskiren binding stabilizes (pro)renin, thereby greatly suppressing its metabolism. Combined with aliskiren's high affinity (virtually excluding dissociation), this explains why the renin inhibitor enhances intracellular renin and prorenin accumulation at 37°C. Importantly, aliskiren also increased prorenin binding to megalin, evidenced by the elevated cell-associated prorenin levels at 4°C in the presence of the renin inhibitor. The latter did not apply to renin, suggesting that the aliskiren-induced conformational change of prorenin, resulting in the removal of the prosegment from the enzymatic cleft,[21, 33] underlies this phenomenon, rather than aliskiren-induced stabilization of the (pro)renin molecule. This indicates that the prosegment, particularly when fully exposed, facilitates prorenin-megalin interaction. In summary, aliskiren facilitates binding only in the case of prorenin, and slowed down degradation for both renin and prorenin. Hence, at 37°C, when both binding and internalization occur, aliskiren's effects were largest for prorenin.

ciPTEC express most of the transporters and efflux pumps physiologically present in the proximal tubule, and possess the complete endocytosis machinery, making these cells an appropriate model to study proximal tubule physiology.[17] In many studies with different cell types such as rat vascular smooth muscle cells, cardiomyocytes, fibroblasts, and human endothelial cells, it has been demonstrated that besides megalin, M6P receptors bind and

internalize renin and prorenin.[32, 34, 35] In the current study, the >80% decrease in prorenin and renin uptake induced by M6P in ciPTEC suggests an important role for M6P receptor-mediated uptake of renin and prorenin in these cells. Not surprisingly, the effect of M6P was best seen at 37°C, since at this temperature (but not at 4°C), M6P receptors cycle continuously between the cell surface and the intracellular compartment, thus allowing substantial (pro)renin accumulation in the cells. In contrast, at 4°C, renin and prorenin can only bind to cell surface M6P receptors, without being internalized,[23] and prorenin activation will not occur. In agreement with a predominant role for M6P receptors in ciPTEC, we observed high M6P receptor expression and low to undetectable megalin expression in these cells. The cells additionally expressed cubilin, and the (P)RR. Interestingly, the M6P receptor has been described as a ligand for megalin.[36, 37] To what degree M6P itself acts as a ligand for the megalin receptor is unknown. Our results revealed that the megalin inhibitor RAP-GST exerted identical effects as M6P: up to 90% inhibition of renin/prorenin uptake at 37°C in ciPTEC, and a comparable, but much smaller effect at 4°C. Given the low expression of megalin in ciPTEC, the simplest explanation of these findings is that RAP-GST additionally blocks M6P receptors. Alternatively, megalin may interact with M6P receptors,[38] or M6P might block megalin-mediated pathways. To evaluate the latter, we studied the effect of M6P on the uptake of BSA by ciPTEC, a widely accepted megalin ligand.[39] It was observed that M6P not only blocked BSA uptake to the same degree as RAP-GST, but that it also decreased RAP-GST endocytosis (data not shown). Although this suggests that M6P is a megalin receptor blocker, an important caveat remains the low expression of megalin in ciPTEC. Given these observations, we focused on BN16 cells rather than ciPTEC to verify megalin-(pro)renin interaction, and we used megalin siRNA knockdown instead of RAP-GST to inhibit megalin in these cells. Conveniently, M6P receptor expression in BN16 cells was low, and M6P did not interfere with (pro)renin binding.

Perspective

Megalin is major determinant of urinary renin and prorenin levels. Given its preference for prorenin, urinary prorenin is normally undetectable. Since even filtered renin is reabsorbed by >95% via megalin, decreases in megalin expression (as occurring in diabetes) may easily result in rises in urinary renin that are entirely unrelated to plasma renin levels. These rises therefore reflect tubular (dys)function rather than upregulation of the intrarenal RAS, as is often advocated.[3, 12] Future studies should now unravel 1) megalin-prosegment interaction, which appears to underlie the preference for prorenin, 2) renal megalin alterations in diseases other than diabetes (like preeclampsia), 3) the potential role of megalin outside the kidney, if any, 4) megalin-(P)RR and megalin-M6P receptor interaction, and 5) the destiny

of megalin-internalized (pro)renin: destruction or abluminal release into the renal interstitium and a contribution to renal angiotensin production? An exciting recent study supports the latter following podocyte injury.[40] The link with the (P)RR might explain why previous studies reported (P)RR-(pro)renin interaction in the kidney – this is unlikely to represent actual (pro)renin binding to the (P)RR, given its low affinity,[41-44] but might simply represent a role for the (P)RR in (pro)renin endocytosis.

Acknowledgments

None.

Sources of Funding

Y. Sun and X. Lu were funded by National Natural Science Foundation of China (grant nrs. 81800383 and 81870605), and the Shenzhen Key Laboratory of Metabolism and Cardiovascular Homeostasis, and Shenzhen Municipal Science and Technology Innovation Council (grant no. JCYJ20160307160819191).

Conflict(s) of Interest/Disclosure(s)

None.

References

1. Liu L, Gonzalez AA, McCormack M, Seth DM, Kobori H, Navar LG, Prieto MC. Increased renin excretion is associated with augmented urinary angiotensin ii levels in chronic angiotensin ii-infused hypertensive rats. Am J Physiol Renal Physiol. 2011;301:F1195-1201
2. Navar LG, Kobori H, Prieto MC, Gonzalez-Villalobos RA. Intratubular renin-angiotensin system in hypertension. Hypertension. 2011;57:355-362
3. Roksnoer LC, Heijnen BF, Nakano D, Peti-Peterdi J, Walsh SB, Garrelds IM, van Gool JM, Zietse R, Struijker-Boudier HA, Hoorn EJ, Danser AH. On the origin of urinary renin: A translational approach. Hypertension. 2016;67:927-933
4. Ye F, Wang Y, Wu C, Howatt DA, Wu CH, Balakrishnan A, Mullick AE, Graham MJ, Danser AHJ, Wang J, Daugherty A, Lu HS. Angiotensinogen and megalin interactions contribute to atherosclerosis. Arterioscler Thromb Vasc Biol. 2019;39:150-155
5. Sun Y, Bovee DM, Danser AHJ. Tubular (pro)renin release. Hypertension. 2019;74:26-28
6. van den Heuvel M, Batenburg WW, Jainandunsing S, Garrelds IM, van Gool JM, Feelders RA, van den Meiracker AH, Danser AH. Urinary renin, but not angiotensinogen or aldosterone, reflects the renal renin-angiotensin-aldosterone system activity and the efficacy of renin-angiotensin-aldosterone system blockade in the kidney. J Hypertens. 2011;29:2147-2155
7. Christensen EI, Devuyst O, Dom G, Nielsen R, Van der Smissen P, Verroust P, Leruth M, Guggino WB, Courtoy PJ. Loss of chloride channel clc-5 impairs endocytosis by defective trafficking of megalin and cubilin in kidney proximal tubules. Proc Natl Acad Sci U S A. 2003;100:8472-8477

8. Verdonk K, Saleh L, Lankhorst S, Smilde JE, van Ingen MM, Garrelds IM, Friesema EC, Russcher H, van den Meiracker AH, Visser W, Danser AH. Association studies suggest a key role for endothelin-1 in the pathogenesis of preeclampsia and the accompanying renin-angiotensin-aldosterone system suppression. Hypertension. 2015;65:1316-1323
9. Nielsen R, Christensen EI, Birn H. Megalin and cubilin in proximal tubule protein reabsorption: From experimental models to human disease. Kidney Int. 2016;89:58-67
10. Christensen EI, Birn H. Megalin and cubilin: Multifunctional endocytic receptors. Nat Rev Mol Cell Biol. 2002;3:256-266
11. Hjalm G, Murray E, Crumley G, Harazim W, Lundgren S, Onyango I, Ek B, Larsson M, Juhlin C, Hellman P, Davis H, Akerstrom G, Rask L, Morse B. Cloning and sequencing of human gp330, a ca(2+)-binding receptor with potential intracellular signaling properties. Eur J Biochem. 1996;239:132-137
12. Pohl M, Kaminski H, Castrop H, Bader M, Himmerkus N, Bleich M, Bachmann S, Theilig F. Intrarenal renin angiotensin system revisited: Role of megalin-dependent endocytosis along the proximal nephron. J Biol Chem. 2010;285:41935-41946
13. Gonzalez-Villalobos R, Klassen RB, Allen PL, Navar LG, Hammond TG. Megalin binds and internalizes angiotensin ii. Am J Physiol Renal Physiol. 2005;288:F420-427
14. Hosojima M, Sato H, Yamamoto K, Kaseda R, Soma T, Kobayashi A, Suzuki A, Kabasawa H, Takeyama A, Ikuyama K, Iino N, Nishiyama A, Thekkumkara TJ, Takeda T, Suzuki Y, Gejyo F, Saito A. Regulation of megalin expression in cultured proximal tubule cells by angiotensin ii type 1a receptor- and insulin-mediated signaling cross talk. Endocrinology. 2009;150:871-878
15. Wilmer MJ, Saleem MA, Masereeuw R, Ni L, van der Velden TJ, Russel FG, Mathieson PW, Monnens LA, van den Heuvel LP, Levtchenko EN. Novel conditionally immortalized human proximal tubule cell line expressing functional influx and efflux transporters. Cell Tissue Res. 2010;339:449-457
16. Caetano-Pinto P, Janssen MJ, Gijzen L, Verscheijden L, Wilmer MJ, Masereeuw R. Fluorescence-based transport assays revisited in a human renal proximal tubule cell line. Mol Pharm. 2016;13:933-944
17. Janssen MJ, Nieskens TTG, Steevels TAM, Caetano-Pinto P, den Braanker D, Mulder M, Ponstein Y, Jones S, Masereeuw R, den Besten C, Wilmer MJ. Therapy with 2'-o-me phosphorothioate antisense oligonucleotides causes reversible proteinuria by inhibiting renal protein reabsorption. Molecular therapy. Nucleic acids. 2019;18:298-307
18. Le Panse S, Verroust P, Christensen EI. Internalization and recycling of glycoprotein 280 in bn/msv yolk sac epithelial cells: A model system of relevance to receptor-mediated endocytosis in the renal proximal tubule. Experimental nephrology. 1997;5:375-383
19. Derkx FH, Tan-Tjiong L, Wenting GJ, Boomsma F, Man in 't Veld AJ, Schalekamp MA. Asynchronous changes in prorenin and renin secretion after captopril in patients with renal artery stenosis. Hypertension. 1983;5:244-256
20. Bu G, Geuze HJ, Strous GJ, Schwartz AL. 39 kda receptor-associated protein is an er resident protein and molecular chaperone for ldl receptor-related protein. EMBO J. 1995;14:2269-2280
21. Krop M, Garrelds IM, de Bruin RJ, van Gool JM, Fisher ND, Hollenberg NK, Jan Danser AH. Aliskiren accumulates in renin secretory granules and binds plasma prorenin. Hypertension. 2008;52:1076-1083
22. Batenburg WW, de Bruin RJ, van Gool JM, Muller DN, Bader M, Nguyen G, Danser AH. Aliskiren-binding increases the half life of renin and prorenin in rat aortic vascular smooth muscle cells. Arterioscler Thromb Vasc Biol. 2008;28:1151-1157
23. Batenburg WW, Krop M, Garrelds IM, de Vries R, de Bruin RJ, Burckle CA, Muller DN, Bader M, Nguyen G, Danser AH. Prorenin is the endogenous agonist of the (pro)renin receptor. Binding kinetics of renin and prorenin in rat vascular smooth muscle cells overexpressing the human (pro)renin receptor. J Hypertens. 2007;25:2441-2453
24. Krop M, Lu X, Verdonk K, Schalekamp MA, van Gool JM, McKeever BM, Gregg R, Danser AH. New renin inhibitor vtp-27999 alters renin immunoreactivity and does not unfold prorenin. Hypertension. 2013;61:1075-1082
25. Tang J, Wysocki J, Ye M, Valles PG, Rein J, Shirazi M, Bader M, Gomez RA, Sequeira-Lopez MS, Afkarian M, Batlle D. Urinary renin in patients and mice with diabetic kidney disease. Hypertension. 2019;74:83-94
26. Hollenberg NK, Fisher ND, Nussberger J, Moukarbel GV, Barkoudah E, Danser AH. Renal responses to three types of renin-angiotensin system blockers in patients with diabetes mellitus on a high-salt diet:

A need for higher doses in diabetic patients? J Hypertens. 2011;29:2454-2461
27. Verdonk K, Visser W, Van Den Meiracker AH, Danser AH. The renin-angiotensin-aldosterone system in pre-eclampsia: The delicate balance between good and bad. Clin Sci (Lond). 2014;126:537-544
28. Tojo A, Kinugasa S, Fujita T, Wilcox CS. A local renal renin-angiotensin system activation via renal uptake of prorenin and angiotensinogen in diabetic rats. Diabetes Metab Syndr Obes. 2016;9:1-10
29. Kang JJ, Toma I, Sipos A, Meer EJ, Vargas SL, Peti-Peterdi J. The collecting duct is the major source of prorenin in diabetes. Hypertension. 2008;51:1597-1604
30. Sun Y, Danser AHJ, Lu X. (pro)renin receptor as a therapeutic target for the treatment of cardiovascular diseases? Pharmacol Res. 2017;125:48-56
31. Gleixner EM, Canaud G, Hermle T, Guida MC, Kretz O, Helmstadter M, Huber TB, Eimer S, Terzi F, Simons M. V-atpase/mtor signaling regulates megalin-mediated apical endocytosis. Cell Rep. 2014;8:10-19
32. Saris JJ, Derkx FH, De Bruin RJ, Dekkers DH, Lamers JM, Saxena PR, Schalekamp MA, Jan Danser AH. High-affinity prorenin binding to cardiac man-6-p/igf-ii receptors precedes proteolytic activation to renin. Am J Physiol Heart Circ Physiol. 2001;280:H1706-1715
33. Schefe JH, Neumann C, Goebel M, Danser J, Kirsch S, Gust R, Kintscher U, Unger T, Funke-Kaiser H. Prorenin engages the (pro)renin receptor like renin and both ligand activities are unopposed by aliskiren. J Hypertens. 2008;26:1787-1794
34. van den Eijnden MM, Saris JJ, de Bruin RJ, de Wit E, Sluiter W, Reudelhuber TL, Schalekamp MA, Derkx FH, Danser AH. Prorenin accumulation and activation in human endothelial cells: Importance of mannose 6-phosphate receptors. Arterioscler Thromb Vasc Biol. 2001;21:911-916
35. Saris JJ, Derkx FH, Lamers JM, Saxena PR, Schalekamp MA, Danser AH. Cardiomyocytes bind and activate native human prorenin : Role of soluble mannose 6-phosphate receptors. Hypertension. 2001;37:710-715
36. Christensen EI, Verroust PJ, Nielsen R. Receptor-mediated endocytosis in renal proximal tubule. Pflugers Arch. 2009;458:1039-1048
37. Yammani RR, Sharma M, Seetharam S, Moulder JE, Dahms NM, Seetharam B. Loss of albumin and megalin binding to renal cubilin in rats results in albuminuria after total body irradiation. Am J Physiol Regul Integr Comp Physiol. 2002;283:R339-346
38. Norden AG, Gardner SC, Van't Hoff W, Unwin RJ. Lysosomal enzymuria is a feature of hereditary fanconi syndrome and is related to elevated ci-mannose-6-p-receptor excretion. Nephrol Dial Transplant. 2008;23:2795-2803
39. Dickson LE, Wagner MC, Sandoval RM, Molitoris BA. The proximal tubule and albuminuria: Really! J Am Soc Nephrol. 2014;25:443-453
40. Koizumi M, Ueda K, Niimura F, Nishiyama A, Yanagita M, Saito A, Pastan I, Fujita T, Fukagawa M, Matsusaka T. Podocyte injury augments intrarenal angiotensin ii generation and sodium retention in a megalin-dependent manner. Hypertension. 2019;74:509-517
41. Batenburg WW, Danser AH. (pro)renin and its receptors: Pathophysiological implications. Clin Sci (Lond). 2012;123:121-133
42. Ramkumar N, Kohan DE. The (pro)renin receptor: An emerging player in hypertension and metabolic syndrome. Kidney Int. 2019;95:1041-1052
43. Prieto MC, Reverte V, Mamenko M, Kuczeriszka M, Veiras LC, Rosales CB, McLellan M, Gentile O, Jensen VB, Ichihara A, McDonough AA, Pochynyuk OM, Gonzalez AA. Collecting duct prorenin receptor knockout reduces renal function, increases sodium excretion, and mitigates renal responses in ang ii-induced hypertensive mice. Am J Physiol Renal Physiol. 2017;313:F1243-F1253
44. Trepiccione F, Gerber SD, Grahammer F, Lopez-Cayuqueo KI, Baudrie V, Paunescu TG, Capen DE, Picard N, Alexander RT, Huber TB, Chambrey R, Brown D, Houillier P, Eladari D, Simons M. Renal atp6ap2/(pro)renin receptor is required for normal vacuolar h+-atpase function but not for the renin-angiotensin system. J Am Soc Nephrol. 2016;27:3320-3330

Novelty and significance

What is new?

Megalin is a novel endocytic receptor for renin and prorenin which displays a preference for the latter.

Megalin-dependent (pro)renin internalization, but not binding, involves the (pro)renin receptor.

What is relevant?

These data explains why urine normally does not contain prorenin, except under conditions where megalin trafficking is disturbed, like in patients with Dent's disease or Lowe syndrome.

Summary

To investigate (pro)renin binding and internalization by megalin, Brown Norway Rat yolk sac cells were incubated with renin and prorenin. The cells bound and internalized much more prorenin than renin, and inhibiting megalin expression with siRNA greatly reduced both binding and internalization, while inhibiting the (pro)renin receptor inhibited the latter only. Exposing prorenin's prosegment with the renin inhibitor aliskiren dramatically increased prorenin binding, while after prosegment cleavage with trypsin prorenin binding was identical to that of renin. In conclusion, megalin is a novel endocytic receptor for (pro) renin which displays a preference for prorenin, and endocytosis depends on the (pro)renin receptor.

Supplemental Materials

Table S1. Primers lists

Gene	Species		Sequences
LRP2	Rat	Forward	5'-TCCGACCGCTGGGTATATGT-3'
		Reverse	5'-GGTGAGAACCATCGCTCCAT-3'
M6PR	Rat	Forward	5'-GGCTGCTGTTTGTCAAGAGA-3'
		Reverse	5'-TGAGATCTCCATCTGAGTACCG-3'
Cubilin	Rat	Forward	5'-GCTCCAGATTCTTGCTTACGA-3'
		Reverse	5'-TGTTTCCTGAAGCGATGATAGA-3'
(P)RR	Rat	Forward	5'-TCTTCTCTGGTGTCGAGTGC-3'
		Reverse	5'-CTTCCTTCACAGAGAAGCCC-3'
β-Actin	Rat	Forward	5'-AGCCATGTACGTAGCCATCCA-3'
		Reverse	5'-TCTCCGGAGTCCATCACAATG-3'
LRP2	Human	Forward	5'-CTGCTCCTGGCTCTCGTC-3'
		Reverse	5'-CTTTGGTCCCATCACACCTC-3'
M6PR	Human	Forward	5'-GGCAGACAGACCACATATACCA-3'
		Reverse	5'-AAAGATGGGGTGGCTGTTC-3'
Cubilin	Human	Forward	5'-CGTGGAACACACAAACTTTAGG-3'
		Reverse	5'-CCAGTGAGGGGATCTGATTG-3'
β-Actin	Human	Forward	5'-CTCCCTGGAGAAGAGCTACG-3'
		Reverse	5'-GAAGGAAGGCTGGAAGAGTG-3'

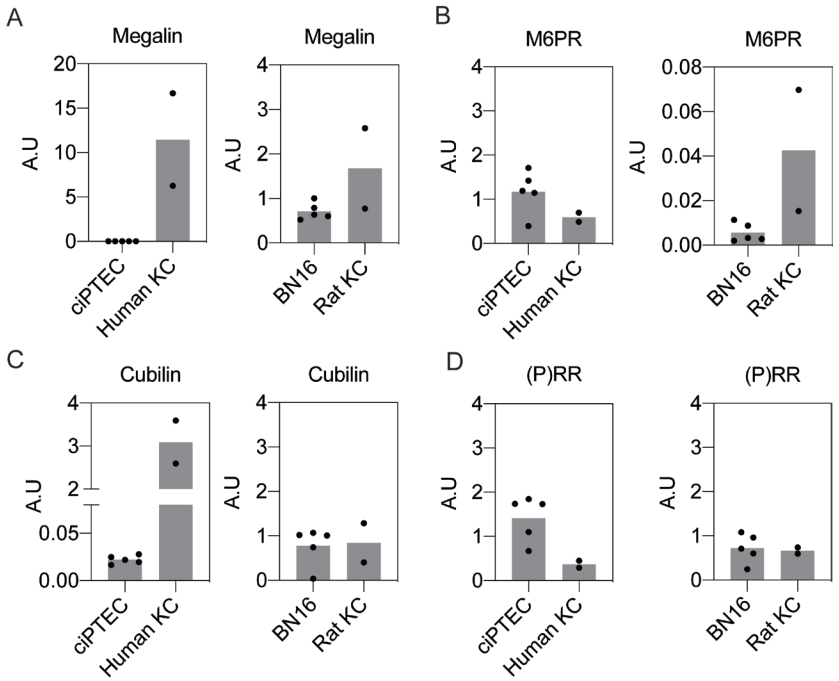

Figure S1. Gene expression of megalin **(panel A)**, mannose 6-phosphate receptor (M6PR, **panel B**), cubilin **(panel C)**, and (pro)renin receptor ((P)RR, **panel D**) in ciPTEC (n=5) and BN16 cells (n=5) compared with human kidney cortex (Human KC, n=1; RNA samples were collected from two different locations) and rat kidney cortex (Rat KC, n=1; RNA samples were collected from two different locations). Arbitrary units (A.U.) were obtained by correcting target gene expression for β-actin expression in the same sample. The bar represents the mean of the individual data points. Regarding megalin, no signal was obtained after 40 cycles in 4 samples, while in one sample a signal was obtained with a Ct value of 39.9.

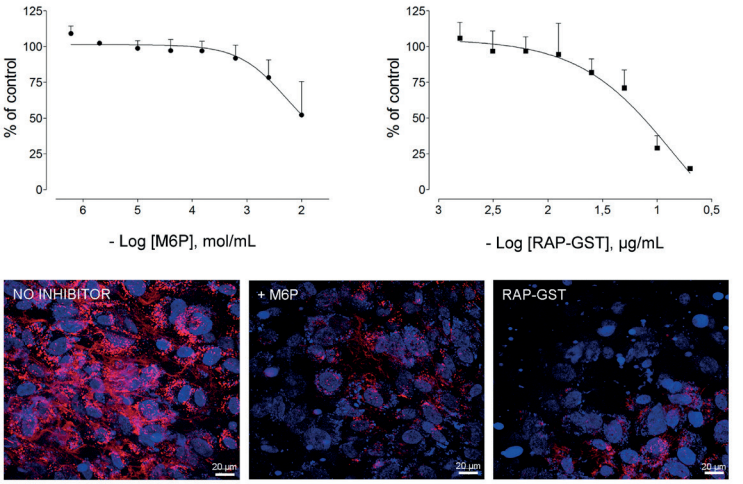

Figure S2. Inhibition of BSA uptake in ciPTEC by M6P and RAP-GST **(top panels)**, and fluorescence staining representing BSA accumulation **(bottom panels)**. Data (2 measurements in duplicate) have been expressed as a percentage of control (cells incubated with BSA in the absence of inhibitor).

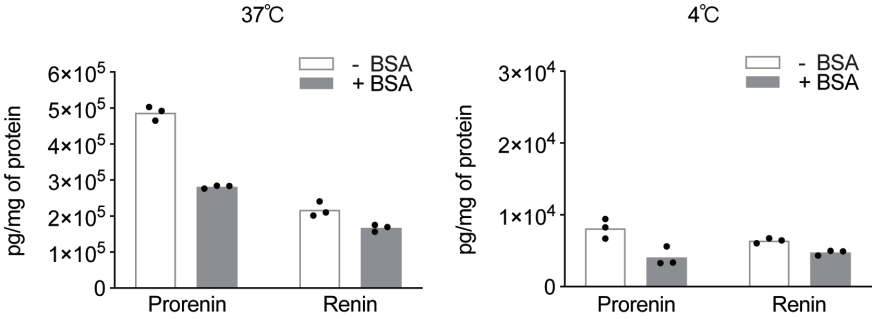

Figure S3. Cell-associated prorenin and renin levels after incubating BN16 cells with 2×10^6 pg/L prorenin or renin with or without 50 µg/mL of bovine serum albumin (BSA). Data represents mean (bar) of n=3. In all cases values with BSA were lower than without BSA.

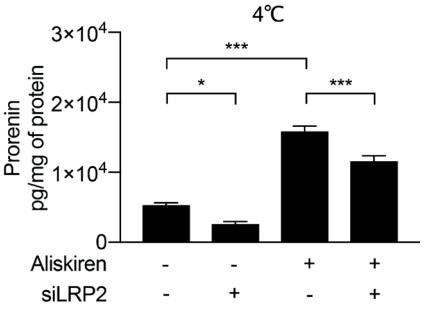

Figure S4. Cell-associated prorenin levels after incubating BN16 cells with 2×10^6 pg/L native prorenin or aliskiren-pretreated ('open') prorenin without or with megalin (LRP2) inhibition. Data are mean±SEMs of n=6. *P<0.05, ***P<0.0005.

CHAPTER 7

Megalin, Proton Pump Inhibitors and the Renin-angiotensin System in Healthy and Preeclamptic Placentas

Yuan Sun, Rugina I. Neuman, Michelle Broekhuizen, Sam Schoenmakers, Xifeng Lu, A.H. Jan Danser

Unpublished chapter

Abstract

Preeclampsia is characterized by elevated serum levels of soluble Fms-like tyrosine kinase-1 (sFlt-1), originating from placental tissue. Proton pump inhibitor (PPI) administration lowers sFlt-1, while angiotensin II stimulates sFlt-1 synthesis. Yet, in preeclampsia, circulating renin and angiotensinogen (AGT) levels are suppressed, while the precursor of renin, prorenin remains unaltered. Since the placenta is believed to synthesize renin-angiotensin system (RAS) components locally, a crucial question is whether placental RAS activity is increased in preeclampsia. Here, we studied gene expression and protein abundance of major RAS components, including megalin, a novel endocytic receptor for prorenin and renin [together denoted as (pro)renin] known to occur at high levels in the placenta, in placental tissue obtained from healthy pregnant women and women with early-onset preeclampsia. We found that renin, ACE, ACE2, and the angiotensin II type 1 and 2 receptors are expressed at identical levels in healthy and preeclamptic placentas, while both the (pro)renin receptor and megalin were increased in the latter. Placental (pro)renin levels were comparable in healthy and preeclamptic pregnancies, and the majority of this (>70%) concerned prorenin. Although placental AGT mRNA levels were at or below detection limit, AGT protein could be detected in healthy placental tissue, implying that placental AGT originates from the maternal systemic circulation. In agreement with this observation, placental AGT levels were markedly reduced in preeclamptic placentas. Moreover, using ex-vivo placental perfusion, we observed that de-novo placental AGT release decreased over time, suggestive for placental washout of blood-derived AGT. In contrast, placental (pro)renin release remained stable over a 3-hour perfusion period, and amounted to quantities that were >5-fold higher than the levels detected in placental tissue, indicating ongoing synthesis. The majority of this (>90%) concerned prorenin. The PPI esomeprazole dose-dependently reduced megalin/(pro)renin receptor-mediated renin uptake in Brown Norway yolk sac epithelial. In conclusion, our data suggest that placental RAS activity depends on AGT taken up from the maternal systemic circulation. They do not support elevated placental RAS activity in preeclampsia, and imply that PPIs might interfere with placental (pro)renin transport, thereby reducing angiotensin II formation as well as angiotensin II-induced sFlt-1 synthesis.

Introduction

Preeclampsia is a hypertensive disorder characterized by new-onset hypertension and proteinuria after 20 weeks of gestation. It is one of the major causes of maternal mortality during pregnancy and end-organ damage occurring after 20 weeks gestation.[1-3] A normal

pregnancy requires a ≈30% increase of extracellular fluid volume to provide an adequate blood supply for the developing uterus, placenta and foetus.[4] The renin-angiotensin system (RAS) plays a key role in this process. Estrogen stimulates hepatic angiotensinogen (AGT) expression, resulting in a 3-5-fold rise in circulating AGT.[4, 5] The plasma renin concentration also rises modestly,[6] and together with the rise in AGT, this results in a significant rise in plasma renin activity (PRA), thus ensuring sufficient RAS activity to allow water and salt retention.[7, 8] Remarkably, plasma prorenin levels increase much more strongly than plasma renin levels,[6, 9] due to prorenin release from the ovaries and to a lesser degree the placenta.[10] The function of this prorenin remains unclear.

In preeclampsia, the rises in renin and AGT in the circulation are suppressed, although sensitivity to angiotensin (Ang) II is enhanced.[11] Circulating prorenin levels in preeclamptic women are in the normal pregnancy range.[12] Given the local production of prorenin in the placenta, while the placenta is a key player in the development of preeclampsia, disturbed placental RAS activity may contribute to this phenomenon. Yet, data on prorenin levels in the uteroplacental unit of preeclamptic women are conflicting, with evidence for decreases, increases and no alteration.[13-15] What exactly determines the distribution of prorenin across the ovaries and uteroplacental unit, as well as its release into the blood stream, is unknown. It may require transcellular transport. For instance, amniotic fluid prorenin is of chorionic origin,[16] implying that chorionic prorenin is capable of crossing the amnion. A novel player in this field is megalin. Megalin not only contributes to renin/prorenin reabsorption in the proximal tubule of the kidney, but also occurs in syncytiotrophoblast and cytotrophoblast cells in the placenta.[17] Membrane recycling of megalin is a fast process which relies on vacuolar H^+-ATPase (V-ATPase)-dependent endosomal acidification.[18] Here it is of interest to note that we and others have recently reported that proton pump inhibitors (PPIs) lower the placental release of soluble Fms-like tyrosine kinase-1 (sFlt-1), a well-known biomarker for the prediction of preeclampsia or adverse outcomes.[19, 20] Angiotensin (Ang) II is one of the stimulators of sFlt-1 release.[21] Although PPIs are capable of inhibiting V-ATPase,[22, 23] such inhibition did not contribute to their acute effects on sFlt-1 release from human trophoblast cells.[24] A further possibility is that PPIs affect sFlt-1 production indirectly, via the placental RAS.

In the present study, we therefore set out to first quantify the expression of major RAS components (including megalin and the (pro)renin receptor [(P)RR]) and their protein abundance in healthy and preeclamptic placentas. Next, we studied the release of RAS components from *ex vivo* perfused placentas of healthy and preeclamptic pregnancies. Finally, we verified whether PPIs modulate megalin-dependent (pro)renin uptake in megalin-expressing

Brown Norway yolk sac epithelial cells (BN16 cells).

Methods

Tissue collection

The experiments were conducted using human placental tissue from women with normal pregnancy or with early-onset preeclampsia based on the ISSHP 2018 criteria.[25] All but one woman with early-onset preeclampsia delivered by caesarean section, and all gave informed consent prior to delivery. Placental tissue was collected immediately after delivery at the Erasmus Medical Center, Rotterdam, the Netherlands. Tissue sections were cut from the decidual side of the placenta and included decidua basalis and chorionic villi. They were snap frozen in liquid nitrogen and stored at -80°C. Areas of necrosis or tissue damage were avoided. The study was exempted from approval by the local institutional Medical Ethics Committee according to the Dutch Medical Research with Human Subjects Law (MEC-2016-418 and MEC-2017-418).

Placenta perfusion experiments

The perfusion method used in this study was previously described by Hitzerd et al.[26] In short, placentas were perfused at 37°C with aerated (95% O_2 and 5% CO_2)perfusion medium consisting of Krebs-Henseleit buffer, supplemented with heparin (2500 IU/L). The fetal circulation (closed-circuit; flow rate 6 mL/minute) was established by cannulating the chorionic artery and corresponding vein of an intact cotyledon. Maternal circulation (closed-circuit; flow rate 12 mL/minute) was created by placing four blunt cannulas in the intervillous space. Perfusion experiments were conducted in healthy and preeclamptic placentas. The healthy group consisted of placentas from uncomplicated, normotensive pregnancies in which the endothelin receptor antagonist ambrisentan (10 mg/L, Sigma-Aldrich Chemie, Schnelldorf, Germany) or the phosphodiesterase-5 inhibitor sildenafil (500 ng/mL) were added to the maternal circulation at t=0.[26, 27] The preeclamptic group consisted of placentas from early-onset preeclamptic pregnancies (<34 weeks) which were perfused with sildenafil or no drug. Samples from the maternal circulations were taken every 30 minutes (until 180 minutes) and immediately stored at −80°C. To control the quality of perfusion, 100 mg/L of antipyrine and 36 mg/L of FITC-dextran (40 kDa) was added to the fetal and maternal buffer, respectively. An experiment was considered successful when the fetal-to-maternal (F/M) ratio of antipyrine was >0.75 and the maternal-to-fetal (M/F) ratio of FITC-dextran <0.03 at t=180. The release of angiotensinogen, renin or prorenin was expressed per hour, correcting for the level that was present in the previous sample.

Homogenization of placenta tissue

About 100 mg of maternal side of placenta tissue (decidua basalis and part of chorionic villi) with grind beads were homogenized with 10 volume of ice-cold buffer C (12 mmol/L $NaH_2PO_4 \cdot 2H_2O$, 86.7 mmol/L Na_2HPO_4, 15.9 mmol/L NaCl) and 1x complete protease inhibitors (Roche, Mannheim, Germany) at 4°C by using Tissue Lyzer 24 (3 × 60s, 60 Hz, Shanghai, China). The lysates were centrifuged at 14.000 ×*g* for 10 minutes at 4°C, then the clear supernatant was transferred to a new tube and kept on ice. The pellet was resuspended in 200 µL of buffer C with protease inhibitor, and was additionally homogenized for 2 × 60s at 60 Hz. After centrifuging at 14.000 ×*g* for 10 minutes at 4°C, the second supernatant was transferred to the first supernatant. Supernatants were stored at −80°C.

Measurement of (pro)renin in placenta and perfusate

Renin in the tissue lysate and perfusates was measured with the Renin III (Cisbio, Gif-sur-Yvette, France) immunoradiometric assay. Total renin was measured with the same assay, after its conversion to the renin conformation (allowing its detection in the assay) by incubating it with 10 µmol/L aliskiren (a kind gift of Novartis, Basel, Switzerland) at 4°C for 48 hours. Prorenin is calculated by subtracting renin from total renin.

Renin binding and uptake

Brown Norway yolk sac epithelial cells (BN16) were cultured in Minimum Essential Media (MEM) (Gibco, Thermo Fisher Scientific, Paisley, UK) supplemented with 1×Gulta^{MAX} (Gibco) and 10% FCS (GE Healthcare, Eindhoven, The Netherlands) at 37°C in a humidified incubator with 5% CO_2. BN16 cells were seeded at a density of 2×10^5 cells per well in 24-well plates and cultured for 48 hours before carrying out experiments. To study the effect of proton pump inhibition on renin binding and internalization, BN16 cells were first washed twice with phosphate buffered saline (PBS), and then pre-incubated with MEM without FCS for 30 minutes at 37°C. Next, cells were washed with ice-cold PBS twice, and incubated with 300 µL MEM containing 0.2 µg/mL of recombinant human renin (a gift from Actelion Pharmaceuticals, Allschwil, Switzerland) in the presence or absence of increasing concentrations of the H^+/K^+ ATPase inhibitor esomeprazole or the V-ATPase inhibitor bafilomycin A1 at either 4°C (to quantify renin binding) or 37°C (to quantify renin internalization). After 2 hours of incubation, the culture medium was discarded, and the cells were washed twice with ice-cold PBS containing 0.5% BSA and twice with ice-cold PBS. Then, the cells were lysed with ice-cold PBS containing 0.2% Triton X-100 (SEEVA, Heidelberg, Germany) and complete protease inhibitors. Lysate was centrifuged at 14.000×*g* for 10 minutes at 4°C to remove any cell debris and the supernatant was stored at -80°C until use. Renin was measured as described above.

Immunoblotting

For protein abundance, frozen pieces of tissue were homogenized in RIPA buffer (150 mmol/L NaCl, 1% Triton X-100, 0.5% sodium deoxycolate, 0.1% SDS, 50 mmol/L Tris pH 8.0) with protease inhibitors cocktail using TissueLyzer (PolyTron PT2100, Littau-Lucerne, Switzerland). Lysates were cleared by centrifugation at 14000×g for 10 minutes at 4°C. The total protein concentration in supernatant was determined by BCA assay (Pierce, Waltham, USA). Equal amounts of proteins (30-40 mg) were loaded and separated on Precast Midi Protein Gel (Bio-Rad, USA), and transferred to PVDF membranes using semi-dry Trans-Blot Turbo Transfer system (Bio-Rad). The blots were then probed with antibodies against angiotensinogen (1:100, ABBIOTEC, Shenzhen, China), GAPDH (1:5000, GeneTex, Hsinchu, China), β-actin (1:5000, Merck Millipore, Darmstadt, Germany), or megalin (1:500, Biotech, Wuhan, China), and detected by using Clarity Western ECL Substrate (Bio-Rad, Hercules, USA). The intensities of bands were analyzed using ImageJ.

RNA isolation and qPCR analysis

Total RNA was extracted using the Direct-zol RNA kit (Zymo Research, Irvine, USA). One microgram total RNA was reverse transcribed using QuantiTect® Reverse Transcription Kit (Qiagen, Hilden, Germany). SYBR Green real-time quantitative PCR assays were performed on QuantStudio 7 Flex Real-Time PCR Systems (Thermo Fisher, Waltham, USA) using SYBR ®Premix Ex TaqTM II kit (Qiagen, Venlo, The Netherlands). Primers used in the study are listed in Supplemental Table 1. β-actin, Pre-mRNA Processing Factor 38A (PRPF38A) and DExD-Box Helicase 50 (DDX50) were used as housekeeping genes for calculating the relative expressions of target genes **(Supplemental Table 1)**, and the geometric mean of the three relative expressions were used for calculating the arbitrary unit (A.U).

Statistics

Data are provided as mean ± SEM or geometric mean and range. When comparing differences between two groups, Student's t-test was used. One-way ANOVA with Bonferroni post-modification was used when comparing differences between more than two groups. Kolmogorov-Smirnov test was used to verify normal distribution. For data that were non-normally distributed, a non-parametric t-test (Mann-Whitney U test) was used to compare the differences between groups. $P<0.05$ was considered significant. Data below detection limit were assumed to equal the detection limit.

Results

Clinical characteristics of the patients are provided in **Table 1**. The data confirm that our PE patients fulfilled the ISSHP 2018 criteria.[25]

Table 1. Clinical Characteristics of placentas

Characteristic	Healthy (n=16)	PE (n=14)
Maternal age (years)	31 (28 - 38)	30 (26 - 39)
Nulliparity (n)	0	9*
Ethnicity (n caucasian / other)	8 / 8	10 / 4
BMI (kg/m^2)	25.7 (22.4 - 33.2)	24.3 (22.4 - 33.2)
Highest diastolic blood pressure (mmHg)	80 (70 - 81)	108.5 (100 - 111.3)*
Urinary protein/creatinine ratio	ND	352.5 (98.0 - 890.5)*
Mode of delivery (n caesarean / spontaneous)	16 / 0	13 /1
Gestational age (weeks)	39.0 (38.7 - 39.0)	29.9 (28,9-31,8)*
Sex (n female / male)	5 / 11	7 / 7
Birth weight (g)	3593 (3383 - 3975)	1125 (915 - 1375)*
Birth centile <10th (n)	0	9*
Placental weight (g)	696.5 (974.5 - 619.3)	293.0 (233.8 - 346.5)*

Data are shown as n (number of cases) or median (interquartile range). *P<0.05, Mann-Whitney U test. ND, not done.

Expression of RAS components in healthy and preeclamptic placentas

Placental expression of renin, AGT, angiotensin-converting enzyme (ACE), ACE2, the Ang II type 1 and type 2 receptor (AT1R, AT2R), and megalin was comparable between healthy and preeclamptic placentas (n=12 for each), while (P)RR expression was increased in the

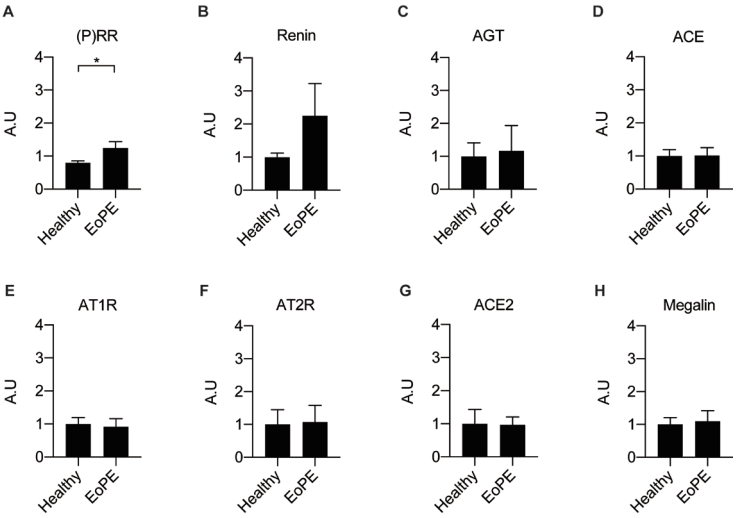

Figure 1. Gene expression levels of RAS components **(A-G)** and megalin **(H)** in healthy and early-onset preeclamptic (EoPE) placental tissue. Data are mean±SEM of n=12. * P<0.05. (P)RR, (pro)renin receptor; AGT, angiotensinogen; ACE, angiotensin-converting enzyme; AT1R, AT2R, angiotensin II type 1 and 2 receptor; A.U., arbitrary unit.

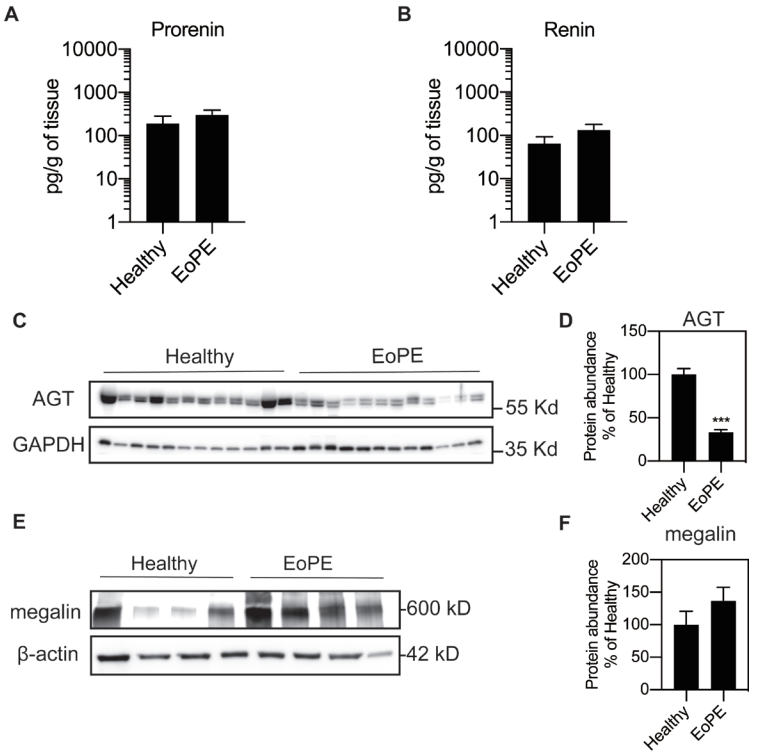

Figure 2. Renin **(A)** and prorenin **(B)** levels measured by immunoradiometric assay and angiotensinogen (AGT; **C+D**) and megalin **(E+F)** protein abundance measured by western blot in healthy and early-onset preeclamptic (EoPE) placental tissue. Panels **C** and **E** are representative blots of AGT and megalin protein. Data have been normalized versus GAPDH and β-actin. Data are mean±SEM of n=12. *** P<0.005.AGT, angiotensinogen.

latter **(Figure 1)**. AGT expression was at or below detection limit (Ct=38) in most of the samples, even when using a second set of primers (Figure S1). Total renin levels in healthy placental tissue amounted to 107 (range 58.1-174) pg/g, and 73.4 ± 6.4% of this was prorenin **(Figure 2A and 2B)**. Total renin levels were non-significantly (P=0.052) higher in preeclamptic placentas (266 [range 145-535] pg/g), while the proportion of prorenin in this group (73.4±7.3%) was identical to that in healthy placentas. Placental AGT abundance was decreased (P<0.0001) in preeclamptic patients versus healthy subjects **(Figure 2C and 2D)**. Megalin protein abundance tended to be increased in preeclamptic placentas (**Figure 2E and 2F)**.

Placental release of (pro)renin and AGT

Prorenin release into the maternal perfusate from healthy placenta (n=5) was stable during the 3-hour perfusion period **(Figure 3A)**, and no differences versus preeclamptic placentas (n=4) were observed. Renin release occurred in parallel, but its levels were >10-fold lower than those of prorenin **(Figure 3B)**. Placental AGT release from healthy placentas (n=5)

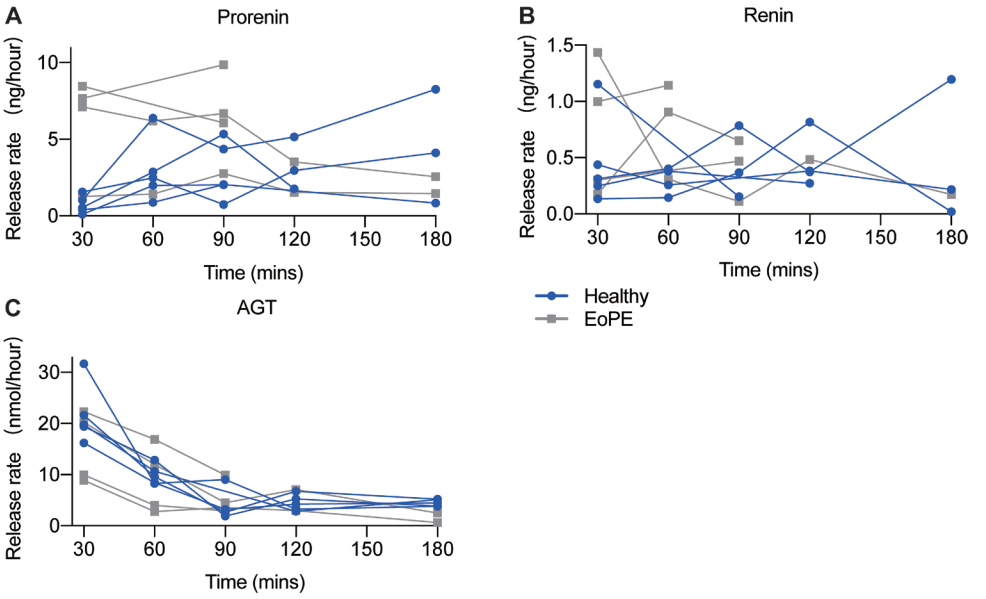

Figure 3. Renin, prorenin and angiotensinogen (AGT) release from isolated perfused healthy (n=5) and early-onset preeclamptic (EoPE, n=4) cotyledons. Perfusate collection from some of the preeclamptic placentas could not be continued over the full 180 minutes due to fetal-to-maternal leakage. In such cases only the samples prior to the occurrence of leakage were used.

peaked at 21.7±2.6 nmol/hour over the first 30 minutes, and then decreased, the release being lowest after 180 minutes **(Figure 3C)**. AGT release from 4 preeclamptic placentas tended to be in the low 'normal' range, i.e., the range observed in the healthy placentas.

Inhibiting V-ATPase decreases renin internalization but not binding

Esomeprazole dose-dependently reduced renin uptake in BN16 cells, and increased renin binding at the highest dose tested only **(Figures 4A and 4B)**. Bafilomycin A1 similarly reduced renin uptake, without affecting renin binding **(Figures 4C and 4D)**.

Discussion

The existence of a placental RAS has been proposed decades ago.[28] Although it is believed that it may contribute to preeclampsia, its exact role is still unknown. This relates to the fact that we still do not fully understand how local Ang II synthesis occurs in the placenta. In the current study, we found that the mRNA levels of most RAS components are comparable in healthy and preeclamptic placentas. This agrees with previous studies showing that renin, AGT, ACE and AT2R expression is similar in normal and preeclamptic decidua basalis.[15, 29, 30] Simultaneously, uteroplacental AT1R[30-32] and renin[32] upregulation have also been claimed

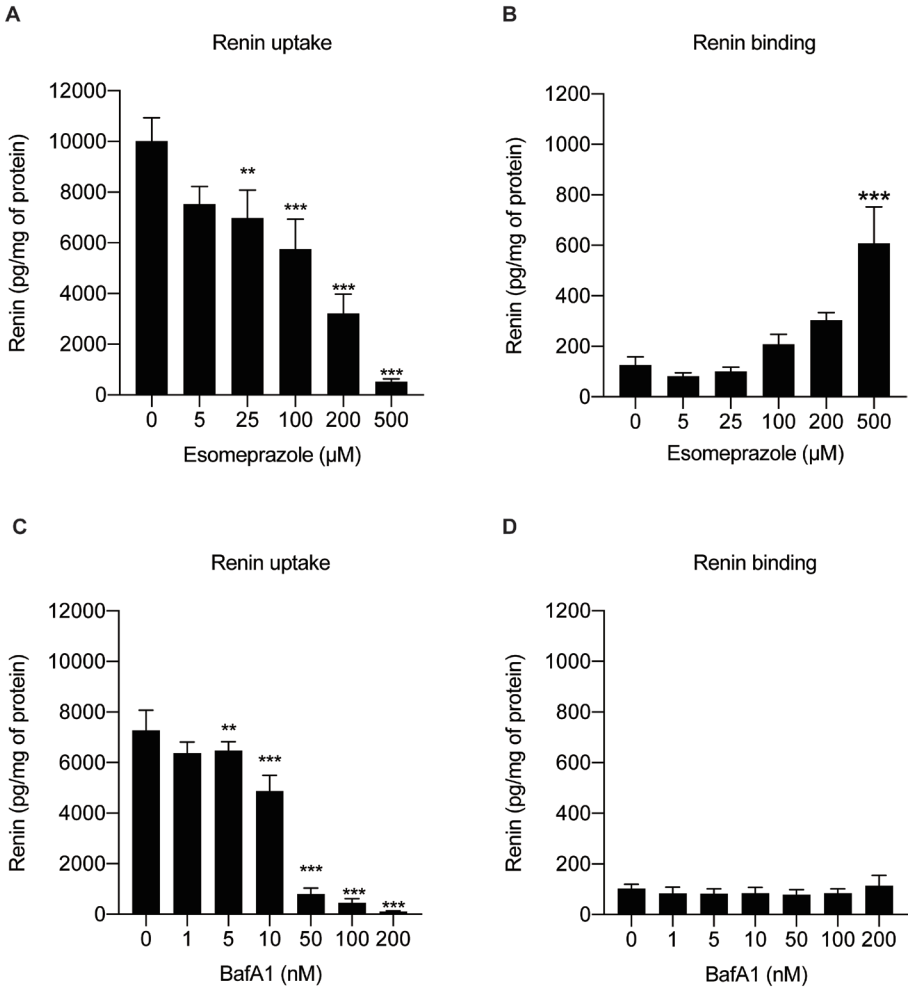

Figure 4. Cell-associated renin levels after incubating BN16 cells with 100 U/L renin at 37°C **(A&C)** or 4°C **(B&D)** for 2 hours in the presence of increasing concentrations of esomeprazole **(A&B)** or bafilomycin A1 **(C&D)**. Data are mean±SEM of n=6. *P<0.05, **P<0.005, ***P<0.0005 vs. 0.

in preeclampsia. One explanation for these conflicting observations is that different tissues were studied, ranging from endometrium and myometrium to decidual tissue. In our study, we collected tissue from the maternal side of the placenta, i.e., decidua basalis and part of chorionic villi. A second explanation is that placental RAS expression may change with increasing gestational age. For example, placental AT1R mRNA levels are highest at 6-9 weeks of gestation, and lowest at term (37±0-41±0 weeks).[32] Thus, the 10 week difference in gestational age between the healthy and preeclamptic women of this study is a confounding factor. Nevertheless, it is important to note that symptoms in early-onset preeclampsia (before 34±0 weeks of gestation, like in our study), develop much earlier,[33] implying that

changes in placental RAS expression, if having a causal effect, might be more drastic even at this early gestational age.

Importantly, placental AGT expression in the present study was low and in most cases undetectable. Such low expression has been observed earlier, when making a comparison with prolactin and renin using Northern blot analysis.[34] Despite the absence of significant expression, AGT protein was easily detectable in placental tissue. This implies that placental AGT must have been taken up from maternal blood. In agreement with this concept, placental AGT levels were lower in preeclamptic women, who are known to have greatly diminished circulating AGT levels. Moreover, perfusing the placenta with buffer resulted in a washout of AGT, again with a tendency for diminished levels in the perfusate from preeclamptic placentas. Animal data similarly support a major role for AGT of maternal origin. When female mice carrying the human renin transgene were crossed with male mice carrying the human AGT transgene (both of which do not react with their mouse counterparts), the pregnant mice remained normotensive. Yet, when crossing female human AGT transgenic mice with male human renin transgenic mice, the pregnant mice did develop a preeclamptic phenotype, characterized by hypertension, elevated sFlt-1 levels and proteinuria.[35] Moreover, specifically inhibiting human AGT expression in the maternal liver with liver-targeted siRNA in the latter model suppressed the preeclamptic phenotype.[36]

Unlike AGT release, which peaked early and then decreased, placental (pro)renin release remained stable over a 3-hour perfusion period. More than 90% of this release was prorenin, and the increase was comparable in the healthy and preeclamptic placentas. Since the total renin release in healthy placentas amounted to ≈5000 pg/hr, and considering that a cotyledon wet weight amounts to ≈25 g, the total renin amount released during the 3 hours perfusion period can be estimated to be 5000/25×3=600 pg/g. Since this is >5 times the amount detected in placental tissue, these data strongly support the synthesis and release of (pro)renin from the placenta, in full agreement with previous findings.[28, 37] Importantly, the circulating renin levels in preeclamptic women are lower than those in healthy pregnant women, while their circulating prorenin levels mimic those in healthy pregnancy. Clearly therefore, placental (pro)renin synthesis occurs independently of renal (pro)renin synthesis. In fact, it has already been estimated that the actual release of (pro)renin from the placenta into the circulation amounts to at most a few percent of the total amount of circulating (pro)renin during pregnancy.[37] Yet, given the simultaneous reduction of placental AGT levels, it is unlikely that placental RAS activity is upregulated in preeclampsia.

The (P)RR is an accessory protein of the V-ATPase. Its upregulation in preeclampsia, com-

bined with a tendency for increased megalin levels favors increased activity of the megalin-V-ATPase pathway in this condition. We recently identified megalin as a novel endocytic receptor for (pro)renin in the kidney,[38] where it simultaneously is a determinant of renal RAS activity.[39, 40] Whether it contributes to RAS activity (e.g., by facilitating (pro)renin transport) in the placenta is still unknown. We now additionally show that the PPI esomeprazole, like the V-ATPase inhibitor bafilomycin A1, can inhibit megalin-mediated renin uptake. We speculate that this might result in suppression of placental RAS activity. Since lower Ang II levels will result in diminished sFlt-1 production, this concept offers an explanation for the observation that PPIs lower sFlt-1 in preeclamptic women, whose sensitivity to Ang II is greatly enhanced(Figure 5).[4] Clearly, more work is needed to fully support this novel concept.

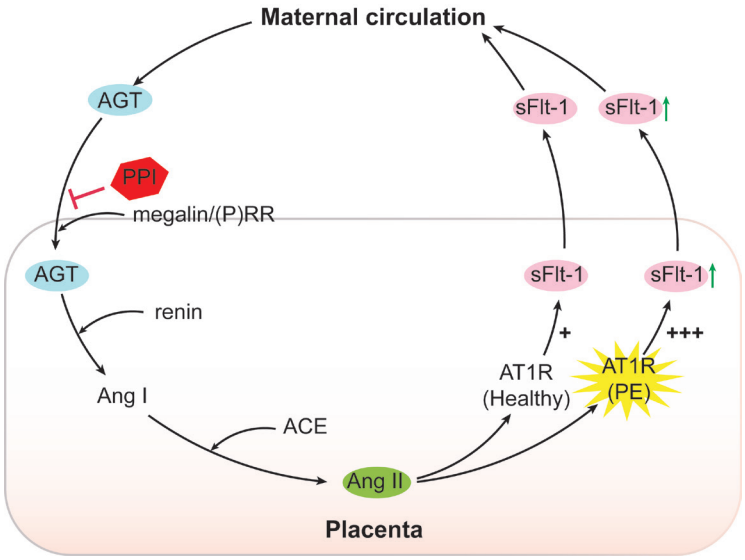

Figure 5. Summarizing picture. See Discussion for explanation.

Sources of Funding

Y. Sun and X. Lu were supported by National Natural Science Foundation of China (grant nrs. 81800383 and 81870605), and the Shenzhen Key Laboratory of Metabolism and Cardiovascular Homeostasis, and Shenzhen Municipal Science and Technology Innovation Council (grant no. JCYJ20170817093928508 and JCYJ2019080817040).

References

1. Mol BWJ, Roberts CT, Thangaratinam S, Magee LA, de Groot CJM, Hofmeyr GJ. Pre-eclampsia. *Lancet*. 2016;387:999-1011
2. Miklus RM, Elliott C, Snow N. Surgical cricothyrotomy in the field: Experience of a helicopter transport team. *J Trauma*. 1989;29:506-508
3. Phipps EA, Thadhani R, Benzing T, Karumanchi SA. Pre-eclampsia: Pathogenesis, novel diagnostics and therapies. *Nat Rev Nephrol*. 2019;15:275-289
4. Verdonk K, Visser W, Van Den Meiracker AH, Danser AH. The renin-angiotensin-aldosterone system in pre-eclampsia: The delicate balance between good and bad. *Clin Sci (Lond)*. 2014;126:537-544
5. Rana S, Powe CE, Salahuddin S, Verlohren S, Perschel FH, Levine RJ, Lim KH, Wenger JB, Thadhani R, Karumanchi SA. Angiogenic factors and the risk of adverse outcomes in women with suspected preeclampsia. *Circulation*. 2012;125:911-919
6. Derkx FH, Alberda AT, de Jong FH, Zeilmaker FH, Makovitz JW, Schalekamp MA. Source of plasma prorenin in early and late pregnancy: Observations in a patient with primary ovarian failure. *J Clin Endocrinol Metab*. 1987;65:349-354
7. Hsueh WA, Luetscher JA, Carlson EJ, Grislis G, Fraze E, McHargue A. Changes in active and inactive renin throughout pregnancy. *J Clin Endocrinol Metab*. 1982;54:1010-1016
8. Irani RA, Xia Y. Renin angiotensin signaling in normal pregnancy and preeclampsia. *Semin Nephrol*. 2011;31:47-58
9. Sealey JE, McCord D, Taufield PA, Ales KA, Druzin ML, Atlas SA, Laragh JH. Plasma prorenin in first-trimester pregnancy: Relationship to changes in human chorionic gonadotropin. *Am J Obstet Gynecol*. 1985;153:514-519
10. Krop M, Danser AH. Circulating versus tissue renin-angiotensin system: On the origin of (pro)renin. *Curr Hypertens Rep*. 2008;10:112-118
11. Irani RA, Xia Y. The functional role of the renin-angiotensin system in pregnancy and preeclampsia. *Placenta*. 2008;29:763-771
12. Verdonk K, Saleh L, Lankhorst S, Smilde JE, van Ingen MM, Garrelds IM, Friesema EC, Russcher H, van den Meiracker AH, Visser W, Danser AH. Association studies suggest a key role for endothelin-1 in the pathogenesis of preeclampsia and the accompanying renin-angiotensin-aldosterone system suppression. *Hypertension*. 2015;65:1316-1323
13. Brar HS, Kjos SL, Dougherty W, Do YS, Tam HB, Hsueh WA. Increased fetoplacental active renin production in pregnancy-induced hypertension. *Am J Obstet Gynecol*. 1987;157:363-367
14. Kalenga MK, Thomas K, de Gasparo M, De Hertogh R. Determination of renin, angiotensin converting enzyme and angiotensin ii levels in human placenta, chorion and amnion from women with pregnancy induced hypertension. *Clin Endocrinol (Oxf)*. 1996;44:429-433
15. Herse F, Dechend R, Harsem NK, Wallukat G, Janke J, Qadri F, Hering L, Muller DN, Luft FC, Staff AC. Dysregulation of the circulating and tissue-based renin-angiotensin system in preeclampsia. *Hypertension*. 2007;49:604-611
16. Pringle KG, Wang Y, Lumbers ER. The synthesis, secretion and uptake of prorenin in human amnion. *Physiol Rep*. 2015;3
17. Storm T, Christensen EI, Christensen JN, Kjaergaard T, Uldbjerg N, Larsen A, Honore B, Madsen M. Megalin is predominantly observed in vesicular structures in first and third trimester cytotrophoblasts of the human placenta. *J Histochem Cytochem*. 2016;64:769-784
18. Gleixner EM, Canaud G, Hermle T, Guida MC, Kretz O, Helmstadter M, Huber TB, Eimer S, Terzi F, Simons M. V-atpase/mtor signaling regulates megalin-mediated apical endocytosis. *Cell Rep*. 2014;8:10-19
19. Hastie R, Bergman L, Cluver CA, Wikman A, Hannan NJ, Walker SP, Wikstrom AK, Tong S, Hesselman S. Proton pump inhibitors and preeclampsia risk among 157 720 women. *Hypertension*. 2019;73:1097-1103
20. Saleh L, Samantar R, Garrelds IM, van den Meiracker AH, Visser W, Danser AHJ. Low soluble fms-like tyrosine kinase-1, endoglin, and endothelin-1 levels in women with confirmed or suspected preeclampsia using proton pump inhibitors. *Hypertension*. 2017;70:594-600
21. Zhou CC, Ahmad S, Mi T, Xia L, Abbasi S, Hewett PW, Sun C, Ahmed A, Kellems RE, Xia Y. Angio-

tensin ii induces soluble fms-like tyrosine kinase-1 release via calcineurin signaling pathway in pregnancy. *Circ Res*. 2007;100:88-95
22. Spugnini EP, Citro G, Fais S. Proton pump inhibitors as anti vacuolar-atpases drugs: A novel anticancer strategy. *J Exp Clin Cancer Res*. 2010;29:44
23. Sabolic I, Brown D, Verbavatz JM, Kleinman J. H(+)-atpases of renal cortical and medullary endosomes are differentially sensitive to sch-28080 and omeprazole. *Am J Physiol*. 1994;266:F868-877
24. Onda K, Tong S, Beard S, Binder N, Muto M, Senadheera SN, Parry L, Dilworth M, Renshall L, Brownfoot F, Hastie R, Tuohey L, Palmer K, Hirano T, Ikawa M, Kaitu'u-Lino T, Hannan NJ. Proton pump inhibitors decrease soluble fms-like tyrosine kinase-1 and soluble endoglin secretion, decrease hypertension, and rescue endothelial dysfunction. *Hypertension*. 2017;69:457-468
25. Brown MA, Magee LA, Kenny LC, Karumanchi SA, McCarthy FP, Saito S, Hall DR, Warren CE, Adoyi G, Ishaku S, International Society for the Study of Hypertension in P. Hypertensive disorders of pregnancy: Isshp classification, diagnosis, and management recommendations for international practice. *Hypertension*. 2018;72:24-43
26. Hitzerd E, Neuman RI, Broekhuizen M, Simons SHP, Schoenmakers S, Reiss IKM, Koch BCP, van den Meiracker AH, Versmissen J, Visser W, Danser AHJ. Transfer and vascular effect of endothelin receptor antagonists in the human placenta. *Hypertension*. 2020;75:877-884
27. Hitzerd E, Broekhuizen M, Mirabito Colafella KM, Glisic M, de Vries R, Koch BCP, de Raaf MA, Merkus D, Schoenmakers S, Reiss IKM, Danser AHJ, Simons SHP. Placental effects and transfer of sildenafil in healthy and preeclamptic conditions. *EBioMedicine*. 2019;45:447-455
28. Poisner AM. Regulation of utero-placental prorenin. *Adv Exp Med Biol*. 1995;377:411-426
29. Shah DM, Banu JM, Chirgwin JM, Tekmal RR. Reproductive tissue renin gene expression in preeclampsia. *Hypertens Pregnancy*. 2000;19:341-351
30. Anton L, Brosnihan KB. Systemic and uteroplacental renin--angiotensin system in normal and pre-eclamptic pregnancies. *Ther Adv Cardiovasc Dis*. 2008;2:349-362
31. Anton L, Merrill DC, Neves LA, Stovall K, Gallagher PE, Diz DI, Moorefield C, Gruver C, Ferrario CM, Brosnihan KB. Activation of local chorionic villi angiotensin ii levels but not angiotensin (1-7) in preeclampsia. *Hypertension*. 2008;51:1066-1072
32. Anton L, Merrill DC, Neves LA, Diz DI, Corthorn J, Valdes G, Stovall K, Gallagher PE, Moorefield C, Gruver C, Brosnihan KB. The uterine placental bed renin-angiotensin system in normal and preeclamptic pregnancy. *Endocrinology*. 2009;150:4316-4325
33. Burton GJ, Redman CW, Roberts JM, Moffett A. Pre-eclampsia: Pathophysiology and clinical implications. *BMJ*. 2019;366:l2381
34. Li C, Ansari R, Yu Z, Shah D. Definitive molecular evidence of renin-angiotensin system in human uterine decidual cells. *Hypertension*. 2000;36:159-164
35. Takimoto E, Ishida J, Sugiyama F, Horiguchi H, Murakami K, Fukamizu A. Hypertension induced in pregnant mice by placental renin and maternal angiotensinogen. *Science*. 1996;274:995-998
36. Haase N, Foster DJ, Cunningham MW, Bercher J, Nguyen T, Shulga-Morskaya S, Milstein S, Shaikh S, Rollins J, Golic M, Herse F, Kraker K, Bendix I, Serdar M, Napieczynska H, Heuser A, Gellhaus A, Thiele K, Wallukat G, Muller DN, LaMarca B, Dechend R. Rna interference therapeutics targeting angiotensinogen ameliorate preeclamptic phenotype in rodent models. *J Clin Invest*. 2020;130:2928-2942
37. Lenz T, James GD, Laragh JH, Sealey JE. Prorenin secretion from human placenta perfused in vitro. *Am J Physiol*. 1991;260:E876-882
38. Sun Y, Goes Martini A, Janssen MJ, Garrelds IM, Masereeuw R, Lu X, Danser AHJ. Megalin: A novel endocytic receptor for prorenin and renin. *Hypertension*. 2020;75:1242-1250
39. Ye F, Wang Y, Wu C, Howatt DA, Wu CH, Balakrishnan A, Mullick AE, Graham MJ, Danser AHJ, Wang J, Daugherty A, Lu HS. Angiotensinogen and megalin interactions contribute to atherosclerosis-brief report. *Arterioscler Thromb Vasc Biol*. 2019;39:150-155
40. Koizumi M, Ueda K, Niimura F, Nishiyama A, Yanagita M, Saito A, Pastan I, Fujita T, Fukagawa M, Matsusaka T. Podocyte injury augments intrarenal angiotensin ii generation and sodium retention in a megalin-dependent manner. *Hypertension*. 2019;74:509-517

Supplemental Materials

Supplemental Table 1. List of qPCR primers sequences.

Gene		Sequence
(P)RR	Forward	5'-TCTCAGTTCACTCCCCCTCAA-3'
	Reverse	5'-GATGCTTATGACGAGACAGCAAG-3'
Renin	Forward	5'-GCCGTCTCTACACTGCCTGT-3'
	Reverse	5'-GGAGGGTGAGTTCTGTTCCA-3'
AGT	Forward	5'-TCAACACCTACGTCCACTTCC-3'
	Reverse	5'-CACTGAGGTGCTGTTGTCCA-3'
AGT	Forward	5'-ACCTACGTCCACTTCCAAGG-3'
(primer 2)	Reverse	5'-GTTGTCCACCCAGAACTCCT-3'
AGT	Forward	5'-ACAAGGTGGAGGGTCTCACT-3'
(primer 3)	Reverse	5'-TGGATGGTCCGGGGAGATAG-3'
ACE	Forward	5'-CCAACCTCGATGTCACCAGT-3'
	Reverse	5'-TCGACCCTTCCCAGAACTC-3'
AT1R	Forward	5'-TGACAGTCCAAAGGCTCCA-3'
	Reverse	5'-TTTGATCACCTGGGTCGAAT-3'
AT2R	Forward	5'-GGCAACTCCACCCTTGCCACT-3'
	Reverse	5'-TGCCAGAGATGTTCACAAGCCCGA-3'
ACE2	Forward	5'-TTCTGTCACCCGATTTTCAA-3'
	Reverse	5'-TCCCAACAATCGTGAGTGC-3'
Megalin	Forward	5'-CTGCTCCTGGCTCTCGTC-3'
	Reverse	5'-CTTTGGTCCCATCACACCTC-3'
β-actin	Forward	5'-CTCCCTGGAGAAGAGCTACG-3'
	Reverse	5'-GAAGGAAGGCTGGAAGAGTG-3'
PRPF38A	Forward	5'-GTTAAGGTTTGTGGGTGGCG-3'
	Reverse	5'-AGCATGCGGACATACTTGAAATC-3'
DDX50	Forward	5'-GCCTCCTGAAAGGAAATATGG-3'
	Reverse	5'-AGTATCCAGTCGGAATCATGC-3'

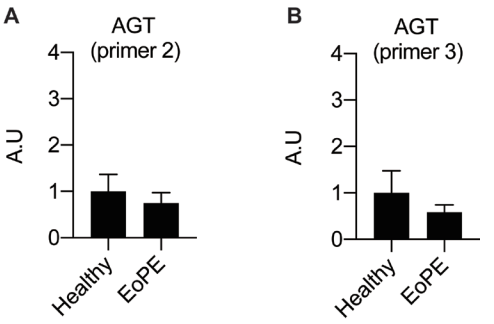

Supplemental Figure 1. AGT gene expression in healthy and EoPE placental tissue. AGT primer 2 **(A)** and AGT primer 3 **(B)** were used in qPCR experiments. Data are mean±SEM of n=12.

CHAPTER 8

Summary and Perspectives

Summary

(Pro)renin receptor in lipid metabolism (Chapters 1-2)

The plasma concentrations of prorenin, the precursor of renin, are normally 10-fold higher than those of renin, and this can go up to ~100-fold under pathophysiological conditions. However, its function, except being an inactive precursor of renin, remains unknown. Previous studies found that elevated plasma prorenin concentrations correlate with the incidence of macro- and micro-vascular complications, such as nephropathy and retinopathy, in diabetes mellitus, despite the normal or even reduced plasma renin concentrations in this condition.[1-3] Moreover, evidence suggests that a local renin-angiotensin system (RAS) exists in multiple organs, which might display increased or decreased activity in the absence of changes in the circulating RAS. Examples are the kidney in diabetes and the placenta in pre-eclampsia.[4, 5] Since renin synthesis is limited to the juxtaglomerular cells in the kidney, these local RAS must rely on a mechanism that either allows uptake of renin and/or prorenin activation. The discovery of the (pro)renin receptor [(P)RR] about two decades ago seemed to provide the solution to this problem, as discussed in **Chapter 1**. The (P)RR binds both renin and prorenin, and displays higher affinity for prorenin.[6] Upon binding, it activates prorenin in a non-proteolytic manner, allowing the generation of angiotensins. Additionally, (P)RR binding of renin and prorenin, denoted herein as (pro)renin, triggers intracellular signaling cascades in an angiotensin-independent manner, resulting in activation of p38 mitogen-activated protein kinase (MAPK) and extracellular signal-regulated kinase 1/2 (Erk1/2), for instance in vascular smooth muscle cells (VSMCs), collecting duct cells, and adipocytes.[7, 8] Activation of p38 MAPK and Erk1/2 leads to upregulation of profibrotic and proliferative gene expression, resulting in accelerated cell proliferation and end-organ damage. However, to observe angiotensin II-dependent and -independent effects, (pro)renin had to be applied at concentrations that are several orders of magnitude above its normal plasma levels and the ultrahigh levels achieved in transgenic rodent models.[9] Moreover, unlike other RAS components, deletion of the (P)RR is lethal, even when it is limited to certain cell types, such as cardiomyocyte and podocytes.[10-12] This questions whether the interaction between (pro)renin and the (P)RR truly is of relevance in vivo.

Interestingly, the cytosolic domain (CD) of the (P)RR was previously identified as an accessory protein of vacuolar H^+-ATPase (V-ATPase).[13]Identification and characterization of a novel 9.2-kDa membrane sector-associated protein of vacuolar proton-ATPase from chromaffin granules. V-ATPase is a multisubunit complex consisting of a H^+- translocating V_o

domain and an ATP-hydrolyzing V_1 domain.[14] V-ATPases are expressed in virtually all cell types and mainly found in the membrane of intracellular compartments, such as signaling endosomes, lysosomes, and the Golgi apparatus.[15] By acidifying the intracellular compartments, they play an important role in the induction of intracellular signaling cascades, receptor-mediated endocytosis, and protein degradation. Intriguingly, global genetic ablation of most, if not all, V-ATPase subunits in mice or zebrafish are embryonically lethal.[16] This indicates a close functional relationship of the (P)RR with V-ATPase. Indeed, inhibiting the (P)RR or blocking V-ATPase using bafilomycin both abolished Wnt-mediated activation of β-catenin.[17] Moreover, deletion of the (P)RR in cardiomyocytes and podocytes resulted in decreased protein abundance of several V-ATPase subunits and a disturbed lysosomal pH, suggesting that the (P)RR is required to maintain V-ATPase integrity. Additionally, our group has previously shown that inhibiting the (P)RR abolishes arginine vasopressin-stimulated V-ATPase activity but not basal V-ATPase in collecting duct cells.[18] These studies thus highlighted that the (P)RR has (pro)renin-independent functions.

In the approach to unravel (pro)renin-independent function(s) of the (P)RR, our group discovered that the (P)RR controls the protein abundance of low-density lipoprotein receptor (LDLR) and sortilin-1 (SORT1), the two key regulators for LDL metabolism, highlighting its potential role in LDL metabolism.[19,20] Thus, in **Chapter 2**, we studied the consequence of inhibiting the hepatic (P)RR on lipid metabolism in vivo. As expected, hepatic (P)RR inhibition indeed raised plasma LDL levels in normal diet (ND) fed C57BL/6J mice, as a consequence of reduced hepatic LDLR and SORT1 abundance. Unexpectedly, we found that hepatic (P)RR deficiency also prevented diet-induced obesity and non-alcoholic fatty liver disease. Using a state-of-the-art comparative proteomics approach, we found that acetyl-CoA carboxylase (ACC) and pyruvate dehydrogenase (PDH) abundance were reduced in (P)RR-inhibited livers. PDH converts pyruvate to acetyl-CoA to flux the carbon sources into complete oxidation in tricarboxylic acid cycle or biosynthetic pathways, such as fatty acid (FA) and cholesterol synthesis. ACC plays a crucial role in regulating FA biosynthesis and oxidation.[21] Genetic ablation of ACC led to reduced lipid synthesis and increased fatty acid oxidation, resulting in a similar phenotype as hepatic (P)RR inhibited mice. Using both human hepatic cells and mouse primary hepatocytes, we confirmed that inhibiting the (P)RR reduced cellular acetyl-CoA levels and promotes FA oxidation. Our study thus revealed a previous unrecognized role of the (P)RR in regulating lipid metabolism.

Angiotensinogen siRNA as a novel blood pressure-lowering tool (Chapter 3)

Increased RAS activity is a major contributor for elevated blood pressure (BP), hence RAS blockers have been widely used in treating hypertension and associated diseases. However, conventional RAS blockers, including angiotensin-converting enzyme inhibitors (ACEi), angiotensin (Ang) II receptor blockers (ARBs), and direct renin inhibitors (DRi), all lead to increased plasma renin levels and may complicate the treatment as such a rise in renin may restore Ang II to pretreatment levels. Moreover, poor adherence with the regular RAS blockers presents another challenge in optimally controlling BP. Since the effector of the RAS derives from angiotensinogen (AGT) originating from the liver, inhibiting hepatic AGT may provide a more effective way in controlling RAS activity. In **Chapter 3**, we thus explored the effects of siRNA targeting AGT in spontaneously hypertensive rats. We found that a single injection of N-acetylgalactosamine (GalNAc)-siRNAs at a dose of 10 mg/kg body weight effectively reduced BP to a similar extent as captopril (ACEi) and valsartan (ARBs) for at least 4 weeks. Although inhibiting hepatic AGT also increased active plasma renin concentrations due to the negative feedback loop, it did not cause the rise in plasma Ang I levels as captopril and valsartan did. However, silencing hepatic AGT did not reduce plasma Ang II levels. This is likely a result of residual AGT presence and the presence of Ang I. However, when combined with valsartan, AGT siRNA treatment greatly reduced plasma Ang I and Ang II levels, paralleled by a further reduction in BP. Thus, our study highlights AGT inhibition alone or in combination with valsartan as an effective mean to control BP.

Megalin and (pro)renin uptake (Chapters 4-6)

Remarkably, although plasma prorenin levels are ≈10-fold higher than those of renin, only renin can be detected in the urine. Furthermore, even when plasma prorenin levels are elevated ≈200-fold, as seen in the Cyp1a1-Ren2 transgenic rats, urinary prorenin is still undetectable. The small differences in their molecular weight are unlikely to result in large discrepancies in glomerular filtration of prorenin and renin,[22] and thus cannot explain why prorenin is undetectable in urine. Interestingly, in patients with Dent's disease or Lowe syndrome, urinary renin and prorenin levels are markedly increased. These patients carry genetic mutations in OCRL1 or CLC-5, resulting in megalin dysfunction. In line with this, genetic ablation or pharmacological inhibition of megalin increases renin levels in urine.[23] These observations thus points towards megalin as an endocytic receptor for (pro)renin **(Chapter 4&5)**. In Chapter 6, we set out to compare megalin-mediated renin and prorenin uptake in BN16 cells which highly express megalin, to study (pro)renin binding and uptake. We found that BN16 cells actively accumulate both renin and prorenin, the latter with much greater efficiency. Blocking the mannose-6-phosphate receptor, a known clearance receptor

for (pro)renin, did not affect this uptake, while knocking down megalin did. These data confirm that megalin is a novel endocytotic receptor for (pro)renin, and given the much greater efficiency of prorenin uptake, they also explain why prorenin is normally lacking in urine.

RAS in preeclampsia (Chapter 7)

As a consequence of drastic increased plasma AGT levels and a modest increase in plasma renin levels, plasma RAS activity is increased during pregnancy, to ensure adequate blood supply for the growing fetus. However, in preeclampsia, a disorder characterized by hypertension and proteinuria after 20 weeks of gestation in women, the rise in circulating AGT and renin are suppressed, which may contribute to the onset of the disease. However, considering the local production of the RAS components in the placenta, it is still possible that placental RAS activity is upregulated in preeclampsia. In **Chapter 7**, we set out to explore if the placental expression of RAS components and their release are altered in early onset preeclampsia. Major RAS components, including renin, ACE, ACE2, AT1R, and AT2R were expressed in the placenta, and their expression levels were comparable in healthy and preeclamptic placentas. Placental (pro)renin levels were also comparable between healthy and preeclamptic pregnancies, in line with unaltered placental renin expression in this condition. Although AGT mRNA levels were at or below detection limit, AGT protein could be detected in healthy placental tissue, implying that placental AGT is taken up from blood. In agreement with this observation, placental AGT levels were markedly reduced in preeclamptic placentas. Moreover, using the placental perfusion technique, we observed that placental AGT release decreased over time, suggestive for washout of blood-derived AGT. In contrast, placental (pro)renin release remained stable over a 3-hour perfusion period, and amounted to quantities that were >5-fold higher than the levels measured in tissue, indicating ongoing synthesis. The majority of this was prorenin. In conclusion, our data suggest that placental RAS activity depends on maternal AGT taken up from blood. They do not support elevated placental RAS activity in preeclampsia.

References

1. Danser AH, Derkx FH, Schalekamp MA, Hense HW, Riegger GA, Schunkert H. Determinants of interindividual variation of renin and prorenin concentrations: Evidence for a sexual dimorphism of (pro) renin levels in humans. J Hypertens. 1998;16:853-862
2. Luetscher JA, Kraemer FB, Wilson DM, Schwartz HC, Bryer-Ash M. Increased plasma inactive renin in diabetes mellitus. A marker of microvascular complications. N Engl J Med. 1985;312:1412-1417
3. Krop M, Danser AH. Circulating versus tissue renin-angiotensin system: On the origin of (pro)renin. Curr Hypertens Rep. 2008;10:112-118
4. van Kats JP, Schalekamp MA, Verdouw PD, Duncker DJ, Danser AH. Intrarenal angiotensin ii: Intersti-

tial and cellular levels and site of production. Kidney Int. 2001;60:2311-2317
5. Campbell DJ, Duncan AM, Kladis A. Angiotensin-converting enzyme inhibition modifies angiotensin but not kinin peptide levels in human atrial tissue. Hypertension. 1999;34:171-175
6. Lu X, Danser AH, Meima ME. Hrp and prorenin: Focus on the (pro)renin receptor and vacuolar h+-atpase. Front Biosci (Schol Ed). 2011;3:1205-1215
7. Achard V, Boullu-Ciocca S, Desbriere R, Nguyen G, Grino M. Renin receptor expression in human adipose tissue. Am J Physiol Regul Integr Comp Physiol. 2007;292:R274-282
8. Sakoda M, Ichihara A, Kaneshiro Y, Takemitsu T, Nakazato Y, Nabi AH, Nakagawa T, Suzuki F, Inagami T, Itoh H. (pro)renin receptor-mediated activation of mitogen-activated protein kinases in human vascular smooth muscle cells. Hypertens Res. 2007;30:1139-1146
9. Batenburg WW, Danser AH. (pro)renin and its receptors: Pathophysiological implications. Clin Sci (Lond). 2012;123:121-133
10. Inoue H, Noumi T, Nagata M, Murakami H, Kanazawa H. Targeted disruption of the gene encoding the proteolipid subunit of mouse vacuolar h(+)-atpase leads to early embryonic lethality. Biochim Biophys Acta. 1999;1413:130-138
11. Kinouchi K, Ichihara A, Sano M, Sun-Wada GH, Wada Y, Kurauchi-Mito A, Bokuda K, Narita T, Oshima Y, Sakoda M, Tamai Y, Sato H, Fukuda K, Itoh H. The (pro)renin receptor/atp6ap2 is essential for vacuolar h+-atpase assembly in murine cardiomyocytes. Circ Res. 2010;107:30-34
12. Riediger F, Quack I, Qadri F, Hartleben B, Park JK, Potthoff SA, Sohn D, Sihn G, Rousselle A, Fokuhl V, Maschke U, Purfurst B, Schneider W, Rump LC, Luft FC, Dechend R, Bader M, Huber TB, Nguyen G, Muller DN. Prorenin receptor is essential for podocyte autophagy and survival. J Am Soc Nephrol. 2011;22:2193-2202
13. Ludwig J, Kerscher S, Brandt U, Pfeiffer K, Getlawi F, Apps DK, Schagger H. Identification and characterization of a novel 9.2-kda membrane sector-associated protein of vacuolar proton-atpase from chromaffin granules. J Biol Chem. 1998;273:10939-10947
14. Wagner CA, Finberg KE, Breton S, Marshansky V, Brown D, Geibel JP. Renal vacuolar h+-atpase. Physiol Rev. 2004;84:1263-1314
15. Nishi T, Forgac M. The vacuolar (h+)-atpases--nature's most versatile proton pumps. Nat Rev Mol Cell Biol. 2002;3:94-103
16. EauClaire SF, Cui S, Ma L, Matous J, Marlow FL, Gupta T, Burgess HA, Abrams EW, Kapp LD, Granato M, Mullins MC, Matthews RP. Mutations in vacuolar h+ -atpase subunits lead to biliary developmental defects in zebrafish. Dev Biol. 2012;365:434-444
17. Cruciat CM, Ohkawara B, Acebron SP, Karaulanov E, Reinhard C, Ingelfinger D, Boutros M, Niehrs C. Requirement of prorenin receptor and vacuolar h+-atpase-mediated acidification for wnt signaling. Science. 2010;327:459-463
18. Lu X, Garrelds IM, Wagner CA, Danser AH, Meima ME. (pro)renin receptor is required for prorenin-dependent and -independent regulation of vacuolar h(+)-atpase activity in mdck.C11 collecting duct cells. Am J Physiol Renal Physiol. 2013;305:F417-425
19. Ren L, Sun Y, Lu H, Ye D, Han L, Wang N, Daugherty A, Li F, Wang M, Su F, Tao W, Sun J, Zelcer N, Mullick AE, Danser AHJ, Jiang Y, He Y, Ruan X, Lu X. (pro)renin receptor inhibition reprograms hepatic lipid metabolism and protects mice from diet-induced obesity and hepatosteatosis. Circ Res. 2018;122:730-741
20. Kjolby M, Andersen OM, Breiderhoff T, Fjorback AW, Pedersen KM, Madsen P, Jansen P, Heeren J, Willnow TE, Nykjaer A. Sort1, encoded by the cardiovascular risk locus 1p13.3, is a regulator of hepatic lipoprotein export. Cell Metab. 2010;12:213-223
21. Herrero L, Rubi B, Sebastian D, Serra D, Asins G, Maechler P, Prentki M, Hegardt FG. Alteration of the malonyl-coa/carnitine palmitoyltransferase i interaction in the beta-cell impairs glucose-induced insulin secretion. Diabetes. 2005;54:462-471
22. Roksnoer LC, Heijnen BF, Nakano D, Peti-Peterdi J, Walsh SB, Garrelds IM, van Gool JM, Zietse R, Struijker-Boudier HA, Hoorn EJ, Danser AH. On the origin of urinary renin: A translational approach. Hypertension. 2016;67:927-933
23. Ye F, Wang Y, Wu C, Howatt DA, Wu CH, Balakrishnan A, Mullick AE, Graham MJ, Danser AHJ, Wang J, Daugherty A, Lu HS. Angiotensinogen and megalin interactions contribute to atherosclerosis-brief report. Arterioscler Thromb Vasc Biol. 2019;39:150-155
24. Binger KJ, Neukam M, Tattikota SG, Qadri F, Puchkov D, Willmes DM, Wurmsee S, Geisberger S,

Dechend R, Raile K, Kurth T, Nguyen G, Poy MN, Solimena M, Muller DN, Birkenfeld AL. Atp6ap2 deletion causes extensive vacuolation that consumes the insulin content of pancreatic beta cells. Proc Natl Acad Sci U S A. 2019;116:19983-19988
25. Koizumi M, Ueda K, Niimura F, Nishiyama A, Yanagita M, Saito A, Pastan I, Fujita T, Fukagawa M, Matsusaka T. Podocyte injury augments intrarenal angiotensin ii generation and sodium retention in a megalin-dependent manner. Hypertension. 2019;74:509-517
26. Lu H, Wu C, Howatt DA, Balakrishnan A, Moorleghen JJ, Chen X, Zhao M, Graham MJ, Mullick AE, Crooke RM, Feldman DL, Cassis LA, Vander Kooi CW, Daugherty A. Angiotensinogen exerts effects independent of angiotensin ii. Arterioscler Thromb Vasc Biol. 2016;36:256-265
27. Corvol P, Lamande N, Cruz A, Celerier J, Gasc JM. Inhibition of angiogenesis: A new function for angiotensinogen and des(angiotensin i)angiotensinogen. Curr Hypertens Rep. 2003;5:149-154

Perspectives

Whether the (P)RR plays a direct role in local RAS activation has been a subject of debate over the past decade. A number of studies have revealed that the (P)RR plays important roles in regulating Wnt signaling, autophagy, lipid metabolism, and glucose metabolism, independent of the RAS. These findings extended our understanding on the functions of the (P)RR, and also questions whether the (P)RR is a true member of the RAS. Yet, inhibiting the (P)RR in BN16 cells did reduce prorenin uptake to a similar extent as achieved by megalin inhibition. However, dual inhibition of the (P)RR and megalin did not further decrease prorenin uptake in BN16, thus suggesting that the (P)RR and megalin lie in the same pathway in regulating cellular prorenin uptake. One plausible explanation is that (P)RR inhibition impairs megalin endocytosis, and the other possibility is that inhibiting the (P)RR reduces prorenin binding. The later seems unlikely since the cellular binding of prorenin was unaltered by (P)RR inhibition in BN16 cells. Therefore, these data further argue that the (P)RR is not a major receptor for prorenin, at least not in BN16 cells. However, how (P)RR deficiency leads to impaired megalin-mediated prorenin endocytosis is still unknown.

In general, ligand endocytosis rate is determined by receptor density at the plasma membrane and receptor recycling rate. For a receptor to recycle back to plasma membrane after delivery of the bound ligand into cells, it is critical to dissociate from its ligand. This requires an acidic pH. If ligand dissociation does not occur, the receptor will be targeted to lysosomes for degradation, thereby eventually reducing receptor-mediated ligand endocytosis. Acidification of the endosomes is achieved by vacuolar H^+-ATPase (V-ATPase). Intriguingly, the (P)RR is an accessory protein of V-ATPase. Hence, it is convenient to hypothesize that inhibiting the (P)RR impairs V-ATPase function and endosomal pH, leading to reduced prorenin endocytosis in BN16 cells. Indeed, we found that inhibiting the V-ATPase using bafilomycin A1 almost completely abolished renin uptake in BN16 cells without affecting

its binding, highlighting that megalin-mediated (pro)renin uptake requires V-ATPase activity.

However, the notion that (P)RR deficiency impairs V-ATPase integrity and activity is challenged by recent findings. The first evidence comes from a study by our group that (P)RR inhibition reduces LDLR endocytosis by accelerating its lysosomal degradation. Since lysosomal protein degradation depends on proteases whose acivities requires acidic pH, one would expect to see reduced lysosomal protein degradation if (P)RR deficiency abolishes V-ATPase activity and lysosomal pH. However, the opposite was observed in case of the LDLR. Moreover, the degradation rate of membrane LDLR (receptor recycling rate) is not affected by (P)RR deficiency, ruling out a defective endosomal pH as the cause for reduced endocytosis. Inhibiting the (P)RR in hepatocytes in vivo reduced the protein abundance of acetyl-CoA carboxylase and pyruvate dehydrogenase without affecting their transcript levels. Additionally, our group recently found that leupeptin, a lysosomal protease inhibitor, could block (P)RR deficiency-induced reduction in protein abundance of lysosomal-associated protein 1 (LAMP1) and LAMP2 (unpublished data). Furthermore, we found that deleting the (P)RR increased, rather than decreased, the protein abundance of most V-ATPase subunits. Taken together, these data support normal or even increased lysosomal activity in the absence of the (P)RR, arguing that V-ATPase activity can stay intact without the (P)RR. Indeed, a recent study by Kissing et al. also concluded that (P)RR deficiency did not affect V-ATPase activity and lysosomal pH, at least in pancreatic b-cells.[24] Hence, the (P)RR may regulate megalin function by controlling its lysosomal degradation rather than its recycling.

It is worthy to notice that megalin is also expressed in syncytiotrophoblasts and cytotrophoblasts in the placenta. Whether it is playing a role in preeclampsia is not yet clear. Megalin recently has been suggested contribute to renal angitotensin II generation.[25] Intriguingly, we and others have recently reported that proton pump inhibitors (PPIs) lower the placental release of soluble Fms-like tyrosine kinase-1 (sFlt-1), a well-known biomarker for the prediction of preeclampsia or adverse pregnancy outcomes. Ang II is known to stimulate sFlt-1 production, and thus we wondered if PPIs could reduce sFlt-1 levels in preeclampsia by inhibiting placental RAS activation. We found that esomeprazole, a type of PPI, dose-dependently reduced renin uptake in BN16 cells, suggesting that PPIs may inhibit cellular RAS activation. However, further studies are required to explore if suppression of megalin-dependent (pro)renin uptake is the underlying cause for reduced sFlt-1 production. Unexpectedly, we found that esomeprazole also increased renin binding in BN16 cells. The exact cause for increased renin binding is not yet clear. Considering the short incubation time of esomeprazole (2h), it is unlikely that it increases renin binding by upregulating

megalin. One possibility is that this PPI may increase plasma membrane density of megalin via an as yet unknown mechanism. However, placental megalin expression did not seem to be altered in preeclamptic pregnancies and its protein abundance only tended to be increased in preeclampsia. Therefore, more studies are needed to clarify the role of placental megalin and its connection with RAS in the onset of preeclampsia.

Blocking RAS activity remains a major therapeutic mean to treat hypertension and its associated diseases. A problem with currently available RAS blockers is that they often raise plasma Ang II levels to their pretreatment stage, thereby overcoming RAS blockade. Since all angiotensin is derived from angiotensinogen (AGT), which is primarily synthesized in the liver, hepatic AGT represents an attractive therapeutic target for blocking RAS activity. We found that inhibiting hepatic AGT indeed effectively reduced BP to a similar extent as ACEi and ARBs. However, hepatic AGT inhibition alone did not reduce plasma Ang II levels. Since AGT siRNA nearly completely abolished hepatic AGT expression and reduced plasma AGT levels by more than 95%, while increasing plasma renin levels, the most likely explanation of this finding is that trace amounts of AGT combined with elevated renin levels are still sufficient to maintain normal plasma Ang II generation. Yet, renal Ang I levels and to a lesser degree renal Ang II levels did decrease during hepatic AGT suppression, implying that this approach particularly affects tissue angiotensin generation. In agreement with this observation, renal NCC and NHE3 activities were lowered by hepatic AGT inhibition. Since NCC and NHE3 are the main regulators of sodium balance, which affects BP, it is likely that the BP lowering effect of hepatic AGT inhibition, at least in part, relies on regulation of sodium balance. Importantly, blocking the AT1R with valsartan on top of AGT inhibition virtually annihilated plasma and renal Ang II levels, due to a further rise in renin, which rapidly metabolized any remaining AGT. As a consequence BP fell synergistically, to a much greater degree than the sum of the effects of valsartan and siRNA alone. Future studies should now evaluate the tissue-protective effects of AGT siRNA, e.g., in the diabetic kidney or the hypertrophied heart in hypertension models, focusing on the possibility that these effects occur in a BP-independent manner. Finally, several studies have reported that AGT and/or des(AngI)AGT (i.e., the product remaining after Ang I has been cleaved off) are biologically active by themselves, regulating body weight gain and liver steatosis independent of Ang II,[26] and inhibiting angiogenesis.[27] The AGT siRNA approach allows further investigation of this possibility, evaluating simultaneously whether such effects contribute to BP lowering and/or organ protection.

In summary, in this thesis, we have clarified the role of the (P)RR in regulating lipid metabolism in vivo, expanding our understanding of the (pro)renin-independent role of the (P)

RR. Moreover, we have identified megalin as a novel endocytic receptor for (pro)renin, and that the (P)RR determines its activity. This discovery allows a unifying concept, i.e., that the (P)RR is not a direct receptor for (pro)renin, but that interference with the (P)RR could indirectly exert effects that normally depend on (pro)renin and megalin. One of these effects might be megalin-mediated transcellular transport of (pro)renin and angiotensinogen into the renal interstitium, thereby allowing local angiotensin generation in this compartment. Future studies should investigate this possibiliy. Finally, hepatic AGT suppression is a new tool to lower BP, displaying effects that are minimally identical to those of classical RAS blockers, but require at most a few injections per year, as opposed to daily intake of tablets. This might annihilate non-adherence.

Nederlandse Samenvatting

De (pro)renine receptor in relatie tot lipidenmetabolisme (Hoofdstukken 1-2)

De plasma concentraties van prorenine, de voorloper van renine, zijn normaliter 10 maal zo hoog als die van renine, hetgeen kan oplopen tot ≈100-maal onder pathofysiologische omstandigheden. Behalve het feit dat het de inactieve voorloper van renine is, is de functie van prorenine nog steeds onbekend. Eerdere studies hebben aangetoond dat verhoogde prorenine concentraties in plasma in verband staan met het optreden van macro- en micro-vasculaire complicaties zoals nefropathie en retinopathie bij patiënten met diabetes mellitus, terwijl de renine concentraties bij deze patiënten juist normaal of zelfs verlaagd zijn.[1-3] Bovendien zijn er aanwijzingen voor een lokaal renine-angiotensine systeem (RAS) in meerdere organen, hetgeen mogelijk zorgt voor verhoogde of verlaagde activiteit bij de afwezigheid van veranderingen in het circulerende RAS. Voorbeelden hiervan zijn de nieren bij diabetes en de placenta bij pre-eclampsie.[4, 5] Aangezien renine synthese zich beperkt tot de juxtaglomerulaire cellen in de nieren, moet dit lokale RAS afhankelijk zijn van een mechanisme dat de opname van renine en/of prorenine activatie toestaat. De ontdekking van de (pro)renine receptor [(P)RR], ongeveer twintig jaar geleden, leek de oplossing voor dit probleem te zijn, zoals besproken wordt in **Hoofdstuk 1**. De (P)RR bindt zich aan zowel renine als prorenine, en vertoont een hogere affiniteit voor prorenine.[6] Bij het binden wordt prorenine op een niet-proteolytische wijze geactiveerd, hetgeen de vorming van angiotensines mogelijk maakt. Daarnaast zorgt (P)RR binding van renine en prorenine, hierna aangeduid als (pro)renine, voor angiotensine-onafhankelijke intracellulaire signaalcascades, wat resulteert in de activatie van p38 mitogeen-geactiveerd proteïne kinase (MAPK) en extracellulair signaal-gereguleerd kinase 1/2 (Erk1/2), bijvoorbeeld in vasculaire gladde spiercellen (VSMCs), verzamelbuiscellen, en vetcellen.[7, 8] Activatie van p38 MAPK and Erk1/2 heeft verhoging van profibrotische en proliferatieve genexpresssie tot gevolg, wat resulteert in versnelde celproliferatie en orgaanschade. Om de angiotensine-afhankelijke en -onafhankelijke effecten te kunnen detecteren, moet (pro)renine wel worden toegediend in concentraties die vele malen hoger zijn dan het reguliere plasma-niveau en die zelfs boven de ultrahoge spiegels in transgene knaagdiermodellen liggen.[9] Bovendien is, in tegenstelling tot andere RAS componenten, volledige afwezigheid van de (P)RR dodelijk, zelfs wanneer dit beperkt wordt tot bepaalde celtypen zoals cardiomyocyten en podocyten.[10-12] Dit gegeven roept de vraag op of de interactie tussen (pro)renine en de (P)RR in vivo werkelijk relevant is.

Interessant is dat het cytosolische domein van de (P)RR reeds eerder is geïdentificeerd als een eiwit behorend bij vacuolair H^+-ATPase (V-ATPase).[13] V-ATPase is een multisubunit complex dat bestaat uit een H^+- translocerend V_o domein en een ATP-hydrolyserend V_1 domein.[14] V-ATPases worden in vrijwel alle celtypen tot expressie gebracht en worden voornamelijk gevonden in de membraan van intracellulaire compartimenten zoals signaalendosomen, lysosomen en het Golgi-apparaat.[15] Door verzuring van de intracellulaire compartementen, spelen deze een belangrijke rol in de inductie van intracellulaire signaalcascades, receptor-gemedieerde endocytose en de afbraak van eiwitten. Genetische ablatie van de meeste, zo niet alle, V-ATPase subeenheden in muizen of zebravissen is embryonaal dodelijk.[16] Dit wijst op een nauw functioneel verband tussen de (P)RR en V-ATPase. Inderdaad leidde remming van de (P)RR of V-ATPase (met bafilomycine) tot verminderde Wnt-gemedieerde activatie van b-catenine.[17] Daarnaast resulteerde (P)RR deletie in cardiomyocyten en podocyten tot afgenomen expressie van diverse V-ATPase subeenheden en een verstoorde lysosomale pH, wat de suggestie wekt dat de (P)RR noodzakelijk is om de V-ATPase-integriteit te bewaren. Bovendien heeft onze groep eerder al aangetoond dat remming van de (P)RR wel de arginine vasopressine-gestimuleerde V-ATPase activiteit onderdrukt, maar niet de basale V-ATPase in verzamelbuiscellen beinvloedt.[18] Deze studies onderstrepen dat de (P)RR inderdaad (pro)renine-onafhankelijke effecten bewerkstelligt.

Tijdens het bestuderen van (pro)renine-onafhankelijk functie(s) van de (P)RR, heeft onze groep ontdekt dat de (P)RR de dichtheid van de low-density lipoproteïn receptor (LDLR) en sortiline-1 (SORT1) reguleert, i.e., de twee belangrijkste regulatoren van het LDL metabolisme, daarmee een potentiële rol van de (P)RR in LDL metabolisme implicerend.[19,20] Daarom bestudeerden we in **Hoofdstuk 2** de consequentie van remming van de hepatische (P)RR op het lipidenmetabolisme in vivo. Zoals verwacht, verhoogde hepatische (P)RR remming inderdaad de plasma LDL concentratie bij een normaal dieet in C57BL/6J muizen, als gevolg van verminderde hepatische LDLR en SORT1 dichtheid. Een onverwachte vondst was dat hepatische (P)RR deficiëntie ook de door een hoog vetdieet veroorzaakte obesitas en non-alcoholic fatty liver disease voorkwam. Dankzij de toepassing van proteomics werd duidelijk dat de concentraties van acetyl-CoA carboxylase (ACC) en pyruvaat dehydrogenase (PDH) verminderd waren in de levers met volledige (P) RR remming. PDH zet pyruvaat om in acetyl-CoA, terwijl ACC een cruciale rol speelt bij de regulatie van vetzuur biosynthese en oxidatie.[21] Genetische ablatie van ACC resulteerde in een afname van synthese van de lipiden en een toename in vetzuur oxidatie, wat leidde tot eenzelfde fenotype als muizen met (P)RR-remming in de lever. Gebruik makend van zowel humane levercellen als primaire hepatocyten van muizen, konden we bevestigen

dat remming van de (P)RR de cellulaire acetyl-CoA spiegels afremt en vetzuur oxidatie bevordert. Onze studie heeft hiermee een niet eerder beschreven rol van de (P)RR in de regulatie van het lipidenmetabolisme aangetoond.

Angiotensinogeen siRNA als nieuw bloeddrukverlagend middel (Hoofdstuk 3)

Verhoogde RAS activiteit is een belangrijke factor bij verhoogde bloeddruk (BD), zodat RAS blokkers veel gebruikt worden voor de behandeling van hypertensie en gerelateerde ziekten. Conventionele RAS blokkers, zoals angiotensine-converterend enzym inhibitoren (ACEi), angiotensine (Ang) II receptor blokkers (ARBs), en directe renine inhibitoren (DRi), kunnen echter allemaal tot een verhoogde renine spiegel in plasma leiden en mogelijk de behandeling bemoeilijken, bijvoorbeeld omdat de toename in renine de Ang II spiegel terugbrengt naar hetzelfde niveau als voor de behandeling. Bovendien vormt slechte therapietrouw van de reguliere RAS blokkers een andere uitdaging voor de optimale controle van de BD. Aangezien al het Ang II voortkomt uit angiotensinogeen (AGT) uit de lever, kan remming van hepatisch AGT mogelijk leiden tot een effectievere RAS onderdrukking. In **Hoofdstuk 3** hebben we daarom de effecten onderzocht van siRNA gericht op AGT in spontaan hypertensieve ratten. We vonden dat een enkele injectie van N-acetylgalactosamine (GalNAc)-siRNA met een dosering van 10 mg/kg lichaamsgewicht effectief de BD verlaagde, in dezelfde mate als captopril (ACEi) en valsartan (ARB) gedurende minimaal 4 weken. Hoewel remming van hepatisch AGT ook de renine concentraties verhoogde als gevolg van het wegvallen van de negatieve feedback loop, veroorzaakte het geen verhoogde Ang I spiegel in het plasma zoals captopril en valsartan. Dat hepatische AGT onderdrukking de Ang II spiegels in plasma niet verlaagde, is waarschijnlijk het gevolg van het nog aanwezig zijn van restanten AGT en Ang I. Behandeling met AGT siRNA in combinatie met valsartan zorgde echter wel voor een sterke afname van Ang I en Ang II in plasma, alsmede een verdere verlaging van de BD. Onze studie onderstreept derhalve dat AGT remming alleen of in combination met valsartan een effectieve methode is om de BD onder controle te krijgen.

Megaline en (pro)renine opname (Hoofdstukken 4-6)

Hoewel de proreninespiegels in plasma ≈10-maal zo hoog zijn als die van renine, kan opmerkelijk genoeg alleen renine gedetecteerd worden in urine. Zelfs wanneer de prorenine spiegels in plasma ≈200-maal verhoogd zijn, zoals het geval is in Cyp1a1-Ren2 transgene ratten, is prorenine in de urine nog steeds niet detecteerbaar. Door de kleine verschillen in hun moleculaire gewicht is het onwaarschijnlijk dat er grote discrepancies ontstaan in

de glomerulaire filtratie van prorenine en renine,[22] en dit kan dus niet de verklaring zijn voor het feit dat prorenine niet detecteerbaar is in urine en renine wel. Opmerkelijk is dat de renine- en proreninespiegels in urine van patiënten met de ziekte van Dent of het Lowe syndroom sterk verhoogd zijn. Deze patiënten zijn drager van genetische mutaties in het OCRL1 of CLC-5 gen, hetgeen tot megalinedisfunctie leidt. In het verlengde hiervan verhoogt genetische ablatie of farmacologische remming van megaline de reninespiegels in urine.[23] Deze observaties wijzen dus op de mogelijke functie van megaline als een endocytische receptor voor (pro)renine (**Hoofdstukken 4&5**). In **Hoofdstuk 6** hebben we de megaline-gemedieerde renine en prorenine binding en opname in BN16 cellen (i.e.., cellen met hoge megaline-expressie) bestudeerd. We vonden dat BN16 cellen zowel renine als prorenine opnemen, waarbij prorenine met grotere efficiëntie werd gebonden. Remming van de mannose-6-fosfaat receptor, een bekende klaringsreceptor voor (pro)renine, had geen effect op deze opname, terwijl blokkade van megaline wel effect had. Deze bevindingen bevestigen dat megaline een nieuwe receptor voor (pro)renine is, en gezien de veel grotere efficiëntie van de opname van prorenine, verklaart dit ook waarom prorenine normaal gesproken niet in urine te vinden is.

Het RAS bij pre-eclampsie (Hoofdstuk 7)

Als gevolg van drastisch verhoogde AGT spiegels in plasma en een bescheiden verhoging van de renine spiegels in plasma, is de activiteit van het RAS in plasma verhoogd tijdens zwangerschap. Dit is o.a. nodig om voldoende toevoer van bloed naar de de groeiende foetus te verzekeren. Bij pre-eclampsie, een aandoening die gekenmerkt wordt door hypertensie en proteïnurie bij vrouwen na 20 weken zwangerschap, wordt de verhoging van circulerend AGT en renine echter onderdrukt, hetgeen mogelijk bijdraagt aan het ontstaan van de ziekte. Gezien de lokale productie van RAS componenten in de placenta is het nog steeds mogelijk dat de RAS activiteit in de placenta juist verhoogd is bij pre-eclampse. In **Hoofdstuk 7** hebben we onderzocht of de expressie van RAS componenten in de placenta en hun afgite veranderen bij pre-eclampsie in een vroeg stadium. Belangrijke RAS componenten, waaronder renine, ACE, ACE2, AT1R, en AT2R, kwamen tot expressie in de placenta, en hun expressie niveaus waren vergelijkbaar in gezonde en pre-eclamptische placentas. De (pro)renine-spiegels in de placenta waren ook hetzelfde bij gezonde en pre-eclamptische zwangerschappen, hetgeen in lijn is met ongewijzigde renine-expressie in de placenta bij deze aandoening. Alhoewel de AGT mRNA spiegels net op of onder de detectiegrens lagen, kon het AGT eiwit wel gemeten worden in gezond placentaweefsel, wat erop wijst dat AGT in de placenta opgenomen wordt vanuit het bloed. In overeenstemming met deze observatie, waren de AGT spiegels in de placenta aanzienlijk verlaagd in de pre-

eclamptische placentas. Placenta perfusie bevestigde dat de afgifte van AGT in de placenta in de tijd afneemt, hetgeen wijst op een 'washout' van uit het bloed opgenomen AGT. In tegenstelling hiermee, bleef de afgifte van (pro)renine uit de placenta juist stabiel tijdens een 3 uur durende perfusie, en steeg tot hoeveelheden die >5-maal hoger lagen dan de spiegels die in placentaweefsel gemeten worden, wat op voortdurende synthese wijst. Dit was overwegend prorenine. Concluderend suggereren onze bevindingen dat de RAS activiteit in de placenta afhankelijk is van maternaal AGT dat opgenomen wordt vanuit het bloed. Er is geen bewijs voor verhoogde RAS-activiteit in de placenta bij pre-eclampsie.

Referenties

1. Danser AH, Derkx FH, Schalekamp MA, Hense HW, Riegger GA, Schunkert H. Determinants of interindividual variation of renin and prorenin concentrations: Evidence for a sexual dimorphism of (pro) renin levels in humans. *J Hypertens*. 1998;16:853-862
2. Luetscher JA, Kraemer FB, Wilson DM, Schwartz HC, Bryer-Ash M. Increased plasma inactive renin in diabetes mellitus. A marker of microvascular complications. *N Engl J Med*. 1985;312:1412-1417
3. Krop M, Danser AH. Circulating versus tissue renin-angiotensin system: On the origin of (pro)renin. *Curr Hypertens Rep*. 2008;10:112-118
4. van Kats JP, Schalekamp MA, Verdouw PD, Duncker DJ, Danser AH. Intrarenal angiotensin ii: Interstitial and cellular levels and site of production. *Kidney Int*. 2001;60:2311-2317
5. Campbell DJ, Duncan AM, Kladis A. Angiotensin-converting enzyme inhibition modifies angiotensin but not kinin peptide levels in human atrial tissue. *Hypertension*. 1999;34:171-175
6. Lu X, Danser AH, Meima ME. Hrp and prorenin: Focus on the (pro)renin receptor and vacuolar h+-atpase. *Front Biosci (Schol Ed)*. 2011;3:1205-1215
7. Achard V, Boullu-Ciocca S, Desbriere R, Nguyen G, Grino M. Renin receptor expression in human adipose tissue. *Am J Physiol Regul Integr Comp Physiol*. 2007;292:R274-282
8. Sakoda M, Ichihara A, Kaneshiro Y, Takemitsu T, Nakazato Y, Nabi AH, Nakagawa T, Suzuki F, Inagami T, Itoh H. (pro)renin receptor-mediated activation of mitogen-activated protein kinases in human vascular smooth muscle cells. *Hypertens Res*. 2007;30:1139-1146
9. Batenburg WW, Danser AH. (pro)renin and its receptors: Pathophysiological implications. *Clin Sci (Lond)*. 2012;123:121-133
10. Inoue H, Noumi T, Nagata M, Murakami H, Kanazawa H. Targeted disruption of the gene encoding the proteolipid subunit of mouse vacuolar h(+)-atpase leads to early embryonic lethality. *Biochim Biophys Acta*. 1999;1413:130-138
11. Kinouchi K, Ichihara A, Sano M, Sun-Wada GH, Wada Y, Kurauchi-Mito A, Bokuda K, Narita T, Oshima Y, Sakoda M, Tamai Y, Sato H, Fukuda K, Itoh H. The (pro)renin receptor/atp6ap2 is essential for vacuolar h+-atpase assembly in murine cardiomyocytes. *Circ Res*. 2010;107:30-34
12. Riediger F, Quack I, Qadri F, Hartleben B, Park JK, Potthoff SA, Sohn D, Sihn G, Rousselle A, Fokuhl V, Maschke U, Purfurst B, Schneider W, Rump LC, Luft FC, Dechend R, Bader M, Huber TB, Nguyen G, Muller DN. Prorenin receptor is essential for podocyte autophagy and survival. *J Am Soc Nephrol*. 2011;22:2193-2202
13. Ludwig J, Kerscher S, Brandt U, Pfeiffer K, Getlawi F, Apps DK, Schagger H. Identification and characterization of a novel 9.2-kda membrane sector-associated protein of vacuolar proton-atpase from chromaffin granules. *J Biol Chem*. 1998;273:10939-10947
14. Wagner CA, Finberg KE, Breton S, Marshansky V, Brown D, Geibel JP. Renal vacuolar h+-atpase. *Physiol Rev*. 2004;84:1263-1314
15. Nishi T, Forgac M. The vacuolar (h+)-atpases--nature's most versatile proton pumps. *Nat Rev Mol Cell Biol*. 2002;3:94-103
16. EauClaire SF, Cui S, Ma L, Matous J, Marlow FL, Gupta T, Burgess HA, Abrams EW, Kapp LD,

Granato M, Mullins MC, Matthews RP. Mutations in vacuolar h+ -atpase subunits lead to biliary developmental defects in zebrafish. *Dev Biol*. 2012;365:434-444

17. Cruciat CM, Ohkawara B, Acebron SP, Karaulanov E, Reinhard C, Ingelfinger D, Boutros M, Niehrs C. Requirement of prorenin receptor and vacuolar h+-atpase-mediated acidification for wnt signaling. *Science*. 2010;327:459-463
18. Lu X, Garrelds IM, Wagner CA, Danser AH, Meima ME. (pro)renin receptor is required for prorenin-dependent and -independent regulation of vacuolar h(+)-atpase activity in mdck.C11 collecting duct cells. *Am J Physiol Renal Physiol*. 2013;305:F417-425
19. Ren L, Sun Y, Lu H, Ye D, Han L, Wang N, Daugherty A, Li F, Wang M, Su F, Tao W, Sun J, Zelcer N, Mullick AE, Danser AHJ, Jiang Y, He Y, Ruan X, Lu X. (pro)renin receptor inhibition reprograms hepatic lipid metabolism and protects mice from diet-induced obesity and hepatosteatosis. *Circ Res*. 2018;122:730-741
20. Kjolby M, Andersen OM, Breiderhoff T, Fjorback AW, Pedersen KM, Madsen P, Jansen P, Heeren J, Willnow TE, Nykjaer A. Sort1, encoded by the cardiovascular risk locus 1p13.3, is a regulator of hepatic lipoprotein export. *Cell Metab*. 2010;12:213-223
21. Herrero L, Rubi B, Sebastian D, Serra D, Asins G, Maechler P, Prentki M, Hegardt FG. Alteration of the malonyl-coa/carnitine palmitoyltransferase i interaction in the beta-cell impairs glucose-induced insulin secretion. *Diabetes*. 2005;54:462-471
22. Roksnoer LC, Heijnen BF, Nakano D, Peti-Peterdi J, Walsh SB, Garrelds IM, van Gool JM, Zietse R, Struijker-Boudier HA, Hoorn EJ, Danser AH. On the origin of urinary renin: A translational approach. *Hypertension*. 2016;67:927-933
23. Ye F, Wang Y, Wu C, Howatt DA, Wu CH, Balakrishnan A, Mullick AE, Graham MJ, Danser AHJ, Wang J, Daugherty A, Lu HS. Angiotensinogen and megalin interactions contribute to atherosclerosis-brief report. *Arterioscler Thromb Vasc Biol*. 2019;39:150-155
24. Binger KJ, Neukam M, Tattikota SG, Qadri F, Puchkov D, Willmes DM, Wurmsee S, Geisberger S, Dechend R, Raile K, Kurth T, Nguyen G, Poy MN, Solimena M, Muller DN, Birkenfeld AL. Atp6ap2 deletion causes extensive vacuolation that consumes the insulin content of pancreatic beta cells. *Proc Natl Acad Sci U S A*. 2019;116:19983-19988
25. Koizumi M, Ueda K, Niimura F, Nishiyama A, Yanagita M, Saito A, Pastan I, Fujita T, Fukagawa M, Matsusaka T. Podocyte injury augments intrarenal angiotensin ii generation and sodium retention in a megalin-dependent manner. *Hypertension*. 2019;74:509-517
26. Lu H, Wu C, Howatt DA, Balakrishnan A, Moorleghen JJ, Chen X, Zhao M, Graham MJ, Mullick AE, Crooke RM, Feldman DL, Cassis LA, Vander Kooi CW, Daugherty A. Angiotensinogen exerts effects independent of angiotensin ii. *Arterioscler Thromb Vasc Biol*. 2016;36:256-265
27. Corvol P, Lamande N, Cruz A, Celerier J, Gasc JM. Inhibition of angiogenesis: A new function for angiotensinogen and des(angiotensin i)angiotensinogen. *Curr Hypertens Rep*. 2003;5:149-154

Ph.D Portfolio

Name:	Yuan Sun
Department:	Internal Medicine, Division of Vascular Medicine and Pharmacology
Research School:	Molecular Medicine
Promotor:	Prof. dr. A.H. Jan Danser
Co-promotors:	Assoc. Prof. dr. Xifeng Lu

Ph.D Training

Courses	**Year**	**ECTs**
Practical Radiation Protection Level 5B	2018	1.0
Biomedical Research Techniques	2018	1.5
Basic Introduction Course on SPSS	2018	1.0
Cardiovascular Pharmacology	2018-2019	0.6
Biomedical Scientific English Writing	2019	2.0
English C1.1 Advanced	2019	3.0
Advanced Course on Applications in Flow Cytometry	2019	0.5
Scientific Integrity	2019	0.3
Biostatistical Methods I: Basic Principles	2019	2.0
The hands-on training: Getting your PhD done - with outlook and onenote	2019	0.3
New pharmacological targets in age-related cardiovascular disease	2019	0.5
Introduction in GraphPad Prism Version 7	2019	0.3
Genetics for Dummies	2019	0.6
20th Winterschool Dutch Kidney Foundation	2020	1.2
Conferences and Symposia		
Dutch Pharmacological Society Spring Meeting (attendance/Poster)	2018-2019	0.9
ATVB/PVD Scientific Sessions (poster)	2018	1.8
ATVB/PVD 2018 Scientific Session Satellite Meeting (attendance)	2018	0.3
The International Society of Hypertension (ISH) 2018 RAAS Satellite meeting (oral)	2018	1.4
29th European Meeting on Hypertension (ESH) and cardiovascular protection (poster)	2019	1.5
AHA Council on Hypertension 2019 (oral)	2019	1.7
Gordon Research Conference: Angiotensin 2020 (oral/poster)	2020	2.6
Gordon Research Seminar (poster)	2020	0.9

Local Research Meetings		
Internal Medicine Science Day (poster)	2019	0.9
Internal Medicine Research Meeting (oral)	2019	0.8
The 23rd Molecular Medicine Day (attendance)	2019	0.3
Weekly Pharmacology research meeting	2018-2020	3.0
Weekly Lipid metabolism research meeting	2016-2017	2.0
Teaching Activities		
Pharmacological control of the autonomous nervous system	2018-2019	2.2
Total ECTs		35.1

Publications (# = equal contribution, *= corresponding author)

Na Wang, Lishu He, Hui Lin, Lunbo Tan, **Yuan Sun**, Xiaoying Zhang, A.H. Jan Danser, Hong S. Lu, Yongcheng He, Xifeng Lu*. MicroRNA-148a regulates low-density lipoprotein metabolism by repressing the (pro)renin receptor, PLoS One 15: e0225356, 2020.

Yuan Sun, Alexandre Goes Martini, Manoe J. Janssen, Ingrid M. Garrelds, Rosalinde Masereeuw, Xifeng Lu, A.H. Jan Danser*. Megalin: a novel endocytic receptor for prorenin and renin? Hypertension 75: 1242-1250, 2020.

Yuan Sun, Xifeng Lu, AH Jan Danser*. Megalin: a novel determinant of renin-angiotensin system activity in the kidney? Curr Hyp Rep 22: 30, 2020.

Yuan Sun, Dominique M. Bovée, A.H. Jan Danser*. Tubular (pro) renin release: the curtain falls. Hypertension 74: 26-28, 2019.

Estrellita Uij[l#], Katrina M. Mirabito Colafella[#], **Yuan Sun**, Liwei Ren, Richard van Veghel, Ingrid M. Garrelds, René de Vries, Marko Poglitsch, Ivan Zlatev, Jae B. Kim, Ewout J. Hoorn, Don Foster, A.H. Jan Danser*. Strong and sustained antihypertensive effect of small interfering RNA targeting liver angiotensinogen. Hypertension 73:1249-1257, 2019

Liwei Ren[#], **Yuan Sun**[#], Hong Lu, Dien Ye, Lijuan Han, Na Wang, Alan Daugherty, Furong Li, Miaomiao Wang, Fengting Su, Wenjun Tao, Jie Sun, Noam Zelcer, Adam E. Mullick, A.H. Jan Danser, Yizhou Jiang, Yongcheng He, Xiongzhong Ruan*, Xifeng Lu*. (Pro) renin receptor inhibition reprograms hepatic lipid metabolism and protects mice from diet-induced obesity and hepatosteatosis, Circ Res 122: 730-741, 2018.

Yuan Sun, A.H. Jan Danser, Xifeng Lu*. (Pro)renin receptor as a therapeutic target for the treatment of cardiovascular diseases? Pharmacol Res 125: 48-56, 2017.

Awards

AHA New Investigator Travel Award	2019
AHA Paul Dudley White International Scholar	2019
Chinese government award for outstanding self-financed students abroad	2019
AHA High impact paper in Hypertension for Summer of 2020	2020

Research Grants

National Natural Science Foundation of China (Grant No. 81800383) 2018-2021

About the Author

Yuan Sun was born on August 8th 1989 in Gansu, China. She achieved her bachelor degree of Biotechnology at Shenzhen University in 2010, and came to the United Kingdom to start her master degree study in industrial and commercial biotechnology at Newcastle University. After she obtained her master degree, she worked as research assistant at Peking University and Shenzhen University. In December 2016, she was enrolled in the PhD program under the supervision of prof. dr. A.H. Jan Danser and assoc. prof. dr. Xifeng Lu. Her research is focused on the link between lipid metabolism and the renin-angiotensin system.

Acknowledgement

Time always pass quickly. The period I spend in Erasmus MC was unforgettable. At the end of this thesis, I would like to express my deepest appreciation to the people that supported me throughout my Ph.D.

To begin with, I would like to thank to my promotor Prof, dr. A.H.Jan Danser. Thank you so much for offering this great opportunity to me to work with you. Your efforts and efficiency made my promotion become true. You are not only a great scientist, but also a tutor mentoring your students. I wish one day I could become a person like you.

My sincere gratitude to my dear co-promotor, dr. Xifeng Lu, who was responsible for my first step in my Ph.D period. Without you, I could not have the chance to start my Ph.D dream. You shed the light on me. I wish we could have more cooperation in the future.

Next, I would like to extend my thanks to the members of reading committee and extended committee: Prof. Ewout. J. Hoorn, Noam Zelcer, Roos Masereeuw, Leo Hofland and Tianxin Yang and Chengchao Ruan. Thank you for taking time to read my thesis and join for the defense.

To Prof. Noam Zelcer, thank you so much you for visiting China to give talks and share brilliant ideas to us. I wish I could have more chance to work with you.

I would also like to thank to Prof dr. Roos Masereeuw, dr. Manoe J. Janssen and dr. Alexandre Goes Martini for helping me with the project. Thank you for all your constructive criticisms in the manuscript. Alexandre, it was nice to meet you at Gordon Conference in Italy. Thank you for your support in my poster session. I wish you have bright further.

Finally, many thanks for all the members of Department of Vascular Pharmacology: Antoinette, Ingrid, Usha, Richard, Rene, Frank (Lejiten), Tessa, Frank, Liwei, Hui, Lunbo, Kuanyu, Linda, Cathy, Rydianne, Dominique, David, Emilie, Charles, Alejandro, Eloisa, Mike, Anusha and all the new Pharma Nerds. Anton, thank you for giving the interesting talks about science and wine. Estrellita and Rugina, we had an unforgettable memory in New Orleans. When I need a friend, you always right there by my side. Michelle, thank you for organizing Vrijmibos and helping me with the placenta work, and also thank to you and Lunbo for being my paranymphs. Annika, thanks for the moments that we had dinners together. I love the cake you made. Edwyn and Eduardo, Cómo está? I enjoyed the days that

we are working together, and the party at your place was unforgettable. Muy gracias! Ehsan, Keivan and Martin, you are the people who always working during weekends, and you are always helping a lot for arranging a great Vrijmibos. Thank you for the happy moments you bring to us. Birgitte, all I can say is thank you. You always willing to help when I turn to you. Thank you, my dear colleagues, it is nice to work with you all. I hope all of you have bright future, we keep in touch!

致谢

阮雄中、管又飞、张炜真、马晓松、华先欣、汪南平、刘宝华教授，感谢你们让我有幸参与团队工作，每一场精彩的学术报，思想火花的激情碰撞，令我对科研之路产生了崇拜和向往之情，你们是我迈向博士道路的一盏引航灯。朱卫国、何前军、苟德明教授，感谢你们对我的鼓励，虽是只言片语，但温暖且有力量！

陈忠丽与岳永恒：我还清晰地记得第一次来到鹿特丹和 EMC，是你们接待的我，感谢你们在工作和生活上对我的关心和帮助，非常幸运能够认识你们这样真挚的朋友，祝福你们的事业和学业一切顺意！

郭元与赵太一：与你们发生的开心的事情太多！感谢有你们，让我的荷兰博士之路不再孤单。祝你们一家幸福安康！

张爽：很喜欢和你聊课题，聊美食，聊旅游，EMC 加班的日子里总能看到你的身影，感谢你在工作和生活上对我的鼎力相助，希望你未来一切顺利！

蔡宗烨：感谢你对我实验和论文答辩的帮助，祝福你在新的工作岗位上大展宏图！

赵静：感谢你，在我们短暂相处的荷兰时光里留下了许多难忘的回忆。祝你的事业一帆风顺，感情圆满！

陈金鸾、小薇、田思雨、缪志江、詹娜、都照宇、翟培培、吴与伦，非常有幸能在 EMC 与你们认识，希望你们科研进展一切顺利！

丁世豪、平臻、老于、高雅、窦莹颖和林展民，感谢师兄师姐们为我指路明灯，愿你们前程似锦！

许健哥与雪野姐，感谢你们在荷兰对我的照顾和关心，愿上帝保守你们。

任丽伟、谭仑波、林惠，我们是嫡系的兄弟姐妹，从深圳课题组到荷兰课题组，这一路都有你们，感谢你们对我的帮助。祝你们研究进展顺利，取得傲人的成绩！

深圳大学实验室小伙伴们：王娜、苗苗、小英、小韦、小陶、凤婷、晓春师兄、一丹、胡悦、孙洁，感谢在我博士生涯中你们与我并肩作战，希望你们事业成功，家庭美满。

昱杰陈总、Fotunatt 胡总、Biotek 刘总和曹总、鼠一鼠二姜总，感谢你们对 EMC 内分泌系 Lab Day 工作的赞助！能够获得国内的慷慨支持，让 EMC 中国留学生感到无比骄傲自豪。

吴吟、张杰、杨琴：有幸能在欧洲大陆重逢大学挚友。愿我们友谊长存！

苏慕：谢谢你的陪伴和鼓励，祝你未来可期。

最后，感谢父母的养育之恩，包容理解与支持，我坚信，我们都是彼此的坚强后盾！

流动的人生，不歇的盛宴，感谢有你，盛装出席。

愿我们未来一切都好！

9 789464 161335